TRANSENDOTHELIAL MOVEMENT OF ADIPONECTIN IN DIABETIC VASCULATURE

NANYOUNG YOON

A DISSERTATION SUBMITTED TO
THE FACULTY OF GRADUATE STUDIES
IN PARTIAL FULFILLMENT OF THE REQUIREMENTS
FOR THE DEGREE OF

DOCTOR OF PHILOSOPHY

GRADUATE PROGRAM IN BIOLOGY
YORK UNIVERSITY
TORONTO, ONTARIO

AUGUST 2019

ABSTRACT

Adiponectin is one of the most abundant circulatory hormone that plays an important role on homeostasis of glucose and lipid, oxidative stress, and inflammation by enhancing insulin sensitivity. It is highly implicated to pathogenesis of metabolic syndrome. This thesis examined: (*study 1*) glucocorticoids effect on adiponectin flux by regulation of permeability and its mechanism involved, (*study 2*) impact of high glucose on transendothelial movement of adiponectin and a whole-body biodistribution to understand functional significance, (*study3*) influence of iron overload on endothelial permeability of adiponectin to investigate the regulatory mechanism.

Findings from study 1 indicated that glucocorticoids altered tight junction profiles that led to reduce endothelial paracellular permeability and to decrease adiponectin contents in rat skeletal muscle. In study 2, the data demonstrated that hyperglycemia decreased vascular permeability and resulted in increased adiponectin transendothelial movement, which observations were tested by multifaceted vasculature platforms in vivo, ex vivo and 2D & 3D in vitro with high glucose treatment. Lastly, study 3 showed that iron overload induced oxidative stress and altered tight junction expression to elevate permeability of endothelial monolayers. This increased adiponectin movement across the endothelial barrier.

In summary, my studies demonstrated that adiponectin transendothelial movement was regulated by vascular permeability. The alteration of permeability relied on expression of tight junction and its regulatory mechanism resulted from diabetic conditions.

TABLE OF CONTENTS

LIST OF FIGURES

Abbreviation	Definition
Å	angstrom, equal to 10^{-10}
AAs	amino acids
ACC	acetyl-CoA carboxylase
Ad	adiponectin
AdipoR1	adiponectin receptor 1
AdipoR2	adiponectin receptor 2
Adn	adiponectin
AJs	adherence junctions
Akt	protein kinase B
AMEM	alpha minimum essential medium
AMP	adenosine-5'-monophosphate
AMPK	5'-AMP-activated protein kinase
ANOVA	analysis of variance
APPL1	adaptor protein, phosphotyrosine interacting with PH domain and leucine zipper 1
APPL2	adaptor protein, phosphotyrosine interacting with PH domain and leucine zipper 2
ATP	adenosine-5'-triphosphate
AUC	area under curve
BBB	blood-brain barrier
BMI	Body Mass Index
C1q	complement component 1q
C57BL/6 mice	C57 black 6, inbred strain of wild-type mice
CaMKII	calcium/calmodulin-dependent protein kinase kinase, isoform II
CaMKK beta	calcium/calmodulin-dependent protein kinase kinase II, beta
cDNA	complementary DNA
CGs	glucocorticoids
CLDN	Claudin

CoQ10	coenzyme Q10
CORT	corticosterone
CPT1	carnitine palmitoyltransferase 1
CSF	cerebrospinal fluid
CT/SPECT	Computed Tomography/Single-photon emission computed tomography
CVD	Cardiovascular Disease
Cyt C	cytochrome c
DAPI	4′,6-diamidino-2-phenylindole
DEX	Dexamethasone
DM	Diabetes Mellitus
DMEM	modification of Basal Medium Eagle (BME)
DMSO	dimethyl sulfoxide
DPPIV	dipeptidyl peptidase-IV
DRP1	GTPase Dynamin-Related Protein 1
E64	irreversible inhibitor of cysteine proteases
ECM	extracellular matrix
EDTA	ethylenediaminetetraacetic acid
EGM	endothelial cell growth medium
ELISA	enzyme-linked immunosorbent assay
ERK 1/2	extracellular signal-regulated kinase 1/2
ETC	electron transport chain
fAd	full-length adiponectin
$FADH_2$	reduced flavin adenine dinucleotide
FAs	fatty acids
FBS	fetal bovine serum
FDG	18F-fluorodeoxyglucose
FFA	free fatty acid
FMT	Fluorescence Molecular Tomography

FMT-PCCT	FMT with emerging X-ray phase-contrast CT
G6Pase	glucose-6-phosphatase
G6PDH	glucose-6-phosphate dehydrogenase
gAd	globular adiponectin
GAPDH	glyceraldehyde 3-phosphate dehydrogenase
GDM	gestational Diabetes Mellitus
GFAT	glutamine:fructose-6-phosphate amidotransferase
GLP-1	glucagon-like peptide-1
GLUT4	glucose transporter 4
GLUTs	glucose transporters
HbA1c	hemoglobin A1C
HDMEC	Human Dermal Microvascular Endothelial Cells
HFE	human factors engineering
HH	hemochromatosis
HJV	hemojuvelin
HMGB1	high mobility group protein B1
HMW	high-molecular weight
HPA	hypothalamic-pituitary-adrenal
HRP	horseradish peroxidase
HUVEC	Human Umbilical Vein Endothelial Cells
IR	insulin receptor
IVGTT	intravenous glucose tolerance test
KO	knockout
LKB1	liver kinase B1
LMW	low-molecular weight
MAPK	mitogen-activated protein kinase
MFN2	GTPase Mitofusin 2
MMPs	Matrix metalloproteinases

MMW	meddle-molecular weight of adiponectin
MRI	Magnetic Resonance Imaging
mRNA	messenger RNA (ribonucleic acid)
Na3VO4	sodium orthovanadate, inhibitor of protein tyrosine phosphatases
NAD+	nicotinamide adenine dinucleotide
NADH	reduced nicotinamide adenine dinucleotide
NADP+	nicotinamide adenine dinucleotide phosphate
NADPH	reduced nicotinamide adenine dinucleotide phosphate
NF-*κ*B/p65	transcription factor p65, a subunit of nuclear factor kappa-light-chain-enhancer of activated B
NIR	near infrared
NLRP3	NACHT, LRR and PYD domains-containing protein 3
NTC	non-targeted control
nu/nu mice	genetic mutant that causes a deteriorated or absent thymus
O-GlcNAc	O-linked N-acetylglucosamine
ob/ob mice	leptin deficient mice
OCLN	Occludin
OGTT	oral glucose tolerance test
PAF	platelet-activating factor
pAMPK	phosphorylated AMP-activated protein kinase
Papp	apparent permeability
PCR	polymerase chain reaction
PDMS	polydimethylsiloxane
PECAM-1	platelet and endothelial cell adhesion molecule 1
PEG	polyethylene glycol
PEPCK	phosphoenolpyruvate carboxykinase
PET	Positron Emission Tomography
PET	polyethylene terephthalate
PFA	paraformaldehyde

PGC-1α	peroxisome proliferator-activated receptor gamma co-activator 1 alpha
PI3K	phosphoinositide 3-kinases
PMSF	phenylmethylsulfonyl fluoride, a serine protease inhibitor
PPAR	peroxisome proliferator-activated receptor
PPARα	peroxisomal proliferator-activated receptor alpha
PPARγ	peroxisomal proliferator-activated receptor gamma
PPP	pentose phosphate pathway
PPRE	PPAR-responsive element
PTB	phosphotyrosine binding
PTM	post-translational modification
qRT-PCR	real-time quantitative reverse transcription PCR
RBP4	retinol binding protein 4
Rho-fAd	rhodamine labeled full-length adiponectin
RIPA	radioimmunoprecipitation assay
RNA	ribonucleic acid
ROI	region of interest
ROS	reactive oxygen species
SDH	sorbitol dehydrogenase
SDS-PAGE	polyacrylamide gel electrophoresis
SEM	standard error of the mean
SGLTs	sodium-glucose linked transporters
shRNA	short hairpin RNA
siRNA	silencing RNA
SIRT1	Sirtuin 1
Sk M	skeletal muscle
STZD	streptozotocin-induced diabetes
T1DM	Type 1 Diabetes Mellitus
T2DM	Type 2 Diabetes Mellitus

TA	tibialis anterior
TEER	transendothelial electrical resistance
TEM	Transmission Electron Microscopy
TfR2	transferrin receptor 2
TJs	tight junctions
TNFα	tumor necrosis factor
TRIC	Tricellulin
TZD	Thiazolidinediones
UDP N-acetylglucosamine	uridine diphosphate N-acetylglucosamine
VE-Cadherin/VE-C	vascular endothelial-cadherin
VEGF	vascular endothelial growth factor
VT750	VivoTag 750,
WGA	wheat germ agglutinin
WHO	World Health Organization
XCT	X-ray Computed Tomography
ZO-1	zonula occludens-1
αSMA	alpha Smooth Muscle Actin

CHAPTER ONE: INTRODUCTION

1.1 METABOLIC SYNDROME AND PATHOPHYSIOLOGY

Metabolic syndrome is defined by a combination of medical issues including insulin resistance, excessive visceral fat, high triglycerides, low HDL cholesterol, dyslipidemia, hypertension, and hyperglycemia, putting individuals at high risk to develop diabetes and/or cardiovascular disease. Furthermore, metabolic syndrome is also highly associated with vascular risk.

1.1.1 DIABETES MELLITUS

Diabetes Mellitus is described as a chronic metabolic disease characterized by a loss of glucose homeostasis due to a lack of or impaired insulin production, secretion or action. The terminology of 'Diabetes Mellitus' comes from the Greek *diabainein* ('to pass through') or *diabetes* ('siphon') and *meli* ('honey (urine)'), and was first defined and named in 400-230 BCE (199). This name is rooted in the fact that untreated Diabetes Mellitus patients suffer from symptoms including experiencing extreme thirst, frequent urination, dehydration, weight loss without intent, ketone bodies in the urine, urine with a sweet smell, and decreased vision or blindness, all associated with high blood glucose levels. In addition, untreated Diabetes Mellitus leads further comorbidities, for example, neuropathy with tingling or numbness in the hands or feet, artery damage with high risk of atherosclerosis, cardiovascular disease (CVD) or heart failure, and damage to the microvasculature resulting in reduced circulation (80). For millennia, Diabetes Mellitus has been a challenging disease in terms of resolving the root causes. The discovery of insulin in 1921, followed by commercialized medications including insulin and other glucose-lowering agents allowed for treatment of the disease, but do not address prevention. As such, the population of diagnosed Diabetes Mellitus patients has increased exponentially in the current era. According to the most updated records from Statistics Canada (Diabetes, 2017), the number of Canadian Diabetes Mellitus patients is 2.3 million (around

7.3% of population aged 12 and older). Following the IDF (International Diabetes Federation), they estimate that more than 600 million of the global population will be Diabetes Mellitus patients by 2040 (270).

1.1.2 PATHOPHYSIOLOGY OF DIABETES MELLITUS

Diabetes Mellitus is well known as the most common heterogeneous disease which has several etiologies (125). It has been reported that the Diabetes Mellitus is imputed by combination of risk factors including both genetic (e.g., family history) and environment (e.g., age, physical inactivity, dietary habits, BMI (obesity), stress, gender, hormonal changes, inflammation, complications associated with medications or surgery, etc) (39). In general, Diabetes Mellitus is categorized into three major types; Type 1 Diabetes Mellitus (T1DM), Type 2 Diabetes Mellitus (T2DM) and Gestational Diabetes Mellitus (GDM). The most prevalent type of diabetes is T2DM, which accounts for >90% of cases. T1DM follows as the second most common type, at 5-10% of the population of diabetic patients. GDM is distinct in that it is a temporary condition that occurs during pregnancy in approximately 5.5% of total births. Different physiological processes cause T1DM and T2DM. T1DM is an autoimmune disease. Pancreatic beta cells are destroyed by abnormal autoimmunity in T1DM, and subsequent insulinopenia eventually leads to hyperglycemia. On the other hand, T2DM is an endocrine disorder that results in a chronic imbalance of glucose homeostasis due to insulin resistance. At the early stages of T2DM development, blood glucose is observed to be in the normal range, and its metabolism looks undistorted. However, the circulating level of insulin increases to compensate for insulin resistance (hyperinsulinemia),. As the disease progresses, depending on the individual, genetic susceptibility and risk factors from the environment trigger pancreatic beta cell dysfunction. They often experience defects in insulin regulation due to beta cell damage, for example, producing insufficient insulin or delaying insulin secretion. Thus, the impaired insulin sensitivity in T2DM combined with insufficient insulin release impacts on glucose uptake

and leads patients to suffer chronic hyperglycemia, not only in the postprandial phase but also after fasting.

1.2 MECHANISMS OF DIABETES MELLITUS

1.2.1 INSULIN RESISTANCE

Insulin resistance is defined as a condition of impaired cellular responses to insulin, a circulating hormone secreted from pancreatic beta cells. The cellular response is activated by insulin binding to its heterodimer receptor, insulin receptor (IR), in insulin-target tissues (166), and followed by activation of an intracellular signaling cascade. To determine change in insulin signaling, activation of Akt by phosphorylation (Ser473) is mainly quantified (262). Alterations in Akt activity have been experimentally observed in Diabetes Mellitus subjects, not only T2DM animal models, but also T1DM (236, 293, 320, 321). It has been well established that T2DM is tightly associated with obesity, metabolic syndrome and subsequent insulin resistance (88). The insulin resistance is observed in tissues in which glucose uptake is mediated by insulin, for example, brain, liver, skeletal muscle, and adipose tissue. Skeletal muscle is particularly important in this context, as it accounts for 75-80% of insulin-stimulated glucose uptake (60). However, insulin resistance is also associated with diabetic complications in numerous other tissues leading to various pathologies (264, 293). In the case of nephropathy, impaired insulin signaling leads to a decrease in glucose uptake by the kidney. Reduced insulin signaling and associated glucose uptake causes the liver to recognize the body as having low glucose availability, triggering aberrant glucose production via gluconeogenesis or glycogenolysis. Impaired insulin-mediated suppression of lipolysis also causes mobilization of free fatty acids (FFA) from adipose tissue. Systemic accumulation of FFAs and excess glucose (hyperglycemia) exacerbates the failing insulin secretion and response mechanisms, ultimately causing diabetes and its complications. Indeed, the loss of insulin action makes changes in molecular localization and expression level of GLUTs (glucose transporters) and SGLTs (sodium-glucose

linked transporters). (74, 167, 195, 284, 322) Thus, insulin resistance has been considered as an important mechanism in the development of Diabetes Mellitus.

1.2.2 COMPENSATORY HYPERINSULINEMIA

In 1966, the Fraser group observed significantly increased plasma insulin levels in 19 non-diabetic patients who had essential hypertension as compared to a group of normotensive controls (292). Around 25 years later, these findings were replicated by other groups, which supported the observation of hyperinsulinemia along with hypertension, although there was no change in glucose levels. Intrestingly, plasma insulin highly increased during oral glucose tolerance test (OGTT) or intravenous glucose tolerance test (IVGTT) in hypertensive individuals as well (77, 162, 176, 206, 237, 253). From the follow up studies, it was concluded that insulin resistance and compensatory hyperinsulinemia is a risk factor for CVD (120, 216, 240). As described above, we currently understand that insulin resistance can lead to compensatory hyperinsulinemia to control insulin-mediated glucose uptake from the blood stream, and that ultimately insulin resistance can develop into overt Diabetes Mellitus without appropriate treatment (215).

Glucocorticoids (GCs) are a medication widely used as the first line therapy for inflammation and autoimmune diseases. More than 1% of the population is prescribed glucocorticoids on any one day for the treatment of inflammation, cancer, or respiratory diseases. Older individuals (70-79yrs) have especially high rates of GC treatment, accounting for around 2.5% of this population (275). Unfortunately, this powerful medication shows detrimental effects on pre-diabetic patients, as it increases insulin resistance (105, 274). GCs are a class of steroid hormone. It was reported in rat and mouse animal models that excess GCs lowered insulin sensitivity and resulted in hyperinsulinemia (215). In addition, overexposure of GCs leads to increased adipose tissue at visceral and trunk sites (86). In adipose tissue, impaired insulin signaling cannot suppress lipolysis and cannot increase glucose uptake. Similarly, glucose uptake was downregulated in muscle. In the liver, GC overload

caused a failure of inhibition of gluconeogenesis and glycogenolysis. As a result of these alterations, circulating glucose and free fatty acids increased and energy metabolism shifted at a level of mitochondrial oxidation.(87)

Dexamethasone is the primary prescribed drug for GC therapy, and some patients experience side effects from overexposure of this exogenous GC based on dose and/or duration of treatment. On the other hand, Cortisol is a steroid hormone that is produced *de novo* by the adrenal cortex under stress conditions. Although endogenous GC overexposure is rare, it is categorized as a chronic endocrine disorder (209). Overall, GCs overexposure by either endogenous or exogenous GCs is named Cushing Syndrome. Without treatment, Cushing Syndrome alters cortisol circadian rhythm, activates the hypothalamic-pituitary-adrenal (HPA) axis, and increases adipose tissue (obesity) with the development of insulin resistance. (16, 87, 228, 250)

1.2.3 HYPERGLYCEMIA; FAILURE OF GLUCOSE CONTROL

Hyperglycemia, a chronic elevation of blood glucose due to a failure of glucose control, is seen in the major two types of diabetes patients. In the progression of diabetes, the most effective way to reduce the risk of vascular complications is by controlling glucose levels (1, 62). Because T1DM is a condition of systemic insulin deficiency, patients have insulin dependency. Additionally, half of T2DM patients eventually require insulin therapy. Studies show the importance of glucose control with exogenous insulin therapy in experimental diabetic models. In a study of insulin infusion into T1DM subjects to improve glucose control (203), the therapy prevented microvascular and macrovascular complications (62, 256, 302). Further, pancreatic islet transplants also have a protective effect against the development of complications (94).

There are some clinical intervention strategies for hyperglycemia. Before starting medications, life style modification and setting the individual hemoglobin A1C (HbA1c) target are required for patients because the most urgent clinical goal is lowering plasma glucose levels. The

lifespan of red blood cell is around 2~3 months (varying between 70 and 140 days) (49), and the HbA1c measures the glycated hemoglobin within red blood cells, thus reflecting the glucose levels over the previous 2 - 3 months (224, 225). The normal range of HbA1c is 4 - 5.6%, while an HbA1c of 6.5% is the diagnostic threshold (232). If the HbA1c is above the threshold, there are numerous pharmaceutical agents to reduce glycemia though various targets and mechanisms; (1) Agents for enhancing insulin secretion from the pancreas (e.g., sulfonylureas (1), glucagon-like peptide-1 receptor (GLP-1R) agonist (97), dipeptidyl peptidase-IV (DPP-IV) inhibitor (207)). (2) Insulin sensitizing agents, which are commonly peroxisome proliferator-activated receptor gamma (PPARg) activators or agonists (e.g., Thiazolidinediones (TZD) (150), metformin (115)). (3) Anti-hyperglycemic drugs that directly eliminate glucose from the bloodstream (e.g., Inhibitors of sodium-dependent glucose transporter 2 (SGLT2) (164, 273)).

1.2.4 REDOX IMBALANCE AND OXIDATIVE STRESS

1.2.4.1 ABERRANT ENERGY PRODUCTION; MITOCHONDRIAL DAMAGE

In general, once cells uptake glucose, energy production starts from the process of glycolysis that produces two pyruvate and two net ATP per one molecule of glucose via anaerobic metabolism (33). The pyruvate then moves into the mitochondria and is processed through oxidative decarboxylation to generate Acetyl-CoA for running the Kreb's cycle. This if followed by oxidative phosphorylation via the electron transport chain (ETC) on the inner mitochondrial membrane. The mitochondrial ETC is composed of complexes I, II, III, IV, and V, as well as electron transporters coenzyme Q10 (CoQ10)/ubiquinone and cytochrome c (Cyt C). The electron flow tightly coupled via complexes I/III/IV or complex II/III/IV, which use NADH, $FADH_2$ and oxygen to produce a proton gradient across the inner membrane. The built-up proton gradient is then used by complex V/ATP synthase to make ATP and H_2O (328). When the cell uses fatty acids (FAs) or amino acids (AAs) as an energy source, the sources go through beta-oxidation and oxidative phosphorylation to

generate large amounts of chemical energy (eg. ~130 ATP/1 FA). The energy production in healthy cells is well managed, however, the cells in diabetes fail to control this energetic flux, resulting in impaired cellular energy generation (101).

Many studies have demonstrated that hyperglycemia induces mitochondrial dysfunction by promoting fragmentation. Mitochondrial fragmentation is facilitated by DRP1 (GTPase Dynamin-Related Protein 1, for fission) activation and MFN2 downregulation (GTPase Mitofusin 2, for fusion) regulated by signaling related to intracellular Ca^{2+} concentrations, CaMKII (calmodulin-dependent kinase II) and ERK 1/2 (extracellular signal-regulated kinase 1/2) activation (28, 246, 317). The induction of mitochondrial fragmentation, and prevention of fission, is closely associated with ROS (reactive oxygen species) overproduction that enhances DRP1-mediated fission (9). In the progression of diabetic complications, superoxide generation from the mitochondria is an early stage event, along with electron leakage to produce H_2O_2 instead of ATP, which usually happens at complex I (NADH dehydrogenase) and in between CoQ10 and complex III (36, 46, 52, 186, 221, 238, 261, 272, 330). Importantly, uncoupling of the ETC not only generates excess ROS, but the loss of mitochondrial membrane potential also stops ATP production and generates heat instead of ATP in diabetic heart. This also slows intracellular glucose transport. In contrast, free fatty acid uptake is increased, which is postulated to be a compensatory mechanism for the loss of glucose metabolism. This has been repeatedly observed to be associated with vascular complications (2, 7, 35, 52, 78, 220).

1.2.4.2 OXIDATIVE STRESS

Oxidative stress relies on the imbalance of cellular ROS production versus the capacity for cellular detoxification. The detoxification includes removing reactive intermediates from oxidative metabolism and repairing cellular damage from excessive ROS. In diabetes, especially in hyperglycemia, the causes of cellular oxidative stress are up-regulation of the sorbitol/polyol

pathway, protein glycosylation, and glucose autoxidation (290). Hexokinase plays an important role in glucose utilization by most cells and it is regulated by glucose-6-phosphate dehydrogenase (G6PDH), the rate limiting step for the pentose phosphate pathway (PPP) (33). The products of the PPP are the sources for the synthesis of nucleotides and aromatic amino acids, as well as NADPH, which gives the cell reducing power (69, 327). Under high glucose conditions, the flux of glucose metabolism is shifted to generate more NADPH via PPP activation, while at the same time the flux of the sorbitol pathway is increased. Sorbitol accumulates by activation of aldose reductase to convert NADPH to $NADP^+$. Then, excess NADH by the following reaction of sorbitol dehydrogenase (SDH) would be the bundle for the mitochondrial ETC. Furthermore, the accumulated sorbitol also provides osmotic stress in cells. (69, 205)

In addition to increases in NADPH and sorbitol under hyperglycemic conditions, because mitochondrial ROS inhibits GADPH activity, the reaction from frunctose-6-phosphate to UDP N-acetylglucosamine by glutamine:fructose-6-phosphate amidotransferase (GFAT) is increased preferentially as compared to glycolysis (68). This enhances O-linked N-acetylglucosamine (O-GlcNAc), which competes with serine/threonine phosphorylation of transcription factors to alter gene expression in diabetes. (68, 137, 227)

1.2.5 IRON OVERLOAD

Iron overload is one of the risk factors for diabetes, observed in clinical hereditary hemochromatosis (HH) cases. Among HH patients, approximately 60% of patients have a high risk of developing diabetes. (70, 297) The leading cause of HH is a homozygous HFE (human factors engineering) mutation at C282Y, followed by other less common mutations in iron metabolism-related proteins, for example, TfR2 (transferrin receptor 2), HJV (hemojuvelin), and hepcidin (75, 204). The mutation in HFE increases iron accumulation in several tissues. The alteration in iron metabolism due to excess iron uptake by tissues leads to a change in glucose homeostasis by affecting

insulin action and secretion. T2DM patients have been shown to have increased serum ferritin levels, which plays roles in iron storage, as well as acting as an iron carrier in plasma. Multiple animal studies have demonstrated the association between serum ferritin level and diabetes risk (41, 83, 116, 117, 239). In addition, iron depletion by deferoxamine, an iron chelator, improved insulin resistance by increasing glucose uptake and insulin sensitivity (67).

This close correlation between iron overload and diabetes risk is not fully understood. However, there are some suggested mechanisms. Iron overload may lead to diabetes by 1) causing insulin deficiency by inducing pancreatic beta cell failure, 2) promoting insulin resistance, and 3) inducing hepatic dysfunction mediated by insulin resistance. Firstly, iron overload induces intracellular oxidative stress. Pancreatic beta cells are particularly susceptible to oxidative stress as there is a comparably weak antioxidative defense system in beta cells as compared to other tissues (151). The central role of beta cells is focused on glucose metabolism, including mitochondrial oxidative phosphorylation and glucose-induced insulin secretion. As energy is produced via mitochondrial metabolism in the beta cell, the occurrence of a redox imbalance from excess ROS leads to beta cell dysfunction, ultimately resulting in the reduction of insulin secretion (263). Next, iron overload is associated with insulin resistance in adipocytes and hepatocytes. A population study showed that increasing plasma ferritin levels correlate with insulin resistance of adipose tissue. *In vitro*, decreased glucose transport and adiponectin expression (a marker of an insulin sensitizer) was observed in adipocytes treated with iron. (66, 298) Above all, however, the strongest correlations with elevated serum ferritin levels are the induction of hepatic insulin resistance, increase in hepatic iron accumulation, as well as plasma levels of adiponectin (223). Cells have a compensatory mechanism to respond to high iron levels, in order to avoid the insulin resistance associated with systemic iron overload. This mechanism involves the upregulation of the iron hormone hepcidin via the iron-sensing pathway. Enhanced hepcidin production contributes to the control of up-taking nutritional iron, as well as releasing stored intracellular iron by inhibition of ferroportin (an iron

exporter). However, in the case of advanced liver injury, the hepatic dysfunction prevents the rapid regulation of hepcidin, and ultimately results in loss of iron control, resulting in hepatic iron accumulation (138). Overall, iron overload is thought to contribute to Diabetes Mellitus by impairing systemic insulin secretion and action.

1.3 ADIPONECTIN

Adiponectin is known as a circulating hormone derived from adipocytes. It is one of a series of adipokines such as leptin, interleukin-6, TNF-alpha, retinol-binding protein 4 (RBP4), and so on that are secreted into the bloodstream. Adiponectin is one of the most abundant proteins in the circulation of normal humans (3~30ug/mL), accounting for 0.01% of all plasma proteins (13). Adiponectin plays a pivotal role in the regulation of metabolism, especially in the conditions of obesity and diabetes. Previous research has shown that the level of adiponectin in serum has a negative correlation with aspects of metabolic syndrome (obesity and insulin resistance) and is associated with an increased risk of cardiovascular disease and diabetes. This section will review the current understanding of signaling mechanisms mediated by adiponectin, including its receptors and other downstream intracellular signaling proteins. Also, it will review the specific effects of adiponectin in target tissues.

1.3.1 STRUCTURE OF ADIPONECTIN

Adiponectin is a highly conserved protein which is encoded by the gene located on chromosome 3q27, which has been identified through genome-wide association studies as a diabetes susceptibility locus (133, 255). Adiponectin is composed of 244 amino acids has three main domains; a signal peptide, an N-terminal collagen-like fibrose region and C-terminal globular domain. The adiponectin sequence shares similarities with collagens X and VIII, and complement factor C1q. In addition, the C-terminal globular domain structure resembles the crystal structure of TNF- α, even

though there is no similarity of primary sequences (235). There are two different types of functional adiponectin; full-length adiponectin (fAd) and globular adiponectin (gAd). The gAd is liberated by cleavage of fAd by leukocyte derived elastase to generate a C-terminal globular fragment of adiponectin which mediates important functional effects. Despite gAd being a shorter sequence of amino acids and structurally smaller than fAd, its potent metabolic effects are similar to fAd. But, importantly, the specific affinities for the two different adiponectin receptors are different. In animal studies to examine the role of gAd in the context of genetic obesity (leptin-deficient ob/ob), even though no change on the body weight of mice was observed, gAd overexpression ameliorated insulin resistance, beta cell degranulation, and diabetes by enhancing fatty acid oxidation (309). The adiponectinemia also raised lipid clearance and lipoprotein lipase activity and suppressed insulin-mediated endogenous glucose production (51). Before secretion into bloodstream, adiponectin undergoes post-translational modification (PTM). A previous mass spectrometry (MS)-based study has mapped the PTM sites for adiponectin. Four proline residues are conserved for hydroxylation in the collagen domain, and five lysine residues are also conserved for hydroxylation and glycosylation subsequently (four sites in the collagen region and one site in the hyper-variable region) (286, 288). The PTM steps are involved in the binding to the putative adiponectin receptor T-cadherin, which is a glycosylphosphatidylinositol-linked cell-surface molecule (109).

1.3.2 ADIPONECTIN OLIGOMERS

Full-length adiponectin exists in the body as three oligomeric forms; LMW (low-molecular weight), MMW (medium-molecular weight) and HMW (high-molecular weight) isoforms. Monomeric adiponectin has not been detected in circulation under physiological conditions. (Fig 1.1)

The LMW form is an adiponectin trimer, and is the basic building block for higher molecular weight forms. LMW adiponectin is formed by hydrophobic interactions between the globular regions of adiponectin and is stabilized by non-covalent interactions of the collagenous domains in a triple-

helix stalk. The structure of the trimer is a ball-and-stick-like shape including a large globular sphere (269). The crystal structure of the globular domain was determined at a resolution of 2.1 Å (1 Å = 0.1 nm) (235).

The MMW form is hexameric adiponectin. MMW adiponectin is formed by two homotrimers by disulfide bond-mediated self-association. The cysteine residue in the adiponectin N-terminal variable domain plays an essential role in the formation of a disulfide bond (Cys36 in human, Cys39 in mouse) (196, 268, 269, 285). MMW adiponectin was visualized by high-resolution electron microscopy as being Y shaped in structure (252).

The HMW form is oligomeric adiponectin, though the structure is still poorly characterized. Through TEM (transmission electron microscopy), bovine HMW adiponectin was reported to be asymmetric bouquet-like in shape within a tight ring of octadecamers (13, 252). But the composition of human HMW adiponectin oligomers differs from those of rodents and cows. Human HMW adiponectin shows the range of oligomers as 18 – 30-mers or even larger (280) .

Oligomerization of adiponectin is important not only for the structural properties, but also functional activity. For example, MMW and HMW forms from adiponectin mutants lacking the cysteine residue in N-terminal domain did not bind to the T-cadherin receptor. (109)

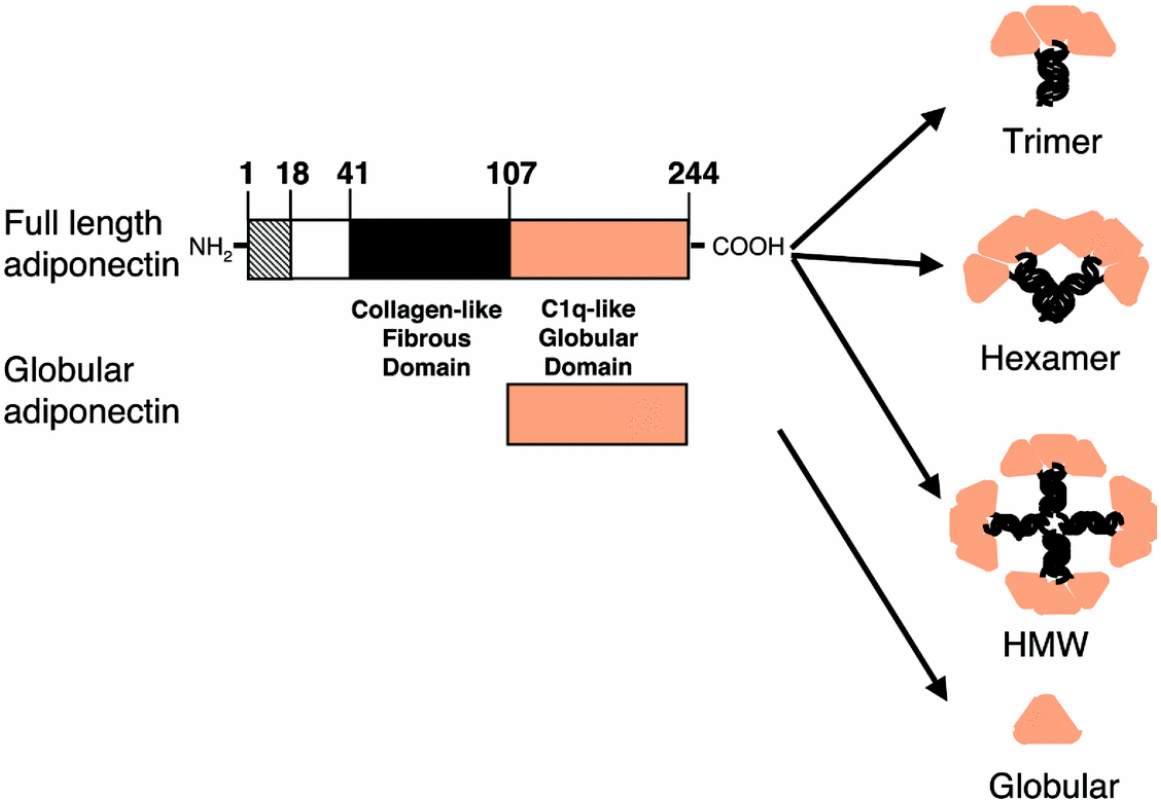

Figure 1.1. Adiponectin structure and oligomers

The full-length adiponectin (fAd) gene encodes 244 AAs. The polypeptide is composed of several domains; a collagen-like fibrous domain (N-term) and a C1q-like globular domain (C-term). fAd has three different isoforms; LMW (trimer), MMW (hexamer) and HMW (oligomer). On the other hand, gAd (globular adiponectin) has only the globular domain (191).

1.3.3. RECEPTORS OF ADIPONECTIN

Secreted and circulating adiponectin is distributed to target tissues. In target tissues, intracellular adiponectin signaling is mediated through adiponectin binding to receptors AdipoR1 and AdipoR2, which are 7-transmembrane adiponectin receptor isomers with an internal N-terminus and an external C-terminus (307). AdipoR1 is found in several types of tissues, but especially abundant in skeletal muscle, whereas AdipoR2 is found commonly in liver (306). These adiponectin receptors show different affinities for the ligand types. Based upon the results of RNA interference of the receptor genes and affinity tests, AdipoR1 is high-affinity receptor for globular adiponectin, while AdipoR2 is low-affinity receptor for globular adiponectin. Conversely, AdipoR2 binds full-length adiponectin with high affinity (123). The adiponectin receptors are highly conserved between human and mouse, with 96.8% of AdipoR1 and 95.3% of AdipoR2 sequence similarity (307)

AdipoR1 and AdipoR2 are key players in the functional role of adiponectin with physiological and pathophysiological significance. Adiponectin receptors are involved in the regulation of several metabolic processes such as glucose and lipid metabolism, inflammation and oxidative stress. A functional study of adiponectin receptors showed that the mRNA expression level of AdipoR1 and AdipoR2 decreased in obese transgenic mice compared with wild type mice (310). Also, disruption of AdipoR1 and AdipoR2 inhibits aidponectin binding to these receptors, and eliminates the metabolic actions of adiponectin. Specifically, AMPK activation was decreased in the AdipoR1 KO mice, and in the AdipoR2 KO mice, PPARα signaling was reduced. Additionally, disruption of both adiponectin receptors increased tissue triglyceride accumulation, inflammation and oxidative stress markers at both mRNA and protein levels. It also induced insulin resistance and glucose intolerance. (310)

1.3.4 ADIPONECTIN SIGNALING

Previous studies have shown (Fig 1.2) that adiponectin binding via AdipoR1 and AdipoR2 mediated signal transduction, mainly through AMPK and PPARα pathways, resulting in increased insulin sensitivity (34, 59, 123), stimulation of fatty acid oxidation and glucose utilization (173), and mitochondria biogenesis (51, 114). Adiponectin also suppressed hepatic glucose production (173). It has also been reported that adiponectin has AdipoR1- and AdipoR2-activated ceramidase activity leading to antiapoptotic function (107, 122).

After binding of adiponectin to its receptors, the very next molecule involved in signaling is APPL. APPL1 (phosphotyrosine interaction, PH domain, and leucine zipper containing 1) is an adaptor protein for adiponectin receptors (168). The phosphotyrosine binding domain (PTB) of APPL1 in its C-terminal site interacts with the N-terminal intracellular domain of AdipoR1 and AdipoR2. In contrast, APPL2 negatively regulates adiponectin signaling, producing a so-called Yin-Yang regulation by APPL1-APPL2. In the basal condition, APPL2 occupies the intracellular N-terminal of AdipoR1, at the same time, it interacts with APPL1 as an APPL1-APPL2 heterodimer. Thus, it interrupts the interaction between AdipoR1 and APPL1 as an adaptor protein, so adiponectin signaling is inhibited. However, once adiponectin signaling is stimulated by binding adiponectin to its receptors, APPL1 and APPL2 dissociate from each other and APPL1 is released. Then AdipoR1 recruits APPL1, which is a limiting step for adiponectin signaling. APPL1 can activate several proteins involved in different signaling pathways by phosphorylation. For example, APPL1 regulates the LKB1/AMPK, MAPK, and PI3K/Akt pathways. PI3K/Akt are also components of the insulin signaling pathway. During the time that APPL1 is bound to APPL2 and inactivated, insulin signaling is inhibited by the active form of dephosphorylated S6K (217, 281). Other adaptor proteins for adiponectin receptors exist, but are not discussed here.

AMPK (5'-AMP-activated protein kinase) belongs to a family of energy sensing enzymes and is a principal mediator of many of the effects of adiponectin. AMPK is activated in response to

and increase in the AMP/ATP ratio and by phosphorylation (98, 282). Upon activation of adiponectin signaling, the activity of AMPK is also directly regulated by adiponectin or adiponectin receptors in an APPL1-mediated manner. When extracellular adiponectin binds its cell surface receptors, Ca^{2+} influx increases and Ca^{2+}/calmodulin-dependent protein kinase kinase β (CaMKK β) is activated to phosphorylate AMPK at the T172 site (114). LKB1 is also a kinase that activates AMPK, and adiponectin also promotes AMPK activation through promoting APPL1-dependent LKB1 cytosolic translocation (331). LKB1 deletion in the liver leads to increased blood glucose levels and impaired glucose tolerance (173). Additionally, AICAR is a small molecule that also can be used to increase pAMPK as a cell permeable activator (308).

Activated AMPK cascades the signal to various downstream targets. Based on the ratio of NAD^+/NADH, pAMPK activates SIRT1 to facilitate deacetylation of the transcription factor PGC-1α to enhance mitochondrial biogenesis and related target gene expression (114). Furthermore, pAMPK induces phosphorylation of ACC (acetyl-CoA carboxylase) at site S79 and it leads to inhibit the ACC activation by cytosolic citrate, as an allosteric activator of ACC (129). This inactivation causes lowering concentration of malonyl-CoA, the product of ACC activity, which inhibits CPT1, the enzyme responsible for converting fatty acyl-CoA to acylcarnitine. Acylcarnitine is the first molecule involved in mitochondrial β-oxidation. In addition, pAMPK is also able to increase suppression of gluconeogenesis-related genes such as PEPCK (phosphoenolpyruvate carboxykinase) and G6Pase (glucose-6-phosphatase) downstream of adiponectin cues. Decreased gluconeogenesis affects both the AMP/ATP ratio as well as NAD+/NADH ratio (265). Thus, elevation in pAMPK leads to increased fatty acid oxidation, glucose uptake (51) and mitochondrial biogenesis (114). In contrast, blocking AMPK activation by dominant negative mutation shows opposite effects on these metabolic parameters (308).

PPARs (peroxisomal proliferator-activated receptors) are a group of nuclear receptor proteins that act as transcription factors, regulating the expression of numerous genes, including the

adiponectin gene (171, 329). Adiponectin gene expression is regulated by binding of PPARs to PPRE (PPAR-responsive element) (329). Agonist treatment to activate PPARα leads to increased expression of both adiponectin and adiponectin receptors at the mRNA level. The effects on carbohydrate and lipid metabolism are also associated with elevated expression of PPARγ (peroxisomal proliferator-activated receptor gamma), caveolin-1, and mitochondrial markers in white adipose tissue (51).

Finally, adiponectin signaling has different effects depending on the target tissue type. For instance, in skeletal muscle, both types of adiponectin (full-length and globular) can activate AMPK, but only full-length adiponectin is able to activate AMPK effectively in the liver (308).

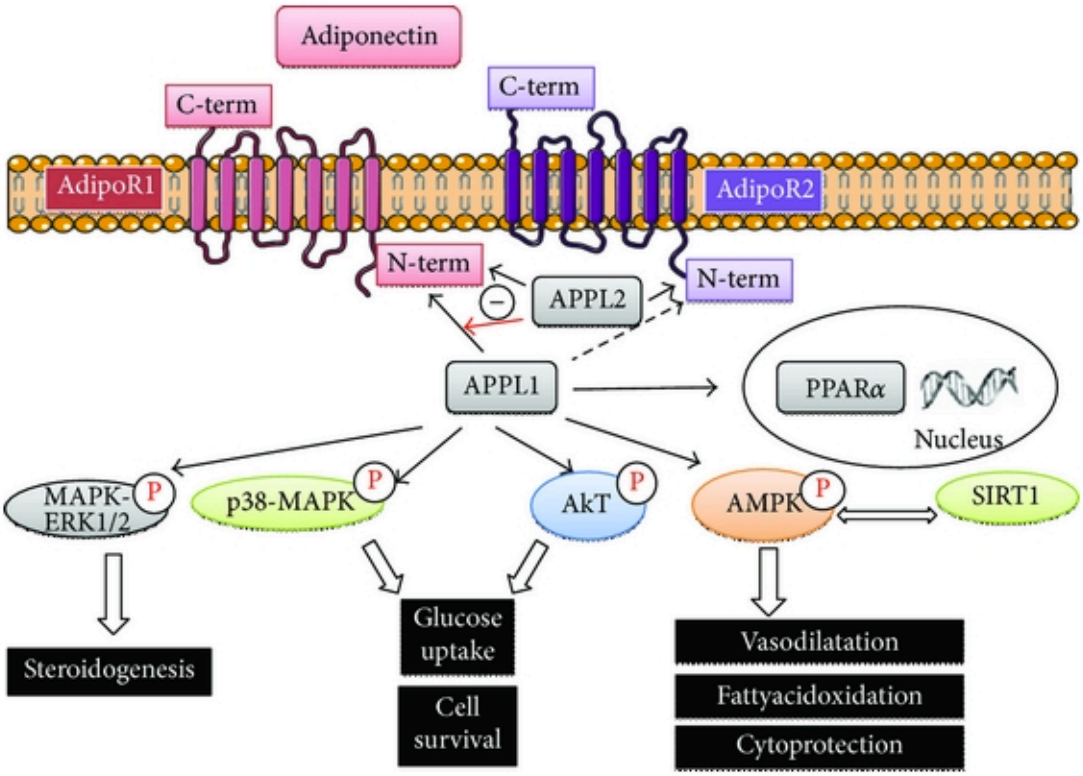

Figure 1.2. Adiponectin Signaling via AdipoR1 and AdipoR2

Adiponectin signaling is mediated by activation of two known receptors, AdipoR1 and AdipoR2. Uplon receptor activation, APPL1 is recruited to AdipoR1 and activates downstream signaling including PPARα, AMPK, AMPK/SIRT1, p38-MAPK, ERK1/2-MAPK, and Akt. APPL1 and APPL2 are controlled by Yin-Yang regulation. (281), (217)

1.4 ENDOTHELIAL MOVEMENT OF HORMONES

1.4.1 STRUCTURE AND FUNCTION OF ENDOTHELIUM

A monolayer of endothelial cells lines the entire circulatory system of the body. This endothelium acts as a barrier, which regulates the exchange of hormones, proteins and small molecules between the vascular compartment and the interstitial space (89, 208). The actions of a hormone or nutrient on a target tissue is implicitly dependent upon the ability of these factors to gain access to the tissue, and numerous studies have indicated that hormone and nutrient concentrations in blood differ from those surrounding cells on the tissue side of the blood vessel endothelium (18, 30, 44, 45, 102, 136, 165, 245, 312). In this regard, it is our contention that the significance of the endothelium as a regulator of hormone and substrate access to target tissues is often underappreciated. Endothelial permeability can be regulated by two distinct pathways: 1) the transcellular pathway where solutes are actively transported across the endothelium, primarily via caveolae-mediated transcytosis; or 2) the paracellular pathway where solutes passively move through the intercellular space between adjacent endothelial cells. (Fig 1.3)

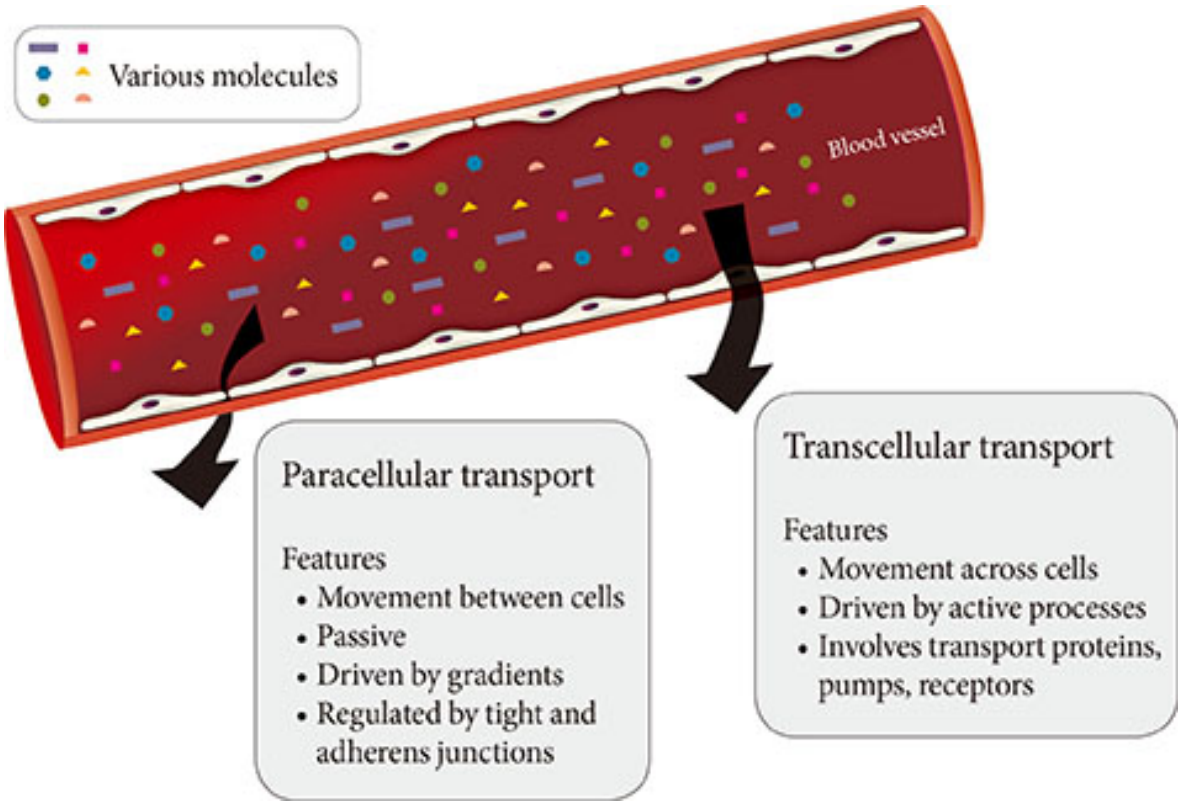

Figure 1.3. Routes of transendothelial transport. A schematic representation of paracellular and transcellular routes for transport of blood-borne hormones and solutes to interstitial space of underlying tissue.

1.4.2 TRANSCELLULAR TRANSPORT

The transcellular movement of solutes involves energy-dependent trafficking of vesicles across the endothelium (89). This often requires their recognition by receptors in caveolae on the luminal surface of the endothelium, and may involve vesiculo-vacuolar organelles or occur via transcellular channels (89). Caveolae, cholesterol- and sphingolipid-rich non-clathrin-coated pits are abundant in endothelial cells. After ligand binding to receptors in caveolae, dynamin-mediated endocytosis occurs followed by vectorial transport and fusion of the vesicle with the basolateral membrane, resulting in the release of contents by exocytosis (89). As a general concept, transcellular vesicle trafficking is important in the transport of larger macromolecules across the endothelium since the paracellular route is typically capable of restricting passage of solutes larger than 3 nm in radius (95, 96).

1.4.3 PARACELLULAR TRANSPORT

The paracellular mode of transport across endothelia depends upon concentration gradients between blood and interstitial fluid. One regulatory mechanism of paracellular movement involves tight junctions (TJs), which are composed of strands of transmembrane and cytosolic proteins that closely control paracellular flux and have been established to be important in regulating hormone transport (96, 134, 136). As a component of the cell-cell junction of endothelia, the TJ provides a selective barrier to solute movement between cells (95). The permselectivity of the TJ barrier is dependent on the variable assemblage of TJ proteins that comprise the complex. Proteins such as occludin, tricellulin, and claudins directly establish the TJ barrier and form the backbone of TJ strands, while the cytosolic proteins, such as ZO-1, provide structural support to the TJ complex. The incorporation of specific TJ protein isoforms can enhance TJ barrier function (i.e., make TJs tighter) or form channels to increase TJ permeability (i.e., make TJs leakier) (95). Importantly, skeletal muscle and heart vasculature have a continuous endothelium with TJs between cells (5, 6). However,

the liver and spleen have a discontinuous endothelium with large holes, which allow rapid equilibration of plasma with the underlying tissue (5, 6). It was suggested that this expedited exposure of the liver to plasma solute changes may partly explain its earlier susceptibility to insulin resistance (132). Indeed, the precise architecture of TJs varies between different vascular beds, with TJs being either dominant at the apical point of intercellular space or intermingled with adherence junctions (AJs). Therefore, there is no doubt that transendothelial paracellular flux in certain vascular beds is more susceptible to changes in TJ composition and structure. Furthermore, changes in paracellular transport leading to endothelial hyperpermeability is a significant problem in vascular inflammation associated with diabetes, cancer, ischemia-reperfusion injury, thrombosis, trauma, sepsis, and T-respiratory distress syndrome (144). Importantly, despite the tremendous interest in adipokines over recent years, very few studies have examined the critical step whereby factors secreted by adipose tissue, or other tissues, must enter the circulation via capillaries or lymph. Paracellular movement is very likely to be a major regulatory step in this process. Indeed, it has been demonstrated that lymph/capillary partitioning of adipokines is dependent upon their molecular size, and it has been proposed that this will have important ramifications for their regional and systemic distribution and subsequent physiological effects (172).

It is also important to realize that crosstalk exists between 1) transcellular and paracellular routes of transport across endothelia and 2) TJs and AJs of endothelia. An example of the former is that in caveolin-1 knockout mice, or upon siRNA-mediated reduction of caveolin-1, altered TJ assembly in small capillaries and veins increased paracellular transport of albumin (175, 214, 230). In the latter case, it has been shown that vascular endothelial (VE)-cadherin mediated signaling can regulate the expression of TJ proteins and consequently alter barrier function (89).

Indeed, evidence suggests that AJs also play a crucial role in regulating vascular permeability. They are comprised of calcium-dependent VE-cadherin in complex with a range of interacting partners, such as β-catenin and p120-catenin (89), and the expression of VE-cadherin is a specific

early developmental marker for the endothelial lineage. Deletion of the VE-cadherin gene induces embryonic lethality due to early collapse of the vasculature (92), and increased vascular permeability occurs when VE-cadherin homophilic binding is inhibited. AJ stability is also critically regulated by phosphorylation (89). More specifically, phosphorylation of VE-cadherin at catenin binding sites induced internalization and thus alterations in vascular permeability. Interestingly, recent work demonstrated that phosphorylation of these residues (Y658 and Y685 of VE-cadherin) occurs constitutively in veins but not arteries, correlating with enhanced leakiness in venous vessels (194). Furthermore, single point mutations in VE-cadherin (Y658F and Y685F) reduce paracellular permeability by blocking internalization of VE-cadherin (194).

1.4.4 ENDOTHELIAL DYSFUNCTION IN DIABETES

The concept of endothelial dysfunction in diabetes is well established (63). However, this typically refers to vascular functions independent of transendothelial solute flux. The endothelium is also a dynamic interface that responds to various stimuli and synthesizes and liberates vasoactive molecules such as nitric oxide, prostaglandins and endothelin. Accordingly, vascular complications in diabetes include outcomes occurring in large (atherosclerosis, cardiomyopathy) and small (retinopathy, nephropathy, neuropathy) vessels (254). Diabetes-induced deleterious alterations in paracellular solute movement also represents a form of endothelial dysfunction which should be fully characterized to establish its physiological significance.

1.4.5 STUDIES ON TRANSENDOTHELIAL TRANSPORT OF HORMONES

Transport of insulin has been perhaps the best studied example of transendothelial hormone transport. The concentration of insulin at the target cell surface has been shown to be very different from that in plasma by approaches including microdialysis (102, 245), direct interstitial sampling (30), and lymph measurements (45, 312). Furthermore, early temporal studies have demonstrated

that insulin-mediated glucose up-take in muscle lags behind increases in plasma insulin (81), In contrast, when using cultured skeletal muscle cells, the addition of recombinant insulin has been shown to stimulate glucose uptake almost immediately (maximal at ~10 minutes) (247). The time delay seen *in vivo* has led to the suggestion that reaching the interstitial space is the limiting factor for insulin-mediated glucose uptake (134). Thus, modification of access to skeletal muscle can have major effects on insulin action and subsequent metabolism (17, 134). Indeed, the efficiency and extent of insulin delivery to the interstitial space can be inhibited physiologically by diet (143). The mechanism via which insulin crosses the endothelium is at least in part via the paracellular pathway, and for more information on this topic readers are referred to recent excellent review articles by Kolka and Bergman (134, 135).

Recent years have seen great interest in the role of adiponectin in the pathophysiology of diabetic complications (161, 229, 313). Numerous studies have now established that adiponectin can act on various targets to mediate antidiabetic, anti-inflammatory, anti-atherosclerotic, and cardioprotective effects (200, 229, 313). Thus, enhancing adiponectin action is considered as a therapeutically beneficial strategy. As described above, adiponectin circulates in the blood as three multimeric complexes; LMW (trimer), MMW (hexamer) and HMW (oligomer), and in obese and diabetic patients reduced circulating levels of adiponectin have been observed. It is likely that delivery of adiponectin to the interstitial space is a major, yet underestimated, determinant of its function. Given the size range of the biologically active forms of adiponectin (16 kDa for globular form and >500 kDa for HMW) there is considerable potential for selective paracellular transport of adiponectin, particularly in different vascular beds. HMW adiponectin is often considered to be the most biologically active and most relevant form with respect to the metabolic syndrome, and we speculate that given the large size of the HMW form, transendothelial movement may prove to be a significant rate-limiting step in its physiological actions (Fig 1.5). Indeed, it has been proposed that HMW adiponectin mediates beneficial metabolic effects primarily by acting on the liver (313),

whereas the globular form is thought to have more potent metabolic effects in skeletal muscle (161). These observations of tissue specificity could be explained by the leaky and moderately tight paracellular barriers, respectively, present in the vascular beds of these respective tissues, although this is likely an oversimplification (Fig. 1.4). As far as we are aware, no studies have directly examined the paracellular movement of adiponectin in skeletal muscle and liver.

Studies of adiponectin movement across the blood-brain barrier (BBB) have indicated that only LMW and MMW, but not HMW forms were found in cerebral spinal fluid (142, 145, 185). Surprisingly, there are only a few studies examining interstitial adiponectin levels. One found that interstitial concentrations of adiponectin in human adipose tissue were ~25-fold lower than plasma (39) while the other found that exercise increased interstitial adiponectin levels, which were around 20% of plasma concentration (106). We hypothesize that the magnitude of gradient between plasma and interstitial levels of adiponectin in skeletal muscle may be higher due to the existence of a tighter endothelial barrier within the muscle vasculature. Indeed, this may be highly significant as it has been shown that hyperinsulinemia differentially affects the compartmental (interstitial and circulating) distribution of the adiponectin complexes in lean and insulin-resistant, obese individuals (179). We have recently shown that adiponectin moves across cultured endothelial monolayers via a paracellular route and that this movement was reduced by hormonal or physical manipulation of TJs.

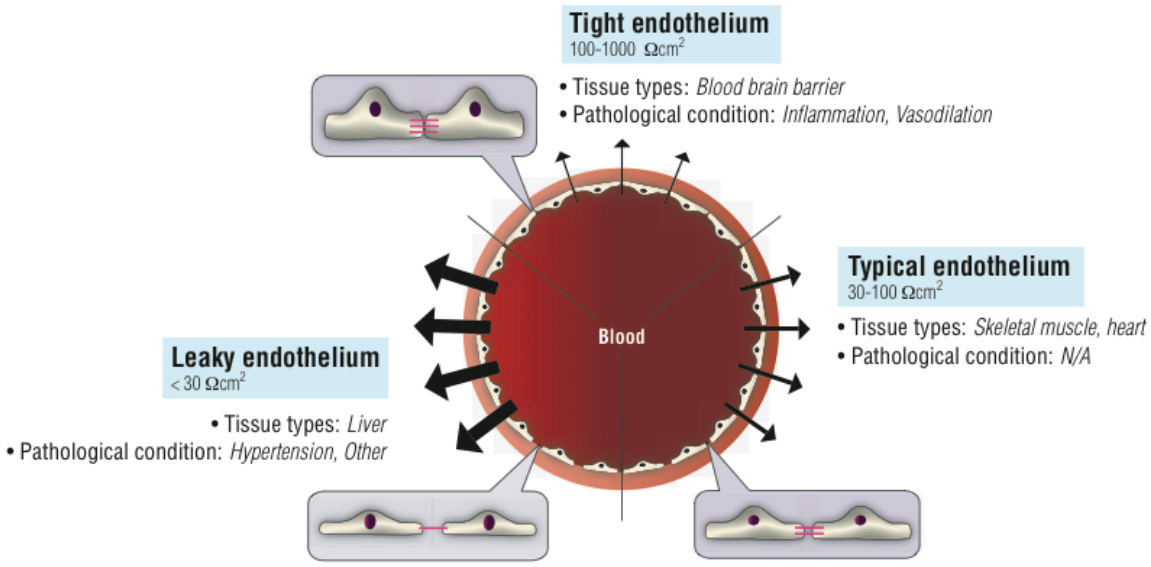

Figure 1.4. Diversity of paracellular transport characteristics in different vascular beds. The size and structure of tight junctions varies significantly between different tissues and in this figure we summarize this by defining three arbitrary categories of leaky, moderately tight and tight endothelia. The typical resistance values associated with these definitions and examples of tissues where each category of endothelium is characteristic is shown. N/A, not applicable.

1.4.6 TJ COMPOSITION AND PROTEIN EXPRESSION IN DIABETES

Studies examining changes in TJ composition and protein expression in diabetes have not been extensive but have so far yielded numerous consistent observations in the study of diabetic complications. For example, reductions in ZO-1 have been observed in kidney glomeruli, the retina, BBB and intestine of various diabetic models (23, 158, 192, 234, 242). Localization of ZO-1 in glomeruli was also investigated by electron microscopy and found to redistribute from the podocyte membrane to the cytoplasm in the diabetic kidney (218). Several reports have indicated that both occludin and claudin-5 were reduced in the diabetic retina and BBB (12, 15, 23, 158, 242). Hence, expression or localization of TJ proteins appears to be susceptible to a diabetic environment and contribute to complications such as retinopathy and nephropathy. More widespread analysis is now needed, particularly in metabolically active tissues. Knockout mouse models have been generated for various TJ proteins, including occludin and claudin-1, 2, 4, 5, 7, 9, 11, 14, 15, 16, 18, and 19 (22, 82, 85, 93, 100, 174, 180, 182, 187, 226, 257, 260, 279, 295). While little to no information is available regarding the metabolic phenotype of most of these models, one study using Cldn2−/−Cldn15−/− double-KO mice demonstrated that the animals died from malnutrition related to defective absorption of glucose, amino acids and fats (279). These models may prove valuable in elucidating the significance of alterations in transendothelial hormone flux in determining metabolic dysfunction in diabetes.

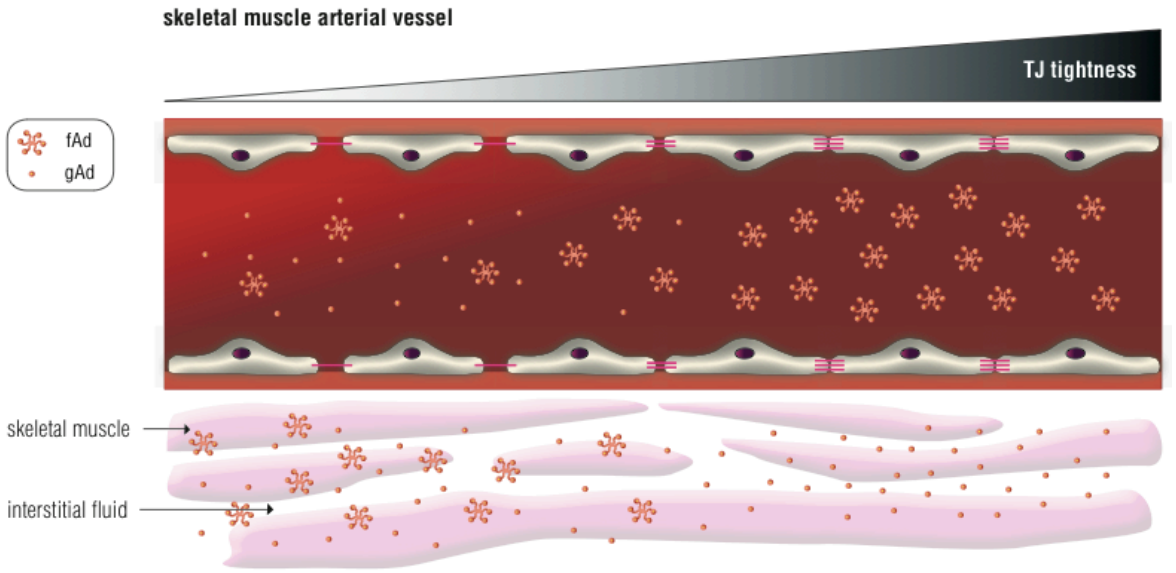

Figure 1.5. Paracellular movement of adiponectin. A conceptual model showing the potential significance of paracellular transendothelial movement of adiponectin. When vascular endothelium is leaky (left side) there is significant flux of all forms of adiponectin from bloodstream to interstitial space. However, as endothelium becomes tighter there is likely to be a gradient of decrease in high molecular weight or other multimeric forms of adiponectin whereas the smaller globular fragment of adiponectin may still be able to access underlying target tissue such as skeletal muscle. TJ, tight junctions; fAd, full length adiponectin; gAd, globular adiponectin.

1.4.7 THERAPEUTIC POTENTIAL OF TARGETING ENDOTHELIAL TRANSPORT

Based on the above description of the importance of endothelial transport in diabetes, it is evident that developing therapeutic strategies that manipulate paracellular flux may prove useful. Indeed, a literature review indicates that various agents are already available; such as peptides which bind to integral TJ proteins, siRNA and antisense oligonucleotides targeting TJ proteins, various toxins, lipids, and activators or inhibitors of kinases and phosphatases that regulate junction assembly and function have all been shown to regulate paracellular permeability (91). Nevertheless, there is an innate risk in therapeutics which globally alter transendothelial permeability, and so it will be desirable to elicit changes in a localized or tissue specific manner, or to target specific components of TJs which allow more controlled and selective changes in permeability (61). One example of a current therapeutic approach targeting TJs is the use of glucocorticoids as a locally applied treatment for diabetic retinopathy. The mechanism of action is thought to involve, at least in part, restoration of barrier function in the retinal vasculature by modifying TJ composition and structure (76). Therefore, it is attractive to speculate that controlled manipulation of paracellular transport may be applicable to improving metabolic dysfunction in diabetes.

1.5 MONITORING MODALITIES OF HORMONE MOVEMENT

1.5.1 IN VIVO IMAGING AND APPLICATION

Imaging technologies in biological research are increasingly becoming a keystone, which provide the chance to understand biological phenomena by bridging or closing the gap between research performed *in vitro* and in *vivo*. Modern approaches have surpassed the anatomical or functional imaging in conventional visualized manners by, for example, using radiological or illuminological tools.

Tomography is imaging by sections or sectioning, through the use of any kind of penetrating wave. A device used in tomography is called a tomograph, while the image produced is a tomogram.

After imaging and gathering the data projected from detectors, tomographic reconstruction is performed using a software algorithm processed by computer. There are several types of tomogram produced using different physical phenomena such as FMT, CT/SPECT, PET and MRI, etc. Here I will review the basic principles and applications in the biological research.

1.5.1.1 FLUORESCENCE MOLECULAR TOMOGRAPHY / NEAR INFRA-RED FLUOROCHROME

Fluorescence molecular tomography (FMT) is a non-invasive optical quantitative technique. FMT functions as a functional and molecular imaging modality to take volumetric two- or three-dimensional images of the targeted fluorescent signals (188).

The basic principle of FMT involves scanning an object and calculating the data from the object to digitally reconstruct it (189). The light sources of the object on the surface, and detectors used for each measured excitation/emission set (light source-detector pairs) provide a number of independent data samples. In 2D imaging mode, wide-field illumination corresponds to an infinite number of points of light sources because it is not mathematically possible to deconvolve the contribution of individual sources. Thus, it prevents 3D reconstruction of probe distribution on the object (188). However, a sequential scan of focal light sources in FMT makes it possible to measure each individual light source-detector pair, even though it also increases the expense of a prolonged measurement time (189, 190).

FMT has shown advantages for use in *in vivo* imaging. It is possible to perform time-course imaging in live animals without tissue depth limitations in small animals like mice and rats. At the time of imaging, small animals are anesthetized with a mixture of isoflorane and oxygen (276). FMT has a high sensitivity for detecting fluorescent signal, thus it is able to take images of the desired fluorescent probe at low concentrations, down to the picomolar level (46). Furthermore, the intensity of the fluorescent signal can be visualized systemically. In addition, using FMT it is also possible to

perform scans using multichannel lasers in the near infrared (NIR) spectrum (276). Because many fluorescent materials absorb in the visible region, but fewer do in the NIR region, NIR lasers are effective to prevent background fluorescence in many cases. Also NIR probes provide greater and more versatile access to fluorescent-imaging biomarkers (276).

Recently, FMT has been applied to various biological research questions, because it functions in the assessment of disease progression and drug response at the molecular, cellular and target levels. These can be assessed by blood volume quantification, angiogenesis measurements, and tumor burden tracking, as examples. In tumor research, tumor size and angiogenesis level can be monitored and compared with anti-tumor or tumor-targeting drug carrier treatments to demonstrate efficacy (153, 178, 323). As a screening tool for assessing biodistribution of biologicals rapidly and cost effectively, FMT has powerful potential for use in the determination of pharmacokinetics, pharmacodynamics, targeting and clearance times and pathways (156, 276). To perform such research and visualize images through FMT, there are some commercial markers, such as fluorescent macromolecules, that are used to monitor specific processes. For example, probes that remain localized to the vasculature during angiogenesis, an apoptosis marker (annexin) which selectively binds phosphatidylserine exposed in the outer leaflet of the cell membrane during the early stages of apoptosis, cathepsins as a marker for a variety of disease states including inflammation and cancer (like autophagy), and matrix metalloproteinases (MMPs) as a marker of inflammation diseases and cancer.

FMT equipment used to be liquid-based, and the sample had to be forced into a regular geometrical configuration of an index-matching cylinder filled with fluid because the liquid-based set up offered high sensitivity and high signal-to noise ratios. However, due to difficulties in handling of the liquid-based system, and non-natural positioning of the animal, a so-called non-contact scanner system was developed. In the non-contact system, an advanced theoretical framework and modeling

capacities were implemented, therefore, gantry based (149) and horizontal positioning of animal can now be performed (249).

However, the performance of FMT is limited by the strong scattering of near-infrared photons (10, 177). It perturbs the ability of the information from the FMT to match the real signal from the body perfectly. Using extra anatomical information derived from the same orientation of animal positioning, it is possible to improve the reconstruction accuracy. Recently, these challenges have been addressed by developing additional tomography techniques to complement FMT and increase anatomical accuracy, such as MRI, X-ray CT and PET (10, 111, 152, 177). For instance, there are now 360 degree rotating scanning FMT approaches (147, 149), hybrid technology with FMT-MRI (152) and FMT-PCCT (177) which have been developed and applied to research.

1.5.1.2 SINGLE-PHOTON EXCITATION COMPUTED TOMOGRAPHY

X-ray Computed Tomography (CT or XCT) is a nondestructive technique for visualizing interior features within solid objects, and for obtaining digital information on their 3D geometries and properties.

The fundamental theory of XCT consists of directing X-rays at an object from multiple orientations and measuring the decrease in intensity along a series of linear paths. Following Beer's Law, intensity is reduced by a function of X-ray energy, path length, and the material linear attenuation coefficient. Using a specialized algorithm, reconstruction of the distribution of X-ray attenuation in the imaged volume is performed. In addition, the most CT X-ray detectors utilize scintillators. In general, smaller detectors provide better resolution for the image, but exhibit reduced count rates because of their reduced area compared to larger detectors. But, when acquisition time is extended to compensate, it is possible to reduce the noise levels. Common scintillation materials are cesium iodide, gadolinium oxysulfide, and sodium metatungstate (127).

In the case of hybrid implementations based on X-ray CT and FMT, a major limitation is the low soft-tissue contrast offered. In particular, bone, lung, and the tissue outline can be visualized with good contrast. But other internal organs and tissues are not visible with high contrast in X-ray CT images as they do not exhibit considerable absorption differences of X-ray photons (324).

In single-photon emission computed tomography (SPECT), there have been recent improvements not only in the reliability and resolution, but also the construction of compact and novel detector geometries (110). It also offers reduced acquisition time or radiation dose and extended application (110). Thus, SPECT can be applied for organ-specific imaging of a broader range of tissues (29).

1.5.1.3 POSITRON EMISSION TOMOGRAPHY

Positron Emission Tomography (PET) is a modality used for the functional or metabolic assessment of tissue, which has been applied for research and diagnostics in the fields of neurology, cardiology and oncology. PET scanners utilize a combination of a scintillator and a photomultiplier to generate images (231). To take images with PET, it is necessary to introduce a labeled positron-emitting radiotracer that is taken up by the tissues that are to be imaged. The PET scanner then detects the location of labeled molecules like glucose, thymidine, methionine, estradiol, annexin V, etc. in the body as the tracer decays. FDG (18F-fluorodeoxyglucose), which is glucose analog, is the most commonly used radiotracer for oncology applications imaged with PET (124).

Recent studies have shown that the PET system not only allows for the detection of bioluminescence, but also fluorescence using the same setup (181). For example, PET/FMT is used to validate FMT as a surrogate for the nuclear imaging modality. Because of the longer half-life of fluorescent signals as compared to positron emitters, the PET/FMT system provides a more stable signal. Hybrid PET also offers the spatial information for tracer signal distribution by correlation (181). In addition, PET can also be used inside the high magnetic field of an MR system, as a hybrid

PET/MR, which was previously considered impossible due to the use photomultiplier tubes in a combined system (291, 315).

1.5.1.4 MAGNETIC RESONANCE IMAGING

The basic principle of magnetic resonance imaging (MRI) is that it relies on the properties of subatomic spin to obtain images. Protons, neutrons and electrons all spin around a central axis. Under conditions where protons and neutrons are balanced within an atom, then it could lead to a zero spin nucleus. Unbalanced atoms like hydrogen create a small magnetic field. This small magnetic field is a magnetic moment. These tiny magnetic moments are balanced against each other to generate a neutral magnetic field under normal conditions. However, these magnetic moments can be influenced by an external magnetic field. A directional magnetic field, or moment, is associated with charged particles in motion. Nuclei containing an odd number of protons or neutrons have a characteristic motion or precession. Because nuclei are charged particles, this precession produces a small magnetic moment that can be distinctly detected by MRI (248, 311, 326).

MRI has superb contrast between different soft tissue structures in the body such as cartilage and soft organs like the brain or the heart with 3D acquisition. There is no involvement of any kind of ionizing radiation in MRI, but the resolution of MRI is higher than CT (248). MRI scanning also can provide information about blood circulation throughout the blood vessels (157).

1.5.2 IN VITRO MICROVASCULATURE

Although many disease models have been utilized to elucidate the underlying mechanisms of vascular complications, and the advanced imaging technologies described above have been developed to monitor the response of pathological conditions in these models, in most cases the studies are limited to animal models, especially rodents. To find direct pathological relevance to vascular impact in human diseases, inevitably we should use human endothelial cells. *In vitro*

vascular cell culture systems with human cells allows us to overcome the confounding effects associated with complex *in vivo* conditions related to disease. Currently, even though many researchers aim to rebuild the complicated vascular environment on a lab scale (e.g., blood vessel on a chip (130)), this *in vitro* culture system is still useful in terms of being able to measure the response to only a few selective factors from many vascular components.

To mimic vasculature *in vitro* with endothelial cells, we should consider the aspects of both structural and functional properties. The most important structural feature of blood vessels is that they are composed of a monolayer of endothelium. The endothelial barrier compartmentalizes the area of the bloodstream lumen from the outside of vessels, while at the same time, it plays a role in controlling molecular transfer in between those two areas (72). In addition, there is the fluidity of bloodstream (146). In this part, I will cover the two types of microvascular systems used *in vitro* with descriptions of notable features and their applications.

1.5.2.1 2D MONOLAYER OF ENDOTHELIUM

There are two different types of 2D endothelial monolayer cell culture systems; 1) the static transwell system and 2) the dynamic *in vitro* system. Firstly, the static transwell system is a conventional way of 2D microvasculature culturing, which has transmembrane inserts hanging on the top of a multi-well plate. The transwell system allows cells to be cultured in a monolayer representative of the endothelial barrier by attaching the cells to the polycarbonate transmembrane of the insert. The insert has a high pore density, with micropores 0.3-0.4μm in size. The insert (apical side) represents the vessel lumen and the well (basolateral side) mimics the interstitial space. This transwell setting lets the system exchange the small molecules across the porous membrane by active or inactive transport mechanisms, but prevents the loss of endothelial cells by migration over the membrane (58, 283). The static model, however, does not reflect systemic fluidity. Thus, there have been attempts to dynamically apply fluid on the *in vitro* 2D vasculature cell culture system. To

provide endothelial shear stress with external medium flow, a microfluidic platform was applied (210). The endothelial monolayer with flow more accurately simulated normal physiology due to allowing for endothelial rearrangement mediated by shear stress (43, 72). Furthermore, long term culture is permissible in this system (301). Using these platforms, there are many options to investigate endothelial barrier function and response, for example, permeability testing of fluorochrome-conjugated target molecules, cell migration assays with a cancer cells or neutrophils, shear stress assay with iPSCs derived brain ECs, and so on.

1.5.2.2 3D PERFUSABLE MICROVASCULATURE

Reconstitution of vascular 3D structure is important not only for studying the behavior of endothelial cells, but also for determining cell fate and other physiologically relevant functions (25). Even though 2D *in vitro* vasculature models consider the fluidic environmental factor, it is difficult to say that this is relevant to the conditions *in vivo* because they are missing major structural properties. The vasculature *in vivo* is an enclosed system of tubular structures, having numerous branches. This feature allows fluid to be circulated throughout the whole body to exchange molecules. Therefore, the application of perfusibility on a 3D *in vitro* system allowed us to understand underlying mechanisms of vasculature better, especially vessel permeability.

From that point of view, there was the important finding that endothelial cells can spontaneously assemble themselves to generate capillary structures (79). When endothelial cells are exposed to an environment with balanced growth factors and a favorable extracellular matrix (ECM), within a few days, the cells will self-assemble into a tubular shaped 3D microvasculature in an *in vitro* system. This endothelial feature can be applied to a PDMS microfluidics platform. The device has open-ended vessels connected to medium channels, making this platform useful to infuse any circulating molecules into the 3D vessel lumen. The platform is used to mimic the brain blood barrier to aid in understand the role of pericytes and astrocytes, and its alteration in permeability under

pathological conditions (314). This system can also be applied in a co-culturing system with other cell types that are also found in endogenous vascular structures, such as smooth muscle cells, pericytes, astrocytes and endothelial cells (103).

1.6 HYPOTHESIS AND RESEARCH AIMS

I hypothesized that altered endothelial permeability in diabetes can regulate the physiological effects of adiponectin. Based upon this hypothesis, I designed the following specific objectives:

Aim 1: To examine adiponectin flux in endothelial cell monolayers treated with glucocorticoids to reduce endothelial permeability and determine the mechanisms involved. My specific hypothesis was that by using glucocorticoids to alter tight junction protein profiles, and thus reduce paracellular permeability, that adiponectin flux would be attenuated.

Aim 2: To investigate the effect of high glucose on transendothelial adiponectin flux, its biodistribution in mice, and the functional significance. This was based on the hypothesis that hyperglycemia in a mouse model of diabetes increases vascular permeability and regulate the extent of adiponectin movement from circulation to the interstitial space in target tissues. The hypothesis was further tested using isolated vessels *ex vivo*, in endothelial monolayers, and a 3D microvasculature network exposed to high glucose.

Aim 3: To determine if iron overload, which is commonly observed in diabetes, influences the endothelial permeability of adiponectin, and to examine the underlying mechanisms. My hypothesis was that iron overload decreases endothelial permeability by elevating oxidative stress and altering the expression of tight junction proteins.

CHAPTER TWO: STUDY 1

Transendothelial movement of adiponectin is restricted by glucocorticoids

Thanh Q. Dang[#1,#], Nanyoung Yoon[#1,#], Helen Chasiotis[1], Emily C. Dunford[2], Qilong Feng[3], Pingnian He[3], Michael C. Riddell[2], Scott P. Kelly[1], and Gary Sweeney[1,*]

[1]Department of Biology, Faculty of Science York University, Toronto, Canada

[2]School of Kinesiology and Health Science, Faculty of Health and Muscle Health Research Center, York University, Toronto, Canada

[3]College of Medicine, Department of Cellular and Molecular Physiology, Penn State University, USA.

[#] These authors contributed equally to this work.

Published in final edited form as:

J Endocrinol. **2017 August ; 234(2): 101–114. doi:10.1530/JOE-16-0363.**

Author Contribution

N.Y., T.D., H.C., S.K., and G.S. conceived and designed research; N.Y., T.D., H.C., E.D., and O.F. performed experiments; N.Y., T.D., H.C., E.D., and O.F. analyzed data; N.Y., T.D., P.H., M.R., S.K., and G.S. interpreted results of experiments; N.Y., T.D., and G.S. prepared figures; T.D., N.Y., and G.S. drafted manuscript; N.Y., T.D., P.H., M.R., S.K., and G.S. edited and revised manuscript; N.Y., T.D., H.C., E.D., O.F., P.H., M.R., S.K., and G.S. approved final version of manuscript. [Following the style of AJP]

2.1. SUMMARY

Altered permeability of the endothelial barrier in a variety of tissues has implications both in disease pathogenesis and treatment. Glucocorticoids are potent mediators of endothelial permeability and this forms the basis for their heavily-prescribed use as medications to treat ocular disease. However, the effect of glucocorticoids on endothelial barriers elsewhere in the body is less well-studied. Here we investigated glucocorticoid-mediated changes in endothelial flux of Adiponectin (Ad), a hormone with a critical role in diabetes. First, we used monolayers of endothelial cells in vitro and found that the glucocorticoid dexamethasone increased transendothelial electrical resistance and reduced permeability of polyethylene glycol (PEG, molecular weight 4000kDa). Dexamethasone reduced flux of Ad from the apical to basolateral side, measured both by ELISA and Western blotting. We then examined a diabetic rat model induced by treatment with exogenous corticosterone, which was characterized by glucose intolerance and hyperinsulinemia. There was no change in circulating Ad but less Ad protein in skeletal muscle homogenates, despite slightly higher mRNA levels, in diabetic versus control muscles. Dexamethasone-induced changes in Ad flux across endothelial monolayers were associated with alterations in the abundance of select claudin (CLDN) tight junction (TJ) proteins. shRNA-mediated knockdown of one such gene, claudin-7, in HUVEC resulted in decreased TEER and increased adiponectin flux, confirming the functional significance of Dex-induced changes in its expression. In conclusion, our study identifies glucocorticoid-mediated reductions in flux of Ad across endothelial monolayers in vivo and in vitro. This suggests that impaired Ad action in target tissues, as a consequence of reduced transendothelial flux, may contribute to the glucocorticoid- induced diabetic phenotype.

2.2. INTRODUCTION

As the primary barrier to the movement of circulating endocrine factors from the bloodstream to the interstitial space, the endothelium plays a critical role in hormone action (134, 316). Endothelial permeability can significantly impact hormone action by preventing or delaying access of the hormone to target tissues (134, 299). Transendothelial solute movement can occur via the transcellular pathway where solutes are transported across the endothelium cell membrane or via the paracellular pathway where solutes passively move through the intercellular space between adjacent endothelial cells (316). Previous work has shown that hormone and nutrient concentrations in blood differ from surrounding cells on the tissue side of the blood vessel endothelium (18, 102, 312). Of note, this has been best documented in the case of insulin where concentrations of the hormone are significantly lower in the target tissue than in the circulation (134).

Glucocorticoids are among the most commonly prescribed anti-inflammatory and immunosuppressive medications worldwide (47). They are also commonly used in oncology treatment (155) and for the treatment of macular edema and, more recently, retinopathy (4, 325). However, glucocorticoids have been shown to have potent effects on restricting endothelial transport (76, 296) and they contribute to the development of diabetes at least in part by increasing hepatic glucose production and reducing GLUT4 translocation in muscle (20). Yet despite these observations, the potential importance of glucocorticoid-induced alterations in the transendothelial flux of circulating glucoregulatory hormones such as Ad is unclear.

Ad is one of the most abundant plasma proteins and exists in three different isoforms: low molecular weight (LMW; trimer), medium molecular weight (MMW; hexamer) and high molecular weight (HMW; oligomer) (54). Ad has important and beneficial anti-diabetic, anti-inflammatory and cardioprotective actions (13, 54). Ad levels, in particular HMW, are decreased in obese individuals and this correlates with development of associated complications, including diabetes and cardiovascular disease (123, 202). Transendothelial movement of Ad across the blood-brain barrier

(BBB) into cerebrospinal fluid (CSF) was studied and only LMW and MMW were found in the CSF, suggesting that passage of HMW complexes were restricted (142, 145, 185). This may be functionally significant since HMW Ad is often considered to be the most biologically active and physiologically relevant form (54) (184). A recent study calculated the Stokes radii for the Ad oligomers and found that endothelial barriers controlled Ad transport in a cell- and tissue-specific manner (222). Thus, emerging evidence suggests that Ad action may be at least in part mediated by endothelial transport, although whether this is influenced by glucocorticoid-induced changes in transendothelial permeability remains unknown.

Given the large size of Ad multimers it seem likely that transendothelial Ad movement is an important variable in determining it presence within, and action on, target tissues. Therefore we hypothesized that glucocorticoid-induced alterations in transendothelial permeability will modulate the transendothelial movement of Ad. In this regard, the objective of this study was to examine how glucocorticoid treatment of a cultured endothelium influences Ad flux in association with changes in permeability and apical junction protein abundance as well as investigate Ad content within the skeletal muscle in a diabetic rat model induced by exogenous glucocorticoid treatment. The overall goal of this work was to significantly advance our understanding of the glucocorticoid-induced diabetic phenotype by determining whether Ad movement out of the circulatory system might play a role in its pathogenesis.

2.3. MATERIALS AND METHODS

2.3.1. HUVEC cell culture and treatments

Normal primary human umbilical vein endothelial cells (HUVECs; Pooled, PCS-100–013) were obtained from ATCC (Manassas, VA, USA) and grown at 37°C and 5% CO2 on uncoated T75 flasks in vascular cell basal medium (ATCC, PCS-100–030) containing 10% fetal bovine serum (FBS), VEGF endothelial cell growth kit (ATCC, PCS-100–041) and treated with DEX using 2% FBS (both medium were prepared without hydrocortisone hemisuccinate), 100 units/mL penicillin and 100 µg/mL streptomycin. Cells were kept frozen in medium containing 10% DMSO (Bio-Rad Laboratories Canada Ltd., Mississauga, ON, Canada). For experiments, passage 3 was used. Cells were counted using a haemocytometer and seeded onto permeable polyethylene terephthalate (PET) filters at the base of BD Falcon cell culture inserts (BD Biosciences, Mississauga, ON, Canada) at a density of 0.5×10^6 cells/insert.

Dexamethasone (DEX) was obtained from Sigma-Aldrich (Oakville, ON, Canada), and full-length Ad was produced in-house using a mammalian expression system (i.e. HEK 293 cells) according to methods described by (288, 303). HUVECs were treated for 5 days with DEX (1 µM) starting 24 h after seeding cells into inserts, HUVECs were treated with DEX added to both apical and basolateral sides of inserts at concentrations indicated above

2.3.2. shRNA-mediated knockdown of claudin 7 in HUVEC

We used pGPU6/Neo-claudin-7 shRNA vector with target sequence (5'-GGCCATCAGATTGTCACAGAC-3') (GenePharma Co., Ltd., Shanghai, China). These were transfected into HUVEC using Lipofectamine™ 3000 Reagent (Invitrogen, Carlsbad, CA, USA) exactly according to manufacturer's protocol. Non-specific scrambed target sequence shRNA vector was used as control. Following selection with 50 µg/ml Neomycin (Sigma-Aldrich, Oakville, ON,

CA) for 24 hours, cells were seeded onto inserts for analysis of TEER, examining adiponectin flux or preparation of cell lysates to confirm claudin 7 knock-down.

2.3.3. Transendothelial electrical resistance (TEER),and [^{3}H]PEG4000 and Adflux

TEER was measured daily using chopstick electrodes (STX-2) connected to an EVOM voltohmmeter (World Precision Instruments, Sarasota, FL, USA). As a measure of paracellular permeability, apical to basolateral flux rates of [^{3}H] polyethylene glycol at 1 μCi; 1 h flux (molecular mass 4000 Da; PEG-4000; PerkinElmer, Woodbridge, ON, Canada) or Ad (10 μg/mL; 24 h flux) to apical culture medium were determined across HUVEC endothelia. [^{3}H] PEG-4000 in basolateral culture medium was detected using a liquid scintillation counter, Ad was detected using a mouse Ad ELISA kit (Antibody Immunoassay Services, Hong Kong) or Western blot. Permeability measurements were expressed according to calculations previously outlined by (300).

2.3.4. L6 and H9C2 cell culture and treatment with HUVEC-conditioned medium

Rat myoblasts and cardiomyocytes at passage 22–30 were grown in α_AMEM(Life Technologies Inc., Manassas, MA, USA) and DMEM containing 10% FBS and 1% antibiotic-antimycotic (Wisent Inc., St- Bruno QC, Canada). Culture media from the basolateral compartment of HUVEC inserts were collected and applied. L6/ H9C2 cells were starved with medium containing 0.5% FBS and 1% antibiotic-antimycotic for 3 h prior to treatment with HUVEC-conditioned medium.

2.3.5. Quantitative real-time PCR analysis

Total RNA was isolated from control and DEX-treated HUVECs and from soleus skeletal muscle using TRIzol Reagent . Extracted RNA was then treated with DNase I and first- strand cDNA was synthesized using SuperScript III reverse transcriptase and oligo(dT)12–18 primers (Life

Technologies Inc.,Manassas MA, USA). Quantitative real-time PCR (qRT- PCR) analyses were conducted using gene specific primers. SYBR Green I Supermix (Bio- Rad Laboratories Canada Ltd.Mississauga, ON, Canada) and a Chromo4 Detection System (CFB-3240; Bio-Rad Laboratories Canada Ltd.) Samples were run in duplicate. For all qRT- PCR analyses, TJ protein mRNA expression was normalized to GAPDH transcript abundance. For the expression profile, TJ protein transcripts were expressed relative to occludin mRNA. For TJ protein transcripts that were not detected in HUVECs, normal human adult kidney cDNA was obtained (BioChain Institute, Inc., Newark, CA, USA) and used as a positive control in qRT-PCR reactions. Agarose gel electrophoresis verified single qRT-PCR products at predicted amplicon sizes from positive control reactions.

2.3.6. Animal model of diabetes induced by exogenous corticosterone treatment

We used a well-established hyperinsulinemic/hyperglycemic rodent model of chronic glucocorticoid treatment (19, 20, 53, 241, 244). Upon experiment cessation, the tibialis anterior (TA) and soleus skeletal muscles were excised and immediately frozen in liquid N_2 and kept at −80ºC until future analysis.

2.3.7. Oral glucose tolerance test

Animals were fasted overnight (16 hours), 11 days after pellet implantation, and were administered an oral glucose tolerance test (OGTT, 1.5 g/kg body mass) on day 12 using glucometer (Bayer One Touch), additional fasted plasma was collected for later analysis of insulin concentrations via an ELISA 96-well kit (Crystal Chem, USA). Plasma for measurement of Ad concentration was obtained 7 days after pellet implantation at 0800 h and assessed using a mouse Ad ELISA kit (AIS, Hong Kong).

2.3.8. Measurement of hydraulic conductivity (Lp) in individually perfused rat mesenteric microvessel

Female Sprague-Dawley rats of 220 to 250 g (2 to 3 mo old, Sage Laboratory Animal, PA) were used for the experiments. All procedures and animal use were approved by the Animal Care and Use Committee at Pennsylvania State University. Inactin hydrate (Sigma) was used for anesthesia and given subcutaneously at 170 mg/kg body weight. Microvessel permeability was assessed by measuring Lp in individually perfused microvessels, which measures the volume of water flux across the microvessel wall. Details have been described previously (318, 319).

2.3.9. Staining for metachromatic myosin ATPase

To identify skeletal muscle fiber type, a metachromatic myosin ATPase stain was performed using a modified protocol (Ogilvie and Feeback 1990). Sections were pre-incubated in an acidic buffer (pH=4.25) to differentially inhibit myosin ATPase within the different fiber types. In this protocol, type I fibers appear dark blue, type IIa appear light blue and type IIb and IIx are not apparent from each other and are classfied as IIb/x. These fibers appear almost white and are the largest. Images were acquired with a Nikon Eclipse 90i microscope and Q-imaging MicroPublisher with Q-Capture software at 10x magnification.

2.3.10. Immunohistochemistry of Ad and dystrophin in skeletal muscle

Tibialis anterior (TA) from Control and CORT treated rats were cryostat sectioned (10 μm thick) for analysis of muscle Ad content. Sections were stained as previously described (139). Quantification was performed using Zen 2.0 software. The total Ad and dystrophin signal was determined by the sum of red/green signal intensity obtained arbitrary values in the field of view. Diagram view intensity was recorded by the software in form of histograms. Intracellular

quantification was done on Ad images (without dystrophin), images were changed to 8-bits on Image and the arbitrary intensity was calculated as mean intensity per area.

2.3.11. Western blot analysis

Control and DEX-treated HUVECs, and L6 or H9C2 cells treated with HUVEC-conditioned medium and soleus skeletal muscle were lysed in sample buffer (80 mM Tris-HCl (pH 6.8), 2% (w/v) SDS, 20% glycerol, 3.3% (v/v) β-mercaptoethanol 0.01% w/v bromophenol blue) containing protease and phosphatase inhibitors (3 mM EDTA, 10 uM E64, 1 mM Na3VO4, 1 μM leupeptin, 1 μM pepstatin A, 1 μM okadaic acid and 200 μM PMSF). Apical and basolateral HUVEC-conditioned media collected from Ad flux experiments were concentrated with Amicon Ultra-4 Centrifugal Filter Units with Ultracel-30 membranes (EMD Millipore, Billerica, MA, USA) and subjected to nondenaturing, nonreducing conditions to allow the analysis of the different forms of Ad (HMW >250 kDa, MMW ~180 kDa, and LMW ~90 kDa). Primary antibodies specific for the following proteins: T-cadherin (1:1000, R&D Systems), occludin (OCLN, 1:3000), tricellulin (TRIC, 1:3000), claudin-7 (CLDN-7, 1:500), CLDN-10 (1:800), CLDN-11 (1:1000), phospho-AMPKα (Thr172) (1:1000), phospho-p38 MAPK [pT180/pY182] (1:1000), Ad (1:1000),β-actin (1:1000).

OCLN, TRIC, CLDN-7, CLDN-10 and phospho-p38 MAPK [pT180/pY182] antibodies were obtained from Life Technologies, CLDN-11 and Ad antibodies were purchased from EMD Millipore and Signalway Antibody (College Park, MD, USA) respectively, and phospho-AMPKα (Thr172) and β-actin antibodies were obtained from Cell Signaling Technology (New England Biolabs Ltd., Whitby, ON, CA). Protein detection using enhanced chemiluminescence (Bio-Rad) and quantification by densitometry using ImageJ analysis software. TJ protein expression was normalized to β-actin, Tubulin protein abundance.

2.3.12. Statistical analysis

All data are expressed as mean values ± SEM. A one-way analysis of variance (ANOVA) followed by a Student-Newman-Keuls test was used to determine significant differences ($P \leq 0.05$) between groups. When appropriate, a Student's t-test was also used. All statistical analyses were conducted using Prism 5, Excel SigmaStat 3.5 softwares.

2.4. RESULTS

2.4.1. Dexamethasone induces endothelial tightening and inhibits Ad movement across endothelial cell monolayers

We first investigated the effect of dexamethasone (DEX), a synthetic glucocorticoid, on tightness of an endothelial monolayer of HUVECs. Addition of DEX to culture media significantly elevated TEER (Fig.2.1.A) and correspondingly reduced the endothelial permeability of the paracellular transport marker [^{3}H] PEG-4000 (Fig.2.1.B). Similar trends regarding permeability were observed in microvessels of DEX-treated rats. DEX treatment (n = 4) did not cause a significant reduction in baseline Lp compared to normal control group (n = 6), but lowered the mean value from 1.5 ± 0.1 to 1.1 ± 0.2 ($\times 10^{-7}$ cm/s/cm H2O). When each vessel was exposed to platelet activating factor (PAF, 10 nM) that is known to cause transient increases in Lp (332), microvessels in DEX-treated rats showed significantly attenuated Lp response. The mean peak Lp value was reduced from 11.1 ± 1.8 (normal control) to 6.0 ± 0.4($\times 10^{-7}$ cm/s/cm H2O, Fig.2.1.C). We then assessed flux of Ad from the apical to basolateral side of HUVEC monolayer and found a reduced total amount of Ad in basolateral media after DEX treatment (Fig.2.1.D-F). When monitoring absolute flux rates in control cells, Ad flux rate was 4.4 ± 0.12 cm s^{-1} × 10^{-9} which significantly decreased after DEX treatment to 3.2 ± 0.30cm s^{-1} × 10^{-9} (Fig.2.1.D). Following a 24 h flux period, Ad levels detected in basolateral media were 64.8 ± 5.7 ng/mL. Using Western blotting to examine various oligomeric forms of Ad LMW (~90 kDa), MMW (~180 kDa) and HMW (>250 kDa), we found that flux of all forms was reduced by DEX (Fig.2.1.E,F). Additionally, the functional activity of Ad appearing in basolateral media was confirmed by using this media to treat L6 skeletal muscle cells and H9C2 cells derived from rat heart ventricle. In both cell types the media increased AMPK phosphorylation (supplementary Fig.2.1.A,B).

2.4.2. Dexamethasone treatment alters transcript and protein abundance of select TJ proteins in HUVEC monolayers

A tissue expression profile of transcripts encoding 26 TJ proteins in HUVECs revealed the presence of 15 (Fig.2.2.A). The most abundant transcript was found to be CLDN-11, while CLDN-7, CLDN-12 and ZO-1 exhibited relatively high abundance and OCLN, TRIC, CLDN-10 and CLDN-15 exhibited moderate levels of abundance (Fig.2.2.A). Transcripts not detected in HUVECs included CLDN-3, −4, −5, −8, −9, −16, −17, −18, −19, −23 and −25 (Fig.2.2.A & Supplementary Fig.2.1.C). Human kidney cDNA was used as a positive control for transcripts that were not detected in HUVECs (Supplementary Fig.2.1.C). To explore the response of TJ proteins to DEX- treatment, we first compared mRNA abundance of expressed target genes in HUVECs. DEX increased CLDN-6 mRNA abundance while CLDN-2, −20, −22, −24 and ZO-1 mRNA showed significant decreases (Fig.2.2.B). DEX treatment had no significant effect on mRNA encoding OCLN, TRIC, CLDN-1, −7, −10, −11, −12 and −15(Fig.2.2.B). Following DEX treatment, the protein abundance of CLDN-1, −7, −11 and ZO-1 was examined and found to be significantly upregulated following DEX treatment when compared to the control group (Fig.2.2C, D). On the other hand, CLDN-10 protein levels were significantly decreased when compared with the expression in control conditions (Fig.2.2.C, D). In order to validate the functional significance of Dex-induced changes in expression of tight juntion proteins we used shRNA to target claudin-7 and this effectively reduced its expression by 71% on average (Fig.2.3.A). Furthermore, HUVEC with reduced levels of claudin-7 showed reduced TEER and a small but significant increase in flux of adiponectin from apical to basolateral side (Fig.2.3.B-D).

2.4.3. Examination of changes in transcellular endothelial flux

The possible contribution of transcellular receptor-mediated Ad movement across HUVEC monolayers was then investigated by analysis of expression levels of three identified Ad receptors.

Intracellular Ad content in these cells was detected, although at low level, and expression levels did not change significantly with DEX treatment (Fig.2.4.A). However, DEX significantly increased T-cadherin protein abundance (Fig.2.4.B), but had no effect on protein abundance of AdipoR1 and AdipoR2 (Fig.2.4.C).

2.4.4. Skeletal muscle Ad content in a rat model of exogenous glucocorticoid-induced diabetes

We then examined whether the increased endothelial cell barrier tightness observed after DEX treatment would be paralleled in a diabetic rodent model of chronic glucocorticoid exposure. As expected based on previously published work (53, 241, 244), two weeks of exogenous corticosterone (CORT) treatment resulted in severe fasting hyperinsulinemia and impaired glucose tolerance (supplementary Fig.2.2.A). In addition, CORT treatment caused mild/moderate elevations in fasted blood glucose concentrations (5.12± 0.2 mM to 8.3 ± 1.88 mM, supplementary Fig.2.2.B) despite the significantly increased fasted insulin concentrations (0.76±0.25 ng/ml to 4.68±0.72 ng/ml , supplementary Fig.2.2.C). CORT treatment also caused a change in skeletal muscle fibre type composition; a switch from predominantly slow to fast-twitch skeletal muscle fibers, within the tibialis anterior muscle (supplementary Fig.2.2.D).

To explore whether CORT-treatment affects circulating Ad levels, we measured plasma Ad levels in these animals before CORT pellet implantation and at 7 days post pellet implantation, at 0800h. Circulating Ad levels were unaffected by CORT treatment (Fig.2.5.A). Interestingly, there was an apparent elevation in skeletal muscle Ad mRNA levels (Fig.2.5.B), yet Ad protein content was significantly reduced (Fig.2.5.C,D). Upon immunohistochemical analyses, we also observed that the total amount of Ad was decreased in skeletal muscle from the COR-treated rats versus control rats (Fig.2.5.E-H). Dystrophin, was used to assess the structural integrity of the skeletal muscle and was unaffected by CORT treatment. Representative images are shown (Fig.2.5.E) with quantification of the total and intracellular Ad signal (Fig.2.5.G-H). Since CORT-treatment is known to

preferentially target fast-twitch skeletal muscle (20), representative images accordingly depict smaller IIb/x fiber area (Fig.2.4.D) within the CORT-treated rats. CORT-treatment was also found to cause a significant reduction in individual myocyte size (Fig.2.5.F).

2.4.5. AdipoR abundance in a rat model of exogenous glucocorticoid-induced diabetes

Both Ad receptor isoforms (AdipoR1 and AdipoR2) genes were expressed in rat soleus skeletal muscle and although an apparent increase in AdipoR1 mRNA abundance was seen in the diabetic rat model, neither was significantly altered (Fig.2.6.A,B). However, a significantly increased level of ADIPO-R1 protein (approximately 3.4 fold compared to the control) was seen (Fig.2.6.F). There were no changes in ADIPO- R2 nor in T- Cadherin protein levels (Fig.2.6.E,G).

2.4.6. CORT treatment altered Tight Junction genes in rat soleus skeletal muscle after 2 weeks

We then measured changes in mRNA abundance of tight junction, Cldn-1, −2, −3, −4,−5,−6, −7, −9, −10, −11, −12, −24,−14, −15, −19, −20, −22, −23 and Ocln, Tricand Z0–1 were found to be no significant changes with in diabetic rat skeletal muscle (Fig.2.6.C), with only Cldn −5, −10, −11, −22 significantly decreased (Fig.2.6.D).

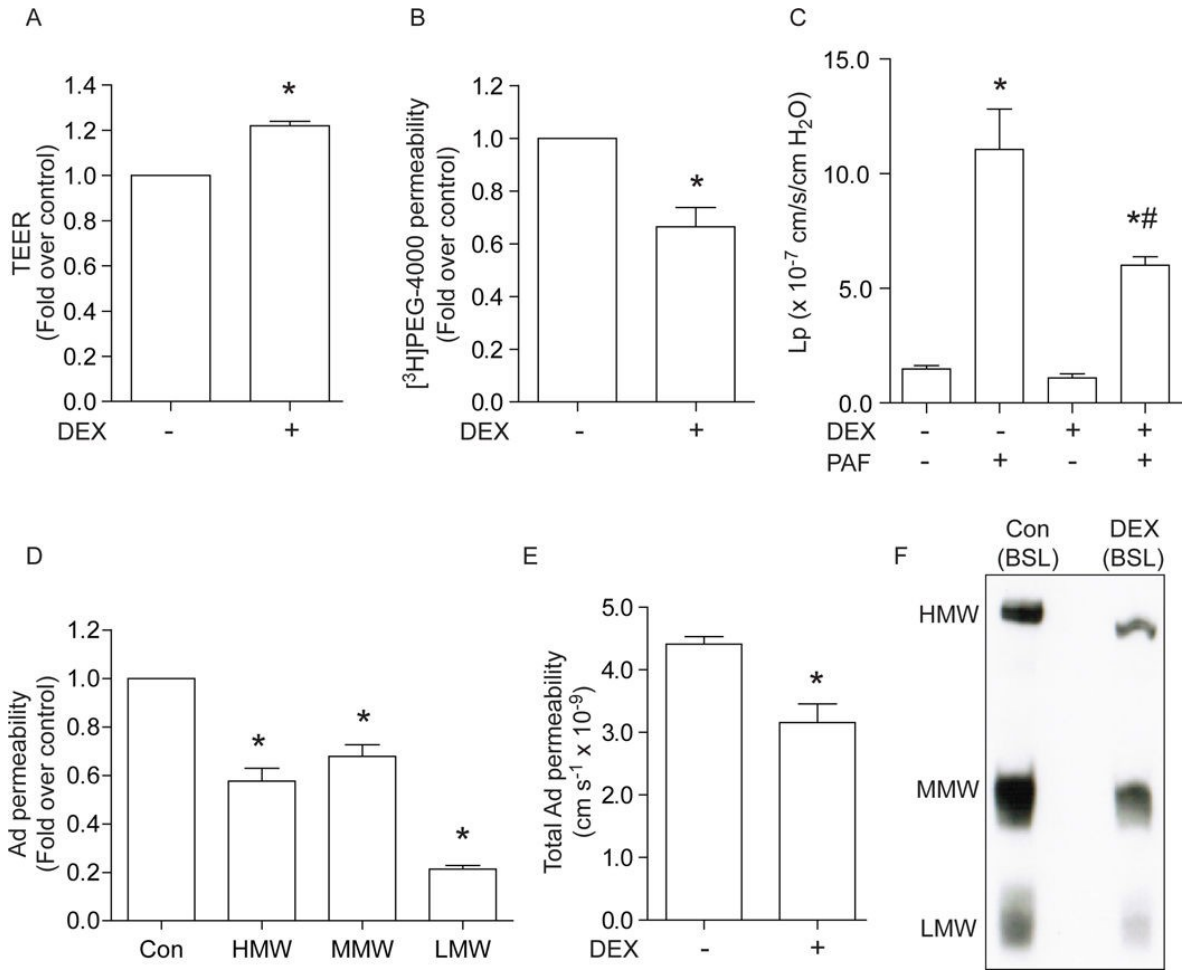
A
TEER
(Fold over control)
1.4
1.2
1.0
0.8
0.6
0.4
0.2
0.0
*
DEX - +
B
[3H]PEG-4000 permeability
(Fold over control)
1.2
1.0
0.8
0.6
0.4
0.2
0.0
*
DEX - +
C
Lp (x 10-7 cm/s/cm H2O)
15.0
10.0
5.0
0.0
*
*#
DEX - - + +
PAF - + - +
D
Ad permeability
(Fold over control)
1.2
1.0
0.8
0.6
0.4
0.2
0.0
*
*
*
Con HMW MMW LMW
E
Total Ad permeability
(cm s-1 x 10-9)
5.0
4.0
3.0
2.0
1.0
0.0
*
DEX - +
F
Con
(BSL)
DEX
(BSL)
HMW
MMW
LMW

Figure 2.1. Effects of DEX on permeability. HUVECs (Human Umbilical Vein Endothelial Cell) were seeded onto permeable polyethylene terephthalate (PET) filters and treated with or without 1μM of DEX every other day in both top and bottom of compartments. Tightness of the monolayer was measured on the 5th day of DEX treatment. A) Transendothelial Electrical Resistance (TEER). B) [3H]PEG-4000 permeability across HUVEC monolayer. C) Measurements of hydraulic conductivity (Lp) in individually perfused mesenteric venulesfrom normal (n = 6) and Dex-treated (n = 4) rats. DEX treatment significantly attenuated the Lp responses to PAF that was known to cause transient increases in Lp. D–F) 10 μg of full-length Ad was added onto the apical side. After 24 hrs, the medium on basolateral was collected. D) Total Ad amount was quantified using ELISA. E) The collected basolateral medium was concentrated and separated by PAGE. 3 forms of Ad are labeled as LMW (~90 kDa), MMW (~180 kDa), HMW (>250 kDa). F) Representative Western blot for full-length Ad flux across control and Dex-treated monolayers. Data are expressed as mean values ± SEM (n=4-8). *Significant difference (P≤0.05) from control (Con) group.

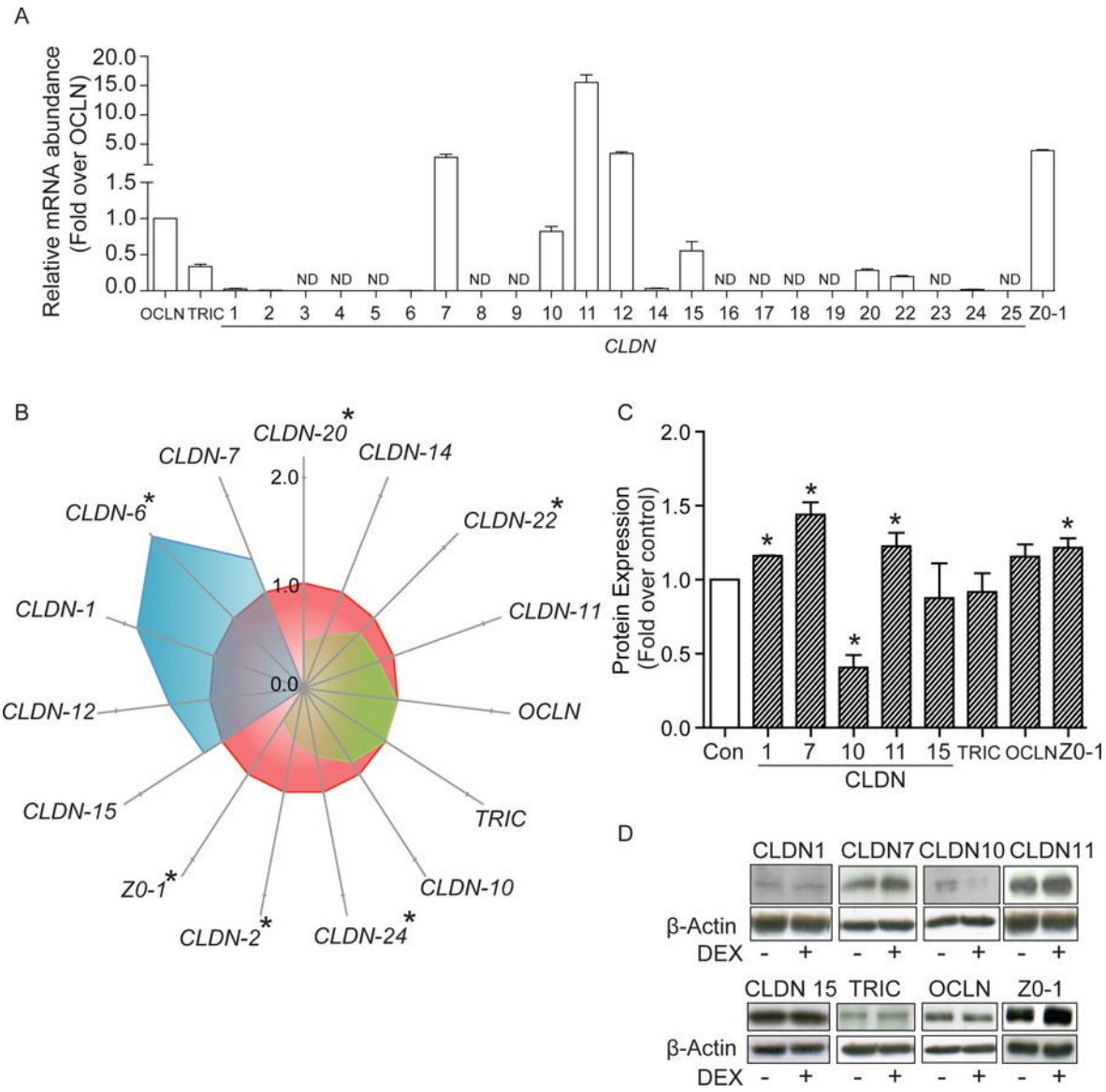
A
Relative mRNA abundance (Fold over OCLN)
20.0
15.0
10.0
5.0
1.5
1.0
0.5
0.0
ND
OCLN TRIC 1 2 3 4 5 6 7 8 9 10 11 12 14 15 16 17 18 19 20 22 23 24 25 Z0-1
CLDN
B
CLDN-20*
CLDN-7
CLDN-14
CLDN-6*
CLDN-22*
2.0
1.0
0.0
CLDN-1
CLDN-11
CLDN-12
OCLN
CLDN-15
TRIC
Z0-1*
CLDN-10
CLDN-2*
CLDN-24*
C
Protein Expression (Fold over control)
2.0
1.5
1.0
0.5
0.0
Con 1 7 10 11 15 TRIC OCLN Z0-1
CLDN
D
CLDN1 CLDN7 CLDN10 CLDN11
β-Actin
DEX - + - + - + - +
CLDN 15 TRIC OCLN Z0-1
β-Actin
DEX - + - + - + - +

Figure 2.2. Effect of DEX on Tight Junction Components. A) mRNA abundance by qRT-PCR analysis. HUVECs grown to confluence on permeable PET inserts. Total RNA was isolated from control cells on the 5th day. Transcript abundance was normalized to GAPDH and each gene examined was expressed relative to OCLN transcript abundance. B) TJ transcript levels in DEX-treated cells were normalized to GAPDH, and expressed relative to the control group (Blue-increasing compared to control; Green-decreasing compared to control). Data are expressed as mean values ± SEM (n = 3-5). C) Protein abundance in HUVECs grown on

cell culture inserts. Protein abundance were normalized toβ-ACTIN, and expressed relative to the control group. D) Representative Western blots of CLDN- 1, -7, -10, -11, -15, TRI, OCC, Z0-1. Data are expressed as mean values ± SEM (n = 3-8). * indicates significant difference ($P \leq 0.05$) from control (Con) group.

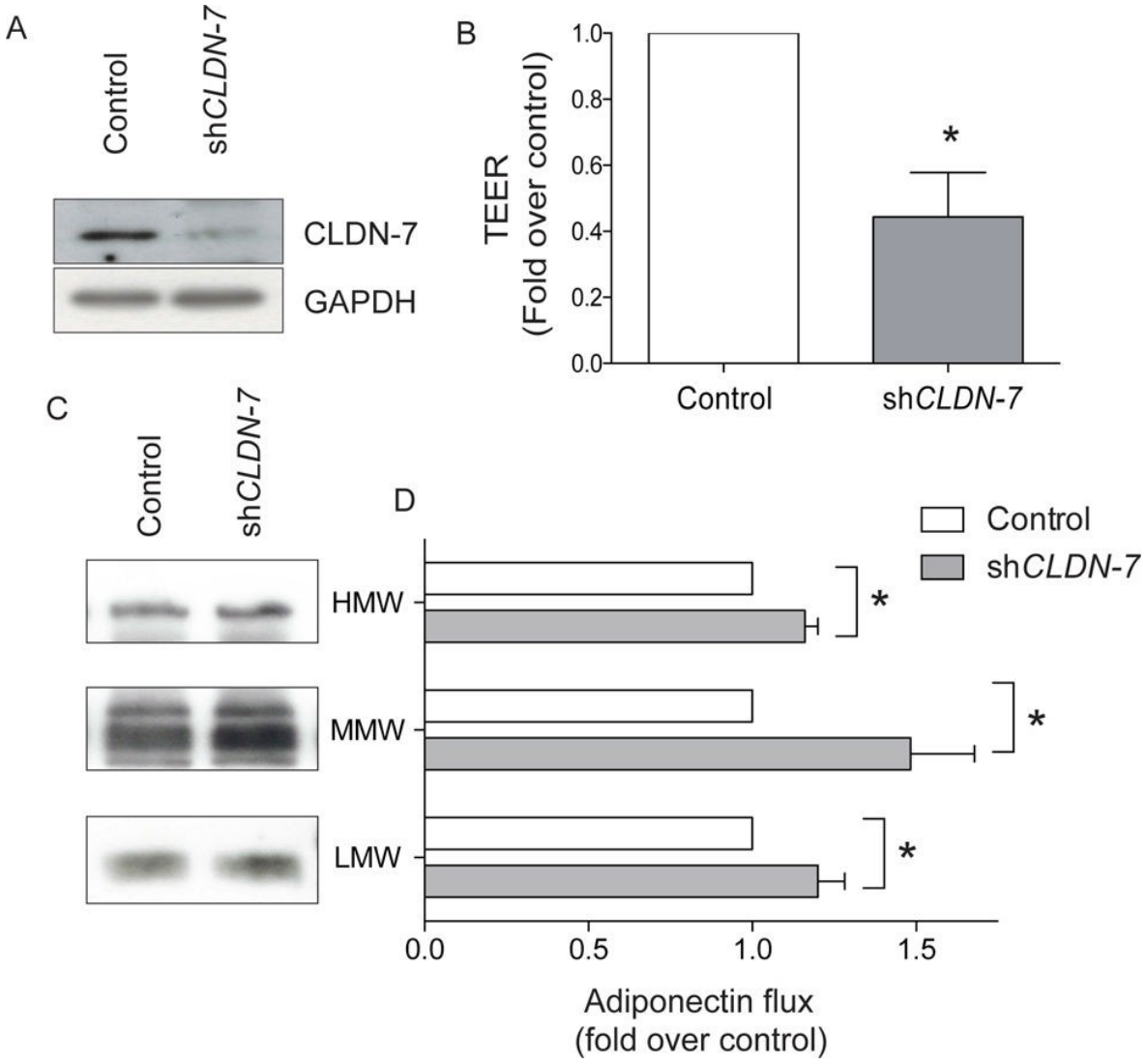

Figure 2.3. Knockdown of claudin-7 alters transendothelial electrical resistance and adiponectin flux. We used shRNA to reduce levels of claudin-7 in HUVEC and average efficiency of knockdown was 71% with a representative Western blot shown in A. In cells transfected with scrambled (Control) or claudin-7 shRNA we then tested TEER (B) and flux of adiponectin with representative Western blot shown in C and quantitation in D. In B and D values are mean ± SEM (n = 3) and *indicates significant difference ($P \leq 0.05$) from control group.

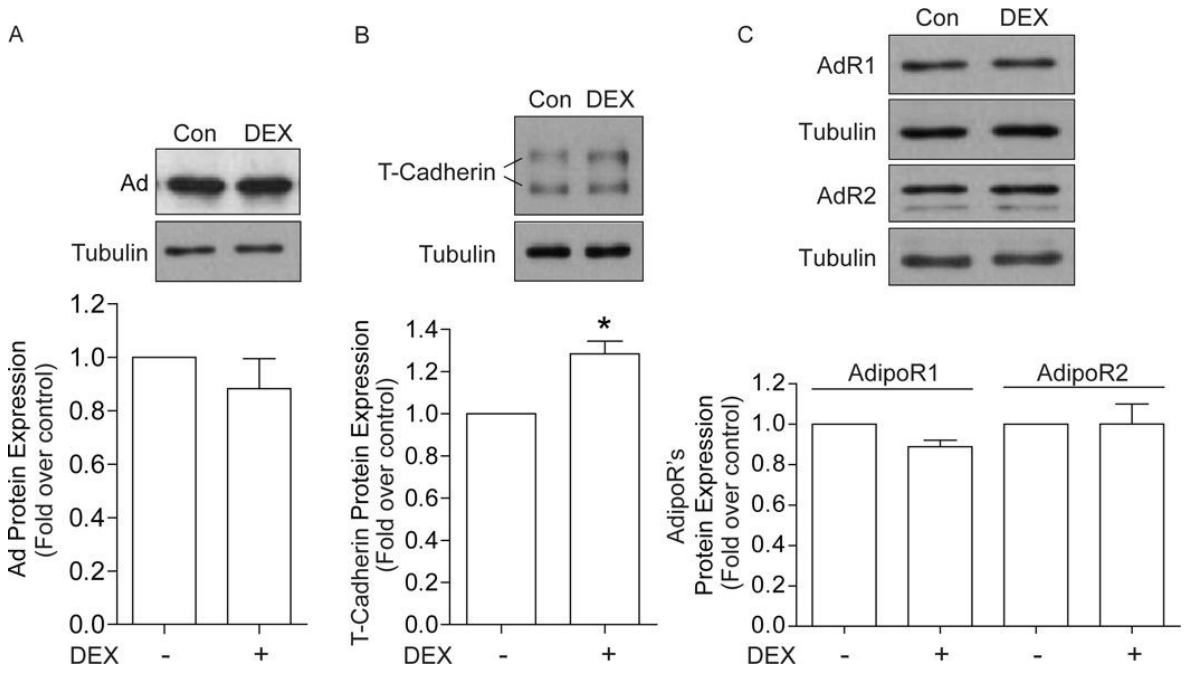

Figure 2.4. Expression of Ad and its receptors in HUVEC. A) Ad expression in HUVECs treated with DEX after 5 days. B) T- CADHERIN expression in HUVECs with DEX treatment. C) ADIPO -R1/ -R2 expression in HUVECs. Data are expressed as mean values ± SEM (n = 3– 6). *indicates significant difference ($P \leq 0.05$) from control (Con) group.

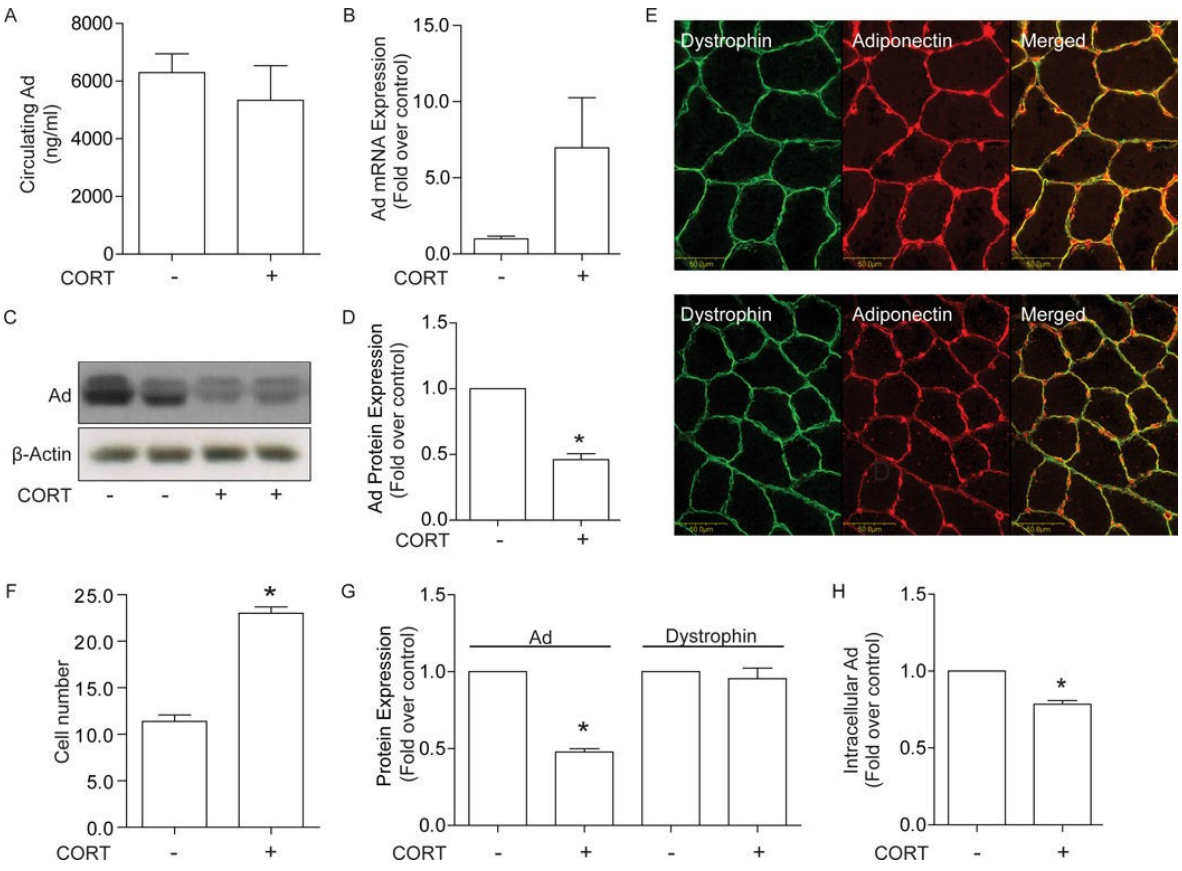

Figure 2.5. Ad level in CORT treated animals. A) Using ELISA, circulating Ad was calculated in 1 week treated rat serum. B) Ad mRNA expression after 14 days of CORT. C&D) Representative Western blotting and quantitation of reduced Ad (~30 kDa) in soleus skeletal muscle. E) Immunohistochemical detection of dystrophin (green), Ad (red) in skeletal muscle isolated from rats after 2 weeks of CORT treatment, together with quantitation in F. G) Quantification of changes in intracellular Ad levels and H) cell number. Quantification of Ad shown as the intensity expressed per cell in arbitrary units and are expressed as mean values ± SEM (n = 3–5).* indicates significant difference ($P \leq 0.05$) from control (Con) group.

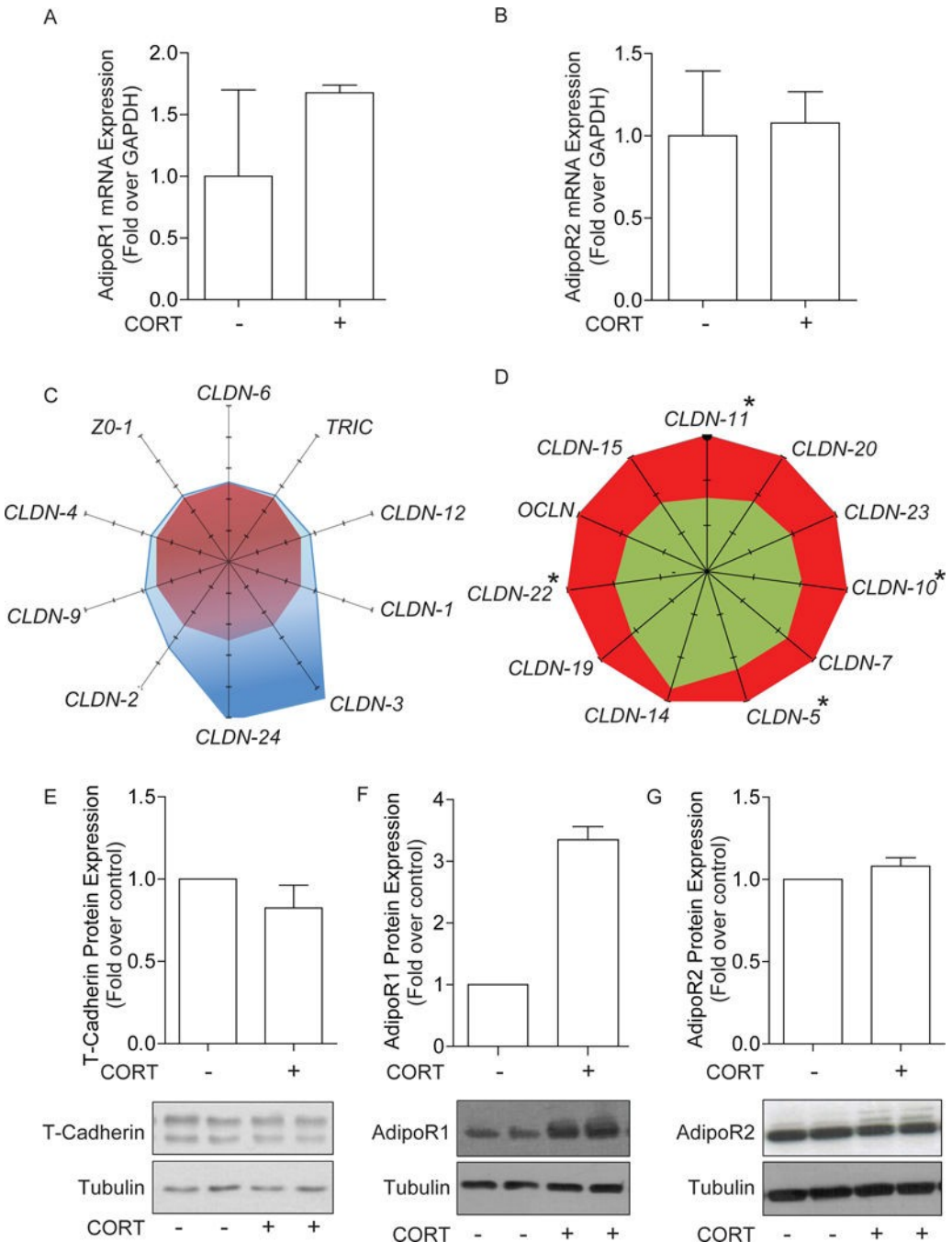
A
AdipoR1 mRNA Expression (Fold over GAPDH)
2.0
1.5
1.0
0.5
0.0
CORT - +
B
AdipoR2 mRNA Expression (Fold over GAPDH)
1.5
1.0
0.5
0.0
CORT - +
C
CLDN-6
Z0-1
TRIC
CLDN-4
CLDN-12
CLDN-9
CLDN-1
CLDN-2
CLDN-3
CLDN-24
D
CLDN-11*
CLDN-15
CLDN-20
OCLN
CLDN-23
CLDN-22*
CLDN-10*
CLDN-19
CLDN-7
CLDN-14
CLDN-5*
E
T-Cadherin Protein Expression (Fold over control)
1.5
1.0
0.5
0.0
CORT - +
T-Cadherin
Tubulin
CORT - - + +
F
AdipoR1 Protein Expression (Fold over control)
4
3
2
1
0
CORT - +
AdipoR1
Tubulin
CORT - - + +
G
AdipoR2 Protein Expression (Fold over control)
1.5
1.0
0.5
0.0
CORT - +
AdipoR2
Tubulin
CORT - - + +

Figure 2.6. Ad receptor expression in skeletal muscle. Rats were treated with CORT for 2 weeks. A,B) mRNA expression of Ad and its receptors after 14 days of CORT. Data are expressed as mean values ± SEM (n = 4–5). C–D) mRNA profile of tight junction in soleus skeletal muscle isolated from 2 weeks CORT- treated rats. mRNA abundance by qRT-PCR analysis. Transcript abundance was normalized to GAPDH mRNA abundance, and mRNA abundance for each gene examined was expressed relative to control group transcript abundance.

Control group gene transcript were normalized to 1. C) mRNA profile of TJ that are increased after 2 weeks CORT treatment compared to control. Blue- CORT- treated, Red- Control. D) TJ genes that are decreased after 2 weeks of CORT treatment. . E–G) Protein expression in soleus. E) T-CADHERIN. F) Ad receptor 1. G) Ad receptor 2. Data are expressed as mean values ± SEM (n = 3). * indicates significant difference ($P \leq 0.05$) from control group.

Supplementary Figure 1

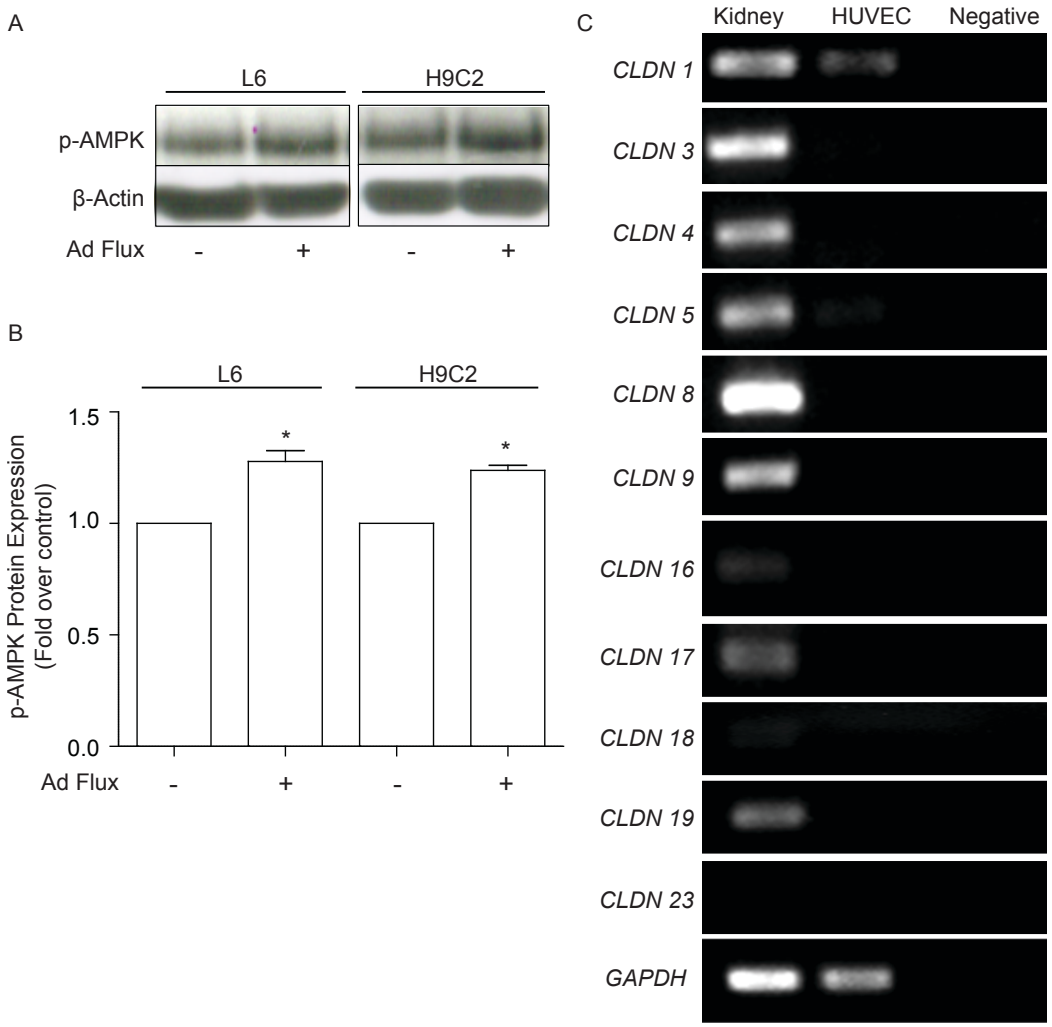

Supplementary Figure 2.1. Validation of Ad functionality and basal level of HUVEC tight junctions A) Effect of treatment with HUVEC-conditioned basolateral medium from Ad flux experiments on p-AMPK and p-p38 MAPK phosphorylation in rat L6 and H9C2. Phosphorylated AMPK and p-p38 MAPK protein abundance was normalized to β-actin, and expressed relative to the corresponding time-matched control group. In (C), Western blots of p-AMPK, phospho-p38 MAPKare shown. Data are expressed as mean values SEM (n = 3). B) Non-detected genes in figure 1(C) was ran on 1% gel in order to confirm the absence. Human kidney was used as positive control. Data are expressed as mean values SEM (n = 3 - 16). *Significant difference (P ≤0.05) from control (Con) group.

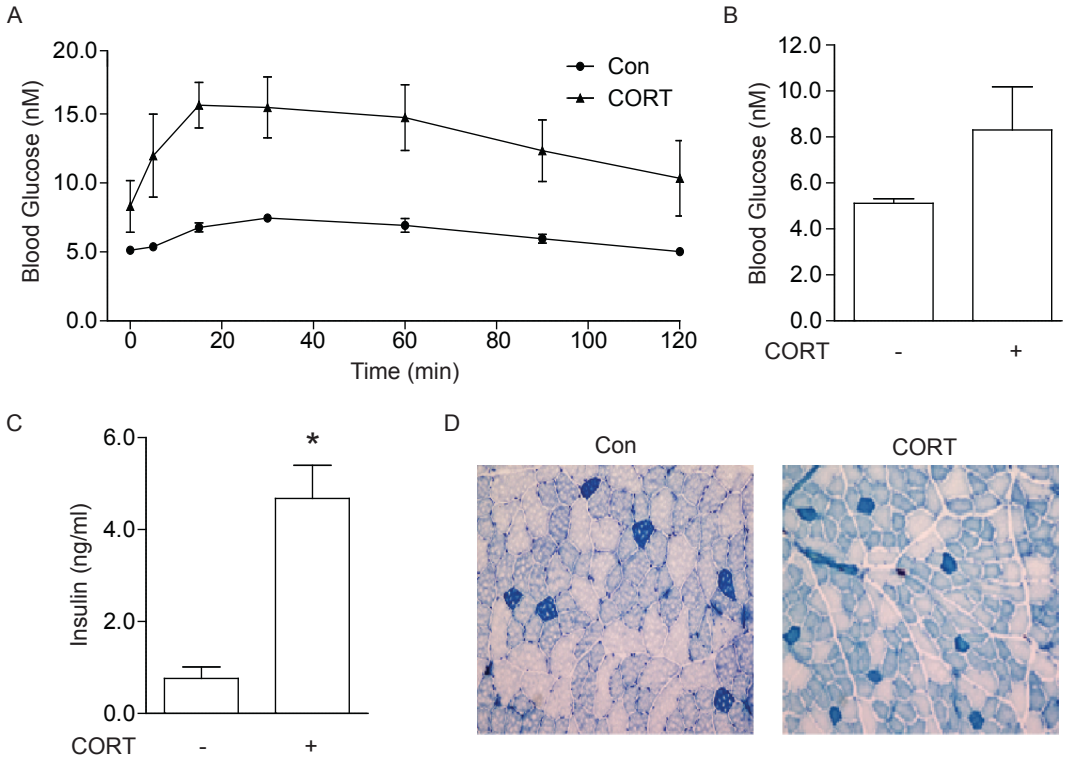

Supplementary Figure 2.2. Circulation of metabolites in CORT treated rats. A) Glucose tolerance in response to an oral glucose tolerance test (OGTT). B) Fasted blood glucose and C) fasted insulin concentrations measured at the onset of the OGTT after 12 days of CORT treatment. D) Representative images of the tibialis anterior (TA) depicting fiber type staining with Metachromatic myosin ATPase. Data are expressed as mean values SEM (n =5). *Significant difference (P≤0.05) from control (Con) group.

2.5. DISCUSSION

Glucocorticoids are potential mediators of endothelium permeability. Our study was designed investigate the its influence on endothelium permeability and consequently the changes in Ad movement across the endothelium barrier and the underlying mechanism. More recently, a similar proposed mechanism for regulation of Ad action was suggested both by us and others (222, 316). To the best of our knowledge, the regulation of this process by glucocorticoids had not been studied before. Our vitro model using DEX treated HUVEC and CORT treated rats to integrate the established observations that glucocorticoids can restrict paracellular transport across various endothelia (126, 212, 219) with the fact that glucocorticoids, commonly prescribed medications, have numerous side effects, including insulin resistance and diabetes (20). Furthermore, we examined whether the emerging phenomenon that transendothelial movement of Ad may regulate the anti-diabetic effects of this hormone and whether this was regulated by glucocorticoids (222, 316). Specifically, our approach involved the use of endothelial cell monolayers and individually perfused intact microvessels to examine whether glucocorticoid altered Ad flux was through reduced microvessel permeability. We also used a rat model of diabetes induced by exogenous glucocorticoid treatment to determine changes in Ad content in muscle as well as peripheral insulin sensitivity.

As indicated in the introduction, strong rationale for this work comes from previous studies with other circulating hormones, most notably insulin. Concentrations of insulin at the cell surface have been shown to be very different from those observed in plasma in microdialysis experiments (102, 245), direct interstitial sampling (30) and lymph measurements (45) (312). It was noted that insulin-mediated glucose uptake lagged behind the increase in plasma insulin (81), whereas in cultured skeletal muscle cells, insulin-mediated glucose uptake occurs within 10 min (247). The time delay seen in vivo (81) reflects a delay in insulin access to the myocyte which is mediated in part via altered paracellular or transcellular endothelial transport. Thus, modification of access to skeletal muscle can have major effects on insulin action and metabolism, suggesting that reaching the

interstitial space is the limiting factor for insulin-mediated glucose uptake (134). Indeed, delivery of insulin to the interstitial space has been shown to be altered by diet (143).

We confirmed the ability of the synthetic glucocorticoid DEX to alter endothelial transport properties, in this case of HUVEC monolayers, as indicated by changes in TEER and PEG-4000. Similar effects were observed in DEX-treated rats, where we saw a significant reduction of permeability in rat mesenteric venules. We then showed that DEX reduced Ad flux across cultured endothelial monolayers by ELISA detection of total Ad content.

Western blotting of Ad isoforms indicated that all three oligomeric forms of Ad (trimer, hexamer and oligomer) were reduced in basolateral media from DEX-treated cells, and although the magnitude of change was more evident in the case of LMW adiponectin, all isoforms were significantly altered and we do not believe this data infers a preferential restriction of LMW flux. This demonstration of restricted flux is important to establish from several perspectives. First, many studies have suggested that oligomeric high molecular weight complexes of Ad are most tightly correlated with insulin resistance (160, 197). Second, the concept that endothelial transport regulated Ad action was also proposed by a recent study which estimated the size of different Ad forms by calculating a Stokes radius (222). The Stokes radii were 3.96 nm for trimeric Ad, 6.01 nm for hexameric Ad and 10.1 nm for various HMW oligomeric forms (222) and these sizes are likely to be in the range that can be physically obstructed or facilitated by changes in endothelial cell tight junction size. Indeed, it was concluded that Ad bioavailability and action in target cells was attenuated under stressed conditions due to reduced trans-endothelial transport (222). We concur that regulation of Ad flux across endothelium is particularly relevant since the target tissues where Ad mediates its physiological effects have a wide-range of endothelial permeability. Liver, for example has highly fenestrated endothelium that may permit the passage of HMW Ad, which has potent effects on hepatic metabolism. In contrast, the central effects of HMW Ad may be limited by its transport across the comparatively tighter blood brain barrier (316).

The well-established effect of glucocorticoids to restrict endothelial transport has been proposed to be mediated via regulation of TJ and adherens junction (AJ) proteins (27, 76). Strands of transmembrane and cytosolic proteins form TJ and AJ complexes that regulate permeability between endothelial cells (95). Functional characteristics of the vertebrate TJ complex are dependent on the variable assemblage of TJ proteins such as occludin (OCLN), tricellulin (TRIC) and in particular, claudins (CLDNs) which directly establish the TJ barrier and form the backbone of TJ strands, while cytosolic ZO-1 and other cortical TJ proteins provide structural support to the TJ complex (95). The CLDN superfamily consists of at least 27 isoforms in mammals and the incorporation of specific CLDN isoforms in TJs can modulate TJ barrier function by making the paracellular pathway tighter or leakier (96). The main observations in our study were increased CLDN-7 and decreased CLDN-10 protein abundance in HUVEC in response to DEX and these changes may underlie the functional properties of paracellular transport limiting Ad flux. Little is known about CLDN-7, although CLDN-7 knockout is lethal in murine models and it seems that CLDN-7 most likely facilitates anion movement across vertebrate epithelia. CLDN-7 was previously found to form a complex with the epithelial cell adhesion molecule (EpCAM) which enhanced cell-cell interaction (140, 277). We suggested that the functional role of CLDN-7 in our model is tightening of the endothelium in association with an increase in abundance, and that this may help to explain, in part, the restricted movement of Ad in DEX-treated HUVEC as well CORT-treated rats. Further supporting this idea, a reprevious studies which have found that CLDN-7 (−/−) can cause colonic inflammation and enhance the paracellular flux of small organic solutes (258), as well as observations that CLDN-7 (−/−) results in the presence of intercellular gaps below TJs and cell matrix loosening (64). Thus, we used shRNA to target claudin-7 in HUVEC and observed that this caused a decrease in TEER and increase in adiponectin flux across monolayers, further indicating an important mechanistic role for Dex-mediated changes in claudin-7 expression. Interestingly, another group found that NLRP3 inflammasome promoted endothelial disruption via production of HMGB1

to disrupt the junctions and increased paracellular permeability (42). Finally, (260) reported that urine Na(+), Cl(−), and K(+) were significantly increased in CLDN-7(−/−) mice compared with that of CLDN-7(+/+) mice. Taken together, the studies outlined above and our data indicate an important functional consequence for CLDN-7 reduction and compromised epithelial permeability as the result of tight junction disruption, and this supports the view that increased CDLN-7 abundance, as seen in these experiments, may contribute to endothelial tightening and reduced Ad flux.

In contrast, CLDN-10 isoforms in vertebrate epithelia have been described to impart both charge and size selective properties to the paracellular pathway. Previous studies investigated the role of CLDN-10 deficient mice using Cre-Lox found that serum phosphate concentration was 28% higher and serum Mg2+ concentration was almost two-fold higher in cKO mice compared with controls. However, the same study also found that CLDN-10 transports molecules in a charged selective manner (31). To the best of our knowledge, Ad is uncharged. Therefore, the transport of Ad is less likely to be affected by CLDN-10. Nevertheless, it would be very interesting to explore whether the consistent decrease in CLDN-10 observed in this study has a functional role in the modulation of Ad transport across the endothelium barrier.

In the glucocorticoid-induced diabetic rodent model used here, a decrease in CLDN-10 mRNA expression in skeletal muscle was also observed. Although changes in expression profiles of other tight junction proteins do not entirely match the changes in HUVEC treated directly with DEX, this is not entirely surprising since there are multiple factors impinging upon tight junction protein expression in skeletal muscle tissue in vivo.

We believe that reduced paracellular transport is the main mechanism of reduced Ad flux observed, yet we also tested possible indicators of altered transendothelial flux (316). In DEX-treated endothelial cells, there was no major change in ADIPO-R1 or ADIPO-R2 mRNA and protein expression, although in skeletal muscle homogenates, ADIPO-R1 protein expression levels increased significantly in CORT-treated animals. This may reflect a compensatory mechanism to reduced Ad

availability in order to increase sensitivity to available Ad. We also observed that DEX increased expression of T-cadherin in HUVEC. T-cadherin has been identified as a non-functional receptor for Ad (109). This is in agreement with a previous study showing that DEX enhanced T-cadherin expression in human osteosarcoma cells (32). One possible interpretation of our finding is that binding to endothelial T-cadherin may trap Ad in the vasculature, as has recently been proposed (169).

We also investigated potential alterations in endothelial transport of Ad in a rodent model of glucocorticoid-induced diabetes (244). In these rats, we found normal circulating Ad levels but significantly reduced total Ad protein content within skeletal muscle without an accompanying decrease in muscle Ad gene expression. This suggests less flux of Ad from circulation could be a contributory mechanism. Indeed, upon immunohistochemical analysis we found reduced Ad content in the interstitial space.

Although not a direct comparison to the in vitro studies we used here, it suggests that skeletal muscle Ad availability, and thus action, may be limited in this animal model possibly contributing to its diabetic phenotype (19-21, 244, 316).

In conclusion, our study indicates that glucocorticoid-mediated tightening can reduce flux of Ad across endothelial monolayers, and that this may be due to alterations in the expression profile of tight junction proteins. Furthermore, in a rat model of diabetes induced by exogenous glucocorticoids, we observed reduced interstitial and intracellular levels of Ad in skeletal muscle. Thus, we propose that reduced Ad action in target tissues, as a consequence of reduced endothelial flux from circulation to interstitial space, may contribute to the diabetic phenotype occurring after glucocorticoid treatment. Since glucocorticoids are one of the most commonly prescribed medications, our discovery of reduced Ad transport in response to glucocorticoids is a particularly important and novel finding with potentially far- reaching consequences.

CHAPTER THREE: STUDY 2

Tracking adiponectin biodistribution via fluorescence molecular tomography indicates increased vascular permeability after streptozotocin-induced diabetes

Nanyoung Yoon[1], Keith Dadson[1], Thanh Dang[1], Teresa Chu[1], Nina Noskovicova[2], Boris Hinz[2], Adeline Raignault[3], Eric Thorin[3], Seunggyu Kim[4], Jessie S. Jeon[4], James Jonkman[5], Trevor McKee[6], Justin Grant[6], Jeffrey D. Peterson[7], Scott P. Kelly[1] & Gary Sweeney[1*]

[1]Department of Biology, York University, Toronto, Canada

[2]Faculty of Dentistry, University of Toronto, Toronto, Canada

[3]Montreal Heart Institute, University of Montreal, Quebec, Canada

[4]Department of Mechanical Engineering, Korea Advanced Institute of Science and Technology, Daejeon, 34141, Republic of Korea

[5]Advanced Optical Microscopy Facility (AOMF), University Health Network, Toronto, Canada

[6]Spatio-temporal Targeting and Amplification of Radiation Response (STTARR), University Health Network, Toronto, Canada

[7]Applied Biology, Life Sciences & Technology, PerkinElmer, Hopkinton, MA, USA.

Published: *Am J Physiol Endocrinol Metab*, accepted on Jun 17, 2019

Author Contribution

N.Y., K.D., J.G., and G.S. conceived and designed research; N.Y., K.D., T.D., T.C., N.N., and A.R. performed experiments; N.Y., K.D., B.H., J.J., T.M., and J.P. analyzed data; N.Y., K.D., B.H., E.T., J.P., S.K., and G.S. interpreted results of experiments; N.Y., K.D., N.N., B.H., and S.K. prepared figures; K.D., N.Y., and G.S. drafted manuscript; N.Y., K.D., N.N., B.H., E.T., S.K., J.S.J., T.M., J.P., S.K., and G.S. edited and revised manuscript; N.Y., K.D., T.D., T.C., N.N., B.H., A.R., E.T., S.K., J.S.J., J.J., T.M., J.G., J.P., S.K., and G.S. approved final version of manuscript. [Following the style of AJP]

3.1. SUMMARY

Adiponectin, a highly abundant polypeptide hormone in plasma, plays an important role in the regulation of energy metabolism in a wide variety of tissues as well as showing important beneficial effects in diabetes, inflammation and cardiovascular disease. To act on target tissues, adiponectin must move from the circulation to the interstitial space, suggesting that vascular permeability plays an important role in regulating adiponectin action. To test this hypothesis, fluorescently labelled adiponectin was used to monitor its biodistribution in mice with streptozotocin-induced diabetes (STZD). Adiponectin was indeed found to have increased sequestration in the highly fenestrated liver and other tissues within 90 min in STZD mice. In addition, increased myocardial adiponectin was detected and confirmed using Computed Tomography (CT) co-registration. This provided support of adiponectin delivery to affected cardiac tissue as a cardioprotective mechanism. A higher adiponectin content in the STZD heart tissues was further examined by ex vivo fluorescence molecular tomography (FMT) imaging, immunohistochemistry and Western blot analysis. In vitro mechanistic studies using an endothelial monolayer model cultured on permeable polyethylene terepthalate inserts further confirmed that adiponectin flux was increased by high glucose. However, in this in vitro model and mouse heart tissue, high glucose levels did not change adiponectin receptor levels. An examination of the tight junction (TJ) complex revealed a decrease in the TJ protein claudin (CLDN)-7 in high glucose-treated endothelial cells and the functional significance of this change was underscored by increased endothelium permeability upon siRNA-mediated knockdown of CLDN-7. Our data support the idea that glucose-induced effects on permeability of the vascular endothelium contribute to the actions of adiponectin by regulating its transendothelial movement from blood to the interstitial space. These observations are physiologically significant and critical when considering ways to harness the therapeutic potential of adiponectin for diabetes.

3.2. INTRODUCTION

Extensive research on adiponectin has validated this hormone as a biomarker for cardiometabolic diseases and as a therapeutic target with enormous potential (289). In order to harness the numerous beneficial effects of adiponectin, it is essential to fully understand the mechanisms governing adiponectin action (161, 200, 271). To date, the vast majority of studies have focused on correlating changes in circulating adiponectin levels and disease markers (11). As a result, reduced adiponectin levels are well established to inversely correlate with diabetes and cardiovascular diseases (289). Adiponectin acts via binding to membrane receptors AdipoR1, AdipoR2 and T-cadherin (113, 306), and reductions in their expression or post-translational modification in disease states has been proposed to lead to adiponectin resistance (71, 233, 287). However, another critical factor that likely determines adiponectin action is vascular permeability (134, 135, 316). More specifically, to directly elicit a response in a target tissue adiponectin must transit from the circulation to interstitial space across the endothelial barrier (316).

The monolayer of endothelial cells lining the circulatory system acts as a barrier that regulates the movement of blood borne factors to the interstitial space. In turn, the barrier properties of the endothelium are regulated by the transcellular pathway (i.e. solute transport across endothelial cells) as well as the paracellular pathway (i.e. solute movement between adjacent endothelial cells) (316). In general, larger macromolecules move via facilitated transcellular trafficking while the paracellular route typically restricts solutes in the range of 3 nm radius (96). Tight junctions (TJ) provide a selective barrier to solute movement between cells and altered expression of components including ZO-1, occludin, tricellulin and claudins alter TJ structure to make a leakier or tighter barrier for paracellular movement of solutes (95). Numerous previous studies, particularly focusing on insulin, have shown that vascular permeability can play an important role in contributing to the development of diabetes and heart failure (134, 316). It is important to note that endothelial permeability varies widely throughout the body in a tissue (and intra-tissue)-specific manner (316).

It has also been shown that endothelial barriers control adiponectin transport in a cell- and tissue-specific manner (222) and we have reported that transendothelial movement of adiponectin was reduced by glucocorticoids (58).

We believe that the role of endothelial permeability as an important determinant of adiponectin action has been somewhat underappreciated. In this study, we further considered a link between vascular permeability, adiponectin flux, and hyperglycaemia/diabetes by producing recombinant adiponectin, which we then conjugated with a near infra-red probe in order to track its biodistribution in live wild type and diabetic mice using fluorescence molecular tomography (FMT). We also examined the effects of high glucose levels on adiponectin flux across isolated arteries and cultured monolayers of endothelial cells. Finally, since the cardioprotective actions of adiponectin are currently the focus in our lab (54-56, 198, 201), we considered the role of the vascular barrier and diabetes on adiponectin access and action in the heart. These studies provide a novel and integrated view on the movement of adiponectin across the endothelial barrier under conditions that relate to diabetes and new insight into the impact that vascular permeability has on the actions of adiponectin on key organs.

3.3. MATERIALS AND METHODS

3.3.1. Experimental animal model

Male Nu/Nu homozygous mice and C57BL6 aged 8-13 weeks were utilized for assessing adiponectin biodistribution. All mice were maintained with access to water and low-fluorescent chow (Teklad global 18% Protein Rodent Diet (Irradiated), Harlan Laboratories, Indianapolis, IN, USA) throughout each experimental period. Age and weight-matched pairs were grouped for each injection (averaging 23~25g). After 12 h starvation, diabetes was induced by single intraperitoneal injection of 150mg kg^{-1} (body weight) STZ (Sigma-Aldrich, St. Louis, MI, USA). Experiments were performed 4 days after STZ injection and diabetes was diagnosed when mice exhibited a blood glucose level > 14mmol/L at this time, whilst all control mice had only saline injection. Circulating adiponectin was detected in serum before and after infusion of VivoTag-750 conjugated adiponectin using a mouse adiponectin ELISA kit (Immunodiagnostics Ltd, Hong Kong) which detects all adiponectin oligomeric forms.

3.3.2. Fluorescence Molecular Tomography (FMT) to Detect VivoTag-750- adiponectin

Recombinant adiponectin prepared in our laboratory was labeled with VivoTag-S 750 (NEV10123, Perkin Elmer, Boston, MA, USA). Importantly, this recombinant protein formed oligomeric forms in a ratio which closely mirror those found in circulation (see supplementary figures 1&2). Labeling efficiency was assessed by running labeled full-length adiponectin on a SDS-PAGE gel then scanned on a LI-COR Odyssey infrared imaging system to visualize the 3 adiponectin isoforms. Labeled proteins were transferred from the gels onto nitrocellulose membranes before probing with adiponectin-specific antibodies to assess fluorescence-to-total protein ratio. Labeled adiponectin was infused into lightly anesthetized mice (1-2% isoflurane) via a surgically placed permanent jugular vein cannula. For cannulation insertion, the mice were first anesthetized with 5% isoflurane then maintained at 2% isoflurane. The surgical site was cleaned with iodine solution and

alcohol before a longitudinal incision of about 15 mm was made in the skin at the neck of the animal, just above the right front leg. Connective tissue surrounding the jugular vein was carefully separated before two sutures of 6-0 Ethilon surgeon's silk (Johnson & Johnson Intl, Brussels, Belgium) were placed ~5-10mm apart on the vein. A fine lateral incision was made between the sutures using micro-scissors, which allowed insertion of a saline-filled polyethylene tube (PE10) into the vein between the sutures. When placement was confirmed, the caudal suture was released and the cannula slowly fed caudally ~ 5mm into the vein towards (but not entering) the heart. To confirm correct placement, 50 µl saline was delivered through the cannula using a 31G insulin needle. The cannula was then securely tied to the jugular vein with silk suture and 85 µg of adiponectin conjugated with VivoTag-S was administered followed by a 50 µl saline flush. The cannula was sealed using a heated haemostat, the skin incision was closed using silk suture, and a serum sample was collected from the tail vein within 2 min of adiponectin infusion. Mice were maintained at 2% isoflurane while being positioned in a glass mouse imaging cassette, then scanned 10, 30, 60, and 90min post-adiponectin infusion with a FMT 2500 LX Quantitative Tomography system (VisEn Medical, Perkin Elmer, Downers Grove, IL, USA) using the 750nm near infra-red channel (750/800nm excitation/emission). Once FMT scanning was completed, mice in the imaging cassette were immediately taken for a computed tomography (CT) scan (Locus eXplore MicroCT, GE Healthcare, London, ON, Canada and XRAD 225Cx, Precision X-Ray, North Banford, CT, USA) under constant anesthesia to ensure identical mouse positioning and accurate alignment between CT and FMT. FMT software (TrueQuant, Perkin Elmer) reconstructs a quantitative 3D dataset in which fluorescence/voxel is expressed in nmol/L. FMT and CT datasets (dicom format) were imported into Inveon Research Workplace (Siemens Healthcare, Germany) or AMIDE (http://amide.sourceforge.net) for FMT-CT co-registration to permit accurate localization of the fluorescent signal.

3.3.3. FMT analysis of tissues ex vivo

To avoid potential scatter from adjacent tissue, heart, liver, kidney, pancreas and skeletal muscle, those tissues were excised from mice after cervical dislocation immediately following FMT and CT scanning (~100-120min post-adiponectin infusion). 2D epifluorescence FMT images were taken of these tissues on an opaque resin imaging block in the FMT imaging cassette. Quantitative analysis of the fluorescent signal was performed using the FMT software (TrueQuant, Perkin Elmer, Downers Grove, IL, USA).

3.3.4. Ex vivo vascular permeability of adiponectin assay

Five weeks old Wistar rats were used. After two weeks of standard diet in the animal facility, rats were fasted 5 hours before induction of diabetes by a single intraperitoneal injection of streptozocin (STZ, Sigma-Aldrich, St. Louis, MI, USA) at a dose of 100 $mg.kg^{-1}$ bodyweight (~200 µl/rat). Diabetes was diagnosed when hyperglycemia was higher than 10 mmol/L (180 mg/dL). Rats developed diabetes within 7 days of STZ injection. A control group of rats was injected with an equivalent volume of the vehicle solution (citrate buffer 0.5M, pH 4.5). Rats that failed to respond to STZ injection were not used for the study. Control or diabetic rats were anesthetized with isoflurane and a mid-line laparotomy was performed to expose and remove the mesenteric bed. Isolated mesenteric arteries were mounted on a glass cannula immerged in a 2-ml organ bath filled with a physiological salt solution (PSS; mmol/L: 130 NaCl; 4.7 KCl; 1.18 KH_2PO_4; 1.17 $MgSO_4$; 14.9 $NaHCO_3$; 1.6 $CaCl_2$; 0.023 EDTA; 10 glucose; pH 7.4) aerated with 12% O_2; 5% CO_2; 83 % N_2 at 37ºC following a method previously described (211). Arterial segments were pressurized at 80 mm Hg in no-flow conditions and equilibrated for 30 min before starting experiments. 10 µg/mL adiponectin (200 µl) was added to the arterial perfusate which circulated at a flow rate of 2 µl/min for 90 min at a constant pressure of 80 mm Hg. At 0, 30, 60, 90 min, 100 µl samples of the extra-vascular bath containing transported adiponectin were collected, and an equivalent volume of

physiological solution was added into the bath. Adiponectin levels were quantitatively determined by ELISA kit (Immunodiagnostics Ltd, Hong Kong).

3.3.5. Cell culture

Human Dermal Microvascular Endothelial Cells HDMEC (ATCC, Manassas, VA, USA) were grown in vascular cell basal medium (ATCC) supplemented with 10% fetal bovine serum (FBS) at 37°C, 5% CO_2. All cells were used at passages 3–4 from the supplier. 500K HDMECs were seeded onto trans-well inserts (Corning, Tewksbury, MA, USA) sized for 12-well plates having 3.0 μm pore sizes. Hyperglycemia was induced with 25 mM glucose in vascular cell basal medium supplemented with 2% FBS for 6 days. To adjust for osmotic pressure differences, control cells were treated with 5.5 mM glucose and 19.5 mM mannitol.

3.3.6. Measurement of Transendothelial Electric Resistance (TEER)

Measurements of TEER were conducted using STX-2 chopstick electrodes attached to an epithelial voltohmmeter (EVOM; World Precision Instruments, Sarasota, FL, USA). All TEER measurements were corrected for background by subtracting TEER recorded across a blank membrane primed with appropriate cell culture medium. Resistance measurements were taken at day 0 and day 6 of treatment with 25 mM glucose and control (5.5 mM glucose + 19.5 mM mannitol).

3.3.7. Permeability Assay using Endothelial Monolayers

HDMECs were seeded onto trans-well inserts and treated with 25mM glucose and 5.5 mM glucose with 19.5 mM mannitol for 5 days prior to the start of experiments. At the start of the experiment, 10μg/mL of adiponectin with the 25mM glucose or 5.5 mM glucose with 19.5 mM mannitol including 2% FBS vascular cell basal medium (ATCC PCS-100-030, Cedarlane, Burlington, ON, CA) was applied to the apical chamber only. After 24 h, apical and basolateral media were

assessed for adiponectin concentration by gel electrophoresis after concentrating with 10,000Da MWCO(molecular weight cutoff) filter (EMD Millipore, Billerica, MA, USA) or by fluorescence intensity reader, respectively, and concentrations calculated by comparison to standard curves prepared in culture medium.

3.3.8. Quantitative RT-PCR

Using aliquots of total extracted RNA, cDNA was synthesized. And pRT-PCR reactions were performed using the SYBR Green PCR Master Mix (Lifetechnologies). Gene-specific primer sets were designed. human CLDN7, F: 5' GGAGACGACAAAGTGAAGAAGG 3', R: 5' GGACAGGAACAGGAGAGCAG 3', human GAPDH, F: 5' AACATCATCCCTGCCTCTACTG 3', R: 5' CCTGCTTCACCACCTTCTTG 3', murine AdipoR1, F: 5' ACGTTGGAGAGTCATCCCGTAT 3', R: 5' CTCTGTGTGGATGCGGAAGAT 3', murine AdipoR2, F: 5' TCCCAGGAAGATGAAGGGTTTAT 3', R: 5' TTCCATTCGTTCCATAGCATGA 3', murine Adiponectin, F: 5' TGTTCCTCTTAATCCTGCCCA 3', R: 5' CCAACCTGCACAAGTTCCCTT 3', murine CLDN7, F: 5' GGACCTGCCATCTTTATCGGC 3', R: 5' AGCTTTGCTTTCACTGCCTGG 3', murine ZO-1, F: 5' GTCCCTGTGAGTCCTTCAGCTG 3', R: 5' ACTCAACACACCACCATTGCTG 3', murine 18s RNA, F: 5' AGTGAAACTGCGAATGGCTCA 3', R: 5' CGAGCGACCAAAGGAACCA 3'.

3.3.9. Claudin-7 Knockdown by shRNA in HDMEC

Claudin-7 gene expression was knocked-down in HDMECs using a pGPU6/Neo-claudin-7 plasmid as shown previously (58) using the following shRNA target sequence: 5′-GGCCATCAG ATTGTCACAGAC-3′ (GenePharma Co., Ltd., Shanghai, China). Lipofectamine 3000 reagent (Life Technologies, Carlsbad, CA, USA) was used for all transfections following manufacturer

instructions. A non-targeted control (NTC) shRNA plasmid was designed with a non-specific scrambled sequence. The transfected cells were stabilized for 24h with 10% FBS medium and subjected to antibiotic selection (500 μg/mL G418 (Sigma-aldrich, Saint Louis, MO, USA)) for 2 days. During antibiotic selection, transfected cells were seeded on trans-well inserts or 6 well-plates for further experiments.

3.3.10. Western Blotting

Proteins from mouse tissues were homogenized by TissueLyser II (QIAGEN, Hilden, Germany) in RIPA buffer with 80mM Tris–HCl (pH 6.8), 2% (w/v) SDS, 20% glycerol, 3.3% (v/v) β-mercaptoethanol and 0.01% (w/v) bromophenol blue, 30mM Hepes (pH 7.4), 2.5mM EGTA, 3mM EDTA, 70mM KCl, 20mM β-glycerolphosphate, 20mM NaF, 1mM Na_3VO_4, 200μM PMSF, 10μM E64, 1μM leupeptin, 1μM pepstatin A, 0.1% NP40, and 0.1μM okadaic acid. To detect the 3 forms of adiponectin, samples were prepared without β-mercaptoethanol or heating. For detection of other protein targets, samples were lysed in complete RIPA buffer and denatured at 95°C for 10min. Transported adiponectin was collected from basolateral HDMEC medium and concentrated using Amicon Ultra-4 Centrifugal Filter Units with Ultracel-10K (EMD Millipore, Billerica, MA, USA). To detect the 3 adiponectin oligomers, concentrated adiponectin samples were prepared without denaturation or reduction. Prepared samples were run on SDS-PAGE gels then transferred onto PVDF membranes (Bio-Rad Laboratories, Hercules CA, USA), before incubation with primary antibody, and detection by chemiluminescence. Polyclonal primary antibody of rabbit anti-Adiponectin (dilution 1:1000) is produced in-house (159). Rabbit anti-AdipoR1/2 antibodies were from Phoenix Biotech (Toronto, ON, CA) (201). Mouse anti-FLAG M2 (dilution 1:1000, F1804, Sigma, Oakville, ON, CA), rabbit anti-Claudin-7 (dilution 1:500, Cat#34-9100, Thermo Fisher, Rockford, Illinois, USA), rabbit anti-α/β-Tubulin (dilution 1:1000, Cat#2148, Cell Signaling, Danvers, MA, USA), rabbit anti-GAPDH(14C10) (dilution 1:1000, Cat#2118, Cell Signaling,

Danvers, MA, USA) were purchased. And the appropriate HRP-conjugated secondary antibody (anti-rabbit IgG-HRP (dilution 1:5000, Cat#7074), anti-mouse IgG-HRP (dilution 1:5000, Cat#7076)) was used from Cell Signaling (Danvers, MA, USA). Bands were quantified by densitometry using Fiji software and normalized to relevant loading controls as indicated.

3.3.11. Immunofluorescence

Mouse hearts were isolated following isoflurane anesthesia and the ventricles excised then cross-sectioned at the mid-line with a surgical blade before being embedded into a mold with Optimal Cutting Temperature compound (O.C.T) (Sakura Finetek USA Inc., Torrance, CA, USA) and frozen on dry ice. 5 µm thick cryosections were made using a cryostat and mounted onto positively charged glass slides (Superfrost, ThermoFisher, CA). Mounted slides were fixed in 4% PFA solution for 10min to stain adiponectin or fixed in 100% ice-cold acetone, air-dried at room temperature, and rehydrated in distilled water followed by washing with phosphate-buffered saline (PBS) buffer. And permeabilization was followed by 0.5% TritonX-100. Before permeabilization, cell border staining was performed by incubating with 5 µg/mL Alexa488 conjugated wheat germ agglutinin (Thermo Fisher, Eugene, OR, USA) for 10min in adiponectin staining. Sections were then incubated with Adiponectin primary antibody (1:100) and Texas-Red secondary antibody (1:250) and DAPI for nuclear visualization. For vasculature staining, primary antibodies directed against Claudin-7 (dilution 1:50, Cat#34-9100, Thermo Fisher, Rockford, Illinois, USA), VE-Cadherin (dilution 1:100, Cat#PA5-17401, Thermo Fisher, Rockford, Illinois, USA), PECAM-1 (dilution 1:50, Cat#SC-376764, Santa Cruz Biotech, Mississauga, CA), ZO-1 (dilution 1:100, Cat#61-7300, ThermoFisher Scientific, Rockford, Illinois, USA), α-SMA (1:100, α-SM1, a kind gift from Dr. Giulio Gabbiani, University of Geneva, Switzerland), and desmin (1:30, Cat#M076029, Dako, Burlington, ON, CA) were used. Isotype-specific secondary antibodies anti-rabbit IgG-TRITC (1:100, Sigma, St. Louis, Missouri, USA), Alexa 568-conjugated IgG (1:100, Abcam, Carlsbad, CA, USA), Alexa647-

conjugated IgG2a (1:100, Molecular Probes, LifeTechnologies Inc., Rockford, Illinois, USA), and anti-mouse IgG1-FITC (1:200, SouthernBiotech, Birmingham, Alabama, USA), and DAPI (Vectashiled mounting medium with DAPI, Cat# H-1200, Burlingame, CA, USA) were used. Images were acquired using a LSM700 (Zeiss) or LSM780 (Zeiss) confocal microscope and an upright Zeiss Axio Observer M35 epifluorescence microscope equipped with structured illumination (Apotome) and Axiocam HR camera (Carl Zeiss, Jena, Germany). All images were processed using Fiji or Adobe Photoshop CS5 (Adobe System, San Jose, CA). Contrast and brightness were enhanced consistently for all representative images used in the publication.

3.3.12. Fabrication of Microfluidic Devices and Cell culture on a Chip

To recapitulate 3D microvascular networks in vitro, we utilized a microfluidic chip that can include cells-trapped hydrogel and cell growth medium with compartmentalization (a central gel channel and two lateral media channels). Previous studies have described the fabrication process of the chips in detail (243). Briefly, silicon-based organic PDMS microfluidic device fabrication includes steps of soft lithography with SU-8 silicon wafer mold (AMED Inc.) and PDMS (1:10, Dow Corning), generating reservoirs with 1, 4 mm diameter biopsy punches (KAI medical), and device assembly by plasma bonding (Femto Science Inc.) to a coverslip (glass, Duran). The devices were sterilized by 15min sonication (Uil Ultrasonic Co., Ltd) in 70% EtOH before the bonding process. An 80°C drying oven was used for curing PDMS mixture, dehydration of devices before plasma treatment and recovering hydrophobicity after bonding (24hr in advanced cell seeding). In this study, 120μm depth of microchannel devices was used.

Human Umbilical Vein Endothelial Cells (HUVECs, Lonza) were grown in endothelial cell growth medium (EGM-2, Lonza) supplemented with 5% fetal bovine serum (FBS) at 37°C, 5% CO_2. All cells were used at passages 6-8 from the supplier. After harvesting of trypsinized cells by centrifugation (125 xg, 7 min), cells were resuspended in concentration of 1.4 x 10^7 cells/mL with

4U/mL thrombin solution. We injected 1:1 mixture of cells (1.4 x 10^7 cells/mL) and fibrinogen solution (5 mg/mL) into a gel inlet to fill it up. After incubating the chips at 37 ° C in a humid chamber for 15 minutes to wait gelation, we injected cell culture medium into the media channels. The cells in the microfluidic chips were incubated for 4 days with daily replacement of medium. Self-assembly of HUVECs into a perfusable vascular network (vasculogenesis) was induced by adding 50 ng/mL VEGF to EGM from day 0 (D0) to day 4 (D4).

3.3.13. Vascular Permeability Assay in Microfluidic Chips

After 4 day culture, medium was washed out with a quick PBS rinse before a fluorescent molecule solution was infused. Due to the hydrostatic pressure drop between the two media channels, the solution in the media channel flows along with the perfusable microvascular networks to the opposite media channel. We monitored the diffusion of fluorescent molecules into the fibrin gel (ECM) through the vessel wall and the images were captured at 6-10 second intervals for 3 min via a fluorescence microscope (Axio Observer Z1, Zeiss). The images were quantified using ImageJ.

3.3.14. Perfusibility test in 3D microvascular network

At day 4, endothelial growth medium was quickly washed with PBS by filling up two reservoirs in only one side channel to rinse out any particles from the 3D vessel lumen efficiently using hydrostatic pressure differences. When the interested field of view was found, bright field of image was captured before the fluorescent molecule infusion. Then, 5.0-5.9 μm of FITC surface labeled beads (0.1% w/v, F1CP-50-2, Spherotech) was infused into one media channel and time-lapse images were taken at 1.4 second interval for 2 min under fluorescence microscope (Axio, Observer Z1, Zeiss). The fluorescent images were overlayed with brightfiled orientation image, and processed to video with ImageJ.

3.3.15. Statistical analysis

Data are expressed as mean ± SEM and the significant differences was determined where $p<0.05$ resulted from performing statistical analysis with Student's t-test or multiple t-test and one-way ANOVA.

3.4. RESULTS

3.4.1. Diabetes increases biodistribution of NIR-labeled full-length adiponectin into target tissues

To accurately investigate adiponectin biodistribution, we developed a model using fluorescence molecular tomography (FMT) in which 3-dimensional localization of fluorescently tagged adiponectin could be tracked in short time intervals *in vivo*. Full-length adiponectin comprising of high, medium and low molecular weight oligomers was tagged with a near-infrared (NIR) peptide (VivoTag-S 750) detectable at 750nm (fAd-VT750). This wavelength, and feeding mice with AIN-76A low-chlorophyll chow diet (Harlan, Indianapolis IN), allowed us to avoid confounding effects of autofluorescence (24). Western blot and fluorescent imaging confirmed that all 3 oligomers of adiponectin were fluorophore conjugated (Supplementary Fig 3.1.A), and we demonstrated a linear relationship between adiponectin concentration and fluorescence measurement (Supplementary Fig 3.1.B, C).

To test the hypothesis that hyperglycemia could alter adiponectin biodistribution, we infused fAd-VT750 (85µg, via jugular vein) into STZ injected (STZD) or control nu/nu mice, then monitored whole body fluorescence in mice by FMT imaging. We found no difference in circulating adiponectin levels between control and STZD mice and also observed the same level of fAd-VT750 in serum of either STZD or wt mice 2 min after injection via jugular vein (Supplementary Fig 3.2.A, B). Consecutive FMT images at 0, 10, 30, 60 and 90 min after fAd-VT750 injection showed increasing tissue accumulation of fluorescent adiponectin throughout the body which appeared to be faster or higher in STZD mice (Fig 3.1.A-C), particularly showing enhanced liver and/or heart accumulation relative to controls. FMT imaging confers the added advantage of providing quantitative analysis of whole body fluorescence and clearly measured an increased overall fluorescence intensity in STZD mice. As a control, infused unconjugated VT750 displayed a completely different biodistribution

pattern, clearing quickly through the kidneys and localized primarily to the bladder within 60 min, with very little signal coming from other peripheral tissues (Supplementary Fig 3.3).

To conduct further analysis of the tissue localization of fluorescent signal, mice also underwent x-ray computed tomography (CT) imaging for fluorescence co-registration (Fig 3.1.D). Coronal and sagittal sections of FMT/CT co-registration data showed accumulation of fAd-VT750 in the heart, liver, kidney, and bladder (Fig 3.1.E). To eliminate potential tissue scattering effects, major target tissues of adiponectin action were removed 90 min following fAd-VT750 infusion and imaged ex-vivo by FMT. Heart, liver, kidney, pancreas, and skeletal muscle (Sk M) of STZD mice exhibited a higher fluorescent signal when compared to wt (Fig 3.1.F), although only heart and liver reached significance upon quantitation (Fig 3.1.G). In agreement with this, Western blot analysis of reduced tissue homogenates, to allow detection of all adiponectin as monomers, clearly showed increased levels in all of these target tissues from STZD versus wt at 90min post fAd-VT750 infusion (Fig 3.1.H).

3.4.2. Adiponectin accumulation in the heart is upregulated by STZD

Because the main research focus of our laboratory is cardioprotective effects of adiponectin, we then used FMT-CT co-registered images to quantify the fluorescence contained within a 3-dimensional region of interest mapped to the heart (Fig 3.2.A). FMT quantitation shows that within 10 minutes fAd-VT750 level in STZD hearts was significantly greater than in wt (Fig 3.2.B). Accordingly, area under the curve analysis showed greater accumulation of fAd-VT750 in the hearts of STZD mice (Fig 3.2.C). Immunofluorescent analysis of cross-sections from myocardium also indicated increased fAd-VT750 in STZD mice 90 min post-infusion compared to wt (Fig 3.2.D,E). Interestingly, higher magnification revealed an apparent co-localization of fAd-VT750 with wheat germ agglutinin (WGA), suggesting a near-membrane location.

Since molecular weight could be an important determinant in the movement of the adiponectin isoforms from circulation into the heart, we assessed the amount of fAd-VT750 in perfused heart homogenates from control and STZD mice under non-denaturing conditions. There was an increased presence of all three oligomeric adiponectin isoforms in STZD heart homogenates when compared to wt (Fig 3.2.G). To verify that increased fAd-VT750 localization was not influenced by presence of the VivoTag-750 fluorophore, Flag-tagged and non-fluorescent recombinant adiponectin was injected into wild-type C57BL/6 mice treated with or without STZ. Similar to fAd-VT750, there was increased total heart localization of Flag-adiponectin in STZ treated mice compared to controls (Fig 3.2.F). Quantitative PCR analysis showed no difference in adiponectin mRNA levels between control and STZD cardiac homogenates (Fig 3.2.H).

3.4.3. High glucose levels regulate claudin-7 expression to increase paracellular movement of adiponectin

We next tested vascular permeability of adiponectin using mesenteric arteries isolated from STZD or control mice. Similar to our *in vivo* findings, adiponectin flux across the arterial wall of STZD mesenteric arteries was greater compared to wt (Fig 3.3.A). We then exposed a monolayer of human dermal endothelial cells (HDMECs) cultured on trans-well inserts to high glucose and found that flux of adiponectin, added to apical chamber, was higher than in normal glucose conditions. Fig 3B shows a Western blot, with quantitation below, indicating a significant increase in flux of HMW-, MMW-, and LMW-adiponectin from apical to basolateral side in cells grown under hyperglycemic conditions (Fig 3.3.B). Immunoblotting of the adiponectin receptors AdipoR1 and AdipoR2 showed that their expression in HDMEC monolayers was not affected by high glucose (Supplementary Fig 3.4.C). Accordingly, we found that endothelial barrier tightness measured by trans-endothelial electrical resistance (TEER) was decreased in high glucose treated cells (Fig 3.3.C). This corresponded to a decrease in claudin-7 (cldn-7) mRNA and protein expression following high

glucose treatment (Fig 3.3.D, E). Immunofluorescence imaging indicated a decrease in cell membrane expression of cldn-7 in high glucose treated cells compared to control (Fig 3.3.F), whereas there was no difference in expression of another tight junction related protein, ZO-1, between groups (Fig 3.3.G). This observation was mirrored when heart homogenates were analyzed. Protein and mRNA levels of adiponectin receptors were unchanged by STZD (Supplementary Fig 3.4.A,B). In cardiac tissue sections analyzed by qPCR for mRNA and immunohistochemistry, ZO-1 level was not significantly lower (Fig 3.3.J, K) while cldn-7 expression was significantly decreased (Fig 3.3.H, I) in STZD hearts compared to wt.

3.4.4. Reduced claudin-7 expression decreased TEER and enhanced adiponectin movement across endothelial monolayer

To test the functional importance of cldn-7 in adiponectin flux across an HDMEC monolayer, knockdown of cldn-7 was induced by transfection of shRNA (shCLDN7), which resulted in approximately 50% decrease in cldn-7 protein compared to cells that received a scrambled shRNA sequence not targeting cldn-7 (shNTC) (Fig 3.4.A). TEER was significantly decreased in monolayers comprised of shCLDN7 cells compared to shNTC (Fig 3.4.B). Furthermore, there was increased flux of LMW-adiponectin from apical to basolateral side of monolayers comprised of shCLDN7 cells compared to shNTC controls (Fig 3.4.C).

3.4.5. Functional 3D perfusable microvascular networks allowed to confirm hyperglycemia effect on permeability of dextran and adiponectin

We finally tested the hyperglycemia effect in microfluidic microvascular network of HUVECs (human umbilical vein endothelial cells). This in vitro platform of 3D vasculature-on-a-chip was generated in the ECM mimetic environment with fibrin hydrogel. PDMS (polydimethylsiloxane) microfluidic device is useful to induce perfusable microvasculature as well

as to monitor the event inside of the highly branched vascular structure. The PDMS mold has a central gel channel containing HUVECs and fibrin hydrogel bordered by triangular posts and two media fluid channels (Fig 3.5.A,B). 1.4 x 10^7 cells/mL of HUVECs were seeded with the fibrin hydrogel at D0 and incubated for 4 days to form endothelial monolayers of in vivo-like vasculature naturally (Fig 3.5.C). Additional VEGF was used to increase the dynamic alignment of HUVECs from D0 to D4 (Fig 3.5.D). At day 4, the formation of open-ended EC monolayer 3D vessels between two PDMS posts were completed. GFP transfected HUVECs showed highly branched features of microvascular networks in a device (Fig 3.5.E) and vascular endothelial cadherin (VE-Cadherin) positive stained structures indicated that vessel-like EC monolayer barrier allows the perfusion of fluids (Fig 3.5.F, Supplementary Video 3). To confirm the functionality of this vasculature, we performed perfusibility test with 5 μm beads conjugated with FITC and timelapes images were taken under fluorescence exposure at every 1.4 sec (Fig 3.5.G, Supplementary Video 4). Next, we wanted to test the effect of hyperglycemia on permeability of 3D microvascular networks using full length adiponectin (fAd) and changes of paracellular movement across of this barrier with 3, 70kDa dextran. Immunofluorescent detection of VE-C showed that the integrity of interconnected vascular structures appeared not to loosen in hyperglycemia compared to control (Supplementary Fig 3.5). To assess the permeability, 10 μg/mL fAd conjugated with rhodamine was injected into one reservoir of a device and fluorescent images were captured overtime. The apparent permeability (Papp, cm/sec) was calculated by the fluorescent intensity measurement from a linear ROI spanning the microvessel-ECM interface. Because the perfused fluorescent molecules were transmoved to ECM from the vessels by concentration gradient, the intensity increase was observed in ECM area overtime (Fig 3.5.H). Permeability of rhodamine labeled fAd (Rho-fAd) increased in hyperglycemia (1.285 x 10^{-5} ± 0.09363 x 10^{-5} cm/sec) compared with 19.5mM mannitol with 5.5mM glucose treated control (2.290 x 10^{-5} ± 0.1651 x 10^{-5} cm/sec) (Fig 3.5.K). 70kDa Dextran which is smaller than LMW adiponectin (around 90kDa) also showed significantly higher permeability in high glucose treated

condition (Papp of HG was $6.812 \times 10^{-5} \pm 1.152 \times 10^{-5}$ cm/sec and control Papp was $2.180 \times 10^{-5} \pm 0.2277 \times 10^{-5}$ cm/sec) (Fig 3.5.J). However, for the small size of dextran (3kDa-FITC), hyperglycemia did not significantly change the permeability (Fig 3.5.I). These suggested that paracellular movement regulates transendothelial accessibility depending on the size of molecules. And it confirmed that hyperglycemia *in vitro* with 25mM glucose altered the movement of full-length adiponectin in microfluidic vessels-on-a-chip.

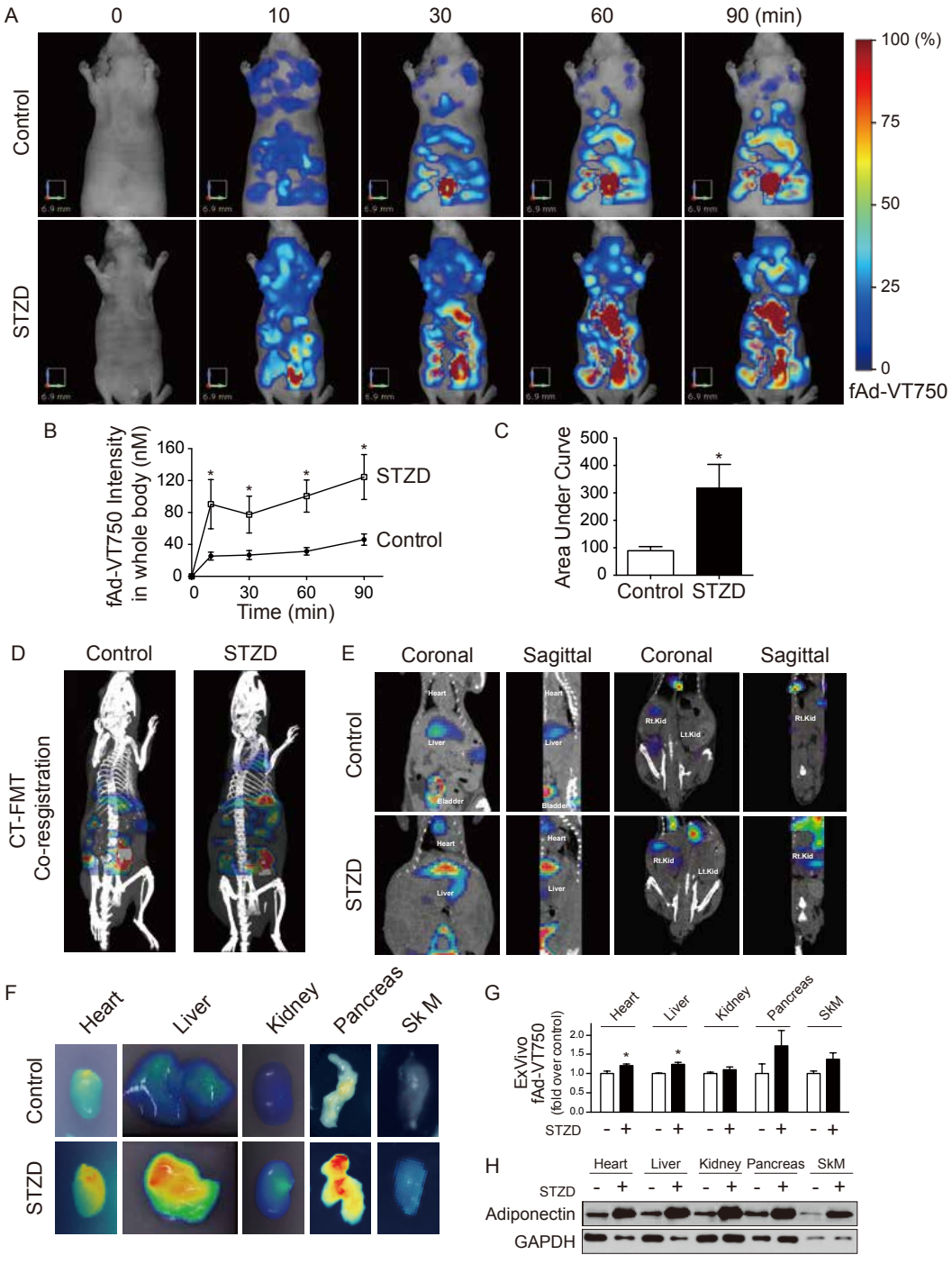
A
0
10
30
60
90 (min)
Control
STZD
100 (%)
75
50
25
0
fAd-VT750
B
fAd-VT750 Intensity in whole body (nM)
160
120
80
40
0
0
30
60
90
Time (min)
STZD
Control
C
Area Under Curve
500
400
300
200
100
0
Control
STZD
D
Control
STZD
CT-FMT Co-resgistration
E
Coronal
Sagittal
Coronal
Sagittal
Control
STZD
Heart
Liver
Bladder
Rt.Kid
Lt.Kid
F
Heart
Liver
Kidney
Pancreas
Sk M
Control
STZD
G
ExVivo fAd-VT750 (fold over control)
Heart
Liver
Kidney
Pancreas
SkM
2.0
1.5
1.0
0.5
0.0
STZD
- + - + - + - + - +
H
Heart
Liver
Kidney
Pancreas
SkM
STZD
- + - + - + - + - +
Adiponectin
GAPDH

Figure 3.1. Fluorescence molecular tomography shows *in vivo* biodistribution of full-length adiponectin is increased in diabetic conditions. (A) 85 µg of near-infrared labeled full-length adiponectin (fAd-VT750) was injected via cannulated jugular vein into control or diabetic (STZD) nu/nu mice. Representative images from a control and STZD mouse before injection and at 10, 30, 60, and 90 minutes post-injection are shown. (B, C) Total signal intensity from whole body 3D field of view were calculated as nM ($n \geq 8$, $^*p<0.05$ from multiple t-test). Time course data was converted to area under curve (AUC) ($^*p<0.05$ from student t-test). (D) Co-registration of FMT (colour) and computed tomography (CT) data (white/grey). (E) Coronal and sagittal view of FMT-CT co-registration with organs of interest identified. (F) Ex-vivo 2D FMT analysis of fAd-VT750 from isolated tissues (heart, liver, kidney, pancreas and skeletal muscle (tibialis anterior)). (G) Quantification of these 2D images using TrueQuant software. * indicates $p < 0.05$, compared to its control ($n \geq 4$). The p values were given by student t-test. (H) Cardiac homogenates from control and STZD mice were analyzed by Western Blot under non-denaturing conditions to compare total amount of reduced (i.e. monomeric, 30 kDa) adiponectin.

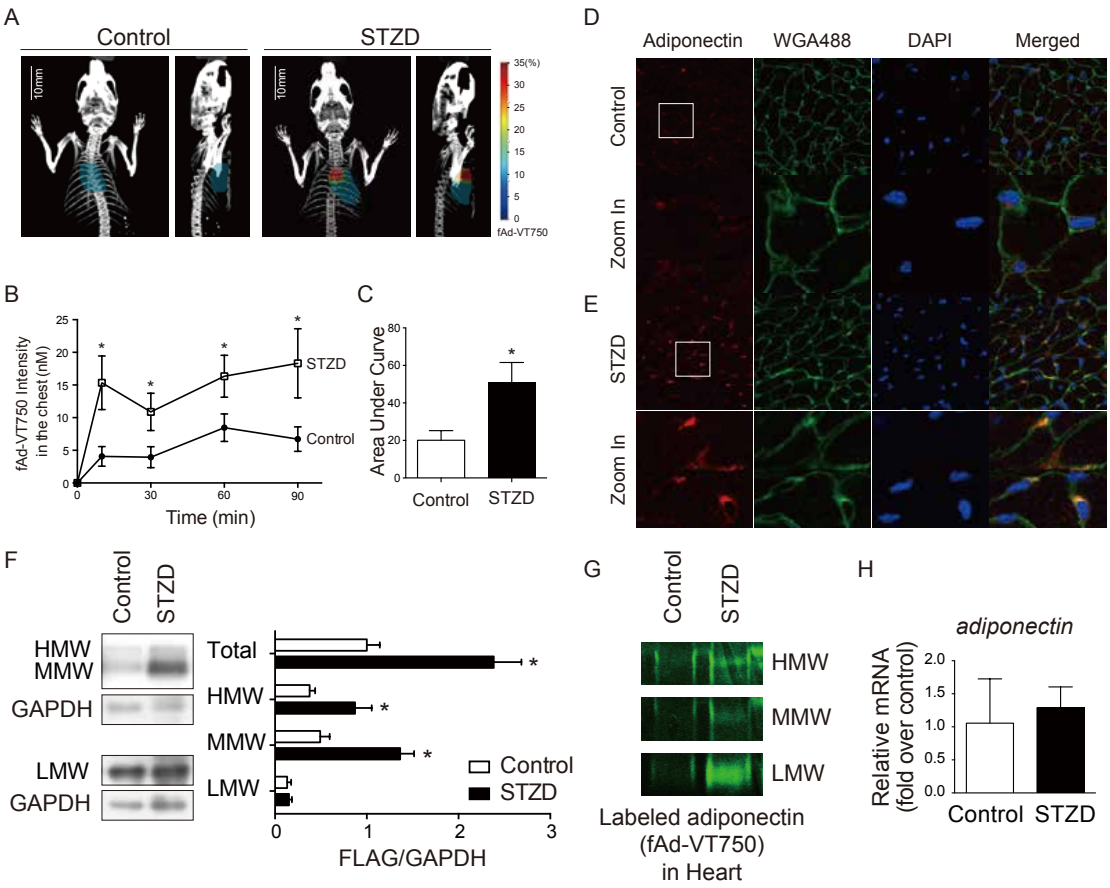
A
Control
STZD
10mm
35(%)
30
25
20
15
10
5
0
fAd-VT750
B
fAd-VT750 Intensity in the chest (nM)
STZD
Control
Time (min)
C
Area Under Curve
Control
STZD
D
Adiponectin
WGA488
DAPI
Merged
Control
Zoom In
E
STZD
Zoom In
F
Control
STZD
HMW
MMW
GAPDH
LMW
GAPDH
Total
HMW
MMW
LMW
Control
STZD
FLAG/GAPDH
G
Control
STZD
HMW
MMW
LMW
Labeled adiponectin (fAd-VT750) in Heart
H
adiponectin
Relative mRNA (fold over control)
Control
STZD

Figure 3.2. Adiponectin uptake into the heart is increased by diabetes.

(A) Representative heart regions of interest (ROIs) generated by alignment of CT and FMT 3D images using IRW software. (B) Quantitation of fAd-VT750 within mapped ROIs. Fluorescence intensity of localized fAd-VT750 (nM) was calculated over time by FMT-CT co-registration analysis ($n \geq 8$). * indicates $p<0.05$ with respect to control at each time point and the p values were from the multiple t-test. (C) Area under curve analysis of fAd-VT750 within the heart ROI (*$p<0.05$) (D, E) Immunofluorescence analysis of transverse heart cryosections stained with adiponectin (red), Wheat Germ Aglutinin (WGA, green), and DAPI (blue). Co-localization of adiponectin and WGA appear orange. (F) Cardiac homogenates from C57BL/6 mice 90 minutes following Flag-tagged adiponectin infusion, run under non-denaturing conditions by SDS-PAGE to detect different adiponectin oligomers: High-Molecular Weight (HMW, >250 kDa), Mid-Molecular Weight (MMW, ~180 kDa), and Low-Molecular Weight (LMW, ~90 kDa). Total adiponectin combines densitometry from all three oligomers, adjusted to GAPDH as loading control (n=5, *$p<0.05$). The quantification analyzed by multiple t-test. (G) Detection of fAd-VT750 by SDS-PAGE in heart homogenates from nu/nu mice 90 min post fAd-VT750 infusion. (H) Real-time quantitative PCR analysis of heart homogenates 90mins post-injection adjusted for GAPDH (n=5).

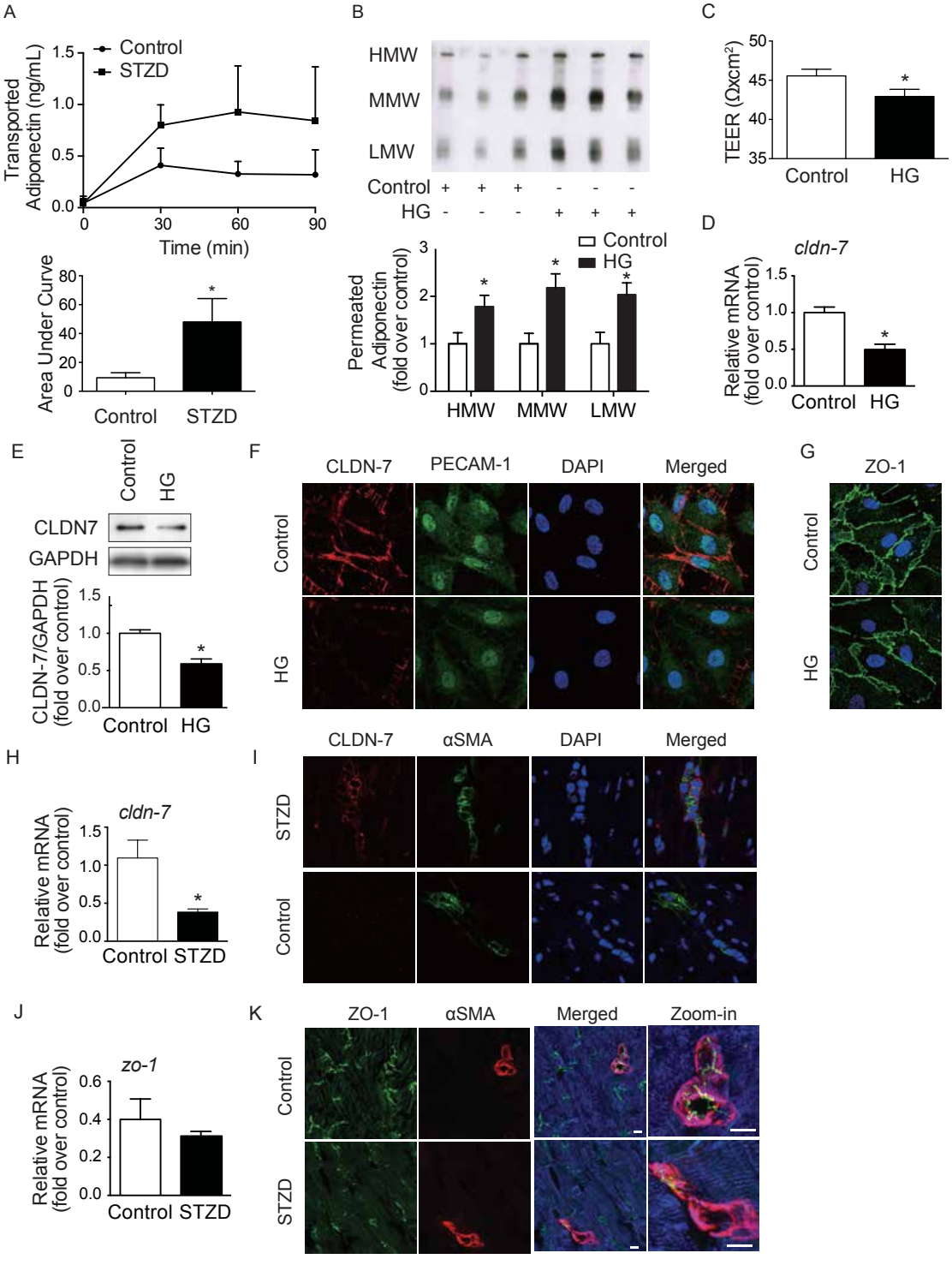
A
Transported Adiponectin (ng/mL)
Control
STZD
Time (min)
Area Under Curve
Control
STZD
B
HMW
MMW
LMW
Control
HG
Permeated Adiponectin (fold over control)
HMW
MMW
LMW
C
TEER (Ωxcm²)
Control
HG
D
cldn-7
Relative mRNA (fold over control)
Control
HG
E
Control
HG
CLDN7
GAPDH
CLDN-7/GAPDH (fold over control)
F
CLDN-7
PECAM-1
DAPI
Merged
Control
HG
G
ZO-1
H
cldn-7
Relative mRNA (fold over control)
I
CLDN-7
αSMA
DAPI
Merged
STZD
Control
J
zo-1
Relative mRNA (fold over control)
K
ZO-1
αSMA
Merged
Zoom-in
Control
STZD

Figure 3.3. Hyperglycemia reduces Claudin-7 expression and permits greater flux of adiponectin movement across the endothelium. (A) Mesenteric arteries extracted from control or STZD rats were perfused with flag-tagged fAd, with samples of extravascular fluid taken at 30, 60, and 90 minutes post adiponectin and analyzed by ELISA. AUC analysis shows greater adiponectin flux from STZD arteries vs control ($n \geq 5$, $^*p<0.05$). (B) HDMEC cells were cultured in a transwell insert before treatment with high glucose (HG) or control. Adiponectin was added to the apical surface then basolateral media was collected 24hr following adiponectin administration. Samples were run under non-denaturing conditions. ($n=3$, * indicates $p<0.05$ with respect to each adiponectin isomer's control.) (C) TEER (transendothelial electrical resistance) was lower in hyperglycemia significantly ($^*p<0.05$, $n \geq 11$). Claudin-7 in hyperglycemia treated endothelial cell also decreased at (D) *cldn-7* mRNA expression ($^*p<0.05$, $n=4$) as well as (E) CLDN-7 protein expression ($^*p<0.05$, $n=3$). (F) Lower CLDN-7 was localized on cell membrane in hyperglycemia. CLDN-7(red) and PECAM-1(green, endothelial marker) are co-staining in HDMEC. (G) However, ZO-1 (green) aligned underneath of cell membrane was not changed by HG treatment. As same as mouse hearts, (H) *cldn-7* mRNA level decreased in diabetic heart induced by STZ ($n=5$, $^*p<0.05$), (J) but no significant different was shown in *zo-1* mRNA level ($n=4$). (I) And lower CLDN-7(red) surrounded by alpha-SMA (green) was observed in heart tissue sections from STZD, (K) although there was no difference of ZO-1. Immunostaining for ZO-1 (green) to identify endothelial cell-specific tight junction structure, α-SMA (red) to identify vascular smooth muscle cells, and desmin (blue) to identify cardiomyocytes. Shown are representative images of $n=3$ mice per experimental group. High magnification images show junction formation between endothelial cells in small vessels. Scale bars: 50 μm and 150 μm, respectively. And all the p values were analyzed by student t-test.

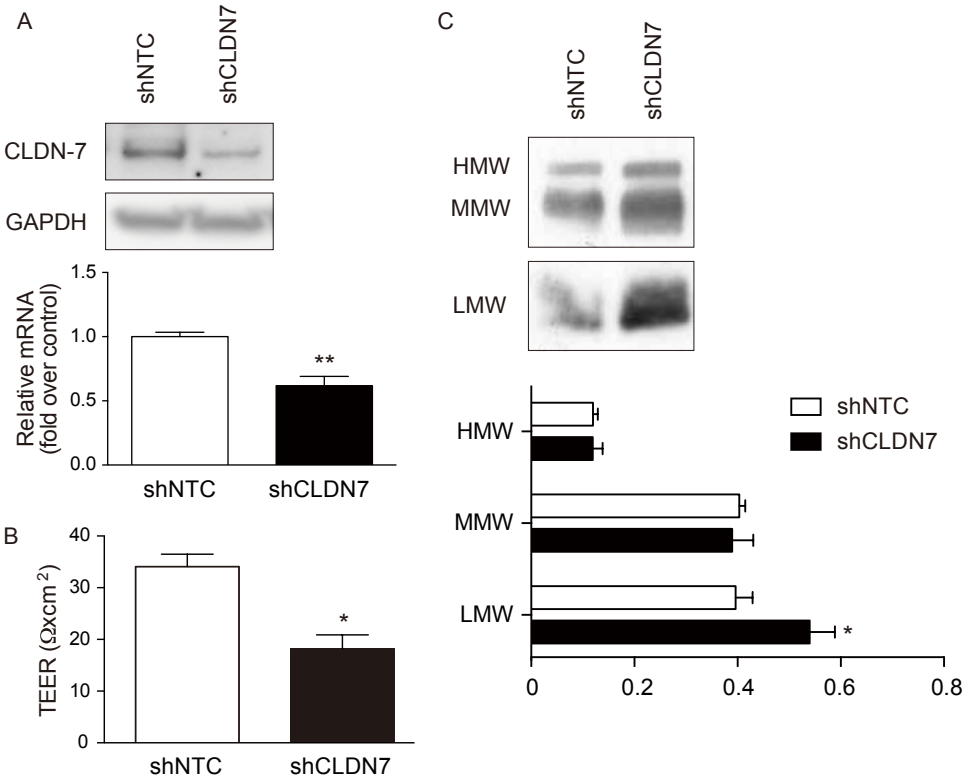

Figure 3.4. Reduced CLDN-7 expression decreased TEER and increased LMW of adiponectin movement across monolayer of HDMECs. (A) One of major component of tight junction proteins, CLDN-7, was targeted to knock down by shRNA transfection after 96h. Transfected HDMECs were transferred into transmembrane culturing system (0.9cm^2) and formed monolayer 72h after transfection. The cells having lower CLDN-7 expression (**$p<0.01$, $n=3$) showed (B) significantly lower TEER (*$p<0.05$, $n\geq7$). TEER was measured at 96hr later from transfection starting. (C) The monolayer of CLDN-7 knockdown HDMECs were used for adiponectin permeability assay for 24hr. The decreased CLDN-7 led adiponectin movement increase, especially in LMW form with statistical significance (*$p<0.05$, $n\geq5$). The values were mean ± SEM and p values were given by statistical analysis from student's t-test.

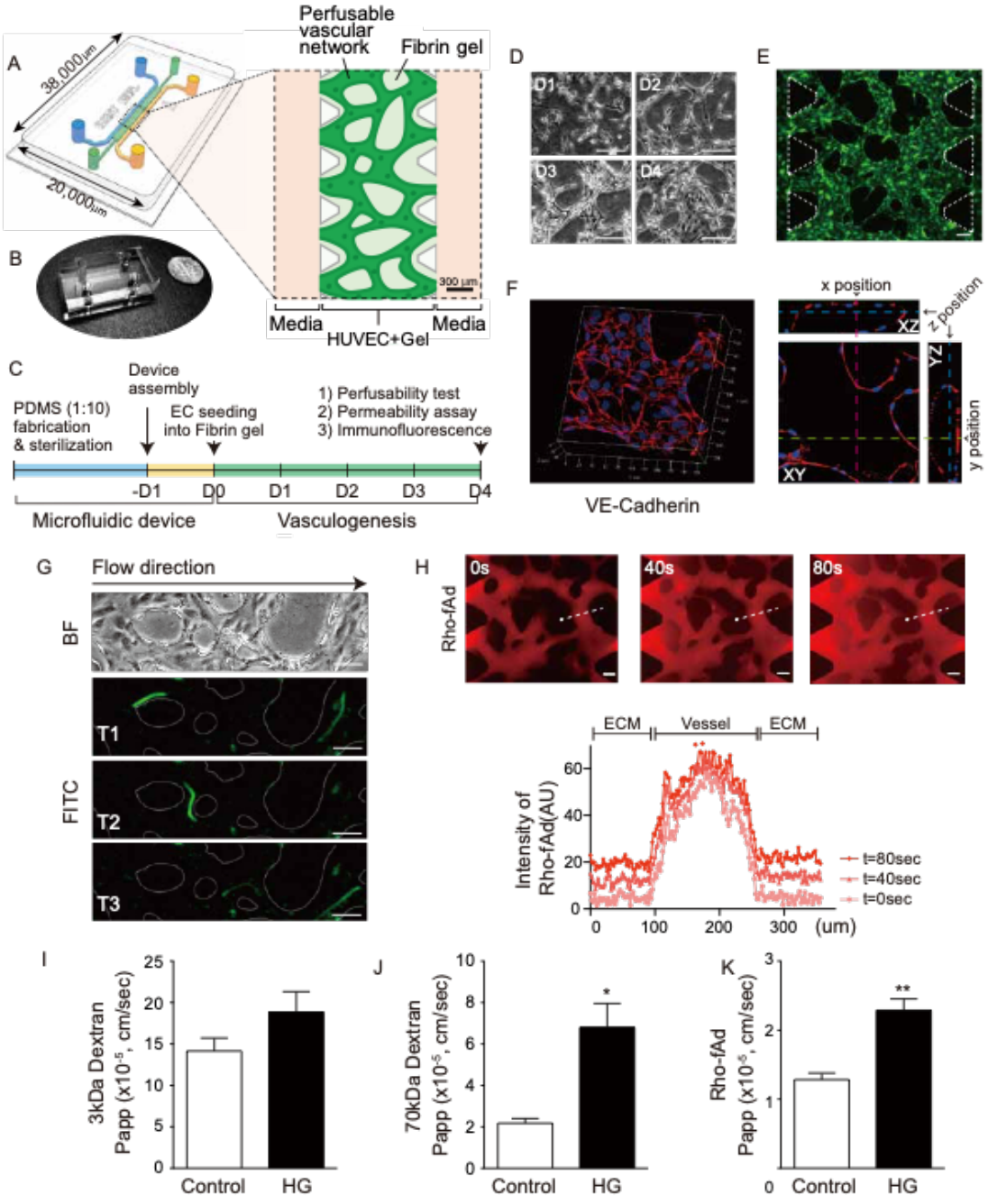

Figure 3.5. Functional 3D microvascular networks of HUVECs in ECM/fibrin hydrogel showed permeability alteration depending on molecular sizes as well as hyperglycemia effect.

(A) Schematic representation of 3D perfusable microvascular network model with HUVECs in a

PDMS (polydimethylsiloxane) microfluidic device. The PDMS mold has a central gel channel containing HUVEC cells and fibrin hydrogel bordered by triangle posts. The HUVEC/fibrin gel channel is flanked on both sides by fluid channels leading to four reservoirs filled with culture medium. (B) A device photo is shown with the area dimension (20,000 μm x 38,000 μm) and a dime as size reference. (C) Experiment timeline is shown. (D) Daily images (D1-D4) of HUVECs in the 3D fibrin gel shows cellular alignment dynamics during vasculogenesis (10X magnification was used). (E) The continuously GFP expressed HUVECs showed the perfusable vasculature on day 4. (F) Confocal reconstructed 3D image of VE-Cadherin (Red) stained with nucleus (DAPI, blue). A single plane from the stacked images showed three ortho-positions (x position/pink at 570 μm, y position/green at 700 μm and z position/blue at 18 μm) of continuous endothelial hollow. (G) To confirm the generated 3D vessels were perfusable, 5 μm beads conjugated with FITC were loaded into one reservoir and timelapes images were taken under fluorescence using Axio Observer Z1 microscope. (Time interval average was 1.4 sec.) (H) Rhodamine labeled full-length adiponectin (Rho-fAd, red) was injected with a concentration of 10 μg/mL. Fluorescent images were captured every 6-10 sec for 3 min from 2 or 3 different fields of view. Three representative images are shown at 0, 40, and 80 sec post infusion. To assess permeability, fluorescent signal intensity (AU) was quantified along a linear ROI spanning the microvessel-ECM interface as shown, and depicted as a distance from the ROI origin (closed circle). Permeabilized fluorescent signal were observed in the ECM (out of vessel) area overtime. Apparent permeability (Papp) was quantified using ImageJ with measurement from randomly selected ROIs. Hyperglycemia with 25mM glucose (J) did not change the permeability of 3kDa-FITC dextran. However, (I) 70kDa-Texas Red dextran and (K) Rho-fAd increased Papp significantly in high glucose (HG) treated condition. (D, E, G, H) The scale bar indicates 100 μm. (I-K) Data presented mean values ± SEM and error bars. Statistical evaluation was done by t-test with the values from 15-25 ROIs (4-6 different fields of view of 2-3 devices) for each condition. * indicates $p=0.0005$ and ** indicates $p<0.0001$.

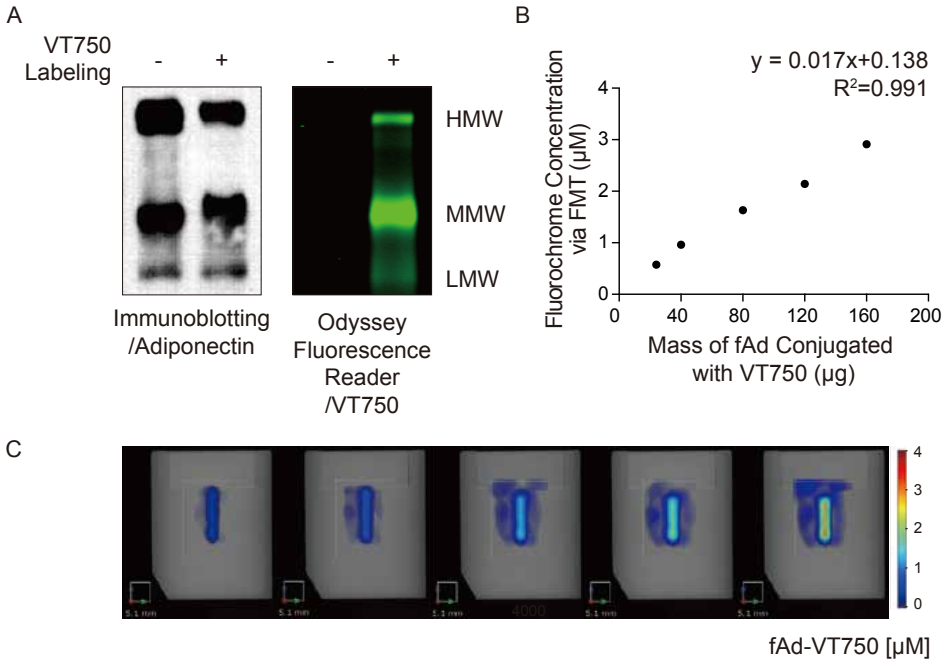

Supplementary Figure 3.1. Full-length adiponectin (fAd) conjugated with VivoTag750 had 3 different forms by adiponectin oligomerization (LMW, MMW and HMW) and gave a linear slope of signal intensity depending on concentration of fAd. (A) To confirm the labeled adiponectin, non-labeled fAd and VT750-conjugated fAd were separated side by side in a SDS-PAGE gel and scanned by Li-Cor image scanner. Then, the both separated fAds were transferred from the SDS-PAGE gel into PVDF membrane to be detected by adiponectin antibody via immunoblotting. It was confirmed that the labeled fAd had 3 different forms as same as non-labeled fAd. (HMW >250 kDa, MMW ~180 kDa and LMW ~90 kDa) (B) To assess the meaning of signal intensity with labeled adiponectin from the field of view under FMT system, fluorochrome concentration was measured in dose dependent conditions. It showed linear regression with R^2=0.991 of the trendline. (C) FMT imaging was taken using a pin-channel imaging block and VT750-conjugated fAd was diluted serially in the range of 0 to 160 μg.

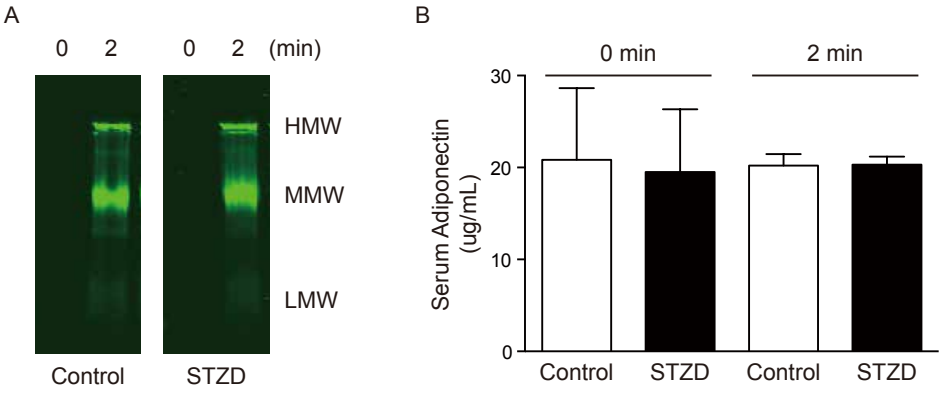

Supplementary Figure 3.2. Equal amount of VT750-conjugated fAd was infused into mice via jugular vein cannula. Serum samples were collected before adiponectin infusion (0min) as well as right after within 2 min. (A) The serum samples were separated in SDS-PAGE gel and scanned it with LiCor imager. 3 forms of labeled adiponectin were only detected from 2min samples with no different level of fluorescence intensity from control vs STZD animals. (B) Before labeled-adiponectin infusion, basal level of circulatory adiponectin amount was compared from control and diabetic, 4 days post induced from 150μg/g STZ injection by i.p., individuals (n>3). Serum level of adiponectin was measured by ELISA. At the same time, the total adiponectin level from the serum showed no changes in STZD mice comparing to control after labeled adiponectin infusion (at 2min).

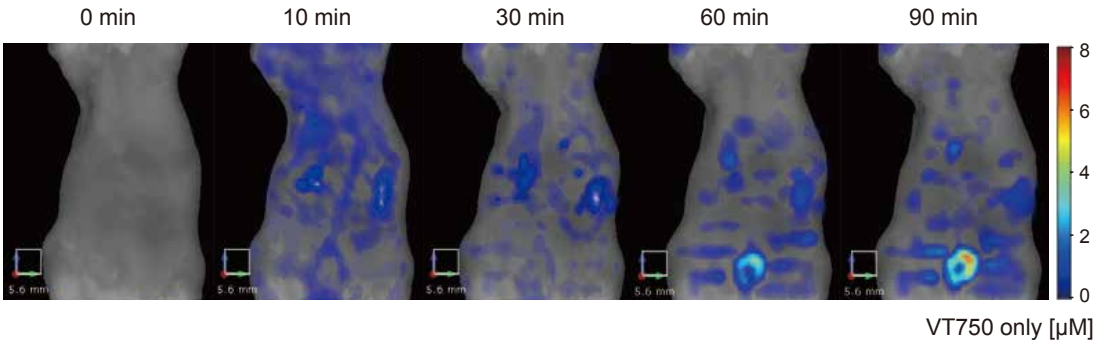

Supplementary Figure 3.3. FMT 2500 system could monitor biodistribution of VT750 over time in a mouse. To validate feasibility of biodistribution monitoring with NIR probe, 2 nmol of protein free VT750 only was infused into mouse via tail vein and imaging with FMT was taken at 0, 10, 30, 60, and 90 min. The pattern of VT750's circulation and accumulation was observed.

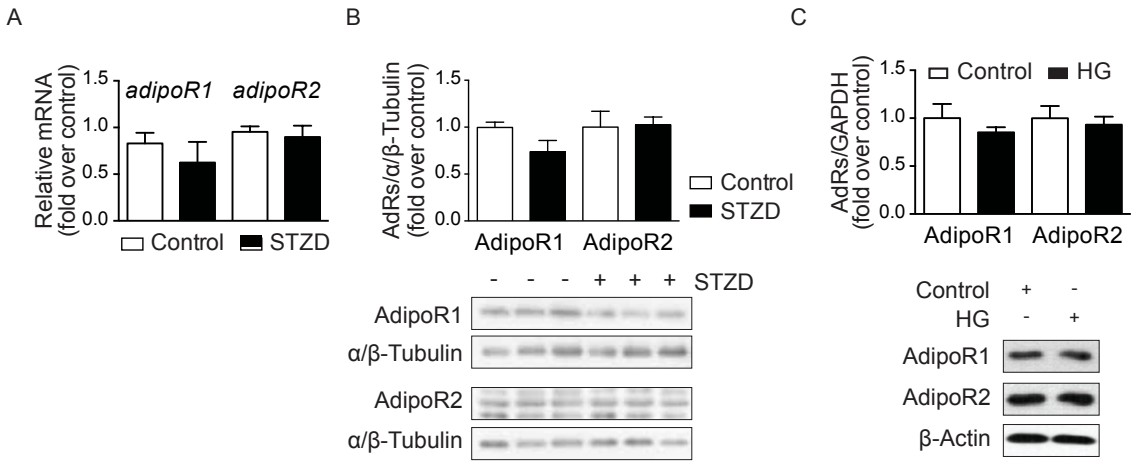

Supplementary Figure 3.4. Hyperglycemia did not change adiponectin receptors. In mouse hearts, STZ-induced hyperglycemina did not change AdipoR1 and AdipoR2 (A) mRNA and (B) protein expression. **(C)** As same as HDMEC, expression of adiponectin receptors (AdipoR1 and AdipoR2) were not changed in between hyperglycemia and control. (n=4)

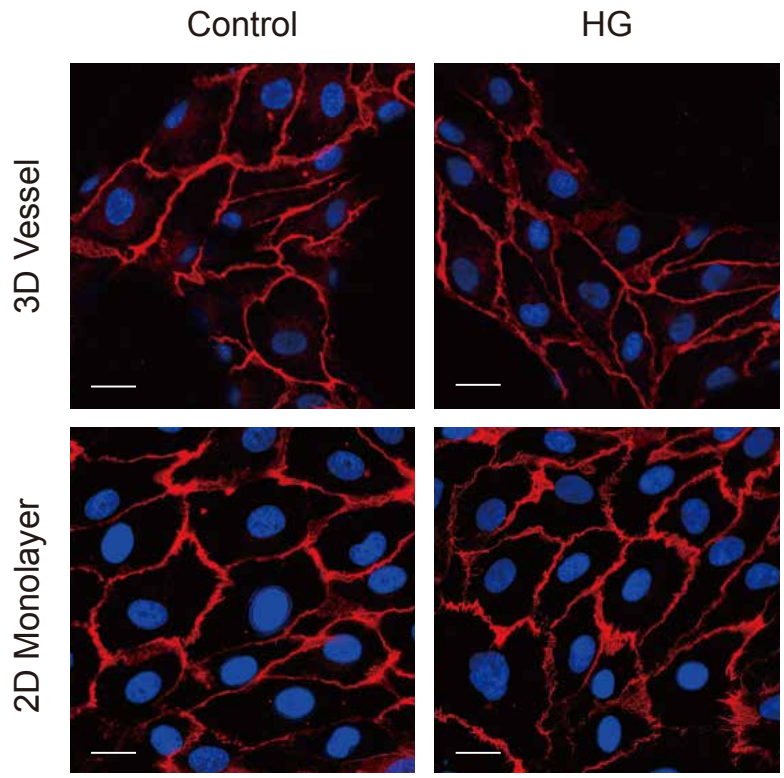

Supplementary Figure 3.5. Vasculature of HUVECs on a chip. VE-Cadherin(red) was stained with DAPI(blue) after 96hr cell culture (at D4) with 50 ng/mL VEGF. During 4 days vasculature formation in hyperglycemia, the integrity of VE-C did not change when it compared to control in 2D endothelial monolayer of HUVECs as well as 3D perfusable vessels of HUVECs. All scale bars indicate 200 μm.

Supplementary Video 3.6. 3D reconstruction of FMT/CT co-registration for control mouse. Vehicle only infused subject was used. FMT data from Infused VT-750 labeled fAd indicates in color, and computed tomography (CT) data showed in white/grey.

Supplementary Video 3.7. 3D reconstruction of FMT/CT co-registration for STZD mouse. Rotated movie showed higher intensity of VT-750 labeled fAd (color) than control subject from FMT data. White/grey scale indicates CT data.

Supplementary Video 3.8. 3D perfusable vasculature of HUVECs. The confocal reconstruction showed 3D microvasculature with VE-Cadherin (Red) and nucleus (DAPI, blue) staining, which has a perfusable lumen aligned with interconnected endothelial cells.

Supplementary Video 3.9. Perfusion of 5μm beads conjugated with FITC in microvascular network. FITC polystyrene particles flow through the continuous 3D microvasculature.

3.5. DISCUSSION

Adiponectin has been shown to mediate widespread physiological effects with resulting anti-diabetic, anti-inflammatory and cardioprotective effects (73). Hence, there has been great interest within academic institutes and pharmaceutical companies to develop therapeutics targeting adiponectin action. To accomplish this, it is critical to fully understand the mechanisms regulating adiponectins cellular effects in various tissues. Whilst we have learned much about adiponectin receptor mediated signaling mechanisms, few studies have focused on examining mechanisms regulating the transit of adiponectin from the circulation to the interstitial space, and thus target cells such as cardiomyocytes, hepatocytes, beta-cells and other cells. We previously proposed that vascular permeability was likely to be an important, and underappreciated, determinant of adiponectin's physiological actions (316). This is particularly relevant since adiponectin is a complex molecule comprised of multiple oligomeric forms, each with a different molecular weight and radial size estimated to be 3.96 to 10.1 nm (222). This is exactly the range within which tight junctions of around 4nm in dimension can be expected to strongly contribute to dictating adiponectin flux. Indeed, we recently demonstrated that glucocorticoid-mediated decreases in transcellular endothelial permeability restricted adiponectin transit across endothelial monolayers (58). The observation that adiponectin in cerebrospinal fluid is almost completely in the small trimeric form, and the total amount is only 0.1% of that in peripheral circulation (145), suggests that the tight blood brain barrier restricts movement of adiponectin oligomers. Conversely, many studies focusing on metabolic effects of adiponectin have focused on liver, which has a highly fenestrated leaky vasculature, and found that the high molecular weight adiponectin is highly bioactive and correlates well with clinical readouts of liver function (50, 259).

In this study, we used a real time non-invasive approach to monitor and quantify the biodistribution of exogenously administered fluorescent adiponectin. The use of FMT as a non-invasive approach to examine biodistribution of a circulating hormone such as adiponectin has strong

advantages (276). The ability to monitor individual mice non-invasively for time-course studies vastly reduces the number of animals required and avoids issues such as inter-animal metabolic variation and variability in fluorophore injection. In addition, time and expense of isolating numerous tissues followed by analysis by western blot can be a significant limiting factor to the identification of novel target tissues. Having a clear, temporal, whole-body indicator of kinetics can provide a wealth of mechanistic insight, potentially leading to new therapeutics. In this study, we complemented FMT imaging with CT, which offered us high-resolution anatomical detail to improve the spatial and temporal localization of adiponectin. Analysis of co-registered FMT-CT data improves upon methodologies which offer only 2D fluorescence acquisition. Through 3-dimensional analysis, we were able to precisely quantify fAd-VT750 in the heart through creation of CT-guided 3D regions of interest (ROIs). This is vital for accuracy as many factors can impair rough localization of a fluorophore including: mouse orientation, variability in organ size, potential "bleed over" from highly targeted tissues (e.g. liver), and spatial overlap of several tissues such as the lungs, heart and thymus, from certain mouse orientations. Analysis of our *in vivo* findings were substantially corroborated by *ex vivo* scanning of target tissues and classic molecular biology techniques including western blot analysis and immunofluorescence imaging. For fluorescence *in vivo* imaging of whole body biodistribution, it is important to avoid autofluorescence which requires near-infrared (NIR) labeling of a target (24). Probes and fluorophores are available in this range, from 680 to 750nm and 800nm, offering the potential for some creative multiplexing studies such as co-tracking of insulin and adiponectin in circulation under various disease models. Imaging at 750-800nm wavelengths completely avoids autofluorescence, and imaging at 680nm only requires the use of low-chlorophyll chow to minimize confounding gastrointestinal background fluorescence.

Using this approach, we studied mice with or without streptozotocin-induced diabetes. Interestingly, an accumulation of adiponectin occurred in the peripheral tissues, particularly liver, and to a greater extent in STZD mice. This was confirmed by quantitative analysis of in vivo FMT

images, ex vivo imaging and by analyzing tissue homogenates by Western blot. It was also interesting to note that we found no difference in endogenous adiponectin between control and STZD animals. As we are interested in the cardioprotective effects of adiponectin(71, 90) when we focused on myocardial adiponectin we again found greater levels in STZD mice. The increased total amount of fAd-VT750 appeared to be accounted for by MMW, plus HMW and to a lesser extent LMW oligomeric forms. It is worth noting that the relative tightness of an endothelial barrier, whether *in vivo*, *ex vivo*, or *in vitro*, and the amount of change induced by a given treatment (e.g. high glucose), can lead to seemingly contradictory results such as the data presented here (Fig 3.2.E vs Fig 3.4.C). This may be explained through an understanding of protein flux dynamics at the cell junction level: slight opening of a tight endothelial barrier may lead to increased flux of only low-molecular weight proteins, while with a leakier barrier, the flux of low-molecular weight proteins may already be maximum. In this case, further opening of a leaky barrier would manifest as increased flux of only higher-molecular weight proteins. STZD is a common diabetic animal model yet data must be interpreted with caution since numerous endogenous changes beyond hyperglycemia may impact vascular permeability (37, 38, 213, 287). It would be of great interest to examine the same phenomenon studied here in models such as high fat diet feeding or in genetically obese models such as *ob/ob* mice (121). Nevertheless, to extend our observations further we examined flux of adiponectin upon addition to isolated mesenteric vessels from wt or STZD animals. We observed again that vascular permeability of adiponectin was higher in STZD vessels. Furthermore, using an endothelial cell monolayer system *in vitro* we found that flux of adiponectin was significantly greater in monolayers cultured in high glucose media versus normal glucose. Collectively, the data suggests that in the STZD model hyperglecemia is likely to be one of the principal determinants of altered vascular permeability of adiponectin.

In this study we also focused on alterations in tight junction proteins as a potential mechanism underlying the effects observed here. We focused on claudin-7 based on rationale from

previous studies which showed that shRNA-mediated reduction in endothelial cell claudin-7 levels increased flux of adiponectin across endothelial monolayers (58). Indeed, our data indicated that a decrease in claudin-7 may be one important alteration leading to incresed vascular permeability in STZD mice. Furthermore, we found ZO-1 was not significantly changed in STZD hearts although previously, hyperglycemia was shown to increase permeability of the blood brain barrier (99), and retinal pigment epithelial cells (99, 278) through downregulation of occludin and ZO-1. Since AdipoR-mediated endocytosis has been shown to have important cellular signaling consequences we also believed that this may contribute to a transcellular route of transport (65, 316). However, our data in supplementary figure 4 showing no significant change in the level of cardiac AdipoR1 or AdipoR2 after hyperglycemia in mice or high glucose level in HDMEC, suggests this is likely not a major player.

We used advanced *in vitro* platform of 3D microvascular networks on a chip to confirm the observation from 2D transwell endothelial monolayer responses in high glucose environment. Generating endothelial monolayer of 3D vessels with multiple branches using programmed cellular dynamics in hydrogel allows to mimic better *in vivo* vascular morphology (130). Another strength of the 3D microvasculature in microfluidic devices is having perfusibility, which allows to test the functionality of the vessels on a chip as well as to better mimic physiological environment with application of fluidic shear stress (119, 131, 294). Using paracellular tracers, many literatures have shown that the basal permeability of comparably large molecules (40, 70kDa dextran) was lower than the permeability of smaller one (4, 10kDa dextran) (84, 104, 118). In this study with the platform, we found that HUVECs exposed to high glucose or the same osmotic pressured control condition showed size-selective behavior where larger molecules, 70kDa dextran and rhodamine labeled full-length adiponectin (~90, ~180, > 280kDa), have smaller permeability than smaller ones, 3kDa dextran. And the access of 70kDa dextran and rhodamine labeled full-length adiponectin was significantly impacted by hyperglycemia-mediated alteration of endothelial permeability.

In summary, we have shown that biodistribution of adiponectin can be altered in a diabetic environment. Data from a combination of temporal non-invasive imaging in mice, isolated vessels *ex vivo* and *in vitro* endothelial cell monolayers suggest that hyperglycemia increased vascular flux of adiponectin. We believe this may be an important determinant of adiponectin's physiological actions and could provide rationale for further investigation and be exploited from a therapeutic perspective.

CHAPTER FOUR: STUDY 3

The study of transendothelial hormone flux in iron overload using endothelial monolayers and microfluidics of 3D perfusable microvascular networks

Nanyoung Yoon[1], Seunggyu Kim[1], Jessie S. Jeon[2], Gary Sweeney[1]

[1]Department of Biology, York University, Toronto, ON, Canada

[2]Department of Mechanical Engineering, Korea Advanced Institute of Science and Technology, Daejeon, Republic of Korea

Author Contribution

N.Y., J.J., and G.S. conceived and designed research; N.Y. performed experiments; N.Y. analyzed data; N.Y., J.J., and G.S. interpreted results of experiments; N.Y. and S.K. prepared figures; N.Y., and G.S. drafted and edited text. [Following the style of AJP]

4.1. SUMMARY

Iron overload is a critical risk factor for the impairment of endothelial integrity and function. Even though the adverse effect of iron overload on insulin resistance-mediated diabetes has been studied, the effects and underlying mechanism of iron overload on the endothelium remains to be elucidated. For the mechanistic studies, it is important to understand whether the endothelial transport of adiponectin is regulated by the effect of iron overload on alterations in vascular permeability. Thus, I hypothesized that iron overload induces intracellular stress to impair transendothelial permeability, and consequently, losing junctional protein alters access of HMW adiponectin for transmovement. In this study, I found that the transendothelial electric resistance (TEER) of human dermal microvascular endothelial cells (HDMEC) and human umbilical vein endothelial cells (HUVEC) decreased under iron overload after 24 hr of tight junction formation. Once the monolayer of endothelium formed, molecular permeability was defined by the molecular size, where 3kDa dextran demonstrated higher permeability than 70kDa dextran and oligomerized adiponectin. In conditions of iron overload, the comparable permeability of the same sized molecules, including adiponectin, increased across the barrier compared to control. Correspondingly, expression levels of CLDN7 and ZO-1 were decreased in iron overload. These experimental aims were also applied to 3D advanced microvascular networks. Under iron overload, increased permeability and the size-dependent endothelial movement were observed consistently. Combined, this suggested that endothelial regulation could play an important role hormone action in the peripheral tissues by regulating the first rate-limiting step of facilitating hormone access to tissue targets.

4.2. INTRODUCTION

Metabolic syndrome is prevalent health problem that is associated with high risk for cardiovascular disease and Diabetes Mellitus. The main concern of metabolic syndrome is in the effects of insulin resistance. Many of previous studies have provided links between insulin resistance and iron overload, from both the systemic and intracellular perspectives (26, 57). Such studies have demonstrated that iron overload-induced oxidative stress impairs glucose utilization and glucose homeostasis, which leads to insulin resistance. Additionally, iron overload results in loss of the pancreatic beta cells due to redox imbalance (223, 263, 298). Ultimately, iron overload plays a causal role in Diabetes Mellitus through mediating loss of both insulin action and insulin secretion.

Adiponectin, as an insulin sensitizer, plays pivotal roles in cardioprotection, anti-inflammatory responses, as well as anti-diabetic activity (3). Interestingly, increased serum ferritin levels were associated with decreased adiponectin expression and its plasma level, likely due to adipocyte damage mediated by oxidative stress (66, 141, 298). On the other hand, overexpression of adiponectin attenuated cardiac accumulation of iron (154), however, the specific roles for adiponectin under conditions of iron excess have not been clearly described. Particularly, in terms of adiponectin action, transendothelial movement of the hormone as a rate-limiting step of its activity have not been elucidated in conditions of iron overload. In this regard, it is important to investigate iron overload effects on the movement of adiponectin across the endothelial layer, and to elucidate the intracellular mechanism of paracellular transport regulation in the environment.

It has been previously reported that one of the activities of adiponectin is to contribute to the suppression of NF-kB activation (266). In contrast, iron overload is known to stimulate NF-kB activation by TNF-α signaling-induced phosphorylation in endothelial cells (183). Systemically, TNF-α has been shown to increase transferrin receptors and divalent metal transporters to promote the accumulation of intracellular iron. Furthermore, Ferroportin 1 was demonstrated to be downregulated by TNF-α stimuli, which led to the inhibition of iron export (183). In addition, TNF-

α signaling regulated not only iron metabolism, but also tight junction proteins (8, 48). Thus, iron-activated TNF-α signaling may induce NF-kB/P65 translocation into nucleus, which is likely to regulate tight junctional protein expression. To examine this, I tested the hypothesis that iron overload alters endothelial tight junction expression and consequently changes the adiponectin permeability across the barrier.

4.3. MATERIAL AND METHODS

4.3.1. Cell culture (conventional)

Human dermal microvascular endothelial cells (HDMECs) and human umbilical vascular endothelial cells (HUVECs) (ATCC, Manassas, VA, USA) were cultured in microvascular endothelial growth medium 2 (EGM2-MV, Lonza, Cat# cc-3202, ON, CA) with 5% fetal bovine serum (FBS) at 37°C, and 5% CO_2. To mimic the vascular monolayer endothelium, 3.0 μm pore size transwell inserts (Corning, Tewksbury, MA, USA) were used, with a surface area of 0.9cm^2 designed for use with 12-well plates. Iron overload in endothelial cells was induced by treating cells with 40μM FeSO4 for 72hr.

4.3.2. Transendothelial electric resistance (TEER)

TEER of HDMECs was measured using an epithelial voltohmmeter (EVOM; World Precision Instruments, Sarasota, FL, USA) and STX-2 chopstick electrodes. All values of TEER were corrected by subtracting the value of blank membrane without cells, and they were calculated by consideration of time and surface area (Ω x cm^2).

4.3.3. Permeability assay

2.5 x 10^5 HDMECs were seeded on 0.9cm^2 transwell inserts. Cells were treated with 40μM $FeSO_4$ for 72hrs. At the beginning of the assay, 10μg/mL of adiponectin was loaded on the apical side of the transwell inserts and an equal amount of plain medium was added into the basolateral side. After 24hr, medium from each side was collected and concentrated using 10,000Da MWCO (molecular weight cutoff) filter (EMD Millipore, Billerica, MA, USA) according to manufacturer's instructions.

4.3.4. Western blotting

Only the conventionally (2D) cultured HDMECs were used for western blotting. Cells were lysed in complete RIPA buffer with 80mM Tris–HCl (pH 6.8), 2% (w/v) SDS, 20% glycerol, 3.3% (v/v) β-mercaptoethanol and 0.01% (w/v) bromophenol blue, 30mM Hepes (pH 7.4), 2.5mM EGTA, 3mM EDTA, 70mM KCl, 20mM β-glycerolphosphate, 20mM NaF, 1mM Na3VO4, 200μM PMSF, 10μM E64, 1μM leupeptin, 1μM pepstatin A, 0.1% NP40, and 0.1μM okadaic acid. And the samples were denatured at 95°C for 10min.

Non-denatured adiponectin samples were prepared without β-mercaptoethanol or heating. After permeabilization assay, transported adiponectin including 3 forms of isomers were collected and concentrated by Amicon Ultra-4 Centrifugal Filter Units with Ultracel-10K (EMD Millipore, Billerica, MA, USA).

After SDS-PAGE electrophoresis and transfer, membranes were incubated in primary antibody: a rabbit polyclonal primary anti-Adiponectin antibody (dilution 1:1000) which was produced in-house (28), rabbit anti-Claudin-7 (dilution 1:500, Cat#34-9100, Thermo Fisher, Rockford, Illinois, USA), and rabbit anti-GAPDH(14C10) (dilution 1:1000, Cat#2118, Cell Signaling, Danvers, MA, USA) were used. Membranes were washed and HRP-conjugated secondary antibody (anti-rabbit IgG-HRP (dilution 1:5000, Cat#7074, Cell signaling, Danvers, MA, USA) was added. Bands were quantified and analyzed by Fiji software.

4.3.5. Immunostaining

$2.5x10^5$ cells/mL of HDMECs were seeded on coverslips and grown for 72hrs with or without 40μM FeSO4. Following treatment, cells were fixed using 4% PFA for 10min and permeabilized with 0.05% triton-x100. After 30min of blocking, primary antibody against anti-ZO-1 (rabbit, dilution 1:100, Cat#61-7300, ThermoFisher Scientific, Rockford, Illinois, USA) was added overnight at 4°C. Secondary antibody was anti-rabbit IgG-TRITC (1:100, Sigma, St. Louis, Missouri,

USA). DAPI (Vectashiled mounting medium with DAPI, Cat# H-1200, Burlingame, CA, USA) was used to stain individual nuclei. Images were taken using an LSM700 (Zeiss) confocal microscope. All images were processed using Fiji or Adobe Photoshop CS5 (Adobe System, San Jose, CA). Contrast and brightness were enhanced consistently for all representative images used in the publication.

4.3.6. Cell culture in microfluidic device

Microfluidic device having 3D microvascular networks in vitro provides culture environment with fibrinogen/ECM in the middle channel and medium supplying in the two side channels. Previous studies showed the fabrication process of the PDMS device and it was followed by this study (37). Human Umbilical Vein Endothelial Cells (HUVECs, Lonza) were used to perform 3D vessel experiments with endothelial cell growth medium (EGM-2, Lonza) supplemented with 5% fetal bovine serum (FBS) at 37°C, 5% CO2. Each device had 1:1 mixture of cells (1.4×10^7 cells/mL) including 4U/mL thrombin solution and fibrinogen solution (5mg/mL) in the middle channel. Vasculogenesis by self-assembly of HUVEC performed during 4 days of culture with adding 50ng/mL VEGF.

4.3.7. Permeability assay in microfluidic device

On day 4 of vasculogenesis with additional 50ng/mL VEGF in endothelial growth medium, one side of each reservoir for a media channel was filled with PBS two times to perform the quick wash out any debris from channel and vessel lumen. Fluorescence microscope (Axio, Observer Z1, Zeiss) was used for monitoring permeability of molecules by time-lapse imaging at every 1.4 seconds for 3 min. Before the fluorescence exposure, the interesting fields of view were selected and memorized by software and the bright field of images were taken first without infusion of fluorochrome conjugated molecules. 35ul of rhodamine labeled adiponectin, 4kDa FITC-dextran and

70kDa TexasRed-dextran were infused into only one reservoir of one side channel. The hydrostatic pressure difference made by 35ul of reagent one direction flow of tested molecules. The taken images were processed and analyzed by image J.

4.4. RESULTS

4.4.1. Iron overload increased permeability of molecules across an endothelial monolayer of HDMECs (2D vasculature system in transwell inserts).

An endothelial monolayer of 2D vasculature cultured HDMECs (Human dermal microvascular endothelial cells) were treated with 40μM $FeSO_4$ in 2% FBS endothelial media for 72hrs to generate an iron overload environment. In iron overloaded cells, TEER graduation of the HDMEC monolayer was attenuated starting from 24hrs and was significantly lower until the 72hr timepoint, where the control cells reached to TEER plateau (Fig 4.1A). This treatment also affected dextran permeability, which indicated endothelial para-cellular movement was altered. Small MW dextran (3kDa) showed significantly higher apparent permeability (Papp), 41.320 x 10^{-7} ± 0.784 x 10^{-7} cm/sec (n=4), than the larger MW dextran (70kDa), 3.134 x 10^{-7} ± 0.062 x 10^{-7} cm/sec, (n=4) (Figure 1B, C). For both 3kDa- and 70kDa-dextran, iron overload led to increased Papp of the HDMECs after 72hr treatment. Papp for 3kDa dextran was 3.503 x 10^{-7} ± 0.0587 x 10^{-7} cm/sec (n=4) and Papp for 70kDa dextran was 44.100 x 10^{-7} ± 0.542 x 10^{-7} cm/sec (n=4) (Fig 4.1 B, C). The permeability of full-length adiponectin (fAd), which included the different isomeric forms (LMW, MMW and HMW adiponectin) showed a similar effect, where the Papp of fAd was increased (1.305 ± 0.0908 folds, n=7) in the iron overload condition (Fig 4.1D). This was confirmed with SDS-PAGE, where specifically LMW adiponectin showed a significant increase in permeability (Fig 4.1E). This indicated that the HDMEC monolayer in a 2D culture system showed size-selective permeability of molecules that can be altered under iron overload conditions.

4.4.2. Iron overload altered tight junction expression in HDMECs.

In my previous observations from the other projects, CLDN-7 expression is considered to be an important tight junction protein that plays a role in regulating adiponectin permeability. CLDN-7 expression was measured by immunoblotting and showed a significant decrease in abundance in iron

overloaded cells compared to controls (Fig 4.2A). The total intensity of ZO-1, which is localized underneath the cell membrane was dramatically reduced, and almost absent in iron overload conditions (Fig 4.2B).

4.4.3. 3D microvascular networks of HUVECs showed decreased permeability of 70kDa dextran as well as rhodamine-labeled adiponectin under iron overload conditions.

HUVECs were cultured in a microfluidic chip designed with 2 sided media channels and a central hydrogel channel containing cells and fibrin gel as an ECM environment (Fig 4.3A). Based on optimization experiments (data not shown), cells were treated with 40μM $FeSO_4$ in 5% FBS endothelium growth media for 48hr, with treatment efficacy confirmed by perfusibility testing with 5μM beads (data not shown). Two different sizes of dextran (3kDa- and 70kDa-) were used to assess size-selective behavior on permeability, and each dextran was conjugated with a different wavelengths of fluorochromes; 3kDa-Alexa488 and 70kDa-texas red (Fig 4.3B). (*analysis of 3kDa Papp results for Figure 3C remains to be completed and I am currently collecting images). The Papp of 70kDa dextran was significantly increased under iron overload when it was analyzed from random ROIs in each field of view (Fig 4.3D). Papp of the control was $1.955 \times 10^{-5} \pm 0.367 \times 10^{-5}$ cm/sec (n=16) and Papp of iron overload was $3.573 \times 10^{-5} \pm 0.600 \times 10^{-5}$ cm/sec (n=24) (Fig 4.3D). Rhodamine-labeled adiponectin was also infused into the 3D microvascular networks and Papp was measured by capturing timelapse images at every 20 sec (Fig 4.3F). The Papp in iron overload ($4.651 \times 10^{-5} \pm 0.585 \times 10^{-5}$ cm/sec, (n=12)) was significantly increased as compared to the Papp of controls, ($2.101 \times 10^{-5} \pm 0.1908 \times 10^{-5}$ cm/sec (n=12)) (Fig 4.3E).

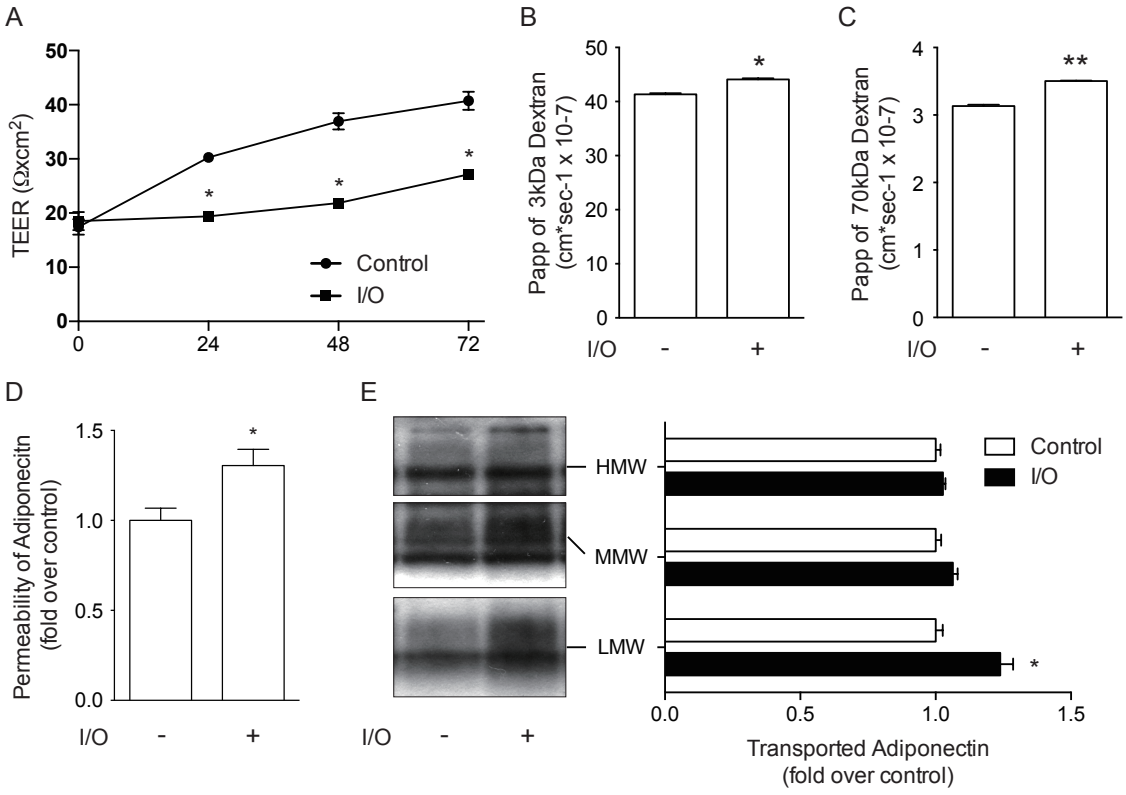

Figure 4.1. Iron overload-induced alteration on TEER and permeability of 2D HDMEC endothelial monolayer in transwell inserts

Iron overload (IO) condition was generated by treatment with 40μM $FeSO_4$ in 2% FBS endothelial media for 72hrs after transferring cells into transwell inserts. (A) TEER was measured every 24hrs. * indicates P<0.05 (n>12). (B, C) Apparent permeability (Papp) of different sizes of dextrans was measured. 3kDa-Alexa488 and 70kDa-Texas red conjugated dextran were loaded into the apical side of the inserts, and 6hr later, the medium from the basolateral side was collected and measured by microplate reader. *indicates p<0.05 and ** indicates p<0.01. (n=4) (D) Papp of full-length adiponectin (fAd) for 24hr. Collected fAd was measured by ELISA. * indicates p<0.05 (n>7). (E) The collected medium including fAd from the basolateral side was concentrated and separated by electrophoresis in SDS-PAGE gel without denaturation. (* indicates p<0.05)

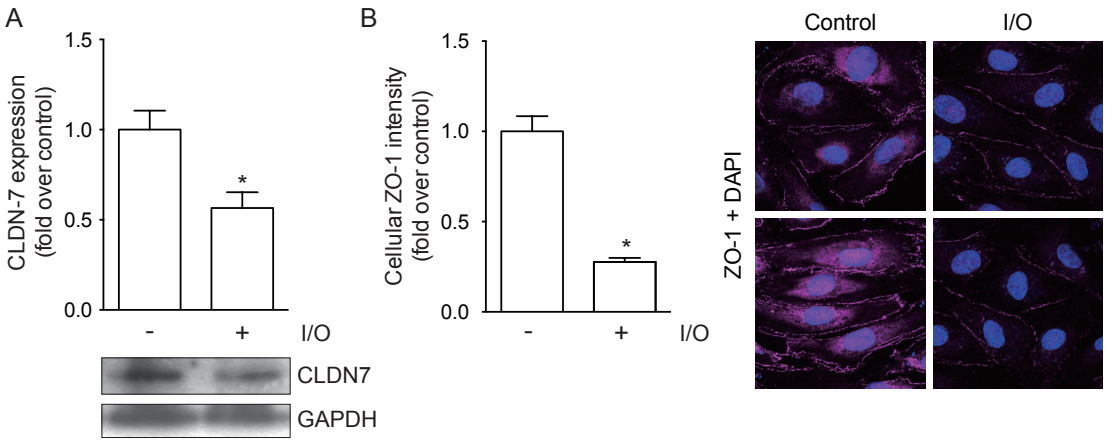

Figure 4.2. Changes of tight junction by iron overload in HDMECs

(A) Immunoblotting for CLDN7 to compare control versus 40μM $FeSO_4$-treated iron overload condition. (B) Immunofluorescence of ZO-1. The total intensity from each field of view was analyzed after normalization with background from the negative control images. * indicates $p<0.05$.

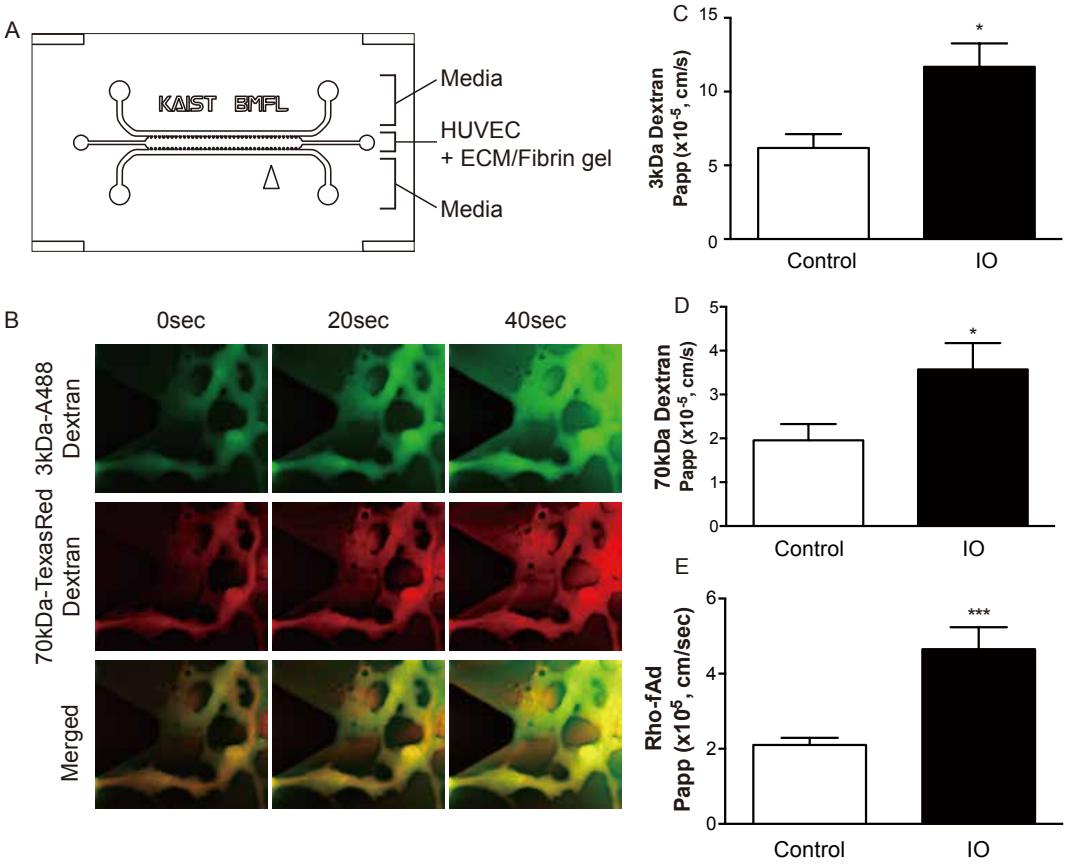
A
KAIST BMFL
Media
HUVEC
+ ECM/Fibrin gel
Media
B
0sec
20sec
40sec
3kDa-A488 Dextran
70kDa-TexasRed Dextran
Merged
C
3kDa Dextran Papp (x10-5, cm/s)
15
10
5
0
*
Control
IO
D
70kDa Dextran Papp (x10-5, cm/s)
5
4
3
2
1
0
*
Control
IO
E
Rho-fAd Papp (x10-5, cm/sec)
6
4
2
0
***
Control
IO
F
0sec
20sec
40sec
HUVEC::GFP (Green)
Rho-fAd (Red)

Figure 4.3. Permeability analysis of dextrans and adiponectin in 3D microvascular networks of HUVECs

(A) Schematic image for a microfluidic device with 2 media channels and a central cell-hydrogel channel. (B) Two different sizes of dextran infused into perfusable vasculature on-a-chip. 3kDa-Alexa dextran (Green) and 70kDa-Texas red (Red) were perfused and time-lapse images were captured at every 20 sec. (C, D) Calculated Papp (cm/sec) for each type of dextran. * indicates $p<0.05$ (n=16~24). (E) Papp of rhodamine labeled adiponectin (Rho-fAd) was measured. *indicates $p<0.05$ (n=12). (F) The representative captured images at each timepoint overlaying with constitutively expressed GFP in HUVECs (Green) and Rho-fAd (Red).

4.5. DISCUSSION

This research was designed to examine endothelial function and integrity, an area of fundamental endocrine importance, with a 2D vessel mimic culture system and a 3D closed circulatory vasculature system using endothelial cells. It is well established that paracellular transport is modulated in response to nutritional factors. Despite this, we know very little about the endothelial "machinery" that implements these changes. Specifically, in the condition of iron overload, I observed that permeability across vessel-like endothelium barriers of HDMECs and HUVECs increased and allowed more transendothelial movement of dextran and full-length adiponectin.

In terms of permeability, there are three main observations confirmed in both types of *in vitro* vasculature systems. Firstly, the paracellular movement of molecules was regulated in a size-selective manner, and the basal permeability of adiponectin was similar to that of 70kDa dextran. The structure of oligomerized adiponectin is asymmetric and not uniform (191), which would suggest it would have an uncertain range of permeability. The permeability assay in the 3D vasculature system allowed me to define the accessibility of adiponectin based on structural specificity. Secondly, iron overload significantly increased paracellular permeability. Even though the extent of the impact of excess iron was represented differently due to differences in the sensitivity for detection in each system (2D vs 3D), the trends and significance of the iron effect reproducible in both systems. Lastly, the major difference in between two *in vitro* systems was sheer stress introduced by the fluidics setting. Having flow in the perfusable vasculature did not affect the observed alteration in permeability mediated by excess intracellular iron.

This alteration of adiponectin flux is strongly associated with changes in tight junction proteins. From the previous studies 1 and 2, CLDN7 plays a key role in adiponectin flux control; increased CLND7 reduced the flux of adiponectin, while in contrast, loss or decreased expression of CLND7 elevated adiponectin movement. The effect of iron overload on downregulation of CLDN7 expression supports the suggested role for iron overload in regulation of endothelial tight junctions.

In addition to CLDN7, the intracellular protein level of ZO-1 was also upon treatment with 40μM $FeSO_4$. However, the mechanism of how the expression of the junctional proteins is altered by iron is not known.

In this study, I will continue to elucidate the underlying mechanism by investigating speculated targets, which are oxidative stress and regulation of NF-kB activation by iron overload. It is well known that iron-mediated oxidative stress comes from the induced ROS production in endothelial cells, and it results in impairing endothelial function (193). The produced intracellular ROS is detectable by 2′,7′-dichlorofluorescein diacetate (DCF-DA) fluorescent assay, which reagent is permeable non-fluorescent molecule and becomes fluorescent by ROS-induced oxidation (108), as well as, by CellROX assay that can detect cellular oxidative stress using reagent turnover from reduced form of non-fluorescent probe to oxidized deep red fluorescent one by ROS (251). Therefore, either ROS detection methods will be applied to test iron effects on ROS production in endothelial cells.

The aberrant free radical is known to give negative impacts on the barrier function of TJs and AJs (163), although the regulatory mechanism is not precise yet. I will examine that the iron-driven free radical activates NF-kB as a redox-sensitive transcription factor, which can deal with the oxidative stress via changes of gene expressions in endothelial cells. In addition, I will also test whether the effect of iron subsequently increases permeability by junctional proteins alteration. To confirm that the major components of the NF-kB complex and its regulator will be studied. The subunits of NF-kB (P50 and P65) and the inhibitor of NF-kB (IkB) are tightly regulated by phosphorylation and ubiquitination. Once NF-kB subunits are phosphorylated, it has less affinity to IkB, and it is translocated into the nucleus. The dissociated IkB is phosphorylated and ready for ubiquitination as well as proteolytic degradation by ATP-dependent 26S proteasome complex. (163) To understand the cellular response to iron overload, the level of phosphorylation for P65 and IkBalpha will be detected by immunoblotting. And the activity of luciferase, as a reporter gene

under the control of NF-kB promoter, will be tested to measure the NF-kB gene regulation from iron overload. This further investigation contributes to a better understanding of the mechanism that iron-induced oxidative stress alters the permeability of adiponectin.

CHAPTER FIVE: DISCUSSION AND CONCLUSION

5.1 RESEARCH SUMMARY

Dysfunctional endothelium driven by metabolic syndrome has been observed in cases of diabetes and cardiovascular disease. Structural and functional damage to the vasculature is caused by a combination of hyperinsulinemia, hyperglycemia, and redox imbalance mediated by cellular and mechanical stress. One of the significant roles of the endothelium in the vascular structure is to regulate molecular transport across the barrier. To study the effect of hormonal transport in the context of metabolic syndrome, particularly in study 1, I examined the effect of glucocorticoids on transendothelial permeability. The most prevalent medication for inflammation, glucocorticoids are known for having a side effect of building up insulin resistance, as well as being a tightening agent of the endothelium. The tightening effect was observed in both *in vivo* and *in vitro* systems. Consequently, adiponectin movement was restricted. (Fig 5.B) Furthermore, I found that exogenous glucocorticoids triggered hyperinsulinemia in the absence of fluctuations in blood glucose levels in rats, which may indicate the progressive development of systemic insulin resistance (Fig 5.A). It is suggested that hyperinsulinemia mediated by glucocorticoid treatment reduced endothelial permeability, which restricted adiponectin movement (Fig 5.A,B). In contrast, in studies 2 and 3, hyperglycemia and iron overload both increased adiponectin movement associated with loosened permeability (Fig 5.B). In the case of hyperglycemia, many studies have indicated that hyperglycemia has a causal relationship to oxidative stress. Additionally, accumulated serum ferritin and increased cellular iron content leads to a redox imbalance status by excess ROS production, which contributes to synergetic pathologies. (Fig 5.A)

The endothelial monolayer is an important rate-limiting determinant of hormone and substrate access to target tissues. Previous studies focusing on insulin suggest that impaired delivery of insulin from the plasma to the interstitial space in obesity may contribute to metabolic insulin

resistance and diabetes. Since adiponectin is known to mediate beneficial antidiabetic effects, and the molecular weight of biologically active forms of adiponectin ranges widely, I proposed that paracellular transport is a major determinant of transendothelial adiponectin flux. This was proven throughout studies 1, 2 and 3 paracellular transport was altered by different risk factors of metabolic syndrome, leading to changes in adiponectin flux. In study 1, glucocorticoid-treated HUVECs and *in vivo* studies in rats consistently showed restricted adiponectin trans-movement.

In contrast, for studies 2 and 3, exposure to excess glucose or iron increased adiponectin flux in the mouse, as well as HUVECs and HDMECs. The alteration in paracellular transport was highly associated with changes in TEER in a monolayer culture system. For example, based on the TEER, which is interpreted as measurable tightness of the endothelium, paracellular movement of dextran was inversely regulated. Similarly, the amount of transported adiponectin across the monolayer showed a negative correlation with TEER.

In addition, paracellular transport is regulated in a size-selective manner. My studies applied two different sizes of dextran (3kDa and 70kDa) to monitor permeability *in vitro*. Expectedly, 70kDa dextran had lower permeability than 3kDa dextran. However, in terms of oligomerized adiponectin movement *in vivo*, it appears as though there is another potential mechanism. In particular, the research community has often accepted that fact that the HMW oligomeric form of adiponectin targets liver and not muscle, whereas the small globular portion has 'more potency' in skeletal muscle. This was initially attributed to the higher binding affinity of the globular fragment of adiponectin to skeletal muscle cell membranes, which were thought to express more of the AdipoR1 receptor isoform. However, such data are not consistent, and easier access of the smaller globular adiponectin across the relatively tight endothelial monolayer found in skeletal muscle vasculature, in comparison with liver, may be significant. Thus, TJ-mediated, or AJ-mediated, alterations in adiponectin access to tissues from the vasculature are likely to be of important functional significance. In this aspect, study 1 showed the comparison of the tight junction protein profile upon glucocorticoid treatment vs

control. Although the profiles seemed different from the species, alterations in claudin 7 and claudin-10 were consistent in their response to glucocorticoids. Particularly, CLDN 7 seemed to play an important role in the maintenance of endothelial monolayer integrity according to the results of increased adiponectin flux across a monolayer of HUVECs with claudin 7 shRNA-mediated knockdown. Based on the findings in the following study 2, CLDN 7 is likely to play a pivotal role to control adiponectin transport.

Indeed, numerous studies in kidney and retina have indicated that expression of various TJ proteins is altered in diabetes. Although the changes in metabolic target tissues of adiponectin and their physiological significance still need to be established, principal mechanisms responsible for altered TJ composition and structure in diabetes are partially elucidated in my thesis studies. In study 3, the underlying mechanism to explain TJ alteration in the endothelium by iron overload was investigated with the clue of oxidative stress. Increased cellular ROS production has been reported to induce NF-kB phosphorylation (170). In retinal ECs, there was a report that TNF-α activation altered TJ proteins (14). Taken together, an NF-kB activation-related cellular response to increased ROS by iron overload may be responsible for the decreased TJ proteins in the endothelium, and consequently, increased access of adiponectin movement across the barrier of the endothelium.

For studies 1,2, and 3, I established advanced technical approaches to monitor adiponectin movement *in vivo*, *ex vivo* and *in vitro*. FMT-CT imaging allowed 3D non-invasive small animal scanning over time, obtaining both temporal and the spatial detailed information. I also applied the 3D perfusable microvascular network, which allowed me to test the functionality of auto-assembled vessels *in vitro*.

Overall, these studies suggested that transendothelial movement of adiponectin via paracellular permeability of the endothelial barrier is a tightly regulated process which can be dynamically adjusted in response to various mediators. The potential contribution to metabolic dysfunction due to metabolic syndrome and diabetes is apparent, yet the precise significance has

likely been somewhat underestimated. I believe that further investigation of TJ-mediated changes in hormone or substrate flux in diabetes, and the characterization of their functional significance, will shed additional light on the pathophysiology of disease and identify potential therapeutic opportunities.

5.2 FUTURE DIRECTION

Future studies will continue to explore the mechanisms underlying hormone physiological action mediated by alterations of endothelial permeability. Studies 1, 2 and 3 claimed that tight junctional alterations directly affected the transendothelial movement of adiponectin. In the case of HDMECs and HUVECs, CLDN7 was a major component of the tight junctions to control adiponectin movement across the endothelial barrier. Extending this observation to an animal model would allow for finding the physiological meaning endothelial permeability regulation, and claudin 7 knock out mice will be the priority model. Unfortunately, conventional or intestinal-specific CLDN7 knockout mice mediated by the Cre/Lox system show a severe phenotype of stunted or perinatal death in mice (258, 304). However, recently, an inducible intestine-specific conditional knockout mouse was developed for targeting CLDN7. These mice showed a normal phenotype before tamoxifen induction via intraperitoneal injection (258). Under conditions of metabolic syndrome, alterations in endothelial permeability occur in cardiac vessels, one of the most susceptible organs to metabolic syndrome. My study 2 showed that exogenous adiponectin content was increased in heart tissue of diabetic mice. Thus, although it could be ambitious to generate an inducible cardiac-specific claudin 7 knockout animal, my preliminary findings demonstrate that this does warrant further investigation. For example, to confirm the physiological importance of claudin 7 on adiponectin endothelial movement, I can compare the biodistribution of adiponectin in the claudin 7 knockout model vs. wildtype using the FMT/CT monitoring system. Furthermore, I can also recover the claudin 7 gene expression via adenovirus-mediated overexpression (148). This type of study

would provide further therapeutic insights into the application of claudin 7 overexpression via adenoviral gene therapy in diabetes.

In addition, the strategy of restoring CLDN7 by overexpression can also be applied to an iron overload animal model to examine changes in adiponectin action in target tissue mediated by recovery of endothelial permeability. The iron overload model is produced by dietary supplement or iron-dextran injection via various routes, for example, intraperitoneal, subcutaneous, intramuscular, parenteral, or intravenous injection (112). In study 3, the presumptive cause of loss of permeability was reduced CLDN7 expression in endothelial cells, which depended on alterations in gene expression of CLDN7 by iron-mediated oxidative stress. If the compensation of tight junctions works on improving endothelial integrity, it also can be a target of future therapy for iron chelator-induced complications.

Both the *in vivo* animal models and *in vitro* vasculature platform have opened opportunities to extend the study of adiponectin action and endothelial regulation. 3D vasculature networks can be applied for diverse purposes and optimized with numerous features. Firstly, even though the simplified system containing only endothelial cells has the benefit of providing clear, direct effects, it is less physiologically relevant than having harmonious effects with several different cell types like pericytes, smooth muscle cells, immune cells or cancer cells (40, 305). In the BBB, renal and retinal vessels, pericytes are known to play a crucial role in managing endothelial integrity (128, 267, 305). To mimic more physiological and functional vasculature *in vitro*, I can apply the co-culturing system used in study 3 in hydrogel ECM with pericytes or smooth muscle cells by taking advantage of the self-assembly feature of endothelial cells. Secondly, I can use this human functional microvasculature network to develop a screening platform for other circulatory molecules including cytokines, other hormones, adipokines ,and immune-related cells under conditions resembling metabolic syndrome. For example, as described in studies 2 and 3, transendothelial adiponectin movement is increased in diabetes-related conditions. In the state, I could examine correlations

between adiponectin and the permeability of other hormones or cells, for example, LCN2, TNF-alpha, neutrophils or monocytes, etc. This approach may contribute to finding future therapeutic targets and strategies.

5.3 CONCLUSION

In summary, all of my studies intended to investigate the mechanisms of physiological adiponectin action via transendothelial movement, which is regulated by endothelial permeability in diabetes. To prove that reduced endothelial permeability restricted adiponectin movement, I used glucocorticoid treatment. The study proved that transendothelial adiponectin moved via the paracellular pathway, and also suggested that decreased adiponectin movement depended on paracellular permeability which was regulated by tight junctional profiles. In contrast, hyperglycemia increased adiponectin transendothelial movement due to increased endothelial permeability, as measured by TEER. Examination of the biodistribution of adiponectin in diabetic mice showed that a higher amount of exogenous adiponectin existed in the peripheral tissues 90min after infusion compared to controls. This *in vivo* observation was validated in *ex vivo* isolated vessels, 2D *in vitro* endothelial monolayers and in 3D perfusable *in vitro* microvasculature. Lastly, I wanted to know underlying mechanisms responsible for the alteration of permeability in adiponectin movement, particularly in iron overload. Elevation in oxidative stress caused by excess iron is likely to change tight junction protein expression. Therefore, I concluded that adiponectin transendothelial movement was determined by endothelial permeability, which was strongly regulated by tight junctional protein expression. The permeability of diabetic vasculature altered adiponectin movement from plasma to peripheral tissues, and thus influenced its action.

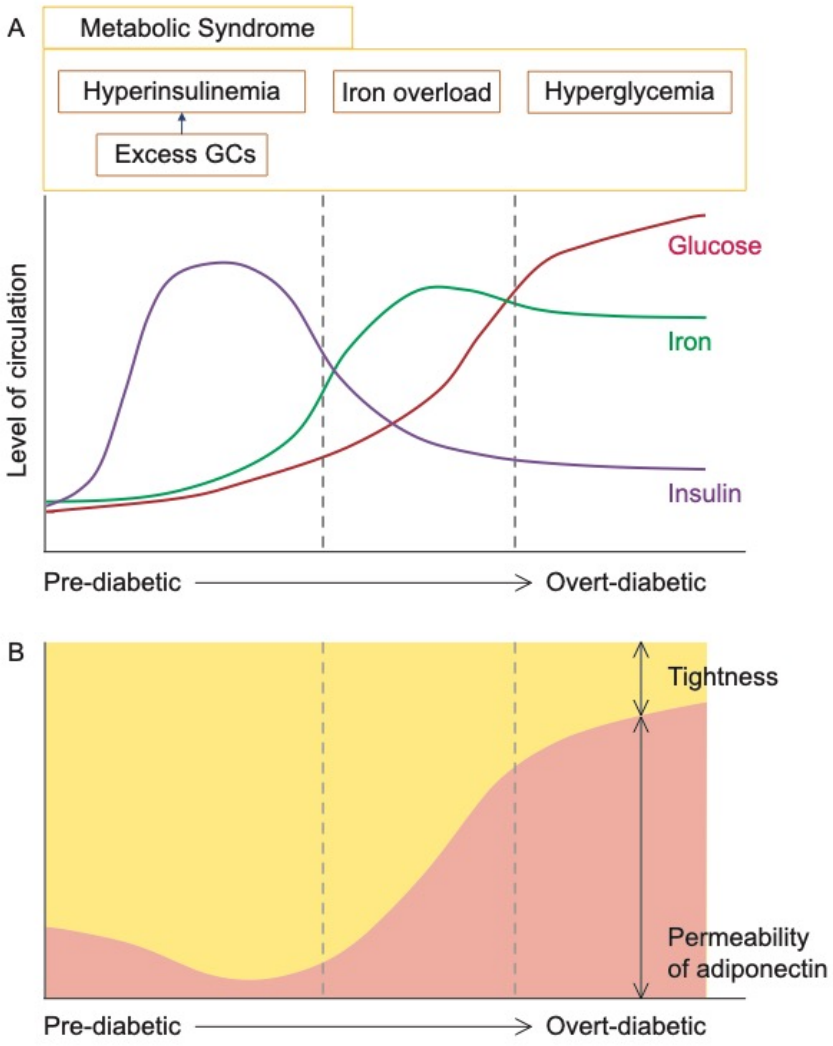

Figure 5.1. Schematic summary of studies for adiponectin permeability in chronic diabetic process

(A) Depending on the chronic process of diabetes from pre-diabetic to overt-diabetic condition, the impaired control of homeostasis reflects alteration of insulin, iron and glucose at the circulatory level. (B) The hyperinsulinemia, iron overload and hyperglycemia leads to changes the tightness of endothelial barrier and it is negatively correlated to permeability of adiponectin.

Uncategorized References

1. Intensive blood-glucose control with sulphonylureas or insulin compared with conventional treatment and risk of complications in patients with type 2 diabetes (UKPDS 33). UK Prospective Diabetes Study (UKPDS) Group. *Lancet* 352: 837-853, 1998.
2. **Abe Y, Sakairi T, Kajiyama H, Shrivastav S, Beeson C, and Kopp JB.** Bioenergetic characterization of mouse podocytes. *Am J Physiol Cell Physiol* 299: C464-476, 2010.
3. **Achari AE and Jain SK.** Adiponectin, a Therapeutic Target for Obesity, Diabetes, and Endothelial Dysfunction. *Int J Mol Sci* 18, 2017.
4. **Agarwal A, Sarwar S, Sepah YJ, and Nguyen QD.** What have we learnt about the management of diabetic macular edema in the antivascular endothelial growth factor and corticosteroid era? *Curr Opin Ophthalmol* 26: 177-183, 2015.
5. **Aird WC.** Phenotypic heterogeneity of the endothelium: I. Structure, function, and mechanisms. *Circ Res* 100: 158-173, 2007.
6. **Aird WC.** Phenotypic heterogeneity of the endothelium: II. Representative vascular beds. *Circ Res* 100: 174-190, 2007.
7. **Akude E, Zherebitskaya E, Chowdhury SK, Smith DR, Dobrowsky RT, and Fernyhough P.** Diminished superoxide generation is associated with respiratory chain dysfunction and changes in the mitochondrial proteome of sensory neurons from diabetic rats. *Diabetes* 60: 288-297, 2011.
8. **Al-Sadi R, Guo S, Ye D, Rawat M, and Ma TY.** TNF-alpha Modulation of Intestinal Tight Junction Permeability Is Mediated by NIK/IKK-alpha Axis Activation of the Canonical NF-kappaB Pathway. *Am J Pathol* 186: 1151-1165, 2016.
9. **Alberts B, Johnson A, Lewis J, Raff M, Roberts K, and Walter P.** Molecular biology of the cell. new york: Garland science; 2002. *Classic textbook now in its 5th Edition*, 2002.
10. **Ale A, Ermolayev V, Herzog E, Cohrs C, de Angelis MH, and Ntziachristos V.** FMT-XCT: in vivo animal studies with hybrid fluorescence molecular tomography-X-ray computed tomography. *Nature methods* 9: 615-620, 2012.
11. **Alipoor E, Mohammad Hosseinzadeh F, and Hosseinzadeh-Attar MJ.** Adipokines in critical illness: A review of the evidence and knowledge gaps. *Biomed Pharmacother* 108: 1739-1750, 2018.
12. **Antonetti DA, Barber AJ, Khin S, Lieth E, Tarbell JM, and Gardner TW.** Vascular permeability in experimental diabetes is associated with reduced endothelial occludin content: vascular endothelial growth factor decreases occludin in retinal endothelial cells. Penn State Retina Research Group. *Diabetes* 47: 1953-1959, 1998.
13. **Arita Y, Kihara S, Ouchi N, Maeda K, Kuriyama H, Okamoto Y, Kumada M, Hotta K, Nishida M, Takahashi M, Nakamura T, Shimomura I, Muraguchi M, Ohmoto Y, Funahashi T, and Matsuzawa Y.** Adipocyte-derived plasma protein adiponectin acts as a platelet-derived growth factor-BB-binding protein and regulates growth factor-induced common postreceptor signal in vascular smooth muscle cell. *Circulation* 105: 2893-2898, 2002.
14. **Aveleira CA, Lin CM, Abcouwer SF, Ambrosio AF, and Antonetti DA.** TNF-alpha signals through PKCzeta/NF-kappaB to alter the tight junction complex and increase retinal endothelial cell permeability. *Diabetes* 59: 2872-2882, 2010.

15. **Barber AJ, Antonetti DA, and Gardner TW.** Altered expression of retinal occludin and glial fibrillary acidic protein in experimental diabetes. The Penn State Retina Research Group. *Invest Ophthalmol Vis Sci* 41: 3561-3568, 2000.
16. **Barbot M, Ceccato F, and Scaroni C.** Diabetes Mellitus Secondary to Cushing's Disease. *Front Endocrinol (Lausanne)* 9: 284, 2018.
17. **Barrett EJ and Rattigan S.** Muscle perfusion: its measurement and role in metabolic regulation. *Diabetes* 61: 2661-2668, 2012.
18. **Barrett EJ, Wang H, Upchurch CT, and Liu Z.** Insulin regulates its own delivery to skeletal muscle by feed-forward actions on the vasculature. *American journal of physiology Endocrinology and metabolism* 301: E252-263, 2011.
19. **Beaudry JL, D'Souza A M, Teich T, Tsushima R, and Riddell MC.** Exogenous glucocorticoids and a high-fat diet cause severe hyperglycemia and hyperinsulinemia and limit islet glucose responsiveness in young male Sprague-Dawley rats. *Endocrinology* 154: 3197-3208, 2013.
20. **Beaudry JL, Dunford EC, Leclair E, Mandel ER, Peckett AJ, Haas TL, and Riddell MC.** Voluntary exercise improves metabolic profile in high-fat fed glucocorticoid-treated rats. *J Appl Physiol (1985)* 118: 1331-1343, 2015.
21. **Beaudry JL, Dunford EC, Teich T, Zaharieva D, Hunt H, Belanoff JK, and Riddell MC.** Effects of selective and non-selective glucocorticoid receptor II antagonists on rapid-onset diabetes in young rats. *PLoS One* 9: e91248, 2014.
22. **Ben-Yosef T, Belyantseva IA, Saunders TL, Hughes ED, Kawamoto K, Van Itallie CM, Beyer LA, Halsey K, Gardner DJ, Wilcox ER, Rasmussen J, Anderson JM, Dolan DF, Forge A, Raphael Y, Camper SA, and Friedman TB.** Claudin 14 knockout mice, a model for autosomal recessive deafness DFNB29, are deaf due to cochlear hair cell degeneration. *Hum Mol Genet* 12: 2049-2061, 2003.
23. **Bhattacharjee PS, Huq TS, Potter V, Young A, Davenport IR, Graves R, Mandal TK, Clement C, McFerrin HE, Muniruzzaman S, Ireland SK, and Hill JM.** High-glucose-induced endothelial cell injury is inhibited by a Peptide derived from human apolipoprotein E. *PLoS One* 7: e52152, 2012.
24. **Bhaumik S, DePuy J, and Klimash J.** Strategies to minimize background autofluorescence in live mice during noninvasive fluorescence optical imaging. *Lab animal* 36: 40-43, 2007.
25. **Bischel LL, Sung KE, Jimenez-Torres JA, Mader B, Keely PJ, and Beebe DJ.** The importance of being a lumen. *FASEB J* 28: 4583-4590, 2014.
26. **Blasco G, Puig J, Daunis IEJ, Molina X, Xifra G, Fernandez-Aranda F, Pedraza S, Ricart W, Portero-Otin M, and Fernandez-Real JM.** Brain iron overload, insulin resistance, and cognitive performance in obese subjects: a preliminary MRI case-control study. *Diabetes Care* 37: 3076-3083, 2014.
27. **Blecharz KG, Drenckhahn D, and Forster CY.** Glucocorticoids increase VE-cadherin expression and cause cytoskeletal rearrangements in murine brain endothelial cEND cells. *J Cereb Blood Flow Metab* 28: 1139-1149, 2008.
28. **Bo T, Yamamori T, Suzuki M, Sakai Y, Yamamoto K, and Inanami O.** Calmodulin-dependent protein kinase II (CaMKII) mediates radiation-induced mitochondrial fission by

regulating the phosphorylation of dynamin-related protein 1 (Drp1) at serine 616. *Biochem Biophys Res Commun* 495: 1601-1607, 2018.

29. **Bocher M, Blevis IM, Tsukerman L, Shrem Y, Kovalski G, and Volokh L.** A fast cardiac gamma camera with dynamic SPECT capabilities: design, system validation and future potential. *European journal of nuclear medicine and molecular imaging* 37: 1887-1902, 2010.

30. **Bodenlenz M, Schaupp LA, Druml T, Sommer R, Wutte A, Schaller HC, Sinner F, Wach P, and Pieber TR.** Measurement of interstitial insulin in human adipose and muscle tissue under moderate hyperinsulinemia by means of direct interstitial access. *American journal of physiology Endocrinology and metabolism* 289: E296-300, 2005.

31. **Breiderhoff T, Himmerkus N, Stuiver M, Mutig K, Will C, Meij IC, Bachmann S, Bleich M, Willnow TE, and Muller D.** Deletion of claudin-10 (Cldn10) in the thick ascending limb impairs paracellular sodium permeability and leads to hypermagnesemia and nephrocalcinosis. *Proc Natl Acad Sci U S A* 109: 14241-14246, 2012.

32. **Bromhead C, Miller JH, and McDonald FJ.** Regulation of T-cadherin by hormones, glucocorticoid and EGF. *Gene* 374: 58-67, 2006.

33. **Brownlee M.** Biochemistry and molecular cell biology of diabetic complications. *Nature* 414: 813, 2001.

34. **Buechler C, Wanninger J, and Neumeier M.** Adiponectin receptor binding proteins--recent advances in elucidating adiponectin signalling pathways. *FEBS letters* 584: 4280-4286, 2010.

35. **Bugger H, Chen D, Riehle C, Soto J, Theobald HA, Hu XX, Ganesan B, Weimer BC, and Abel ED.** Tissue-specific remodeling of the mitochondrial proteome in type 1 diabetic akita mice. *Diabetes* 58: 1986-1997, 2009.

36. **Bugger H, Chen D, Riehle C, Soto J, Theobald HA, Hu XX, Ganesan B, Weimer BC, and Abel ED.** Tissue-specific remodeling of the mitochondrial proteome in type 1 diabetic akita mice. *Diabetes* 58: 1986-1997, 2009.

37. **Capucci MS, Hoffmann ME, De Groot A, and Natarajan AT.** Streptozotocin-induced toxicity in CHO-9 and V79 cells. *Environ Mol Mutagen* 26: 72-78, 1995.

38. **Chang KS and Stevens WC.** Endothelium-dependent increase in vascular sensitivity to phenylephrine in long-term streptozotocin diabetic rat aorta. *Br J Pharmacol* 107: 983-990, 1992.

39. **Chen L, Magliano DJ, and Zimmet PZ.** The worldwide epidemiology of type 2 diabetes mellitus--present and future perspectives. *Nat Rev Endocrinol* 8: 228-236, 2011.

40. **Chen MB, Whisler JA, Frose J, Yu C, Shin Y, and Kamm RD.** On-chip human microvasculature assay for visualization and quantification of tumor cell extravasation dynamics. *Nat Protoc* 12: 865-880, 2017.

41. **Chen X, Scholl TO, and Stein TP.** Association of elevated serum ferritin levels and the risk of gestational diabetes mellitus in pregnant women: The Camden study. *Diabetes Care* 29: 1077-1082, 2006.

42. **Chen Y, Pitzer AL, Li X, Li PL, Wang L, and Zhang Y.** Instigation of endothelial Nlrp3 inflammasome by adipokine visfatin promotes inter-endothelial junction disruption: role of HMGB1. *J Cell Mol Med* 19: 2715-2727, 2015.

43. **Chistiakov DA, Orekhov AN, and Bobryshev YV.** Effects of shear stress on endothelial cells: go with the flow. *Acta Physiol (Oxf)* 219: 382-408, 2017.
44. **Chiu JD, Kolka CM, Richey JM, Harrison LN, Zuniga E, Kirkman EL, and Bergman RN.** Experimental hyperlipidemia dramatically reduces access of insulin to canine skeletal muscle. *Obesity (Silver Spring)* 17: 1486-1492, 2009.
45. **Chiu JD, Richey JM, Harrison LN, Zuniga E, Kolka CM, Kirkman E, Ellmerer M, and Bergman RN.** Direct administration of insulin into skeletal muscle reveals that the transport of insulin across the capillary endothelium limits the time course of insulin to activate glucose disposal. *Diabetes* 57: 828-835, 2008.
46. **Chowdhury SK, Smith DR, and Fernyhough P.** The role of aberrant mitochondrial bioenergetics in diabetic neuropathy. *Neurobiol Dis* 51: 56-65, 2013.
47. **Clark AR and Belvisi MG.** Maps and legends: the quest for dissociated ligands of the glucocorticoid receptor. *Pharmacol Ther* 134: 54-67, 2012.
48. **Clark PR, Kim RK, Pober JS, and Kluger MS.** Tumor necrosis factor disrupts claudin-5 endothelial tight junction barriers in two distinct NF-kappaB-dependent phases. *PLoS One* 10: e0120075, 2015.
49. **Cohen RM, Franco RS, Khera PK, Smith EP, Lindsell CJ, Ciraolo PJ, Palascak MB, and Joiner CH.** Red cell life span heterogeneity in hematologically normal people is sufficient to alter HbA1c. *Blood* 112: 4284-4291, 2008.
50. **Combs TP and Marliss EB.** Adiponectin signaling in the liver. *Rev Endocr Metab Disord* 15: 137-147, 2014.
51. **Combs TP, Pajvani UB, Berg AH, Lin Y, Jelicks LA, Laplante M, Nawrocki AR, Rajala MW, Parlow AF, Cheeseboro L, Ding YY, Russell RG, Lindemann D, Hartley A, Baker GR, Obici S, Deshaies Y, Ludgate M, Rossetti L, and Scherer PE.** A transgenic mouse with a deletion in the collagenous domain of adiponectin displays elevated circulating adiponectin and improved insulin sensitivity. *Endocrinology* 145: 367-383, 2004.
52. **Coughlan MT, Thorburn DR, Penfold SA, Laskowski A, Harcourt BE, Sourris KC, Tan AL, Fukami K, Thallas-Bonke V, Nawroth PP, Brownlee M, Bierhaus A, Cooper ME, and Forbes JM.** RAGE-induced cytosolic ROS promote mitochondrial superoxide generation in diabetes. *J Am Soc Nephrol* 20: 742-752, 2009.
53. **D'Souza A M, Beaudry JL, Szigiato AA, Trumble SJ, Snook LA, Bonen A, Giacca A, and Riddell MC.** Consumption of a high-fat diet rapidly exacerbates the development of fatty liver disease that occurs with chronically elevated glucocorticoids. *Am J Physiol Gastrointest Liver Physiol* 302: G850-863, 2012.
54. **Dadson K, Liu Y, and Sweeney G.** Adiponectin action: a combination of endocrine and autocrine/paracrine effects. *Front Endocrinol (Lausanne)* 2: 62, 2011.
55. **Dadson K, Turdi S, Boo S, Hinz B, and Sweeney G.** Temporal and Molecular Analyses of Cardiac Extracellular Matrix Remodeling following Pressure Overload in Adiponectin Deficient Mice. *PLoS One* 10: e0121049, 2015.
56. **Dadson K, Turdi S, Hashemi S, Zhao J, Polidovitch N, Beca S, Backx PH, McDermott JC, and Sweeney G.** Adiponectin is required for cardiac MEF2 activation during pressure overload induced hypertrophy. *J Mol Cell Cardiol* 86: 102-109, 2015.

57. **Dandona P, Hussain MA, Varghese Z, Politis D, Flynn DM, and Hoffbrand AV.** Insulin resistance and iron overload. *Ann Clin Biochem* 20 Pt 2: 77-79, 1983.
58. **Dang TQ, Yoon N, Chasiotis H, Dunford EC, Feng Q, He P, Riddell MC, Kelly SP, and Sweeney G.** Transendothelial movement of adiponectin is restricted by glucocorticoids. *J Endocrinol* 234: 101-114, 2017.
59. **Deepa SS and Dong LQ.** APPL1: role in adiponectin signaling and beyond. *American journal of physiology Endocrinology and metabolism* 296: E22-36, 2009.
60. **Defronzo RA.** Banting Lecture. From the triumvirate to the ominous octet: a new paradigm for the treatment of type 2 diabetes mellitus. *Diabetes* 58: 773-795, 2009.
61. **Deli MA.** Potential use of tight junction modulators to reversibly open membranous barriers and improve drug delivery. *Biochim Biophys Acta* 1788: 892-910, 2009.
62. **Diabetes C, Complications Trial Research G, Nathan DM, Genuth S, Lachin J, Cleary P, Crofford O, Davis M, Rand L, and Siebert C.** The effect of intensive treatment of diabetes on the development and progression of long-term complications in insulin-dependent diabetes mellitus. *N Engl J Med* 329: 977-986, 1993.
63. **Ding H and Triggle CR.** Endothelial dysfunction in diabetes: multiple targets for treatment. *Pflugers Arch* 459: 977-994, 2010.
64. **Ding L, Lu Z, Foreman O, Tatum R, Lu Q, Renegar R, Cao J, and Chen YH.** Inflammation and disruption of the mucosal architecture in claudin-7-deficient mice. *Gastroenterology* 142: 305-315, 2012.
65. **Ding Q, Wang Z, and Chen Y.** Endocytosis of adiponectin receptor 1 through a clathrin- and Rab5-dependent pathway. *Cell Res* 19: 317-327, 2009.
66. **Dongiovanni P, Ruscica M, Rametta R, Recalcati S, Steffani L, Gatti S, Girelli D, Cairo G, Magni P, Fargion S, and Valenti L.** Dietary iron overload induces visceral adipose tissue insulin resistance. *Am J Pathol* 182: 2254-2263, 2013.
67. **Dongiovanni P, Valenti L, Ludovica Fracanzani A, Gatti S, Cairo G, and Fargion S.** Iron depletion by deferoxamine up-regulates glucose uptake and insulin signaling in hepatoma cells and in rat liver. *Am J Pathol* 172: 738-747, 2008.
68. **Du XL, Edelstein D, Rossetti L, Fantus IG, Goldberg H, Ziyadeh F, Wu J, and Brownlee M.** Hyperglycemia-induced mitochondrial superoxide overproduction activates the hexosamine pathway and induces plasminogen activator inhibitor-1 expression by increasing Sp1 glycosylation. *Proc Natl Acad Sci U S A* 97: 12222-12226, 2000.
69. **Dvornik E, Simard-Duquesne N, Krami M, Sestanj K, Gabbay KH, Kinoshita JH, Varma SD, and Merola LO.** Polyol accumulation in galactosemic and diabetic rats: control by an aldose reductase inhibitor. *Science* 182: 1146-1148, 1973.
70. **Dymock IW, Cassar J, Pyke DA, Oakley WG, and Williams R.** Observations on the pathogenesis, complications and treatment of diabetes in 115 cases of haemochromatosis. *Am J Med* 52: 203-210, 1972.
71. **Engin A.** Adiponectin-Resistance in Obesity. *Adv Exp Med Biol* 960: 415-441, 2017.
72. **Eskin SG, Ives CL, McIntire LV, and Navarro LT.** Response of cultured endothelial cells to steady flow. *Microvasc Res* 28: 87-94, 1984.
73. **Esmaili S, Hemmati M, and Karamian M.** Physiological role of adiponectin in different tissues: a review. *Arch Physiol Biochem*: 1-7, 2018.

74. **Fang ZY, Prins JB, and Marwick TH.** Diabetic cardiomyopathy: evidence, mechanisms, and therapeutic implications. *Endocr Rev* 25: 543-567, 2004.
75. **Feder JN, Gnirke A, Thomas W, Tsuchihashi Z, Ruddy DA, Basava A, Dormishian F, Domingo R, Jr., Ellis MC, Fullan A, Hinton LM, Jones NL, Kimmel BE, Kronmal GS, Lauer P, Lee VK, Loeb DB, Mapa FA, McClelland E, Meyer NC, Mintier GA, Moeller N, Moore T, Morikang E, Prass CE, Quintana L, Starnes SM, Schatzman RC, Brunke KJ, Drayna DT, Risch NJ, Bacon BR, and Wolff RK.** A novel MHC class I-like gene is mutated in patients with hereditary haemochromatosis. *Nat Genet* 13: 399-408, 1996.
76. **Felinski EA and Antonetti DA.** Glucocorticoid regulation of endothelial cell tight junction gene expression: novel treatments for diabetic retinopathy. *Curr Eye Res* 30: 949-957, 2005.
77. **Ferrannini E, Buzzigoli G, Bonadonna R, Giorico MA, Oleggini M, Graziadei L, Pedrinelli R, Brandi L, and Bevilacqua S.** Insulin resistance in essential hypertension. *N Engl J Med* 317: 350-357, 1987.
78. **Flarsheim CE, Grupp IL, and Matlib MA.** Mitochondrial dysfunction accompanies diastolic dysfunction in diabetic rat heart. *Am J Physiol* 271: H192-202, 1996.
79. **Folkman J and Haudenschild C.** Angiogenesis in vitro. *Nature* 288: 551-556, 1980.
80. **Ford ES, Zhao G, and Li C.** Pre-diabetes and the risk for cardiovascular disease: a systematic review of the evidence. *J Am Coll Cardiol* 55: 1310-1317, 2010.
81. **Freidenberg GR, Suter S, Henry RR, Nolan J, Reichart D, and Olefsky JM.** Delayed onset of insulin activation of the insulin receptor kinase in vivo in human skeletal muscle. *Diabetes* 43: 118-126, 1994.
82. **Fujita H, Hamazaki Y, Noda Y, Oshima M, and Minato N.** Claudin-4 deficiency results in urothelial hyperplasia and lethal hydronephrosis. *PLoS One* 7: e52272, 2012.
83. **Fumeron F, Pean F, Driss F, Balkau B, Tichet J, Marre M, Grandchamp B, and Insulin Resistance Syndrome Study G.** Ferritin and transferrin are both predictive of the onset of hyperglycemia in men and women over 3 years: the data from an epidemiological study on the Insulin Resistance Syndrome (DESIR) study. *Diabetes Care* 29: 2090-2094, 2006.
84. **Funamoto K, Yoshino D, Matsubara K, Zervantonakis IK, Funamoto K, Nakayama M, Masamune J, Kimura Y, and Kamm RD.** Endothelial monolayer permeability under controlled oxygen tension. *Integr Biol (Camb)* 9: 529-538, 2017.
85. **Furuse M, Hata M, Furuse K, Yoshida Y, Haratake A, Sugitani Y, Noda T, Kubo A, and Tsukita S.** Claudin-based tight junctions are crucial for the mammalian epidermal barrier: a lesson from claudin-1-deficient mice. *J Cell Biol* 156: 1099-1111, 2002.
86. **Gathercole LL, Morgan SA, Bujalska IJ, Hauton D, Stewart PM, and Tomlinson JW.** Regulation of lipogenesis by glucocorticoids and insulin in human adipose tissue. *PLoS One* 6: e26223, 2011.
87. **Geer EB, Islam J, and Buettner C.** Mechanisms of glucocorticoid-induced insulin resistance: focus on adipose tissue function and lipid metabolism. *Endocrinol Metab Clin North Am* 43: 75-102, 2014.
88. **Ginsberg HN and MacCallum PR.** The obesity, metabolic syndrome, and type 2 diabetes mellitus pandemic: Part I. Increased cardiovascular disease risk and the

importance of atherogenic dyslipidemia in persons with the metabolic syndrome and type 2 diabetes mellitus. *J Cardiometab Syndr* 4: 113-119, 2009.

89. **Goddard LM and Iruela-Arispe ML.** Cellular and molecular regulation of vascular permeability. *Thromb Haemost* 109: 407-415, 2013.

90. **Goldstein BJ, Scalia RG, and Ma XL.** Protective vascular and myocardial effects of adiponectin. *Nat Clin Pract Cardiovasc Med* 6: 27-35, 2009.

91. **Gonzalez-Mariscal L, Hernandez S, and Vega J.** Inventions designed to enhance drug delivery across epithelial and endothelial cells through the paracellular pathway. *Recent Pat Drug Deliv Formul* 2: 145-176, 2008.

92. **Gory-Faure S, Prandini MH, Pointu H, Roullot V, Pignot-Paintrand I, Vernet M, and Huber P.** Role of vascular endothelial-cadherin in vascular morphogenesis. *Development* 126: 2093-2102, 1999.

93. **Gow A, Southwood CM, Li JS, Pariali M, Riordan GP, Brodie SE, Danias J, Bronstein JM, Kachar B, and Lazzarini RA.** CNS myelin and sertoli cell tight junction strands are absent in Osp/claudin-11 null mice. *Cell* 99: 649-659, 1999.

94. **Gronbaek H, Vogel I, Osterby R, Lancranjan I, Flyvbjerg A, and Orskov H.** Effect of octreotide, captopril or insulin on renal changes and UAE in long-term experimental diabetes. *Kidney Int* 53: 173-180, 1998.

95. **Gunzel D and Fromm M.** Claudins and other tight junction proteins. *Compr Physiol* 2: 1819-1852, 2012.

96. **Gunzel D and Yu AS.** Claudins and the modulation of tight junction permeability. *Physiol Rev* 93: 525-569, 2013.

97. **Gutniak M, Orskov C, Holst JJ, Ahren B, and Efendic S.** Antidiabetogenic effect of glucagon-like peptide-1 (7-36)amide in normal subjects and patients with diabetes mellitus. *N Engl J Med* 326: 1316-1322, 1992.

98. **Hardie DG and Carling D.** The AMP-activated protein kinase--fuel gauge of the mammalian cell? *European journal of biochemistry / FEBS* 246: 259-273, 1997.

99. **Hawkins BT, Lundeen TF, Norwood KM, Brooks HL, and Egleton RD.** Increased blood-brain barrier permeability and altered tight junctions in experimental diabetes in the rat: contribution of hyperglycaemia and matrix metalloproteinases. *Diabetologia* 50: 202-211, 2007.

100. **Hayashi D, Tamura A, Tanaka H, Yamazaki Y, Watanabe S, Suzuki K, Suzuki K, Sentani K, Yasui W, Rakugi H, Isaka Y, and Tsukita S.** Deficiency of claudin-18 causes paracellular H+ leakage, up-regulation of interleukin-1beta, and atrophic gastritis in mice. *Gastroenterology* 142: 292-304, 2012.

101. **Heilig CW, Concepcion LA, Riser BL, Freytag SO, Zhu M, and Cortes P.** Overexpression of glucose transporters in rat mesangial cells cultured in a normal glucose milieu mimics the diabetic phenotype. *J Clin Invest* 96: 1802-1814, 1995.

102. **Herkner H, Klein N, Joukhadar C, Lackner E, Langenberger H, Frossard M, Bieglmayer C, Wagner O, Roden M, and Muller M.** Transcapillary insulin transfer in human skeletal muscle. *Eur J Clin Invest* 33: 141-146, 2003.

103. **Herland A, van der Meer AD, FitzGerald EA, Park TE, Sleeboom JJ, and Ingber DE.** Distinct Contributions of Astrocytes and Pericytes to Neuroinflammation Identified in a 3D Human Blood-Brain Barrier on a Chip. *PLoS One* 11: e0150360, 2016.
104. **Ho YT, Adriani G, Beyer S, Nhan PT, Kamm RD, and Kah JCY.** A Facile Method to Probe the Vascular Permeability of Nanoparticles in Nanomedicine Applications. *Sci Rep* 7: 707, 2017.
105. **Hoes JN, Jacobs JW, Boers M, Boumpas D, Buttgereit F, Caeyers N, Choy EH, Cutolo M, Da Silva JA, Esselens G, Guillevin L, Hafstrom I, Kirwan JR, Rovensky J, Russell A, Saag KG, Svensson B, Westhovens R, Zeidler H, and Bijlsma JW.** EULAR evidence-based recommendations on the management of systemic glucocorticoid therapy in rheumatic diseases. *Ann Rheum Dis* 66: 1560-1567, 2007.
106. **Hojbjerre L, Rosenzweig M, Dela F, Bruun JM, and Stallknecht B.** Acute exercise increases adipose tissue interstitial adiponectin concentration in healthy overweight and lean subjects. *Eur J Endocrinol* 157: 613-623, 2007.
107. **Holland WL, Miller RA, Wang ZV, Sun K, Barth BM, Bui HH, Davis KE, Bikman BT, Halberg N, Rutkowski JM, Wade MR, Tenorio VM, Kuo MS, Brozinick JT, Zhang BB, Birnbaum MJ, Summers SA, and Scherer PE.** Receptor-mediated activation of ceramidase activity initiates the pleiotropic actions of adiponectin. *Nature medicine* 17: 55-63, 2011.
108. **Hsu CP, Lin CH, and Kuo CY.** Endothelial-cell inflammation and damage by reactive oxygen species are prevented by propofol via ABCA1-mediated cholesterol efflux. *Int J Med Sci* 15: 978-985, 2018.
109. **Hug C, Wang J, Ahmad NS, Bogan JS, Tsao TS, and Lodish HF.** T-cadherin is a receptor for hexameric and high-molecular-weight forms of Acrp30/adiponectin. *Proc Natl Acad Sci U S A* 101: 10308-10313, 2004.
110. **Hutton BF.** New SPECT technology: potential and challenges. *European journal of nuclear medicine and molecular imaging* 37: 1883-1886, 2010.
111. **Hyde D, de Kleine R, MacLaurin SA, Miller E, Brooks DH, Krucker T, and Ntziachristos V.** Hybrid FMT-CT imaging of amyloid-beta plaques in a murine Alzheimer's disease model. *NeuroImage* 44: 1304-1311, 2009.
112. **Italia K, Colah R, and Ghosh K.** Experimental animal model to study iron overload and iron chelation and review of other such models. *Blood Cells Mol Dis* 55: 194-199, 2015.
113. **Iwabu M, Okada-Iwabu M, Yamauchi T, and Kadowaki T.** Adiponectin/adiponectin receptor in disease and aging. *NPJ Aging Mech Dis* 1: 15013, 2015.
114. **Iwabu M, Yamauchi T, Okada-Iwabu M, Sato K, Nakagawa T, Funata M, Yamaguchi M, Namiki S, Nakayama R, Tabata M, Ogata H, Kubota N, Takamoto I, Hayashi YK, Yamauchi N, Waki H, Fukayama M, Nishino I, Tokuyama K, Ueki K, Oike Y, Ishii S, Hirose K, Shimizu T, Touhara K, and Kadowaki T.** Adiponectin and AdipoR1 regulate PGC-1alpha and mitochondria by Ca(2+) and AMPK/SIRT1. *Nature* 464: 1313-1319, 2010.
115. **Janka HU, Plewe G, Riddle MC, Kliebe-Frisch C, Schweitzer MA, and Yki-Jarvinen H.** Comparison of basal insulin added to oral agents versus twice-daily premixed insulin as initial insulin therapy for type 2 diabetes. *Diabetes Care* 28: 254-259, 2005.
116. **Jehn M, Clark JM, and Guallar E.** Serum ferritin and risk of the metabolic syndrome in U.S. adults. *Diabetes Care* 27: 2422-2428, 2004.

117. **Jehn ML, Guallar E, Clark JM, Couper D, Duncan BB, Ballantyne CM, Hoogeveen RC, Harris ZL, and Pankow JS.** A prospective study of plasma ferritin level and incident diabetes: the Atherosclerosis Risk in Communities (ARIC) Study. *Am J Epidemiol* 165: 1047-1054, 2007.
118. **Jeon JS, Bersini S, Gilardi M, Dubini G, Charest JL, Moretti M, and Kamm RD.** Human 3D vascularized organotypic microfluidic assays to study breast cancer cell extravasation. *Proc Natl Acad Sci U S A* 112: 214-219, 2015.
119. **Jeon JS, Bersini S, Whisler JA, Chen MB, Dubini G, Charest JL, Moretti M, and Kamm RD.** Generation of 3D functional microvascular networks with human mesenchymal stem cells in microfluidic systems. *Integr Biol (Camb)* 6: 555-563, 2014.
120. **Jeppesen J, Hein HO, Suadicani P, and Gyntelberg F.** High triglycerides and low HDL cholesterol and blood pressure and risk of ischemic heart disease. *Hypertension* 36: 226-232, 2000.
121. **Johnson AM, Costanzo A, Gareau MG, Armando AM, Quehenberger O, Jameson JM, and Olefsky JM.** High fat diet causes depletion of intestinal eosinophils associated with intestinal permeability. *PLoS One* 10: e0122195, 2015.
122. **Kadowaki T and Yamauchi T.** Adiponectin receptor signaling: a new layer to the current model. *Cell Metab* 13: 123-124, 2011.
123. **Kadowaki T, Yamauchi T, Kubota N, Hara K, Ueki K, and Tobe K.** Adiponectin and adiponectin receptors in insulin resistance, diabetes, and the metabolic syndrome. *J Clin Invest* 116: 1784-1792, 2006.
124. **Kaira K, Oriuchi N, Shimizu K, Ishikita T, Higuchi T, Imai H, Yanagitani N, Sunaga N, Hisada T, Ishizuka T, Kanai Y, Endou H, Nakajima T, Endo K, and Mori M.** Evaluation of thoracic tumors with (18)F-FMT and (18)F-FDG PET-CT: a clinicopathological study. *International journal of cancer Journal international du cancer* 124: 1152-1160, 2009.
125. **Karalliedde J and Gnudi L.** Diabetes mellitus, a complex and heterogeneous disease, and the role of insulin resistance as a determinant of diabetic kidney disease. *Nephrol Dial Transplant* 31: 206-213, 2016.
126. **Keaney J and Campbell M.** The dynamic blood-brain barrier. *FEBS J* 282: 4067-4079, 2015.
127. **Kelcz F, Joseph PM, and Hilal SK.** Noise considerations in dual energy CT scanning. *Medical physics* 6: 418-425, 1979.
128. **Kim J, Chung M, Kim S, Jo DH, Kim JH, and Jeon NL.** Engineering of a Biomimetic Pericyte-Covered 3D Microvascular Network. *PLoS One* 10: e0133880, 2015.
129. **Kim KH, Lopez-Casillas F, Bai DH, Luo X, and Pape ME.** Role of reversible phosphorylation of acetyl-CoA carboxylase in long-chain fatty acid synthesis. *FASEB J* 3: 2250-2256, 1989.
130. **Kim S, Kim W, Lim S, and Jeon JS.** Vasculature-On-A-Chip for In Vitro Disease Models. *Bioengineering (Basel)* 4, 2017.
131. **Kim S, Lee H, Chung M, and Jeon NL.** Engineering of functional, perfusable 3D microvascular networks on a chip. *Lab Chip* 13: 1489-1500, 2013.
132. **Kim SP, Ellmerer M, Van Citters GW, and Bergman RN.** Primacy of hepatic insulin resistance in the development of the metabolic syndrome induced by an isocaloric moderate-fat diet in the dog. *Diabetes* 52: 2453-2460, 2003.

133. **Kissebah AH, Sonnenberg GE, Myklebust J, Goldstein M, Broman K, James RG, Marks JA, Krakower GR, Jacob HJ, Weber J, Martin L, Blangero J, and Comuzzie AG.** Quantitative trait loci on chromosomes 3 and 17 influence phenotypes of the metabolic syndrome. *Proc Natl Acad Sci U S A* 97: 14478-14483, 2000.
134. **Kolka CM and Bergman RN.** The barrier within: endothelial transport of hormones. *Physiology (Bethesda)* 27: 237-247, 2012.
135. **Kolka CM and Bergman RN.** The endothelium in diabetes: its role in insulin access and diabetic complications. *Rev Endocr Metab Disord* 14: 13-19, 2013.
136. **Kolka CM, Harrison LN, Lottati M, Chiu JD, Kirkman EL, and Bergman RN.** Diet-induced obesity prevents interstitial dispersion of insulin in skeletal muscle. *Diabetes* 59: 619-626, 2010.
137. **Kolm-Litty V, Sauer U, Nerlich A, Lehmann R, and Schleicher ED.** High glucose-induced transforming growth factor beta1 production is mediated by the hexosamine pathway in porcine glomerular mesangial cells. *J Clin Invest* 101: 160-169, 1998.
138. **Kowdley KV.** Iron Overload in Patients With Chronic Liver Disease. *Gastroenterol Hepatol (N Y)* 12: 695-698, 2016.
139. **Krause MP, Liu Y, Vu V, Chan L, Xu A, Riddell MC, Sweeney G, and Hawke TJ.** Adiponectin is expressed by skeletal muscle fibers and influences muscle phenotype and function. *Am J Physiol Cell Physiol* 295: C203-212, 2008.
140. **Krug SM, Gunzel D, Conrad MP, Lee IF, Amasheh S, Fromm M, and Yu AS.** Charge-selective claudin channels. *Ann N Y Acad Sci* 1257: 20-28, 2012.
141. **Ku BJ, Kim SY, Lee TY, and Park KS.** Serum ferritin is inversely correlated with serum adiponectin level: population-based cross-sectional study. *Dis Markers* 27: 303-310, 2009.
142. **Kubota N, Yano W, Kubota T, Yamauchi T, Itoh S, Kumagai H, Kozono H, Takamoto I, Okamoto S, Shiuchi T, Suzuki R, Satoh H, Tsuchida A, Moroi M, Sugi K, Noda T, Ebinuma H, Ueta Y, Kondo T, Araki E, Ezaki O, Nagai R, Tobe K, Terauchi Y, Ueki K, Minokoshi Y, and Kadowaki T.** Adiponectin stimulates AMP-activated protein kinase in the hypothalamus and increases food intake. *Cell Metab* 6: 55-68, 2007.
143. **Kubota T, Kubota N, Kumagai H, Yamaguchi S, Kozono H, Takahashi T, Inoue M, Itoh S, Takamoto I, Sasako T, Kumagai K, Kawai T, Hashimoto S, Kobayashi T, Sato M, Tokuyama K, Nishimura S, Tsunoda M, Ide T, Murakami K, Yamazaki T, Ezaki O, Kawamura K, Masuda H, Moroi M, Sugi K, Oike Y, Shimokawa H, Yanagihara N, Tsutsui M, Terauchi Y, Tobe K, Nagai R, Kamata K, Inoue K, Kodama T, Ueki K, and Kadowaki T.** Impaired insulin signaling in endothelial cells reduces insulin-induced glucose uptake by skeletal muscle. *Cell Metab* 13: 294-307, 2011.
144. **Kumar P, Shen Q, Pivetti CD, Lee ES, Wu MH, and Yuan SY.** Molecular mechanisms of endothelial hyperpermeability: implications in inflammation. *Expert Rev Mol Med* 11: e19, 2009.
145. **Kusminski CM, McTernan PG, Schraw T, Kos K, O'Hare JP, Ahima R, Kumar S, and Scherer PE.** Adiponectin complexes in human cerebrospinal fluid: distinct complex distribution from serum. *Diabetologia* 50: 634-642, 2007.

146. **Langille BL and Adamson SL.** Relationship between blood flow direction and endothelial cell orientation at arterial branch sites in rabbits and mice. *Circ Res* 48: 481-488, 1981.
147. **Lapointe E, Pichette J, and Berube-Lauziere Y.** A multi-view time-domain non-contact diffuse optical tomography scanner with dual wavelength detection for intrinsic and fluorescence small animal imaging. *The Review of scientific instruments* 83: 063703, 2012.
148. **Lee CS, Bishop ES, Zhang R, Yu X, Farina EM, Yan S, Zhao C, Zheng Z, Shu Y, Wu X, Lei J, Li Y, Zhang W, Yang C, Wu K, Wu Y, Ho S, Athiviraham A, Lee MJ, Wolf JM, Reid RR, and He TC.** Adenovirus-Mediated Gene Delivery: Potential Applications for Gene and Cell-Based Therapies in the New Era of Personalized Medicine. *Genes Dis* 4: 43-63, 2017.
149. **Lee JH, Kim HK, Chandhanayingyong C, Lee FY, and Hielscher AH.** Non-contact small animal fluorescence imaging system for simultaneous multi-directional angular-dependent data acquisition. *Biomedical optics express* 5: 2301-2316, 2014.
150. **Lehmann JM, Moore LB, Smith-Oliver TA, Wilkison WO, Willson TM, and Kliewer SA.** An antidiabetic thiazolidinedione is a high affinity ligand for peroxisome proliferator-activated receptor gamma (PPAR gamma). *J Biol Chem* 270: 12953-12956, 1995.
151. **Lenzen S.** Oxidative stress: the vulnerable beta-cell. *Biochem Soc Trans* 36: 343-347, 2008.
152. **Li B, Maafi F, Berti R, Pouliot P, Rheaume E, Tardif JC, and Lesage F.** Hybrid FMT-MRI applied to in vivo atherosclerosis imaging. *Biomedical optics express* 5: 1664-1676, 2014.
153. **Li R, Zheng K, Hu P, Chen Z, Zhou S, Chen J, Yuan C, Chen S, Zheng W, Ma E, Zhang F, Xue J, Chen X, and Huang M.** A novel tumor targeting drug carrier for optical imaging and therapy. *Theranostics* 4: 642-659, 2014.
154. **Lin H, Lian WS, Chen HH, Lai PF, and Cheng CF.** Adiponectin ameliorates iron-overload cardiomyopathy through the PPARalpha-PGC-1-dependent signaling pathway. *Mol Pharmacol* 84: 275-285, 2013.
155. **Lin KT and Wang LH.** New dimension of glucocorticoids in cancer treatment. *Steroids* 111: 84-88, 2016.
156. **Lin SA, Patel M, Suresch D, Connolly B, Bao B, Groves K, Rajopadhye M, Peterson JD, Klimas M, Sur C, and Bednar B.** Quantitative Longitudinal Imaging of Vascular Inflammation and Treatment by Ezetimibe in apoE Mice by FMT Using New Optical Imaging Biomarkers of Cathepsin Activity and alpha(v)beta(3) Integrin. *International journal of molecular imaging* 2012: 189254, 2012.
157. **Liu B, Li Z, and Xie P.** Angioplasty and stenting for severe vertebral artery orifice stenosis: effects on cerebellar function remodeling verified by blood oxygen level-dependent functional magnetic resonance imaging. *Neural regeneration research* 9: 2095-2101, 2014.
158. **Liu C, Wu J, and Zou MH.** Activation of AMP-activated protein kinase alleviates high-glucose-induced dysfunction of brain microvascular endothelial cell tight-junction dynamics. *Free Radic Biol Med* 53: 1213-1221, 2012.

159. **Liu Y, Palanivel R, Rai E, Park M, Gabor TV, Scheid MP, Xu A, and Sweeney G.** Adiponectin stimulates autophagy and reduces oxidative stress to enhance insulin sensitivity during high-fat diet feeding in mice. *Diabetes* 64: 36-48, 2015.
160. **Liu Y, Retnakaran R, Hanley A, Tungtrongchitr R, Shaw C, and Sweeney G.** Total and high molecular weight but not trimeric or hexameric forms of adiponectin correlate with markers of the metabolic syndrome and liver injury in Thai subjects. *J Clin Endocrinol Metab* 92: 4313-4318, 2007.
161. **Liu Y and Sweeney G.** Adiponectin action in skeletal muscle. *Best practice & research Clinical endocrinology & metabolism* 28: 33-41, 2014.
162. **Lucas CP, Estigarribia JA, Darga LL, and Reaven GM.** Insulin and blood pressure in obesity. *Hypertension* 7: 702-706, 1985.
163. **Lum H and Roebuck KA.** Oxidant stress and endothelial cell dysfunction. *Am J Physiol Cell Physiol* 280: C719-741, 2001.
164. **Ly JP, Onay T, Sison K, Sivaskandarajah G, Sabbisetti V, Li L, Bonventre JV, Flenniken A, Paragas N, Barasch JM, Adamson SL, Osborne L, Rossant J, Schnermann J, and Quaggin SE.** The Sweet Pee model for Sglt2 mutation. *J Am Soc Nephrol* 22: 113-123, 2011.
165. **Maggs DG, Jacob R, Rife F, Lange R, Leone P, During MJ, Tamborlane WV, and Sherwin RS.** Interstitial fluid concentrations of glycerol, glucose, and amino acids in human quadricep muscle and adipose tissue. Evidence for significant lipolysis in skeletal muscle. *J Clin Invest* 96: 370-377, 1995.
166. **Malaguarnera R and Belfiore A.** The insulin receptor: a new target for cancer therapy. *Front Endocrinol (Lausanne)* 2: 93, 2011.
167. **Malatiali S, Francis I, and Barac-Nieto M.** Phlorizin prevents glomerular hyperfiltration but not hypertrophy in diabetic rats. *Exp Diabetes Res* 2008: 305403, 2008.
168. **Mao X, Kikani CK, Riojas RA, Langlais P, Wang L, Ramos FJ, Fang Q, Christ-Roberts CY, Hong JY, Kim RY, Liu F, and Dong LQ.** APPL1 binds to adiponectin receptors and mediates adiponectin signalling and function. *Nature cell biology* 8: 516-523, 2006.
169. **Matsuda K, Fujishima Y, Maeda N, Mori T, Hirata A, Sekimoto R, Tsushima Y, Masuda S, Yamaoka M, Inoue K, Nishizawa H, Kita S, Ranscht B, Funahashi T, and Shimomura I.** Positive feedback regulation between adiponectin and T-cadherin impacts adiponectin levels in tissue and plasma of male mice. *Endocrinology* 156: 934-946, 2015.
170. **Matsunaga T, Hokari S, Koyama I, Harada T, and Komoda T.** NF-kappa B activation in endothelial cells treated with oxidized high-density lipoprotein. *Biochem Biophys Res Commun* 303: 313-319, 2003.
171. **Michalik L, Auwerx J, Berger JP, Chatterjee VK, Glass CK, Gonzalez FJ, Grimaldi PA, Kadowaki T, Lazar MA, O'Rahilly S, Palmer CN, Plutzky J, Reddy JK, Spiegelman BM, Staels B, and Wahli W.** International Union of Pharmacology. LXI. Peroxisome proliferator-activated receptors. *Pharmacological reviews* 58: 726-741, 2006.
172. **Miller NE, Michel CC, Nanjee MN, Olszewski WL, Miller IP, Hazell M, Olivecrona G, Sutton P, Humphreys SM, and Frayn KN.** Secretion of adipokines by human adipose tissue in vivo: partitioning between capillary and lymphatic transport. *American journal of physiology Endocrinology and metabolism* 301: E659-667, 2011.

173. **Miller RA, Chu Q, Le Lay J, Scherer PE, Ahima RS, Kaestner KH, Foretz M, Viollet B, and Birnbaum MJ.** Adiponectin suppresses gluconeogenic gene expression in mouse hepatocytes independent of LKB1-AMPK signaling. *J Clin Invest* 121: 2518-2528, 2011.
174. **Miyamoto T, Morita K, Takemoto D, Takeuchi K, Kitano Y, Miyakawa T, Nakayama K, Okamura Y, Sasaki H, Miyachi Y, Furuse M, and Tsukita S.** Tight junctions in Schwann cells of peripheral myelinated axons: a lesson from claudin-19-deficient mice. *J Cell Biol* 169: 527-538, 2005.
175. **Miyawaki-Shimizu K, Predescu D, Shimizu J, Broman M, Predescu S, and Malik AB.** siRNA-induced caveolin-1 knockdown in mice increases lung vascular permeability via the junctional pathway. *Am J Physiol Lung Cell Mol Physiol* 290: L405-413, 2006.
176. **Modan M, Halkin H, Almog S, Lusky A, Eshkol A, Shefi M, Shitrit A, and Fuchs Z.** Hyperinsulinemia. A link between hypertension obesity and glucose intolerance. *J Clin Invest* 75: 809-817, 1985.
177. **Mohajerani P, Hipp A, Willner M, Marschner M, Trajkovic-Arsic M, Ma X, Burton NC, Klemm U, Radrich K, Ermolayev V, Tzoumas S, Siveke JT, Bech M, Pfeiffer F, and Ntziachristos V.** FMT-PCCT: hybrid fluorescence molecular tomography-x-ray phase-contrast CT imaging of mouse models. *IEEE transactions on medical imaging* 33: 1434-1446, 2014.
178. **Montet X, Figueiredo JL, Alencar H, Ntziachristos V, Mahmood U, and Weissleder R.** Tomographic fluorescence imaging of tumor vascular volume in mice. *Radiology* 242: 751-758, 2007.
179. **Murdolo G, Hammarstedt A, Schmelz M, Jansson PA, and Smith U.** Acute hyperinsulinemia differentially regulates interstitial and circulating adiponectin oligomeric pattern in lean and insulin-resistant, obese individuals. *J Clin Endocrinol Metab* 94: 4508-4516, 2009.
180. **Muto S, Hata M, Taniguchi J, Tsuruoka S, Moriwaki K, Saitou M, Furuse K, Sasaki H, Fujimura A, Imai M, Kusano E, Tsukita S, and Furuse M.** Claudin-2-deficient mice are defective in the leaky and cation-selective paracellular permeability properties of renal proximal tubules. *Proc Natl Acad Sci U S A* 107: 8011-8016, 2010.
181. **Nahrendorf M, Keliher E, Marinelli B, Waterman P, Feruglio PF, Fexon L, Pivovarov M, Swirski FK, Pittet MJ, Vinegoni C, and Weissleder R.** Hybrid PET-optical imaging using targeted probes. *Proc Natl Acad Sci U S A* 107: 7910-7915, 2010.
182. **Nakano Y, Kim SH, Kim HM, Sanneman JD, Zhang Y, Smith RJ, Marcus DC, Wangemann P, Nessler RA, and Banfi B.** A claudin-9-based ion permeability barrier is essential for hearing. *PLoS Genet* 5: e1000610, 2009.
183. **Nanami M, Ookawara T, Otaki Y, Ito K, Moriguchi R, Miyagawa K, Hasuike Y, Izumi M, Eguchi H, Suzuki K, and Nakanishi T.** Tumor necrosis factor-alpha-induced iron sequestration and oxidative stress in human endothelial cells. *Arterioscler Thromb Vasc Biol* 25: 2495-2501, 2005.
184. **Nanayakkara G, Kariharan T, Wang L, Zhong J, and Amin R.** The cardio-protective signaling and mechanisms of adiponectin. *Am J Cardiovasc Dis* 2: 253-266, 2012.
185. **Neumeier M, Weigert J, Buettner R, Wanninger J, Schaffler A, Muller AM, Killian S, Sauerbruch S, Schlachetzki F, Steinbrecher A, Aslanidis C, Scholmerich J, and Buechler**

C. Detection of adiponectin in cerebrospinal fluid in humans. *American journal of physiology Endocrinology and metabolism* 293: E965-969, 2007.

186. **Nishikawa T, Edelstein D, Du XL, Yamagishi S, Matsumura T, Kaneda Y, Yorek MA, Beebe D, Oates PJ, Hammes HP, Giardino I, and Brownlee M.** Normalizing mitochondrial superoxide production blocks three pathways of hyperglycaemic damage. *Nature* 404: 787-790, 2000.

187. **Nitta T, Hata M, Gotoh S, Seo Y, Sasaki H, Hashimoto N, Furuse M, and Tsukita S.** Size-selective loosening of the blood-brain barrier in claudin-5-deficient mice. *J Cell Biol* 161: 653-660, 2003.

188. **Ntziachristos V, Bremer C, Graves EE, Ripoll J, and Weissleder R.** In vivo tomographic imaging of near-infrared fluorescent probes. *Molecular imaging* 1: 82-88, 2002.

189. **Ntziachristos V, Tung CH, Bremer C, and Weissleder R.** Fluorescence molecular tomography resolves protease activity in vivo. *Nature medicine* 8: 757-760, 2002.

190. **Ntziachristos V and Weissleder R.** Charge-coupled-device based scanner for tomography of fluorescent near-infrared probes in turbid media. *Medical physics* 29: 803-809, 2002.

191. **Okamoto Y, Kihara S, Funahashi T, Matsuzawa Y, and Libby P.** Adiponectin: a key adipocytokine in metabolic syndrome. *Clin Sci (Lond)* 110: 267-278, 2006.

192. **Omran OM.** Effects of thymoquinone on STZ-induced diabetic nephropathy: an immunohistochemical study. *Ultrastruct Pathol* 38: 26-33, 2014.

193. **Ooi BK, Goh BH, and Yap WH.** Oxidative Stress in Cardiovascular Diseases: Involvement of Nrf2 Antioxidant Redox Signaling in Macrophage Foam Cells Formation. *Int J Mol Sci* 18, 2017.

194. **Orsenigo F, Giampietro C, Ferrari A, Corada M, Galaup A, Sigismund S, Ristagno G, Maddaluno L, Koh GY, Franco D, Kurtcuoglu V, Poulikakos D, Baluk P, McDonald D, Grazia Lampugnani M, and Dejana E.** Phosphorylation of VE-cadherin is modulated by haemodynamic forces and contributes to the regulation of vascular permeability in vivo. *Nat Commun* 3: 1208, 2012.

195. **Osorio H, Bautista R, Rios A, Franco M, Arellano A, Vargas-Robles H, Romo E, and Escalante B.** Effect of phlorizin on SGLT2 expression in the kidney of diabetic rats. *J Nephrol* 23: 541-546, 2010.

196. **Pajvani UB, Du X, Combs TP, Berg AH, Rajala MW, Schulthess T, Engel J, Brownlee M, and Scherer PE.** Structure-function studies of the adipocyte-secreted hormone Acrp30/adiponectin. Implications fpr metabolic regulation and bioactivity. *J Biol Chem* 278: 9073-9085, 2003.

197. **Pajvani UB, Hawkins M, Combs TP, Rajala MW, Doebber T, Berger JP, Wagner JA, Wu M, Knopps A, Xiang AH, Utzschneider KM, Kahn SE, Olefsky JM, Buchanan TA, and Scherer PE.** Complex distribution, not absolute amount of adiponectin, correlates with thiazolidinedione-mediated improvement in insulin sensitivity. *J Biol Chem* 279: 12152-12162, 2004.

198. **Palanivel R, Ganguly R, Turdi S, Xu A, and Sweeney G.** Adiponectin stimulates Rho-mediated actin cytoskeleton remodeling and glucose uptake via APPL1 in primary cardiomyocytes. *Metabolism* 63: 1363-1373, 2014.
199. **Papaspyros NS.** *The history of diabetes mellitus*: G. Thieme, 1964.
200. **Park M and Sweeney G.** Direct effects of adipokines on the heart: focus on adiponectin. *Heart Fail Rev* 18: 631-644, 2013.
201. **Park M, Youn B, Zheng XL, Wu D, Xu A, and Sweeney G.** Globular adiponectin, acting via AdipoR1/APPL1, protects H9c2 cells from hypoxia/reoxygenation-induced apoptosis. *PLoS One* 6: e19143, 2011.
202. **Peters KE, Beilby J, Cadby G, Warrington NM, Bruce DG, Davis WA, Davis TM, Wiltshire S, Knuiman M, McQuillan BM, Palmer LJ, Thompson PL, and Hung J.** A comprehensive investigation of variants in genes encoding adiponectin (ADIPOQ) and its receptors (ADIPOR1/R2), and their association with serum adiponectin, type 2 diabetes, insulin resistance and the metabolic syndrome. *BMC Med Genet* 14: 15, 2013.
203. **Pickup J, Mattock M, and Kerry S.** Glycaemic control with continuous subcutaneous insulin infusion compared with intensive insulin injections in patients with type 1 diabetes: meta-analysis of randomised controlled trials. *BMJ* 324: 705, 2002.
204. **Pietrangelo A.** Hereditary hemochromatosis: pathogenesis, diagnosis, and treatment. *Gastroenterology* 139: 393-408, 408 e391-392, 2010.
205. **Pingle SC, Mishra S, Marcuzzi A, Bhat SG, Sekino Y, Rybak LP, and Ramkumar V.** Osmotic diuretics induce adenosine A1 receptor expression and protect renal proximal tubular epithelial cells against cisplatin-mediated apoptosis. *J Biol Chem* 279: 43157-43167, 2004.
206. **Pollare T, Lithell H, and Berne C.** Insulin resistance is a characteristic feature of primary hypertension independent of obesity. *Metabolism* 39: 167-174, 1990.
207. **Pratley RE, Nauck M, Bailey T, Montanya E, Cuddihy R, Filetti S, Thomsen AB, Sondergaard RE, Davies M, and Group L-D-S.** Liraglutide versus sitagliptin for patients with type 2 diabetes who did not have adequate glycaemic control with metformin: a 26-week, randomised, parallel-group, open-label trial. *Lancet* 375: 1447-1456, 2010.
208. **Pries AR and Kuebler WM.** Normal endothelium. *Handb Exp Pharmacol*: 1-40, 2006.
209. **Protzek AO, Rezende LF, Costa-Junior JM, Ferreira SM, Cappelli AP, de Paula FM, de Souza JC, Kurauti MA, Carneiro EM, Rafacho A, and Boschero AC.** Hyperinsulinemia caused by dexamethasone treatment is associated with reduced insulin clearance and lower hepatic activity of insulin-degrading enzyme. *J Steroid Biochem Mol Biol* 155: 1-8, 2016.
210. **Raasch M, Rennert K, Jahn T, Peters S, Henkel T, Huber O, Schulz I, Becker H, Lorkowski S, Funke H, and Mosig A.** Microfluidically supported biochip design for culture of endothelial cell layers with improved perfusion conditions. *Biofabrication* 7: 015013, 2015.
211. **Raignault A, Bolduc V, Lesage F, and Thorin E.** Pulse pressure-dependent cerebrovascular eNOS regulation in mice. *J Cereb Blood Flow Metab* 37: 413-424, 2017.
212. **Rao A, Pandya V, and Whaley-Connell A.** Obesity and insulin resistance in resistant hypertension: implications for the kidney. *Adv Chronic Kidney Dis* 22: 211-217, 2015.

213. **Raza H and John A.** Streptozotocin-induced cytotoxicity, oxidative stress and mitochondrial dysfunction in human hepatoma HepG2 cells. *Int J Mol Sci* 13: 5751-5767, 2012.
214. **Razani B, Engelman JA, Wang XB, Schubert W, Zhang XL, Marks CB, Macaluso F, Russell RG, Li M, Pestell RG, Di Vizio D, Hou H, Jr., Kneitz B, Lagaud G, Christ GJ, Edelmann W, and Lisanti MP.** Caveolin-1 null mice are viable but show evidence of hyperproliferative and vascular abnormalities. *J Biol Chem* 276: 38121-38138, 2001.
215. **Reaven GM.** Insulin resistance/compensatory hyperinsulinemia, essential hypertension, and cardiovascular disease. *J Clin Endocrinol Metab* 88: 2399-2403, 2003.
216. **Reaven GM.** Relationship between insulin resistance and hypertension. *Diabetes Care* 14 Suppl 4: 33-38, 1991.
217. **Reverchon M, Rame C, Bertoldo M, and Dupont J.** Adipokines and the female reproductive tract. *International journal of endocrinology* 2014: 232454, 2014.
218. **Rincon-Choles H, Vasylyeva TL, Pergola PE, Bhandari B, Bhandari K, Zhang JH, Wang W, Gorin Y, Barnes JL, and Abboud HE.** ZO-1 expression and phosphorylation in diabetic nephropathy. *Diabetes* 55: 894-900, 2006.
219. **Rochfort KD and Cummins PM.** The blood-brain barrier endothelium: a target for pro-inflammatory cytokines. *Biochem Soc Trans* 43: 702-706, 2015.
220. **Rosca MG, Monnier VM, Szweda LI, and Weiss MF.** Alterations in renal mitochondrial respiration in response to the reactive oxoaldehyde methylglyoxal. *Am J Physiol Renal Physiol* 283: F52-59, 2002.
221. **Roy Chowdhury SK, Smith DR, Saleh A, Schapansky J, Marquez A, Gomes S, Akude E, Morrow D, Calcutt NA, and Fernyhough P.** Impaired adenosine monophosphate-activated protein kinase signalling in dorsal root ganglia neurons is linked to mitochondrial dysfunction and peripheral neuropathy in diabetes. *Brain* 135: 1751-1766, 2012.
222. **Rutkowski JM, Halberg N, Wang QA, Holland WL, Xia JY, and Scherer PE.** Differential transendothelial transport of adiponectin complexes. *Cardiovasc Diabetol* 13: 47, 2014.
223. **Ryan JD, Armitage AE, Cobbold JF, Banerjee R, Borsani O, Dongiovanni P, Neubauer S, Morovat R, Wang LM, Pasricha SR, Fargion S, Collier J, Barnes E, Drakesmith H, Valenti L, and Pavlides M.** Hepatic iron is the major determinant of serum ferritin in NAFLD patients. *Liver Int* 38: 164-173, 2018.
224. **Sacks DB.** Measurement of hemoglobin A(1c): a new twist on the path to harmony. *Diabetes Care* 35: 2674-2680, 2012.
225. **Sacks DB, Arnold M, Bakris GL, Bruns DE, Horvath AR, Kirkman MS, Lernmark A, Metzger BE, and Nathan DM.** Guidelines and recommendations for laboratory analysis in the diagnosis and management of diabetes mellitus. *Clin Chem* 57: e1-e47, 2011.
226. **Saitou M, Furuse M, Sasaki H, Schulzke JD, Fromm M, Takano H, Noda T, and Tsukita S.** Complex phenotype of mice lacking occludin, a component of tight junction strands. *Mol Biol Cell* 11: 4131-4142, 2000.
227. **Sayeski PP and Kudlow JE.** Glucose metabolism to glucosamine is necessary for glucose stimulation of transforming growth factor-alpha gene transcription. *J Biol Chem* 271: 15237-15243, 1996.

228. **Scaroni C, Zilio M, Foti M, and Boscaro M.** Glucose Metabolism Abnormalities in Cushing Syndrome: From Molecular Basis to Clinical Management. *Endocr Rev* 38: 189-219, 2017.
229. **Scheid MP and Sweeney G.** The role of adiponectin signaling in metabolic syndrome and cancer. *Rev Endocr Metab Disord* 15: 157-167, 2014.
230. **Schubert W, Frank PG, Woodman SE, Hyogo H, Cohen DE, Chow CW, and Lisanti MP.** Microvascular hyperpermeability in caveolin-1 (-/-) knock-out mice. Treatment with a specific nitric-oxide synthase inhibitor, L-NAME, restores normal microvascular permeability in Cav-1 null mice. *J Biol Chem* 277: 40091-40098, 2002.
231. **Seco J, Clasie B, and Partridge M.** Review on the characteristics of radiation detectors for dosimetry and imaging. *Physics in medicine and biology* 59: R303-347, 2014.
232. **Selvin E, Steffes MW, Zhu H, Matsushita K, Wagenknecht L, Pankow J, Coresh J, and Brancati FL.** Glycated hemoglobin, diabetes, and cardiovascular risk in nondiabetic adults. *N Engl J Med* 362: 800-811, 2010.
233. **Sente T, Van Berendoncks AM, Hoymans VY, and Vrints CJ.** Adiponectin resistance in skeletal muscle: pathophysiological implications in chronic heart failure. *J Cachexia Sarcopenia Muscle* 7: 261-274, 2016.
234. **Shan CY, Yang JH, Kong Y, Wang XY, Zheng MY, Xu YG, Wang Y, Ren HZ, Chang BC, and Chen LM.** Alteration of the intestinal barrier and GLP2 secretion in Berberine-treated type 2 diabetic rats. *J Endocrinol* 218: 255-262, 2013.
235. **Shapiro L and Scherer PE.** The crystal structure of a complement-1q family protein suggests an evolutionary link to tumor necrosis factor. *Current biology : CB* 8: 335-338, 1998.
236. **Sharma K, Ramachandrarao S, Qiu G, Usui HK, Zhu Y, Dunn SR, Ouedraogo R, Hough K, McCue P, Chan L, Falkner B, and Goldstein BJ.** Adiponectin regulates albuminuria and podocyte function in mice. *J Clin Invest* 118: 1645-1656, 2008.
237. **Shen DC, Shieh SM, Fuh MM, Wu DA, Chen YD, and Reaven GM.** Resistance to insulin-stimulated-glucose uptake in patients with hypertension. *J Clin Endocrinol Metab* 66: 580-583, 1988.
238. **Shenouda SM, Widlansky ME, Chen K, Xu G, Holbrook M, Tabit CE, Hamburg NM, Frame AA, Caiano TL, Kluge MA, Duess MA, Levit A, Kim B, Hartman ML, Joseph L, Shirihai OS, and Vita JA.** Altered mitochondrial dynamics contributes to endothelial dysfunction in diabetes mellitus. *Circulation* 124: 444-453, 2011.
239. **Sheu WH, Chen YT, Lee WJ, Wang CW, and Lin LY.** A relationship between serum ferritin and the insulin resistance syndrome is present in non-diabetic women but not in non-diabetic men. *Clin Endocrinol (Oxf)* 58: 380-385, 2003.
240. **Sheu WH, Jeng CY, Shieh SM, Fuh MM, Shen DD, Chen YD, and Reaven GM.** Insulin resistance and abnormal electrocardiograms in patients with high blood pressure. *Am J Hypertens* 5: 444-448, 1992.
241. **Shikatani EA, Trifonova A, Mandel ER, Liu ST, Roudier E, Krylova A, Szigiato A, Beaudry J, Riddell MC, and Haas TL.** Inhibition of proliferation, migration and proteolysis contribute to corticosterone-mediated inhibition of angiogenesis. *PLoS One* 7: e46625, 2012.

242. **Shin JY, Sohn J, and Park KH.** Chlorogenic acid decreases retinal vascular hyperpermeability in diabetic rat model. *J Korean Med Sci* 28: 608-613, 2013.
243. **Shin Y, Han S, Jeon JS, Yamamoto K, Zervantonakis IK, Sudo R, Kamm RD, and Chung S.** Microfluidic assay for simultaneous culture of multiple cell types on surfaces or within hydrogels. *Nat Protoc* 7: 1247-1259, 2012.
244. **Shpilberg Y, Beaudry JL, D'Souza A, Campbell JE, Peckett A, and Riddell MC.** A rodent model of rapid-onset diabetes induced by glucocorticoids and high-fat feeding. *Dis Model Mech* 5: 671-680, 2012.
245. **Sjostrand M, Holmang A, and Lonnroth P.** Measurement of interstitial insulin in human muscle. *Am J Physiol* 276: E151-154, 1999.
246. **Smirnova E, Griparic L, Shurland DL, and van der Bliek AM.** Dynamin-related protein Drp1 is required for mitochondrial division in mammalian cells. *Mol Biol Cell* 12: 2245-2256, 2001.
247. **Somwar R, Kim DY, Sweeney G, Huang C, Niu W, Lador C, Ramlal T, and Klip A.** GLUT4 translocation precedes the stimulation of glucose uptake by insulin in muscle cells: potential activation of GLUT4 via p38 mitogen-activated protein kinase. *Biochem J* 359: 639-649, 2001.
248. **Stelter L, Pinkernelle JG, Michel R, Schwartlander R, Raschzok N, Morgul MH, Koch M, Denecke T, Ruf J, Baumler H, Jordan A, Hamm B, Sauer IM, and Teichgraber U.** Modification of aminosilanized superparamagnetic nanoparticles: feasibility of multimodal detection using 3T MRI, small animal PET, and fluorescence imaging. *Molecular imaging and biology : MIB : the official publication of the Academy of Molecular Imaging* 12: 25-34, 2010.
249. **Stuker F, Ripoll J, and Rudin M.** Fluorescence molecular tomography: principles and potential for pharmaceutical research. *Pharmaceutics* 3: 229-274, 2011.
250. **Suh S and Park MK.** Glucocorticoid-Induced Diabetes Mellitus: An Important but Overlooked Problem. *Endocrinol Metab (Seoul)* 32: 180-189, 2017.
251. **Sung HK, Song E, Jahng JWS, Pantopoulos K, and Sweeney G.** Iron induces insulin resistance in cardiomyocytes via regulation of oxidative stress. *Sci Rep* 9: 4668, 2019.
252. **Suzuki S, Wilson-Kubalek EM, Wert D, Tsao TS, and Lee DH.** The oligomeric structure of high molecular weight adiponectin. *FEBS letters* 581: 809-814, 2007.
253. **Swislocki AL, Hoffman BB, and Reaven GM.** Insulin resistance, glucose intolerance and hyperinsulinemia in patients with hypertension. *Am J Hypertens* 2: 419-423, 1989.
254. **Symons JD and Abel ED.** Lipotoxicity contributes to endothelial dysfunction: a focus on the contribution from ceramide. *Rev Endocr Metab Disord* 14: 59-68, 2013.
255. **Takahashi M, Arita Y, Yamagata K, Matsukawa Y, Okutomi K, Horie M, Shimomura I, Hotta K, Kuriyama H, Kihara S, Nakamura T, Yamashita S, Funahashi T, and Matsuzawa Y.** Genomic structure and mutations in adipose-specific gene, adiponectin. *International journal of obesity and related metabolic disorders : journal of the International Association for the Study of Obesity* 24: 861-868, 2000.
256. **Takimoto C, Kumagai H, Osaka M, Sakata K, Onami T, Kamayachi T, Iigaya K, Hayashi K, Saruta T, and Itoh H.** Candesartan and insulin reduce renal sympathetic nerve activity in hypertensive type 1 diabetic rats. *Hypertens Res* 31: 1941-1951, 2008.

257. **Tamura A, Kitano Y, Hata M, Katsuno T, Moriwaki K, Sasaki H, Hayashi H, Suzuki Y, Noda T, Furuse M, Tsukita S, and Tsukita S.** Megaintestine in claudin-15-deficient mice. *Gastroenterology* 134: 523-534, 2008.
258. **Tanaka H, Takechi M, Kiyonari H, Shioi G, Tamura A, and Tsukita S.** Intestinal deletion of Claudin-7 enhances paracellular organic solute flux and initiates colonic inflammation in mice. *Gut* 64: 1529-1538, 2015.
259. **Tao C, Sifuentes A, and Holland WL.** Regulation of glucose and lipid homeostasis by adiponectin: effects on hepatocytes, pancreatic beta cells and adipocytes. *Best practice & research Clinical endocrinology & metabolism* 28: 43-58, 2014.
260. **Tatum R, Zhang Y, Salleng K, Lu Z, Lin JJ, Lu Q, Jeansonne BG, Ding L, and Chen YH.** Renal salt wasting and chronic dehydration in claudin-7-deficient mice. *Am J Physiol Renal Physiol* 298: F24-34, 2010.
261. **Tewari S, Santos JM, and Kowluru RA.** Damaged mitochondrial DNA replication system and the development of diabetic retinopathy. *Antioxid Redox Signal* 17: 492-504, 2012.
262. **Tian R.** Another role for the celebrity: Akt and insulin resistance. *Circ Res* 96: 139-140, 2005.
263. **Tiedge M, Lortz S, Drinkgern J, and Lenzen S.** Relation between antioxidant enzyme gene expression and antioxidative defense status of insulin-producing cells. *Diabetes* 46: 1733-1742, 1997.
264. **Tiwari S, Halagappa VK, Riazi S, Hu X, and Ecelbarger CA.** Reduced expression of insulin receptors in the kidneys of insulin-resistant rats. *J Am Soc Nephrol* 18: 2661-2671, 2007.
265. **Tomas E, Tsao TS, Saha AK, Murrey HE, Zhang Cc C, Itani SI, Lodish HF, and Ruderman NB.** Enhanced muscle fat oxidation and glucose transport by ACRP30 globular domain: acetyl-CoA carboxylase inhibition and AMP-activated protein kinase activation. *Proc Natl Acad Sci U S A* 99: 16309-16313, 2002.
266. **Tomizawa A, Hattori Y, Kasai K, and Nakano Y.** Adiponectin induces NF-kappaB activation that leads to suppression of cytokine-induced NF-kappaB activation in vascular endothelial cells: globular adiponectin vs. high molecular weight adiponectin. *Diab Vasc Dis Res* 5: 123-127, 2008.
267. **Trost A, Lange S, Schroedl F, Bruckner D, Motloch KA, Bogner B, Kaser-Eichberger A, Strohmaier C, Runge C, Aigner L, Rivera FJ, and Reitsamer HA.** Brain and Retinal Pericytes: Origin, Function and Role. *Front Cell Neurosci* 10: 20, 2016.
268. **Tsao TS, Murrey HE, Hug C, Lee DH, and Lodish HF.** Oligomerization state-dependent activation of NF-kappa B signaling pathway by adipocyte complement-related protein of 30 kDa (Acrp30). *J Biol Chem* 277: 29359-29362, 2002.
269. **Tsao TS, Tomas E, Murrey HE, Hug C, Lee DH, Ruderman NB, Heuser JE, and Lodish HF.** Role of disulfide bonds in Acrp30/adiponectin structure and signaling specificity. Different oligomers activate different signal transduction pathways. *J Biol Chem* 278: 50810-50817, 2003.
270. **Tuomilehto J and Bahijri S.** Epidemiology: Lifetime risk of diabetes mellitus--how high? *Nat Rev Endocrinol* 12: 127-128, 2016.

271. **Turer AT and Scherer PE.** Adiponectin: mechanistic insights and clinical implications. *Diabetologia* 55: 2319-2326, 2012.
272. **Turrens JF and Boveris A.** Generation of superoxide anion by the NADH dehydrogenase of bovine heart mitochondria. *Biochem J* 191: 421-427, 1980.
273. **Vallon V, Platt KA, Cunard R, Schroth J, Whaley J, Thomson SC, Koepsell H, and Rieg T.** SGLT2 mediates glucose reabsorption in the early proximal tubule. *J Am Soc Nephrol* 22: 104-112, 2011.
274. **van der Goes MC, Jacobs JW, Boers M, Andrews T, Blom-Bakkers MA, Buttgereit F, Caeyers N, Cutolo M, Da Silva JA, Guillevin L, Kirwan JR, Rovensky J, Severijns G, Webber S, Westhovens R, and Bijlsma JW.** Monitoring adverse events of low-dose glucocorticoid therapy: EULAR recommendations for clinical trials and daily practice. *Ann Rheum Dis* 69: 1913-1919, 2010.
275. **van Staa TP, Leufkens HG, Abenhaim L, Begaud B, Zhang B, and Cooper C.** Use of oral corticosteroids in the United Kingdom. *QJM* 93: 105-111, 2000.
276. **Vasquez KO, Casavant C, and Peterson JD.** Quantitative whole body biodistribution of fluorescent-labeled agents by non-invasive tomographic imaging. *PLoS One* 6: e20594, 2011.
277. **Verma SK and Molitoris BA.** Renal endothelial injury and microvascular dysfunction in acute kidney injury. *Semin Nephrol* 35: 96-107, 2015.
278. **Villarroel M, Garcia-Ramirez M, Corraliza L, Hernandez C, and Simo R.** Effects of high glucose concentration on the barrier function and the expression of tight junction proteins in human retinal pigment epithelial cells. *Exp Eye Res* 89: 913-920, 2009.
279. **Wada M, Tamura A, Takahashi N, and Tsukita S.** Loss of claudins 2 and 15 from mice causes defects in paracellular Na+ flow and nutrient transport in gut and leads to death from malnutrition. *Gastroenterology* 144: 369-380, 2013.
280. **Waki H, Yamauchi T, Kamon J, Ito Y, Uchida S, Kita S, Hara K, Hada Y, Vasseur F, Froguel P, Kimura S, Nagai R, and Kadowaki T.** Impaired multimerization of human adiponectin mutants associated with diabetes. Molecular structure and multimer formation of adiponectin. *J Biol Chem* 278: 40352-40363, 2003.
281. **Wang C, Xin X, Xiang R, Ramos FJ, Liu M, Lee HJ, Chen H, Mao X, Kikani CK, Liu F, and Dong LQ.** Yin-Yang regulation of adiponectin signaling by APPL isoforms in muscle cells. *J Biol Chem* 284: 31608-31615, 2009.
282. **Wang W, Yang X, Lopez de Silanes I, Carling D, and Gorospe M.** Increased AMP:ATP ratio and AMP-activated protein kinase activity during cellular senescence linked to reduced HuR function. *J Biol Chem* 278: 27016-27023, 2003.
283. **Wang Y and Alexander JS.** Analysis of endothelial barrier function in vitro. *Methods Mol Biol* 763: 253-264, 2011.
284. **Wang Y, Heilig K, Saunders T, Minto A, Deb DK, Chang A, Brosius F, Monteiro C, and Heilig CW.** Transgenic overexpression of GLUT1 in mouse glomeruli produces renal disease resembling diabetic glomerulosclerosis. *Am J Physiol Renal Physiol* 299: F99-F111, 2010.

285. **Wang Y, Lam KS, Xu JY, Lu G, Xu LY, Cooper GJ, and Xu A.** Adiponectin inhibits cell proliferation by interacting with several growth factors in an oligomerization-dependent manner. *J Biol Chem* 280: 18341-18347, 2005.
286. **Wang Y, Lu G, Wong WP, Vliegenthart JF, Gerwig GJ, Lam KS, Cooper GJ, and Xu A.** Proteomic and functional characterization of endogenous adiponectin purified from fetal bovine serum. *Proteomics* 4: 3933-3942, 2004.
287. **Wang Y, Ma XL, and Lau WB.** Cardiovascular Adiponectin Resistance: The Critical Role of Adiponectin Receptor Modification. *Trends Endocrinol Metab* 28: 519-530, 2017.
288. **Wang Y, Xu A, Knight C, Xu LY, and Cooper GJ.** Hydroxylation and glycosylation of the four conserved lysine residues in the collagenous domain of adiponectin. Potential role in the modulation of its insulin-sensitizing activity. *J Biol Chem* 277: 19521-19529, 2002.
289. **Wang ZV and Scherer PE.** Adiponectin, the past two decades. *J Mol Cell Biol* 8: 93-100, 2016.
290. **Watts GF and Playford DA.** Dyslipoproteinaemia and hyperoxidative stress in the pathogenesis of endothelial dysfunction in non-insulin dependent diabetes mellitus: an hypothesis. *Atherosclerosis* 141: 17-30, 1998.
291. **Wehrl HF, Sauter AW, Divine MR, and Pichler BJ.** Combined PET/MR: A Technology Becomes Mature. *Journal of nuclear medicine : official publication, Society of Nuclear Medicine* 56: 165-168, 2015.
292. **Welborn TA, Breckenridge A, Rubinstein AH, Dollery CT, and Fraser TR.** Serum-insulin in essential hypertension and in peripheral vascular disease. *Lancet* 1: 1336-1337, 1966.
293. **Welsh GI, Hale LJ, Eremina V, Jeansson M, Maezawa Y, Lennon R, Pons DA, Owen RJ, Satchell SC, Miles MJ, Caunt CJ, McArdle CA, Pavenstadt H, Tavare JM, Herzenberg AM, Kahn CR, Mathieson PW, Quaggin SE, Saleem MA, and Coward RJM.** Insulin signaling to the glomerular podocyte is critical for normal kidney function. *Cell Metab* 12: 329-340, 2010.
294. **Whisler JA, Chen MB, and Kamm RD.** Control of perfusable microvascular network morphology using a multiculture microfluidic system. *Tissue Eng Part C Methods* 20: 543-552, 2014.
295. **Will C, Breiderhoff T, Thumfart J, Stuiver M, Kopplin K, Sommer K, Gunzel D, Querfeld U, Meij IC, Shan Q, Bleich M, Willnow TE, and Muller D.** Targeted deletion of murine Cldn16 identifies extra- and intrarenal compensatory mechanisms of Ca2+ and Mg2+ wasting. *Am J Physiol Renal Physiol* 298: F1152-1161, 2010.
296. **Witt KA and Sandoval KE.** Steroids and the blood-brain barrier: therapeutic implications. *Adv Pharmacol* 71: 361-390, 2014.
297. **Witte DL, Crosby WH, Edwards CQ, Fairbanks VF, and Mitros FA.** Practice guideline development task force of the College of American Pathologists. Hereditary hemochromatosis. *Clin Chim Acta* 245: 139-200, 1996.
298. **Wlazlo N, van Greevenbroek MM, Ferreira I, Jansen EH, Feskens EJ, van der Kallen CJ, Schalkwijk CG, Bravenboer B, and Stehouwer CD.** Iron metabolism is associated with adipocyte insulin resistance and plasma adiponectin: the Cohort on Diabetes and Atherosclerosis Maastricht (CODAM) study. *Diabetes Care* 36: 309-315, 2013.

299. **Won SM, Lee JH, Park UJ, Gwag J, Gwag BJ, and Lee YB.** Iron mediates endothelial cell damage and blood-brain barrier opening in the hippocampus after transient forebrain ischemia in rats. *Exp Mol Med* 43: 121-128, 2011.
300. **Wood CM, Gilmour KM, Perry SF, Part P, and Walsh PJ.** Pulsatile urea excretion in gulf toadfish (Opsanus beta): evidence for activation of a specific facilitated diffusion transport system. *J Exp Biol* 201: 805-817, 1998.
301. **Wu W-H, Punde TH, Shih P-C, Fu C-Y, Wang T-P, Hsu L, Chang H-Y, and Liu C-H.** A capillary-endothelium-mimetic microfluidic chip for the study of immune responses. *Sensors and Actuators B: Chemical* 209: 470-477, 2015.
302. **Wu X, Zha D, Xiang G, Zhang B, Xiao SY, and Jia R.** Combined MMF and insulin therapy prevents renal injury in experimental diabetic rats. *Cytokine* 36: 229-236, 2006.
303. **Xu A, Yin S, Wong L, Chan KW, and Lam KS.** Adiponectin ameliorates dyslipidemia induced by the human immunodeficiency virus protease inhibitor ritonavir in mice. *Endocrinology* 145: 487-494, 2004.
304. **Xu C, Wang K, Ding YH, Li WJ, and Ding L.** Claudin-7 gene knockout causes destruction of intestinal structure and animal death in mice. *World J Gastroenterol* 25: 584-599, 2019.
305. **Yamamoto K, Tanimura K, Watanabe M, Sano H, Uwamori H, Mabuchi Y, Matsuzaki Y, Chung S, Kamm RD, Tanishita K, and Sudo R.** Construction of Continuous Capillary Networks Stabilized by Pericyte-like Perivascular Cells. *Tissue Eng Part A* 25: 499-510, 2019.
306. **Yamauchi T, Iwabu M, Okada-Iwabu M, and Kadowaki T.** Adiponectin receptors: a review of their structure, function and how they work. *Best practice & research Clinical endocrinology & metabolism* 28: 15-23, 2014.
307. **Yamauchi T, Kamon J, Ito Y, Tsuchida A, Yokomizo T, Kita S, Sugiyama T, Miyagishi M, Hara K, Tsunoda M, Murakami K, Ohteki T, Uchida S, Takekawa S, Waki H, Tsuno NH, Shibata Y, Terauchi Y, Froguel P, Tobe K, Koyasu S, Taira K, Kitamura T, Shimizu T, Nagai R, and Kadowaki T.** Cloning of adiponectin receptors that mediate antidiabetic metabolic effects. *Nature* 423: 762-769, 2003.
308. **Yamauchi T, Kamon J, Minokoshi Y, Ito Y, Waki H, Uchida S, Yamashita S, Noda M, Kita S, Ueki K, Eto K, Akanuma Y, Froguel P, Foufelle F, Ferre P, Carling D, Kimura S, Nagai R, Kahn BB, and Kadowaki T.** Adiponectin stimulates glucose utilization and fatty-acid oxidation by activating AMP-activated protein kinase. *Nature medicine* 8: 1288-1295, 2002.
309. **Yamauchi T, Kamon J, Waki H, Imai Y, Shimozawa N, Hioki K, Uchida S, Ito Y, Takakuwa K, Matsui J, Takata M, Eto K, Terauchi Y, Komeda K, Tsunoda M, Murakami K, Ohnishi Y, Naitoh T, Yamamura K, Ueyama Y, Froguel P, Kimura S, Nagai R, and Kadowaki T.** Globular adiponectin protected ob/ob mice from diabetes and ApoE-deficient mice from atherosclerosis. *J Biol Chem* 278: 2461-2468, 2003.
310. **Yamauchi T, Nio Y, Maki T, Kobayashi M, Takazawa T, Iwabu M, Okada-Iwabu M, Kawamoto S, Kubota N, Kubota T, Ito Y, Kamon J, Tsuchida A, Kumagai K, Kozono H, Hada Y, Ogata H, Tokuyama K, Tsunoda M, Ide T, Murakami K, Awazawa M, Takamoto I, Froguel P, Hara K, Tobe K, Nagai R, Ueki K, and Kadowaki T.** Targeted disruption of AdipoR1 and

AdipoR2 causes abrogation of adiponectin binding and metabolic actions. *Nature medicine* 13: 332-339, 2007.
311. **Yang L, Peng XH, Wang YA, Wang X, Cao Z, Ni C, Karna P, Zhang X, Wood WC, Gao X, Nie S, and Mao H.** Receptor-targeted nanoparticles for in vivo imaging of breast cancer. *Clinical cancer research : an official journal of the American Association for Cancer Research* 15: 4722-4732, 2009.
312. **Yang YJ, Hope ID, Ader M, and Bergman RN.** Importance of transcapillary insulin transport to dynamics of insulin action after intravenous glucose. *Am J Physiol* 266: E17-25, 1994.
313. **Ye R and Scherer PE.** Adiponectin, driver or passenger on the road to insulin sensitivity? *Mol Metab* 2: 133-141, 2013.
314. **Yeon JH, Na D, Choi K, Ryu SW, Choi C, and Park JK.** Reliable permeability assay system in a microfluidic device mimicking cerebral vasculatures. *Biomed Microdevices* 14: 1141-1148, 2012.
315. **Yoo HJ, Lee JS, and Lee JM.** Integrated Whole Body MR/PET: Where Are We? *Korean journal of radiology : official journal of the Korean Radiological Society* 16: 32-49, 2015.
316. **Yoon N, Dang TQ, Chasiotis H, Kelly SP, and Sweeney G.** Altered transendothelial transport of hormones as a contributor to diabetes. *Diabetes Metab J* 38: 92-99, 2014.
317. **Yu T, Robotham JL, and Yoon Y.** Increased production of reactive oxygen species in hyperglycemic conditions requires dynamic change of mitochondrial morphology. *Proc Natl Acad Sci U S A* 103: 2653-2658, 2006.
318. **Yuan D and He P.** Vascular remodeling alters adhesion protein and cytoskeleton reactions to inflammatory stimuli resulting in enhanced permeability increases in rat venules. *J Appl Physiol (1985)* 113: 1110-1120, 2012.
319. **Yuan D, Xu S, and He P.** Enhanced permeability responses to inflammation in streptozotocin-induced diabetic rat venules: Rho-mediated alterations of actin cytoskeleton and VE-cadherin. *Am J Physiol Heart Circ Physiol* 307: H44-53, 2014.
320. **Zdychova J and Komers R.** Emerging role of Akt kinase/protein kinase B signaling in pathophysiology of diabetes and its complications. *Physiol Res* 54: 1-16, 2005.
321. **Zdychova J, Vesela J, Kazdova L, and Komers R.** Renal activity of Akt kinase in experimental Type 1 diabetes. *Physiol Res* 57: 709-715, 2008.
322. **Zhang H, Schin M, Saha J, Burke K, Holzman LB, Filipiak W, Saunders T, Xiang M, Heilig CW, and Brosius FC, 3rd.** Podocyte-specific overexpression of GLUT1 surprisingly reduces mesangial matrix expansion in diabetic nephropathy in mice. *Am J Physiol Renal Physiol* 299: F91-98, 2010.
323. **Zhang Q, Bindokas V, Shen J, Fan H, Hoffman RM, and Xing HR.** Time-course imaging of therapeutic functional tumor vascular normalization by antiangiogenic agents. *Molecular cancer therapeutics* 10: 1173-1184, 2011.
324. **Zhang X, Badea CT, Hood G, Wetzel AW, Stiles JR, and Johnson GA.** Free-space fluorescence tomography with adaptive sampling based on anatomical information from microCT. *Proceedings - Society of Photo-Optical Instrumentation Engineers* 7757, 2010.

325. **Zhang X, Wang N, Schachat AP, Bao S, and Gillies MC.** Glucocorticoids: structure, signaling and molecular mechanisms in the treatment of diabetic retinopathy and diabetic macular edema. *Curr Mol Med* 14: 376-384, 2014.
326. **Zhang Y, Zhang B, Liu F, Luo J, and Bai J.** In vivo tomographic imaging with fluorescence and MRI using tumor-targeted dual-labeled nanoparticles. *International journal of nanomedicine* 9: 33-41, 2014.
327. **Zhang Z, Apse K, Pang J, and Stanton RC.** High glucose inhibits glucose-6-phosphate dehydrogenase via cAMP in aortic endothelial cells. *J Biol Chem* 275: 40042-40047, 2000.
328. **Zhao RZ, Jiang S, Zhang L, and Yu ZB.** Mitochondrial electron transport chain, ROS generation and uncoupling (Review). *Int J Mol Med* 44: 3-15, 2019.
329. **Zheng F, Zhang S, Lu W, Wu F, Yin X, Yu D, Pan Q, and Li H.** Regulation of insulin resistance and adiponectin signaling in adipose tissue by liver X receptor activation highlights a cross-talk with PPARgamma. *PLoS One* 9: e101269, 2014.
330. **Zhong Q and Kowluru RA.** Diabetic retinopathy and damage to mitochondrial structure and transport machinery. *Invest Ophthalmol Vis Sci* 52: 8739-8746, 2011.
331. **Zhou L, Deepa SS, Etzler JC, Ryu J, Mao X, Fang Q, Liu DD, Torres JM, Jia W, Lechleiter JD, Liu F, and Dong LQ.** Adiponectin activates AMP-activated protein kinase in muscle cells via APPL1/LKB1-dependent and phospholipase C/Ca2+/Ca2+/calmodulin-dependent protein kinase kinase-dependent pathways. *J Biol Chem* 284: 22426-22435, 2009.
332. **Zhou X and He P.** Temporal and spatial correlation of platelet-activating factor-induced increases in endothelial [Ca(2)(+)]i, nitric oxide, and gap formation in intact venules. *Am J Physiol Heart Circ Physiol* 301: H1788-1797, 2011.

APPENDICES

Appendix A: A list of publication

1. **Yoon N**, Dadson K, Dang T, Chu T, Noskovicova N, Hinz B, Raignault A, Thorin E, Kim S, Jeon JS, Jonkman J, McKee T, Grant J, Peterson JD, Kelly SP, Sweeney G.
Tracking adiponectin biodistribution via fluorescence molecular tomography indicates increased vascular permeability after streptozotocin-induced diabetes.
Am J Physiol Endocrinol Metab. 2019 Jul 16. doi: 10.1152/ajpendo.00564.2018. (Appendix B)

2. Dang TQ[#], **Yoon N**[#], Chasiotis H, Dunford EC, Feng Q, He P, Riddell MC, Kelly SP, Sweeney G.
Transendothelial movement of adiponectin is restricted by glucocorticoids.
J Endocrinol. 2017 Aug;234(2):101-114. doi: 10.1530/JOE-16-0363. (Appendix C) [#]co-first authors

3. **Yoon N**, Dang TQ, Chasiotis H, Kelly SP, Sweeney G.
Altered transendothelial transport of hormones as a contributor to diabetes.
Diabetes Metab J. 2014 Apr;38(2):92-9. doi: 10.4093/dmj.2014.38.2.92. Review (Appendix D)

Appendix B

Tracking adiponectin biodistribution via fluorescence molecular tomography indicates increased vascular permeability after streptozotocin-induced diabetes.

Yoon N, Dadson K, Dang T, Chu T, Noskovicova N, Hinz B, Raignault A, Thorin E, Kim S, Jeon JS, Jonkman J, McKee T, Grant J, Peterson JD, Kelly SP, Sweeney G.

Am J Physiol Endocrinol Metab. 2019 Jul 16.

Am J Physiol Endocrinol Metab 317: E760–E772, 2019.
First published July 16, 2019; doi:10.1152/ajpendo.00564.2018.

RESEARCH ARTICLE | *Translational Physiology*

Tracking adiponectin biodistribution via fluorescence molecular tomography indicates increased vascular permeability after streptozotocin-induced diabetes

Nanyoung Yoon,[1] Keith Dadson,[1] Thanh Dang,[1] Teresa Chu,[1] Nina Noskovicova,[2] Boris Hinz,[2] Adeline Raignault,[3] Eric Thorin,[3] Seunggyu Kim,[4,5] Jessie S. Jeon,[4,5] James Jonkman,[6] Trevor D. McKee,[7] Justin Grant,[7] Jeffrey D. Peterson,[8] Scott P. Kelly,[1] and Gary Sweeney[1]

[1]*Department of Biology, York University, Toronto, Canada;* [2]*Faculty of Dentistry, University of Toronto, Toronto, Canada;* [3]*Montreal Heart Institute, University of Montreal, Quebec, Canada;* [4]*Department of Mechanical Engineering, Korea Advanced Institute of Science and Technology, Daejeon, Republic of Korea;* [5]*KAIST Institute for Health Science and Technology, Korea & Advanced Institute of Science and Technology, Daejeon, Republic of Korea;* [6]*Advanced Optical Microscopy Facility, University Health Network, Toronto, Canada;* [7]*Spatio-temporal Targeting and Amplification of Radiation Response, University Health Network, Toronto, Canada; and* [8]*Applied Biology, Life Sciences & Technology, PerkinElmer, Hopkinton, Massachusetts*

Submitted 24 December 2018; accepted in final form 27 June 2019

Yoon N, Dadson K, Dang T, Chu T, Noskovicova N, Hinz B, Raignault A, Thorin E, Kim S, Jeon JS, Jonkman J, McKee TD, Grant J, Peterson JD, Kelly SP, Sweeney G. Tracking adiponectin biodistribution via fluorescence molecular tomography indicates increased vascular permeability after streptozotocin-induced diabetes. *Am J Physiol Endocrinol Metab* 317: E760–E772, 2019. First published July 16, 2019; doi:10.1152/ajpendo.00564.2018.—Adiponectin, a highly abundant polypeptide hormone in plasma, plays an important role in the regulation of energy metabolism in a wide variety of tissues, as well as providing important beneficial effects in diabetes, inflammation, and cardiovascular disease. To act on target tissues, adiponectin must move from the circulation to the interstitial space, suggesting that vascular permeability plays an important role in regulating adiponectin action. To test this hypothesis, fluorescently labeled adiponectin was used to monitor its biodistribution in mice with streptozotocin-induced diabetes (STZD). Adiponectin was, indeed, found to have increased sequestration in the highly fenestrated liver and other tissues within 90 min in STZD mice. In addition, increased myocardial adiponectin was detected and confirmed using computed tomography (CT) coregistration. This provided support of adiponectin delivery to affected cardiac tissue as a cardioprotective mechanism. Higher adiponectin content in the STZD heart tissues was further examined by ex vivo fluorescence molecular tomography (FMT) imaging, immunohistochemistry, and Western blot analysis. In vitro mechanistic studies using an endothelial monolayer on inserts and three-dimensional microvascular networks on microfluidic chips further confirmed that adiponectin flux was increased by high glucose. However, in the in vitro model and mouse heart tissue, high glucose levels did not change adiponectin receptor levels. An examination of the tight junction (TJ) complex revealed a decrease in the TJ protein claudin (CLDN)-7 in high glucose-treated endothelial cells, and the functional significance of this change was underscored by increased endothelium permeability upon siRNA-mediated knockdown of *CLDN-7*. Our data support the idea that glucose-induced effects on permeability of the vascular endothelium contribute to the actions of adiponectin by regulating its transendothelial movement from blood to the interstitial space. These observations are physiologically significant and critical when considering ways to harness the therapeutic potential of adiponectin for diabetes.

adiponectin; diabetes; endothelial; fluorescence molecular tomography; heart; vascular permeability

INTRODUCTION

Extensive research on adiponectin has validated this hormone as a biomarker for cardiometabolic diseases and as a therapeutic target with enormous potential (43). To harness the numerous beneficial effects of adiponectin, it is essential to fully understand the mechanisms governing adiponectin action (29, 31, 39). To date, the vast majority of studies have focused on correlating changes in circulating adiponectin levels and disease markers (1). As a result, reduced adiponectin levels are well established to inversely correlate with diabetes and cardiovascular diseases (43). Adiponectin acts via binding to membrane receptors AdipoR1, AdipoR2, and T-cadherin (19, 45), and reductions in their expression or posttranslational modification in disease states has been proposed to lead to adiponectin resistance (11, 36, 42). However, another critical factor that likely determines adiponectin action is vascular permeability (25, 26, 46). More specifically, to directly elicit a response in a target tissue, adiponectin must transit from the circulation to interstitial space across the endothelial barrier (46).

The monolayer of endothelial cells lining the circulatory system acts as a barrier that regulates the movement of blood-borne factors to the interstitial space. In turn, the barrier properties of the endothelium are regulated by the transcellular pathway (i.e., solute transport across endothelial cells), as well as the paracellular pathway (i.e., solute movement between adjacent endothelial cells) (46). In general, larger macromolecules move via facilitated transcellular trafficking, while the paracellular route typically restricts solutes in the range of 3 nm radius (16). Tight junctions (TJ) provide a selective barrier to solute movement between cells, and altered expression of components, including zona occludens-1 (ZO-1), occludin, tricellulin, and claudins alter TJ structure to make a leakier or

Address for reprint requests and other correspondence: G. Sweeney, Dept. of Biology, York Univ., Toronto, M3J 1P3, Ontario, Canada (e-mail: gsweeney@yorku.ca).

tighter barrier for paracellular movement of solutes (15). Numerous previous studies, particularly focusing on insulin, have shown that vascular permeability can play an important role in contributing to the development of diabetes and heart failure (25, 46). It is important to note that endothelial permeability varies widely throughout the body in a tissue (and intra-tissue)-specific manner (46). It has also been shown that endothelial barriers control adiponectin transport in a cell- and tissue-specific manner (35), and we have reported that transendothelial movement of adiponectin was reduced by glucocorticoids (9).

We believe that the role of endothelial permeability as an important determinant of adiponectin action has been somewhat underappreciated. In this study, we further considered a link between vascular permeability, adiponectin flux, and hyperglycemia/diabetes by producing recombinant adiponectin, which we then conjugated with a near-infrared probe to track its biodistribution in live wild-type control and diabetic mice using fluorescence molecular tomography (FMT). We also examined the effects of high glucose levels on adiponectin flux across isolated arteries and cultured monolayers of endothelial cells. Finally, because the cardioprotective actions of adiponectin are currently the focus in our laboratory (6–8, 30, 32), we considered the role of the vascular barrier and diabetes on adiponectin access and action in the heart. These studies provide a novel and integrated view on the movement of adiponectin across the endothelial barrier under conditions that relate to diabetes and offers new insight on the impact that vascular permeability has on the actions of adiponectin on key organs.

MATERIALS AND METHODS

Experimental animal model. Male *nu/nu* homozygous mice and C57BL6 aged 8–13 wk were used for assessing adiponectin biodistribution. All mice were maintained with access to water and low-fluorescent chow [Teklad Global 18% protein rodent diet (Irradiated), Harlan Laboratories, Indianapolis, IN] throughout each experimental period. Age- and weight-matched pairs were grouped for each injection (averaging 23–25 g). After 12 h of starvation, diabetes was induced by single intraperitoneal injection of 150 mg/kg (body weight) streptozotocin (STZ; Sigma-Aldrich, St. Louis, MO). Experiments were performed 4 days after STZ injection, and diabetes was diagnosed when mice exhibited a blood glucose level >14 mmol/l at this time, while all control mice received only a saline injection. Circulating adiponectin was detected in serum before and after infusion of VivoTag-750-conjugated adiponectin using a mouse adiponectin ELISA kit with a sensitivity of 3.12–200 ng/ml (Immunodiagnostics, Hong Kong, China), which detects all adiponectin oligomeric forms.

Fluorescence molecular tomography to detect VivoTag-750-adiponectin. Recombinant adiponectin prepared in our laboratory was labeled with VivoTag-S 750 (NEV10123, Perkin Elmer, Boston, MA). Importantly, this recombinant protein formed oligomeric forms in a ratio, which closely mirrors those found in circulation (see Supplemental Figs. S1 and S2; all Supplemental material is available at https://doi.org/10.5281/zenodo.3332774). Labeling efficiency was assessed by running labeled full-length adiponectin on a SDS-PAGE gel and then scanned on a LI-COR Odyssey infrared imaging system to visualize the three adiponectin isoforms. Labeled proteins were transferred from the gels onto nitrocellulose membranes before probing with adiponectin-specific antibodies to assess fluorescence-to-total protein ratio. Labeled adiponectin was infused into lightly anesthetized mice (1–2% isoflurane) via a surgically placed permanent jugular vein cannula. For cannulation insertion, the mice were first anesthetized with 5% isoflurane then maintained at 2% isoflurane. The surgical site was cleaned with iodine solution and alcohol before a longitudinal incision of ~15 mm was made in the skin at the neck of the animal, just above the right front leg. Connective tissue surrounding the jugular vein was carefully separated before two sutures of 6-0 Ethilon surgeon's silk (Johnson & Johnson, Brussels, Belgium) were placed ~5–10 mm apart on the vein. A fine lateral incision was made between the sutures using microscissors, which allowed insertion of a saline-filled polyethylene (PE-10) tube into the vein between the sutures. When placement was confirmed, the caudal suture was released, and the cannula was slowly fed caudally ~5 mm into the vein toward (but not entering) the heart. To confirm correct placement, 50 μL saline was delivered through the cannula using a 31-gauge insulin needle. The cannula was then securely tied to the jugular vein with silk suture and 85 μg of adiponectin conjugated with VivoTag-S was administered followed by a 50-μL saline flush. The cannula was sealed using a heated hemostat, the skin incision was closed using silk suture, and a serum sample was collected from the tail vein within 2 min of adiponectin infusion. Mice were maintained at 2% isoflurane, while being positioned in a glass mouse imaging cassette, then scanned 10, 30, 60, and 90 min postadiponectin infusion with a fluorescence molecular tomography (FMT) 2500 LX quantitative tomography system (VisEn Medical, Perkin Elmer, Downers Grove, IL) using the 750-nm near-infrared channel (750/800 nm excitation/emission). Once FMT scanning was completed, mice in the imaging cassette were immediately taken for a computed tomography (CT) scan (Locus eXplore MicroCT, GE Healthcare, London, ON, Canada and XRAD 225Cx, Precision X-Ray, North Banford, CT) under constant anesthesia to ensure identical mouse positioning and accurate alignment between CT and FMT. FMT software (TrueQuant, Perkin Elmer) reconstructs a quantitative three-dimensional (3D) data set, in which fluorescence/voxel is expressed in nanomoles per liter. FMT and CT data sets (dicom format) were imported into Inveon Research Workplace (Siemens Healthcare, Erlangen, Germany) or AMIDE (http://amide.sourceforge.net) for FMT-CT coregistration to permit accurate localization of the fluorescent signal.

FMT analysis of tissues ex vivo. To avoid potential scatter from adjacent tissue, heart, liver, kidney, pancreas, and skeletal muscle, those tissues were excised from mice after cervical dislocation immediately following FMT and CT scanning (~100–120 min postadiponectin infusion). Two-dimensional (2D) epifluorescence FMT images were taken of these tissues on an opaque resin imaging block in the FMT imaging cassette. Quantitative analysis of the fluorescent signal was performed using the FMT software (TrueQuant, Perkin Elmer).

Ex vivo vascular permeability of adiponectin assay. Five-week-old Wistar rats were used. After 2 wk of standard diet in the animal facility, rats were fasted 5 h before induction of diabetes by a single intraperitoneal injection of streptozotocin (STZ; Sigma-Aldrich) at a dose of 100 mg/kg body wt (~200 μL/rat). Diabetes was diagnosed when hyperglycemia was higher than 10 mmol/L (180 mg/dL). Rats developed diabetes within 7 days of STZ injection. A control group of rats was injected with an equivalent volume of the vehicle solution (citrate buffer 0.5 mM, pH 4.5). Rats that failed to respond to STZ injection were not used for the study. Control or diabetic rats were anesthetized with isoflurane, and a midline laparotomy was performed to expose and remove the mesenteric bed. Isolated mesenteric arteries were mounted on a glass cannula immersed in a 2-mL organ bath filled with a physiological salt solution (PSS; in mmol/L: 130 NaCl, 4.7 KCl, 1.18 KH_2PO_4, 1.17 $MgSO_4$, 14.9 $NaHCO_3$, 1.6 $CaCl_2$, 0.023 EDTA, 10 glucose; pH 7.4) aerated with 12% O_2; 5% CO_2; 83% N_2 at 37°C following a method previously described (33). Arterial segments were pressurized at 80 mmHg in no-flow conditions and equilibrated for 30 min before starting experiments. Ten micrograms per milliliter adiponectin (200 μL) was added to the arterial perfusate, which circulated at a flow rate of 2 μL/min for 90 min at a constant pressure of 80 mmHg. At 0, 30, 60, and 90 min, 100-μL samples of

the extra-vascular bath containing transported adiponectin were collected, and an equivalent volume of physiological solution was added to the bath. Adiponectin levels were quantitatively determined by ELISA kit (Immunodiagnostics).

Cell culture. Human dermal microvascular endothelial cells (HDMEC; American Type Culture Collection, Manassas, VA) were grown in vascular cell basal medium (American Type Culture Collection) supplemented with 10% FBS at 37°C, 5% CO_2. All cells were used at passages 3 and 4 from the supplier. 500K HDMECs were seeded onto Transwell inserts (Corning, Tewksbury, MA) sized for 12-well plates having 3.0-μm pore sizes. Hyperglycemia was induced with 25 mM glucose in vascular cell basal medium supplemented with 2% FBS for 6 days. To adjust for osmotic pressure differences, control cells were treated with 5.5 mM glucose and 19.5 mM mannitol.

Measurement of transendothelial electric resistance. Measurements of transendothelial electric resistance (TEER) were conducted using STX-2 chopstick electrodes attached to an epithelial voltohmmeter (EVOM; World Precision Instruments, Sarasota, FL). All TEER measurements were corrected for background by subtracting TEER recorded across a blank membrane primed with appropriate cell culture medium. Resistance measurements were taken at *day 0* and *day 6* of treatment with 25 mM glucose and control (5.5 mM glucose + 19.5 mM mannitol).

Permeability assay using endothelial monolayers. HDMECs were seeded onto Transwell inserts and treated with 25 mM glucose and 5.5 mM glucose with 19.5 mM mannitol for 5 days before the start of experiments. At the start of the experiment, 10 μg/mL of adiponectin with the 25 mM glucose or 5.5 mM glucose with 19.5 mM mannitol, including 2% FBS vascular cell basal medium (American Type Culture Collection PCS-100-030; Cedarlane, Burlington, ON, Canada), was applied to the apical chamber only. After 24 h, apical and basolateral media were assessed for adiponectin concentration by gel electrophoresis after concentrating with 10,000 Da MWCO (molecular weight cutoff) filter (EMD Millipore, Billerica, MA) or by fluorescence intensity reader, respectively, and concentrations were calculated by comparison to standard curves prepared in culture medium.

Quantitative RT-PCR. Using aliquots of total extracted RNA, we synthesized cDNA, and we performed quantitative RT-PCR (qRT-PCR) reactions using the SYBR Green PCR Master Mix (Life Technologies, Carlsbad, CA). Gene-specific primer sets were designed: human CLDN7, forward: 5′-GGAGACGACAAAGTGAAGAAGG-3′ and reverse: 5′-GGACAGGAACAGGAGAGCAG-3′; human GAPDH, forward: 5′-AACATCATCCCTGCCTCTACTG-3′ and reverse: 5′-CCTGCTTCACCACCTTCTTG-3′; murine AdipoR1, forward: 5′-ACGTTGGAGAGTCATCCCGTAT-3′and reverse: 5′-CTCTGTGTGGATGCGGAAGAT-3′; murine AdipoR2, forward: 5′-TCCCAGGAAGATGAAGGGTTTAT-3′ and reverse: 5′-TTCCATTCGTTCCATAGCATGA-3′; murine adiponectin, forward: 5′-TGTTCCTCTTAATCCTGCCCA-3′ and reverse: 5′-CCAACCTGCACAAGTTCCCTT-3′; murine CLDN7, forward: 5′-GGACCTGCCATCTTTATCGGC-3′ and reverse: 5′-AGCTTTGCTTTCACTGCCTGG-3′; murine ZO-1, forward: 5′-GTCCCTGTGAGTCCTTCAGCTG-3′ and reverse: 5′-ACTCAACACACCACCATTGCTG-3′; murine 18s RNA, forward: 5′-AGTGAAACTGCGAATGGCTCA-3′ and reverse: 5′-CGAGCGACCAAAGGAACCA-3′.

Claudin-7 knockdown by shRNA in HDMEC. Claudin-7 gene expression was knocked-down in HDMECs using a pGPU6/Neo-claudin-7 plasmid, as shown previously (9) using the following shRNA target sequence: 5′-GGCCATCAG ATTGTCACAGAC-3′ (GenePharma, Shanghai, China). Lipofectamine 3000 reagent (Life Technologies, Carlsbad, CA) was used for all transfections following the manufacturer's instructions. A nontargeted control (NTC) shRNA plasmid was designed with a nonspecific scrambled sequence. The transfected cells were stabilized for 24 h with 10% FBS medium and subjected to antibiotic selection (500 μg/mL G418; Sigma-Aldrich) for 2 days. During antibiotic selection, transfected cells were seeded on Transwell inserts or six-well plates for further experiments.

Western blot analysis. Proteins from mouse tissues were homogenized by TissueLyser II (QIAGEN, Hilden, Germany) in RIPA buffer with 80 mM Tris·HCl (pH 6.8), 2% (wt/vol) SDS, 20% glycerol, 3.3% (vol/vol) β-mercaptoethanol, 0.01% (wt/vol) bromophenol blue, 30 mM HEPES (pH 7.4), 2.5 mM EGTA, 3 mM EDTA, 70 mM KCl, 20 mM β-glycerolphosphate, 20 mM NaF, 1 mM Na_3VO_4, 200 μM PMSF, 10 μM E64, 1 μM leupeptin, 1 μM pepstatin A, 0.1% NP40, and 0.1 μM okadaic acid. To detect the three forms of adiponectin, samples were prepared without β-mercaptoethanol or heating. For detection of other protein targets, samples were lysed in complete RIPA buffer and denatured at 95°C for 10 min. Transported adiponectin was collected from basolateral HDMEC medium and concentrated using Amicon Ultra-4 centrifugal filter units with Ultracel-10K (EMD Millipore, Billerica, MA). To detect the three adiponectin oligomers, concentrated adiponectin samples were prepared without denaturation or reduction. Prepared samples were run on SDS-PAGE gels and then transferred onto PVDF membranes (Bio-Rad Laboratories, Hercules CA), before incubation with primary antibody and detection by chemiluminescence. Polyclonal primary antibody of rabbit anti-adiponectin (dilution 1:1,000) is produced in-house (28). Rabbit anti-AdipoR1/2 antibodies were from Phoenix Biotech (Toronto, ON, Canada) (32). Mouse anti-FLAG M2 (dilution 1:1,,000, F1804; Sigma, Oakville, ON, Canada), rabbit anti-claudin-7 (dilution 1:500, cat. no. 34-9100; Thermo Fisher Scientific, Waltham, MA), rabbit anti-α/β-tubulin (dilution 1:1,000, cat. no. 2148; Cell Signaling, Danvers, MA), and rabbit anti-GAPDH(14C10) (dilution 1:1,000, cat. no. 2118; Cell Signaling) were purchased. The appropriate HRP-conjugated secondary antibody [anti-rabbit IgG-HRP (dilution 1:5,000, cat. no. 7074), anti-mouse IgG-HRP (dilution 1:5,000; cat. no. 7076)] was used from Cell Signaling. Bands were quantified by densitometry using Fiji software and normalized to relevant loading controls as indicated.

Immunofluorescence. Mouse hearts were isolated following isoflurane anesthesia, and the ventricles were excised and then cross-sectioned at the midline with a surgical blade before being embedded into a mold with optimal cutting temperature compound (OCT) (Sakura Finetek, Torrance, CA) and frozen on dry ice. Five-μm-thick cryosections were made using a cryostat and mounted onto positively charged glass slides (Superfrost; Thermo Fisher Scientific). Mounted slides were fixed in 4% PFA solution for 10 min to stain adiponectin or fixed in 100% ice-cold acetone, air-dried at room temperature, and rehydrated in distilled water followed by washing with PBS buffer. Permeabilization was followed by 0.5% Triton X-100. Before permeabilization, cell border staining was performed by incubating with 5 μg/mL Alexa Fluor 488-conjugated wheat germ agglutinin (WGA; Thermo Fisher Scientific) for 10 min in adiponectin staining. Sections were then incubated with adiponectin primary antibody (1:100), Texas-red secondary antibody (1:250), and DAPI for nuclear visualization. For vasculature staining, primary antibodies directed against claudin-7 (dilution 1:50, cat. no. 34-9100; Thermo Fisher Scientific), VE-cadherin (dilution 1:100; cat. no. PA5-17401; Thermo Fisher Scientific), PECAM-1 (dilution 1:50; cat. no. SC-376764; Santa Cruz Biotech, Mississauga, CA), ZO-1 (dilution 1:100, cat. no. 61-7300; Thermo Fisher Scientific), α-SMA (1:100; α-SM1, a kind gift from Dr. Giulio Gabbiani, University of Geneva, Switzerland), and desmin (1:30, cat. no. M076029; Dako, Burlington, ON, Canada) were used. Isotype-specific secondary antibodies anti-rabbit IgG-TRITC (1:100; Sigma), Alexa Fluor 568-conjugated IgG (1:100; Abcam, Cambridge, MA), Alexa Fluor 647-conjugated IgG2a (1:100; Molecular Probes, LifeTechnologies), and anti-mouse IgG1-FITC (1:200; SouthernBiotech, Birmingham, AL), and DAPI (Vectashield mounting medium with DAPI, cat. no. H-1200; Vector Laboratories, Burlingame, CA) were used. Images were acquired using a LSM700 (Zeiss, Jena, Germany) or LSM780 (Zeiss) confocal microscope and an upright Zeiss Axio Observer M35 epifluorescence microscope equipped with structured illumination (Apotome) and Axiocam HR camera (Carl Zeiss). All images were processed using Fiji or Adobe Photoshop CS5 (Adobe System, San

Jose, CA). Contrast and brightness were enhanced consistently for all representative images used in this article.

Fabrication of microfluidic devices and cell culture on a chip. To recapitulate 3D microvascular networks in vitro, we used a microfluidic chip that included cells embedded in hydrogel. Previous studies have described the fabrication process of the chips in detail (37). Briefly, silicon-based organic PDMS microfluidic device fabrication includes steps of soft lithography with SU-8 silicon wafer mold (A-Med, Conroe, TX) and PDMS (1:10; Dow Corning, Midland, MI), generating reservoirs with 1–4-mm diameter biopsy punches (KAI Medical, Rockville, MD), and device assembly by plasma bonding (Femto Science, Somerset, NJ) to a coverslip (glass; Duran). The devices were sterilized by 15 min of sonication (Uil Ultrasonic, Wa-dong, South Korea) in 70% EtOH before the bonding process. An 80°C drying oven was used for curing PDMS mixture, dehydration of devices before plasma treatment, and recovering hydrophobicity after bonding (24 h in advanced cell seeding). In this study, a 120-μm depth of microchannel devices was used.

Human umbilical vein endothelial cells (HUVECs; Lonza) were grown in endothelial cell growth medium (EGM-2, Lonza) supplemented with 5% FBS at 37°C, 5% CO_2. All cells were used at passages 6–8 from the supplier. After harvesting of trypsinized cells by centrifugation (125 *g*, 7 min), cells were resuspended in a concentration of 1.4×10^7 cells/mL within a 4 U/mL thrombin solution. We injected a 1:1 mixture of cells (1.4×10^7 cells/mL) and fibrinogen solution (5 mg/mL) into a gel inlet to fill it up. After incubating the chips at 37°C in a humid chamber for 15 min to produce gelation, we injected cell culture medium into the media channels. The cells in the microfluidic chips were incubated for 4 days with daily replacement of medium. Self-assembly of HUVECs into a perfusable vascular network (vasculogenesis) was induced by adding 50 ng/mL VEGF to EGM from *day 0* (D0) to *day 4* (D4).

Vascular permeability assay in microfluidic chips. After a 4-day culture, the medium was washed out with a quick PBS rinse before a fluorescent molecule solution was infused. Because of the hydrostatic pressure drop between the two media channels, the solution in the media channel flows along with the perfusable microvascular networks to the opposite media channel. We monitored the diffusion of fluorescent molecules into the fibrin gel (extracellular matrix, ECM) through the vessel wall, and the images were captured at 6–10-s intervals for 3 min via a fluorescence microscope (Axio Observer Z1, Zeiss). The images were quantified using ImageJ.

Perfusibility test in three-dimensional microvascular network. At *day 4*, endothelial growth medium was quickly washed with PBS by filling up two reservoirs in only one side channel to rinse out any particles from the 3D vessel lumen efficiently using hydrostatic pressure differences. When a desired field of view was found, bright-field images were captured. Then, 5.0–5.9 μm of FITC surface-labeled beads (0.1% wt/vol, F1CP-50-2; Spherotech) was infused into one media channel and time-lapse images were taken at 1.4-s intervals for 2 min using the fluorescence microscope (Axio, Observer Z1; Zeiss). The fluorescent images were overlaid with bright-field orientation image, and processed to video with ImageJ.

Statistical analysis. Data are expressed as means ± SE, and the significant differences were determined where $P < 0.05$ resulted from performing statistical analysis with Student's *t*-test or multiple *t*-test and one-way ANOVA.

RESULTS

Diabetes increases biodistribution of NIR-labeled full-length adiponectin into target tissues. To accurately investigate adiponectin biodistribution, we developed a model using FMT in which three-dimensional localization of fluorescently tagged adiponectin could be tracked in short time intervals in vivo. Full-length adiponectin comprising high-, medium-, and low-molecular weight oligomers was tagged with a near-infrared (NIR) peptide (VivoTag-S 750) detectable at 750 nm [full-length adiponectin (fAd)-VT750]. Using this wavelength and feeding mice with AIN-76A low-chlorophyll chow diet (Harlan, Indianapolis IN) allowed us to avoid confounding effects of autofluorescence (2). Western blot and fluorescent imaging confirmed that all three oligomers of adiponectin were fluorophore conjugated (Supplemental Fig. S1*A*, https://doi.org/10.5281/zenodo.3332774), and we demonstrated a linear relationship between adiponectin concentration and fluorescence measurement (Supplemental S1, *A–C*).

To test the hypothesis that hyperglycemia could alter adiponectin biodistribution, we infused fAd-VT750 (85 μg, via jugular vein) into STZ-injected (STZD) or control *nu/nu* mice, and then we monitored whole body fluorescence in mice by FMT imaging. We found no difference in circulating adiponectin levels between control and STZD mice and also observed the same level of fAd-VT750 in serum of either STZD or wt mice 2 min after injection via jugular vein (Supplemental Fig. S2*A*). Consecutive FMT images at 0, 10, 30, 60, and 90 min after fAd-VT750 injection showed increasing tissue accumulation of fluorescent adiponectin throughout the body, which appeared to be faster or higher in STZD mice (Fig. 1, *A–C*), particularly showing enhanced liver and/or heart accumulation relative to controls. FMT imaging confers the added advantage of providing quantitative analysis of whole body fluorescence and clearly measured an increased overall fluorescence intensity in STZD mice. As a control, infused unconjugated VT750 displayed a completely different biodistribution pattern, clearing quickly through the kidneys and localized primarily to the bladder within 60 min, with very little signal coming from other peripheral tissues (Supplemental Fig S3).

To conduct further analysis of the tissue localization of fluorescent signal, mice also underwent X-ray computed tomography (CT) imaging for fluorescence coregistration (Fig. 1*D*). Coronal and sagittal sections of FMT/CT coregistration data showed accumulation of fAd-VT750 in the heart, liver, kidney, and bladder (Fig. 1*E*). To eliminate potential tissue-scattering effects, major target tissues of adiponectin action were removed 90 min following fAd-VT750 infusion and imaged ex vivo by FMT. Heart, liver, kidney, pancreas, and skeletal muscle (Sk M) of STZD mice exhibited a higher fluorescent signal when compared with control (Fig. 1*F*), although only heart and liver reached significance upon quantitation (Fig. 1*G*). In agreement with this, Western blot analysis of reduced tissue homogenates, to allow detection of all adiponectin as monomers, clearly showed increased levels in all of these target tissues from STZD versus wild-type control mice at 90 min post fAd-VT750 infusion (Fig. 1*H*).

Adiponectin accumulation in the heart is upregulated by STZD. Because the main research focus of our laboratory is the cardioprotective effect of adiponectin, we then used FMT-CT coregistered images to quantify the fluorescence contained within a three-dimensional region of interest mapped to the heart (Fig. 2*A*). FMT quantitation shows that within 10 min, fAd-VT750 level in STZD hearts was significantly greater than that in wild-type control mice (Fig. 2*B*). Accordingly, area under the curve analysis showed greater accumulation of fAd-VT750 in the hearts of STZD mice (Fig. 2*C*). Immunofluorescent analysis of cross sections from myocardium also indicated

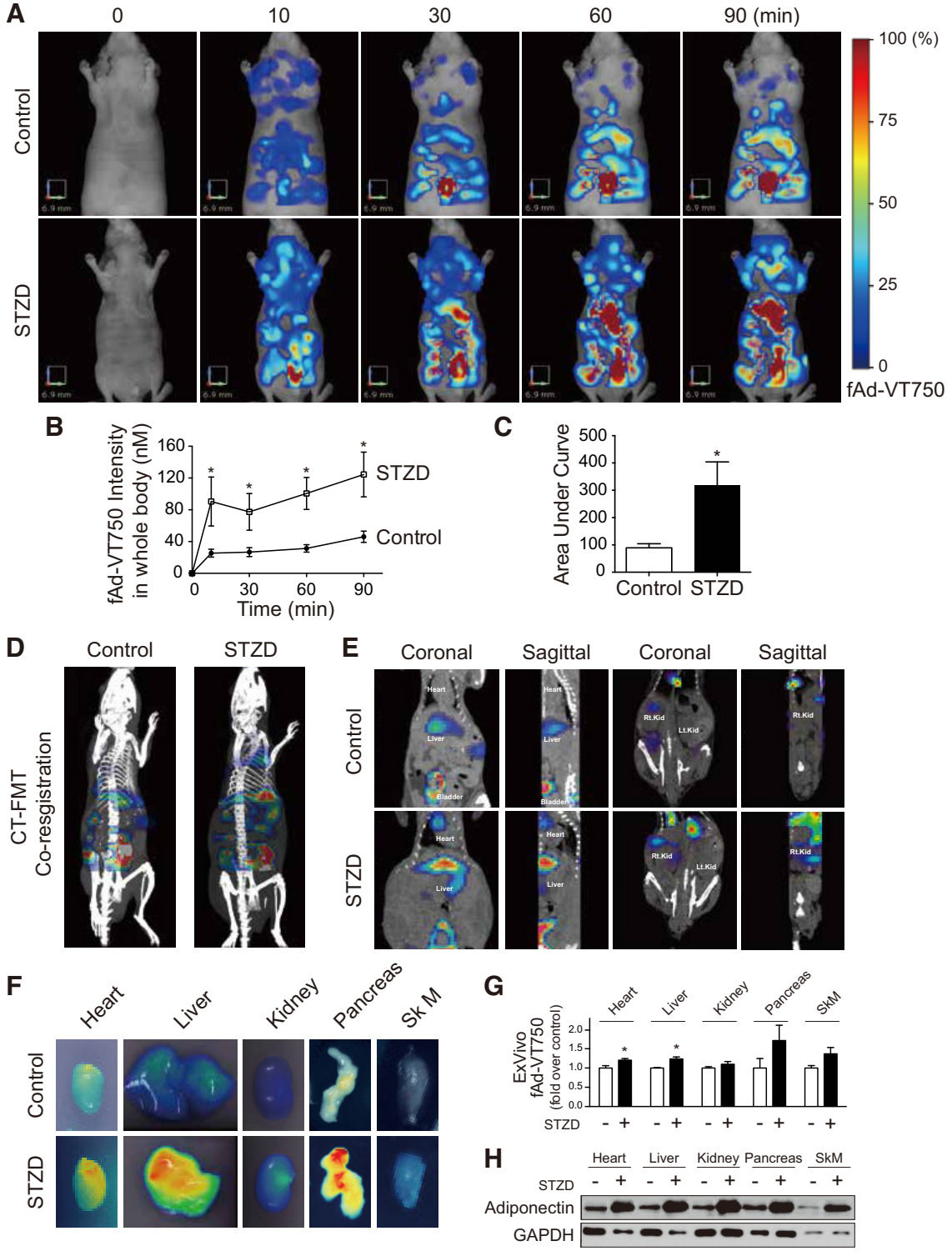

Fig. 1. Fluorescence molecular tomography shows in vivo biodistribution of full-length adiponectin is increased in diabetic conditions. *A*: 85 μg of near-infrared labeled full-length adiponectin (fAd-VT750) was injected via cannulated jugular vein into control or diabetic (streptozotocin-induced diabetes, STZD) *nu/nu* mice. Representative images from a control and STZD mouse before injection and at 10, 30, 60, and 90 min postinjection are shown. *B* and *C*: total signal intensity from whole body three-dimensional (3D) field of view was calculated as nM ($n \geq 8$; $^*P < 0.05$ from multiple *t*-test). Time course data were converted to area under curve (AUC) ($^*P < 0.05$ from Student's *t*-test). *D*: coregistration of fluorescence molecular tomography (FMT) (color) and computed tomography (CT) data (white/gray). *E*: coronal and sagittal view of FMT-CT coregistration with organs of interest identified. *F*: ex vivo two-dimensional (2D) FMT analysis of fAd-VT750 from isolated tissues [heart, liver, kidney, pancreas, and skeletal muscle (tibialis anterior)]. *G*: quantification of these 2D images using TrueQuant software. $^*P < 0.05$, compared with its control ($n \geq 4$). Statistical analysis was performed using Student's *t*-test. *H*: cardiac homogenates from control and STZD mice were analyzed by Western blot analysis under nondenaturing conditions to compare total amount of reduced (i.e., monomeric, 30 kDa) adiponectin.

increased fAd-VT750 in STZD mice 90 min postinfusion compared with wild-type control mice (Fig. 2, *D* and *E*). Interestingly, higher magnification revealed an apparent colocalization of fAd-VT750 with WGA, suggesting a near-membrane location.

Because molecular weight could be an important determinant in the movement of the adiponectin isoforms from circulation into the heart, we assessed the amount of fAd-VT750 in perfused heart homogenates from control and STZD mice under nondenaturing conditions. There was an increased presence of all three oligomeric adiponectin isoforms in STZD heart homogenates when compared with those of wild-type control mice (Fig. 2*G*). To verify that increased fAd-VT750 localization was not influenced by the presence of the VivoTag-750 fluorophore, Flag-tagged and nonfluorescent recombinant adiponectin was injected into wild-type C57BL/6 mice treated with or without STZ. Similar to fAd-VT750, there was increased total heart localization of Flag-adiponectin in STZ-treated mice compared with controls (Fig. 2*F*). Quantitative PCR analysis showed no difference in adiponectin mRNA levels between control and STZD cardiac homogenates (Fig. 2*H*).

High glucose levels regulate claudin-7 expression to increase paracellular movement of adiponectin. We next tested vascular permeability of adiponectin using mesenteric arteries isolated from STZD or control mice. Similar to our in vivo

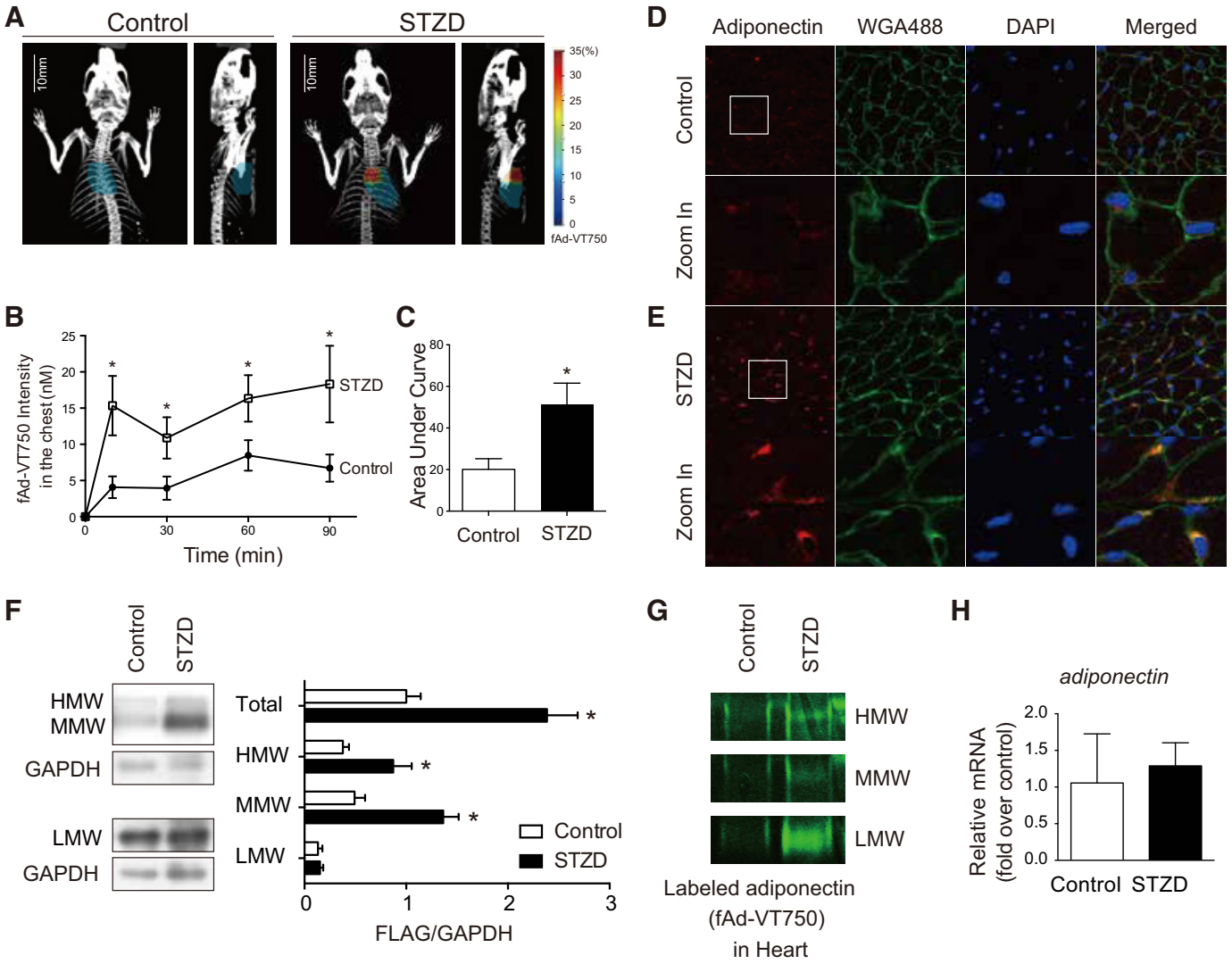

Fig. 2. Adiponectin uptake into the heart is increased by diabetes. *A*: representative heart regions of interest (ROIs) generated by alignment of computed tomography (CT) and fluorescence molecular tomography (FMT) three-dimensional (3D) images using Inveon Research Workplace software. *B*: quantitation of fAd-VT750 within mapped ROIs. Fluorescence intensity of localized fAd-VT750 (nM) was calculated over time by FMT-CT coregistration analysis ($n \geq 8$). *$P < 0.05$ with respect to control at each time point, and the *P* values were obtained from the multiple *t*-test. *C*: area under the curve analysis of fAd-VT750 within the heart ROI (*$P < 0.05$). *D* and *E*: immunofluorescence analysis of transverse heart cryosections stained with adiponectin (red), wheat germ agglutinin (WGA; green), and DAPI (blue). Colocalization of adiponectin and WGA appears orange. *F*: cardiac homogenates from C57BL/6 mice 90 min following Flag-tagged adiponectin infusion, run under nondenaturing conditions by SDS-PAGE to detect different adiponectin oligomers: high-molecular weight (HMW; >250 kDa), middle-molecular weight (MMW; ~180 kDa), and low-molecular weight (LMW; ~90 kDa). Total adiponectin combines densitometry from all three oligomers, adjusted to GAPDH as a loading control ($n = 5$; *$P < 0.05$). The quantification analyzed by multiple *t*-test. *G*: detection of fAd-VT750 by SDS-PAGE in heart homogenates from *nu/nu* mice 90 min post fAd-VT750 infusion. *H*: real-time quantitative PCR analysis of heart homogenates 90 min postinjection adjusted for GAPDH ($n = 5$).

findings, adiponectin flux across the arterial wall of STZD mesenteric arteries was greater compared with those of wild-type control mice (Fig. 3*A*). We then exposed a monolayer of human dermal endothelial cells (HDMECs) cultured on Transwell inserts to high glucose and found that the flux of adiponectin, added to the apical chamber, was higher than in normal glucose conditions. Figure 3*B* shows a Western blot, with quantitation below, indicating a significant increase in flux of high-molecular weight (HMW)-, middle-molecular weight (MMW)-, and low-molecular weight (LMW)-adiponectin from apical to basolateral side in cells grown under hyperglycemic conditions (Fig. 3*B*). Immunoblotting of the adiponectin receptors AdipoR1 and AdipoR2 showed that their expression in HDMEC monolayers was not affected by high glucose (Supplemental Fig. S4*C*). Accordingly, we found that endothelial barrier tightness measured by transendothelial electrical resistance (TEER) was decreased in high glucose-treated cells (Fig. 3*C*). This corresponded to a decrease in claudin-7 (cldn-7) mRNA and protein expression following high glucose treatment (Fig. 3, *D* and *E*). Immunofluorescence imaging indicated a decrease in cell membrane expression of cldn-7 in high glucose-treated cells compared with control (Fig. 3*F*), whereas there was no difference in expression of another tight junction-related protein, ZO-1, between groups (Fig. 3*G*). This observation was mirrored when heart homogenates were analyzed. Protein and mRNA levels of adiponectin receptors were unchanged by STZD (Supplemental Fig. S4, *A* and *B*). In cardiac tissue sections analyzed by qPCR for mRNA and immunohistochemistry, ZO-1 level was not significantly lower (Fig. 3, *J* and *K*), while cldn-7 expression was significantly decreased (Fig. 3, *H* and *I*) in STZD hearts compared with that in wild-type control mice.

Reduced claudin-7 expression decreased TEER and enhanced adiponectin movement across the endothelial monolayer. To test the functional importance of cldn-7 in adiponectin flux across an HDMEC monolayer, knockdown of cldn-7 was induced by transfection of shRNA (shCLDN7), which resulted in ~50% decrease in cldn-7 protein compared with cells that received a scrambled shRNA sequence not targeting cldn-7 (shNTC) (Fig. 4*A*). TEER was significantly decreased in monolayers comprising shCLDN7 cells compared with shNTC (Fig. 4*B*). Furthermore, there was increased flux of LMW-adiponectin from apical to basolateral side of monolayers comprising shCLDN7 cells compared with shNTC controls (Fig. 4*C*).

Functional 3D perfusable microvascular networks allowed to confirm hyperglycemia effect on permeability of dextran and adiponectin. Finally, we tested the hyperglycemia effect in microfluidic microvascular network of HUVECs. This in vitro platform of 3D vasculature-on-a-chip was generated in the ECM mimetic environment with fibrin hydrogel. PDMS (polydimethylsiloxane) microfluidic device is useful to induce perfusable microvasculature, as well as to monitor the event inside of the highly branched vascular structure. The PDMS mold has a central gel channel containing HUVECs and fibrin hydrogel bordered by triangular posts and two media fluid channels (Fig. 5, *A* and *B*). 1.4×10^7 cells/mL of HUVECs were seeded with the fibrin hydrogel at D0 and incubated for 4 days to form endothelial monolayers of in vivo-like vasculature naturally (Fig. 5*C*). Additional VEGF was used to increase the dynamic alignment of HUVECs from D0 to D4 (Fig. 5*D*). At *day 4*, the formation of open-ended EC monolayer 3D vessels between two PDMS posts were completed. GFP transfected HUVECs showed highly branched features of microvascular networks in a device (Fig. 5*E*) and vascular endothelial cadherin (VE-cadherin)-positive-stained structures indicated that vessel-like EC monolayer barrier allows the perfusion of fluids (Fig. 5*F*; Supplemental Video S3). To confirm the functionality of this vasculature, we performed perfusibility test with 5-μm beads conjugated with FITC, and time-lapse images were taken under fluorescence exposure at every 1.4 s (Fig. 5*G*, Supplemental Video S4). Next, we wanted to test the effect of hyperglycemia on permeability of 3D microvascular networks using fAd and changes of paracellular movement across this barrier with 70 kDa dextran at several time intervals. Immunofluorescent detection of VE-C showed that the integrity of interconnected vascular structures appeared not to loosen in hyperglycemia compared with control (Supplemental Fig. S5). To assess the permeability, 10 μg/mL fAd conjugated with rhodamine was injected into one reservoir of a device, and fluorescent images were captured over time. The apparent permeability (Papp, cm/s) was calculated by the fluorescent intensity measurement from a linear region of interest (ROI) spanning the microvessel-ECM interface. Because the perfused fluorescent molecules were transferred to the ECM from the vessels via the concentration gradient, the intensity increase was observed in ECM area over time (Fig. 5*H*). Permeability of rhodamine-labeled fAd (Rho-fAd) increased in hyperglycemia ($1.285 \times 10^{-5} \pm 0.09363 \times 10^{-5}$ cm/s) compared with 19.5 mM mannitol with 5.5 mM glucose-treated control ($2.290 \times 10^{-5} \pm 0.1651 \times$

Fig. 3. Hyperglycemia reduces claudin-7 expression and permits greater flux of adiponectin movement across the endothelium. *A*: mesenteric arteries extracted from control or streptozotocin-induced diabetes (STZD) rats were perfused with flag-tagged fAd, with samples of extravascular fluid taken at 30, 60, and 90 min postadiponectin and analyzed by ELISA. Area under the curve (AUC) analysis shows greater adiponectin flux from STZD arteries vs. control ($n \geq 5$; $^*P < 0.05$). *B*: human dermal microvascular endothelial cells (HDMEC) were cultured in a Transwell insert before treatment with high glucose (HG) or control. Adiponectin was added to the apical surface, and then basolateral media were collected 24 h following adiponectin administration. Samples were run under nondenaturing conditions; $n = 3$; $^*P < 0.05$, with respect to each adiponectin isomer's control. *C*: TEER (transendothelial electrical resistance) was lower in hyperglycemia significantly ($^*P < 0.05$; $n \geq 11$). Claudin-7 in hyperglycemia-treated endothelial cells also decreased at *cldn-7* mRNA expression ($^*P < 0.05$; $n = 4$) (*D*), as well as claudin-7 (CLDN-7) protein expression ($^*P < 0.05$; $n = 3$) (*E*). *F*: lower CLDN-7 was localized on the cell membrane in hyperglycemia. CLDN-7 (red) and PECAM-1 (green; endothelial marker) costain in HDMEC. *G*: however, zona occludens (ZO-1; green), aligning under the cell membrane, was not changed by high glucose (HG) treatment. *H*: *cldn-7* mRNA level decreased in the hearts of mice with STZ-induced diabetes ($n = 5$; $^*P < 0.05$). *J*: no significant difference was shown in *zo-1* mRNA level ($n = 4$). Statistical analysis was performed using the Student's *t*-test. *I*: lower CLDN-7(red) surrounded by α-SMA (green) was observed in heart tissue sections from STZD (*K*), although there was no difference of ZO-1. Immunostaining for ZO-1 (green) to identify endothelial cell-specific tight junction structure, α-SMA (red) to identify vascular smooth muscle cells, and desmin (blue) to identify cardiomyocytes. Shown are representative images of $n = 3$ mice per experimental group. High-magnification images show junction formation between endothelial cells in small vessels. Scale bars: 50 μm and 150 μm, respectively.

10^{-5} cm/s) (Fig. 5*K*). 70 kDa dextran, which is smaller than LMW adiponectin (around 90 kDa), also showed significantly higher permeability in high glucose-treated condition (Papp of HG was $6.812 \times 10^{-5} \pm 1.152 \times 10^{-5}$ cm/s and control Papp was $2.180 \times 10^{-5} \pm 0.2277 \times 10^{-5}$ cm/s) (Fig. 5*J*). However, for the small size of dextran (3 kDa-FITC), hyperglycemia did not significantly change the permeability (Fig. 5*I*). These suggested that paracellular movement regulates transendothe-

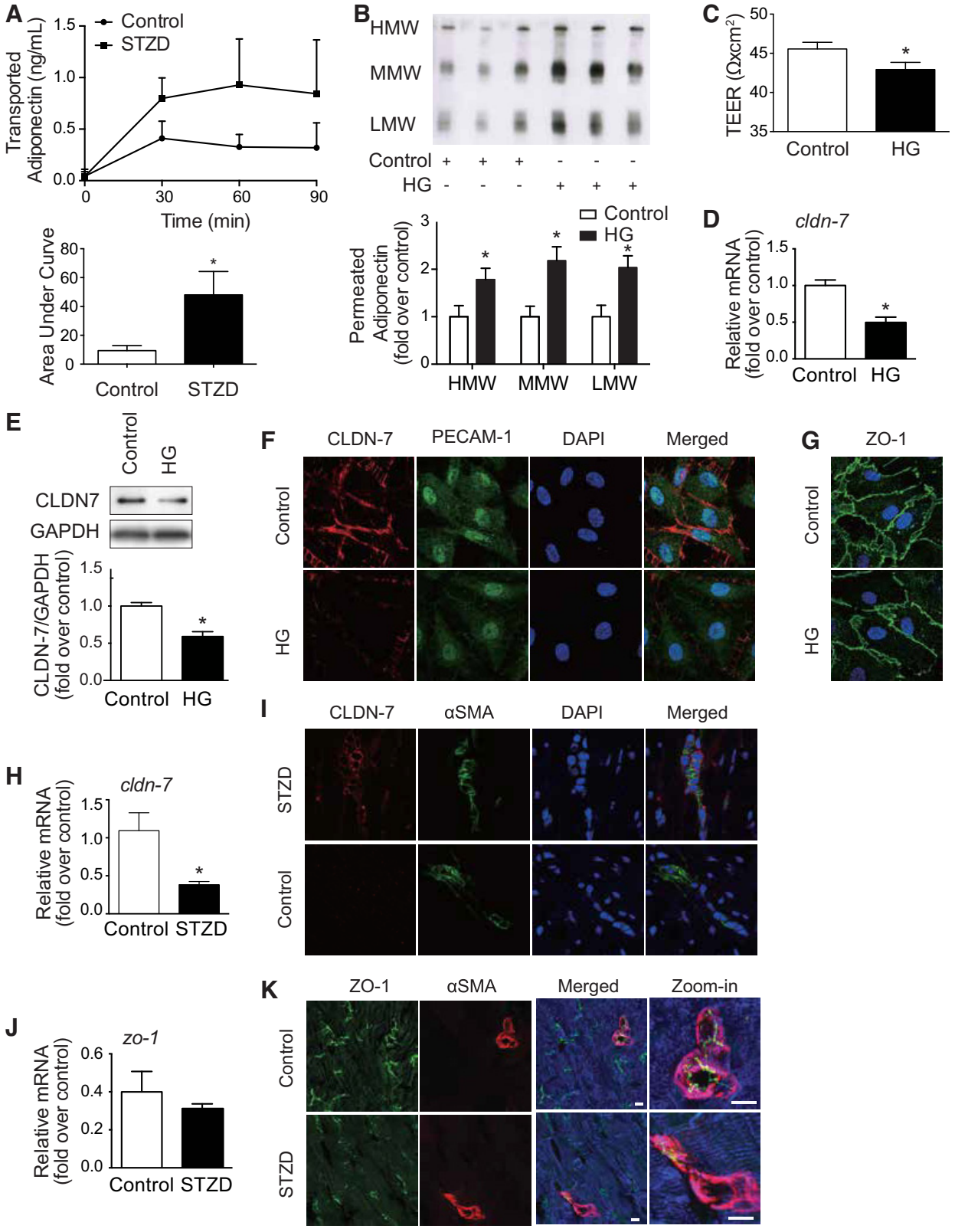

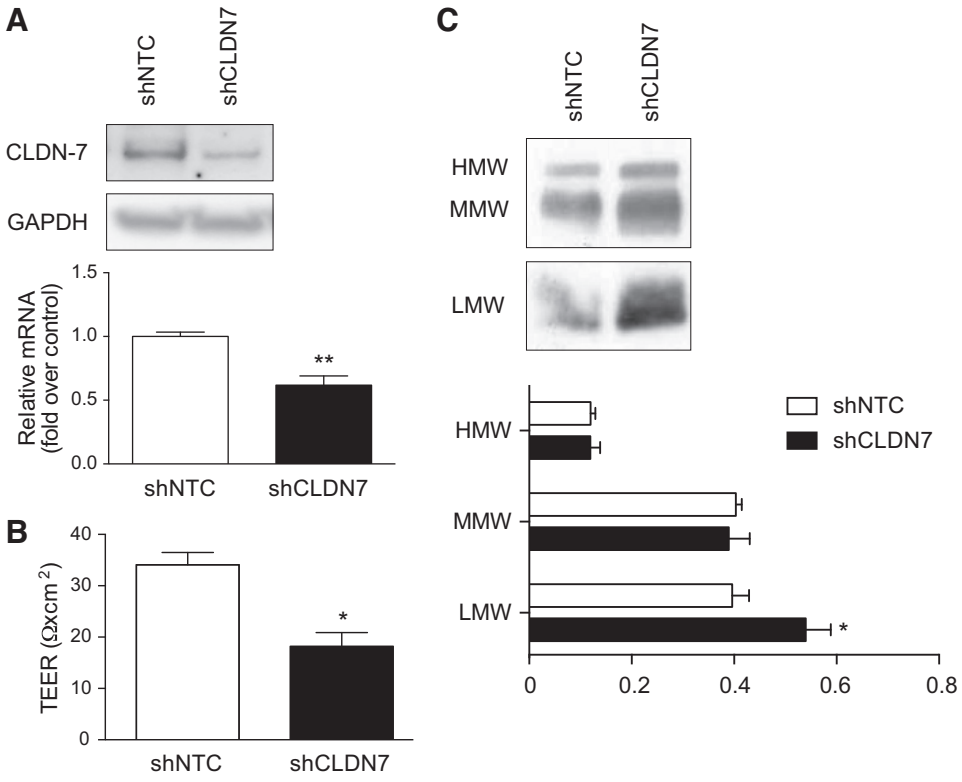

Fig. 4. Reduced claudin-7 (CLDN-7) expression decreased transendothelial electric resistance (TEER) and increased low-molecular-weight (LMW) adiponectin movement across the monolayer of human dermal microvascular endothelial cells (HDMECs). *A*: one of the major components of tight junction proteins, CLDN-7, was targeted to knock down by shRNA transfection after 96 h. Transfected HDMECs were transferred into the transmembrane culturing system (0.9 cm^2) and formed a monolayer 72 h after transfection. *B*: the cells with lower CLDN-7 expression (**$P < 0.01$; $n = 3$) showed significantly lower TEER (*$P < 0.05$; $n \geq 7$). TEER was measured at 96 h after transfection had started. *C*: monolayer of CLDN-7 knockdown HDMECs was used for adiponectin permeability assay for 24 h. The decreased CLDN-7 led the adiponectin movement increase, especially in LMW form with statistical significance (*$P < 0.05$; $n \geq 5$). The values were expressed as means ± SE, and statistical analysis was performed using Student's *t*-test.

lial accessibility depending on the size of molecules. It also confirmed that hyperglycemia in vitro with 25 mM glucose altered the movement of full-length adiponectin in microfluidic vessels-on-a-chip.

DISCUSSION

Adiponectin has been shown to mediate widespread physiological effects with resulting antidiabetic, anti-inflammatory, and cardioprotective effects (12). Hence, there has been great interest within academic institutes and pharmaceutical companies to develop therapeutics targeting adiponectin action. To accomplish this, it is critical to fully understand the mechanisms regulating adiponectin's cellular effects in various tissues. Although we have learned much about adiponectin receptor-mediated signaling mechanisms, few studies have focused on examining mechanisms regulating the transit of adiponectin from the circulation to the interstitial space and, thus, target cells, such as cardiomyocytes, hepatocytes, β-cells, and other cells. We previously proposed that vascular permeability was likely to be an important, and underappreciated, determinant of adiponectin's physiological actions (46). This is particularly relevant since adiponectin is a complex molecule comprising multiple oligomeric forms, each with a different molecular weight and radial size estimated to be 3.96 to 10.1 nm (35). This is exactly the range within which tight junctions of around 4 nm in dimension can be expected to strongly contribute to dictating adiponectin flux. Indeed, we recently demonstrated that glucocorticoid-mediated decreases in transcellular endothelial permeability-restricted adiponectin transit across endothelial monolayers (9). The observation that adi-

Fig. 5. Functional three-dimensional (3D) microvascular networks demonstrated size-dependent permeability and the effect of hyperglycemia on adiponectin transport. *A*: schematic representation of 3D perfusable microvascular network model with human umbilical vein endothelial cells (HUVECs) in a polydimethylsiloxane (PDMS) microfluidic device. The PDMS mold has a central gel channel containing HUVEC cells and fibrin hydrogel bordered by triangle posts. The HUVEC/fibrin gel channel is flanked on both sides by fluid channels, leading to four reservoirs filled with culture medium. *B*: a device photo is shown with an area dimension of 20,000 μm × 38,000 μm; a dime is shown alongside of it as a size reference. *C*: experimental timeline is shown. *D*: daily images (D1–D4) of HUVECs in the 3D fibrin gel shows cellular alignment dynamics during vasculogenesis (×10 magnification was used). *E*: continuously green fluorescent protein (GFP)-expressed HUVECs showed the perfusable vasculature on *day 4*. *F*: confocal reconstructed 3D image of VE-cadherin (red) stained with nucleus (DAPI, blue). A single plane from the stacked images showed three ortho-positions (*x* position/pink at 570 μm, *y* position/green at 700 μm, and *z* position/blue at 18 μm) of continuous endothelial hollow. *G*: to confirm the generated 3D vessels were perfusable, 5-μm beads conjugated with FITC were loaded into one reservoir, and time-lapse images were taken under fluorescence using Axio Observer Z1 microscope. Time interval average was 1.4 s. *H*: rhodamine-labeled, full-length adiponectin (Rho-fAd, red) was injected with a concentration of 10 μg/ml. Fluorescent images were captured every 6–10 s for 3 min from two or three different fields of view. Three representative images are shown at 0, 40, and 80 s postinfusion. To assess permeability, fluorescent signal intensity (arbitrary units, AU) was quantified along a linear region of interest (ROI) spanning the microvessel-ECM interface as shown and depicted as a distance from the ROI origin (●). Permeabilized fluorescent signals were observed in the extracellular matrix (ECM) (out of vessel) area over time. Apparent permeability (Papp) was quantified using ImageJ with measurement from randomly selected ROIs. Hyperglycemia with 25 mM glucose (*J*) did not change the permeability of 3 kDa-FITC dextran. However, 70-kDa Texas red dextran (*I*) and Rho-fAd (*K*) increased Papp significantly in high glucose (HG)-treated condition. *D*, *E*, *G*, *H*: scale bar indicates 100 μm. *I*–*K*: data presented are means ± SE. Statistical evaluation was done by Student's *t*-test with the values from 15 to 25 ROIs (four to six different fields of view from two or three devices) for each condition. *$P = 0.0005$. **$P < 0.0001$.

ponectin in cerebrospinal fluid is almost completely in the small trimeric form, and the total amount is only 0.1% of that in peripheral circulation (27), suggests that the tight blood-brain barrier restricts movement of adiponectin oligomers. Conversely, many studies focusing on metabolic effects of adiponectin have focused on liver, which has a highly fenestrated leaky vasculature, and found that the HMW adiponectin is highly bioactive and correlates well with clinical readouts of

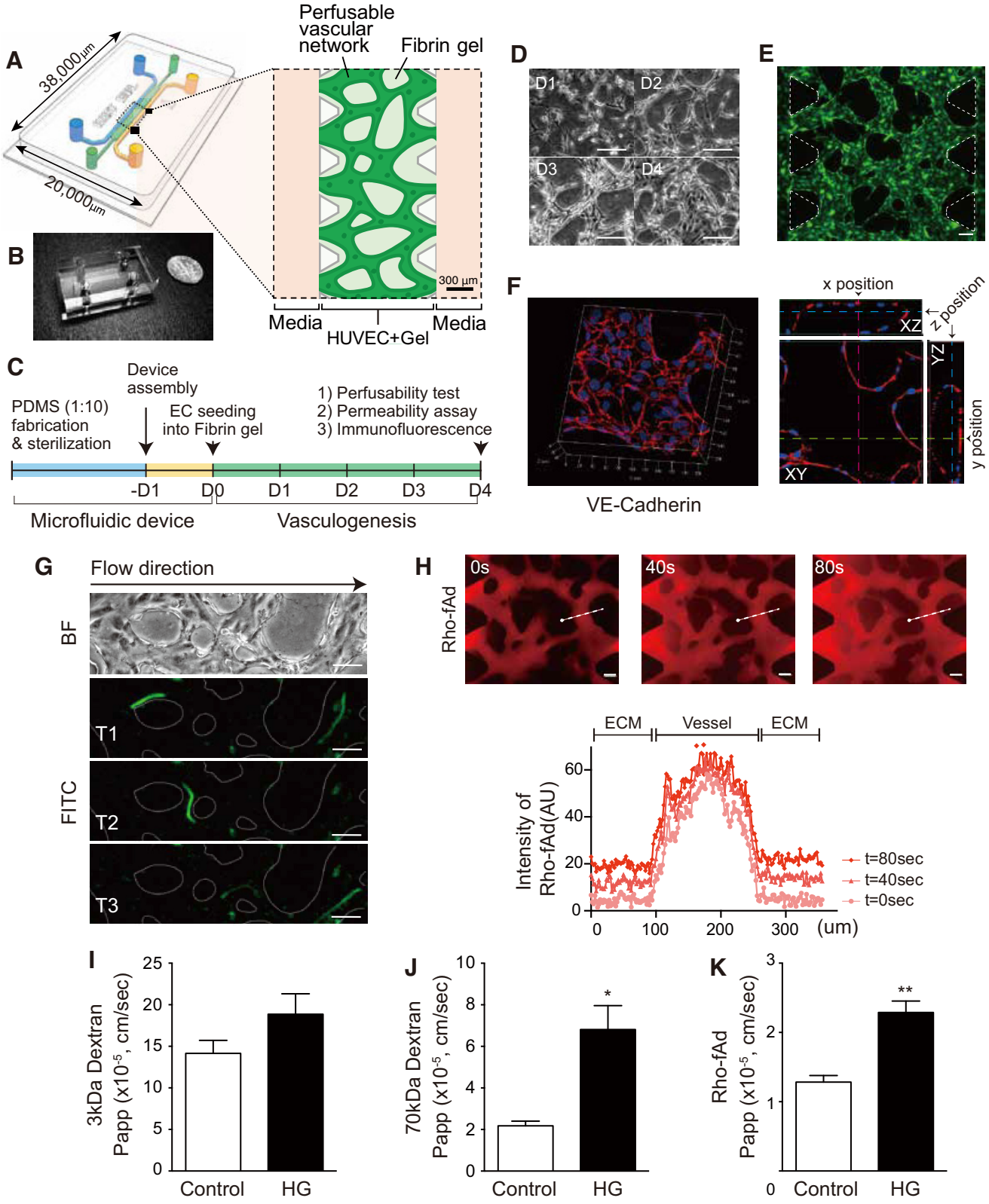

liver function (5, 38). Hence, this study was designed to use FMT to investigate distribution of fluorescently labeled adiponectin after systemic introduction in diabetic versus wild-type control mice. Given the critical need for adiponectin to access target tissues and the well-established regulatory role of vascular permeability in both physiology and therapeutics, we believe this work has widespread relevance.

We used a real-time noninvasive approach to monitor and quantify the biodistribution of exogenously administered fluorescent adiponectin. The use of FMT as a noninvasive approach to examine biodistribution of a circulating hormone, such as adiponectin, has strong advantages (40). The ability to monitor individual mice noninvasively for time-course studies vastly reduces the number of animals required and avoids issues, such as interanimal metabolic variation and variability in fluorophore injection. In addition, time and expense of isolating numerous tissues followed by analysis by Western blot can be a significant limiting factor to the identification of novel target tissues. Having a clear, temporal, whole body indicator of kinetics can provide a wealth of mechanistic insight, potentially leading to new therapeutics. In this study, we complemented FMT imaging with CT, which offered us high-resolution anatomical detail to improve the spatial and temporal localization of adiponectin. Analysis of coregistered FMT-CT data improves upon methodologies, which offer only 2D fluorescence acquisition. Through 3D analysis, we were able to precisely quantify fAd-VT750 in the heart through creation of CT-guided 3D ROIs. This is vital for accuracy, as many factors can impair rough localization of a fluorophore, including mouse orientation, variability in organ size, potential "bleed over" from highly targeted tissues (e.g., liver), and spatial overlap of several tissues, such as the lungs, heart, and thymus, from certain mouse orientations. Analysis of our in vivo findings were substantially corroborated by ex vivo scanning of target tissues and classic molecular biology techniques, including Western blot analysis and immunofluorescence imaging. For fluorescence in vivo imaging of whole body biodistribution, it is important to avoid autofluorescence, which requires near-infrared (NIR) labeling of a target (2). Probes and fluorophores are available in this range, from 680 to 750 nm and 800 nm, offering the potential for some creative multiplexing studies such as cotracking of insulin and adiponectin in circulation under various disease models. Imaging at 750–800 nm wavelengths completely avoids autofluorescence, and imaging at 680 nm only requires the use of low-chlorophyll chow to minimize confounding gastrointestinal background fluorescence.

Using this approach, we studied mice with or without streptozotocin-induced diabetes. Interestingly, an accumulation of adiponectin occurred in the peripheral tissues, particularly the liver, and to a greater extent in STZD mice. This was confirmed by quantitative analysis of in vivo FMT images, ex vivo imaging, and by analyzing tissue homogenates by Western blot. It was also interesting to note that we found no difference in endogenous adiponectin between control and STZD animals. As we are interested in the cardioprotective effects of adiponectin (11, 14), when we focused on myocardial adiponectin, we again found greater levels in STZD mice. The increased total amount of fAd-VT750 appeared to be accounted for by MMW, plus HMW and to a lesser extent LMW oligomeric forms. It is worth noting that the relative tightness of an endothelial barrier, whether in vivo, ex vivo, or in vitro, and the amount of change induced by a given treatment (e.g., high glucose), can lead to seemingly contradictory results, such as the data presented here (Fig. 2*E* vs. Fig. 4*C*). This may be explained through an understanding of protein flux dynamics at the cell junction level: slight opening of a tight endothelial barrier may lead to increased flux of only low-molecular weight proteins, while with a leakier barrier, the flux of low-molecular weight proteins may already be maximum. In this case, further opening of a leaky barrier would manifest as increased flux of only higher-molecular weight proteins. STZD is a common diabetic animal model, yet data must be interpreted with caution, since numerous endogenous changes beyond hyperglycemia may impact vascular permeability (3, 4, 34, 42). It would be of great interest to examine the same phenomenon studied here in models such as a high-fat diet feeding or in genetically obese models such as *ob/ob* mice (22). Nevertheless, to extend our observations further, we examined flux of adiponectin upon its addition to isolated mesenteric vessels from wild-type control or STZD animals. We observed again that vascular permeability of adiponectin was higher in STZD vessels. Furthermore, using an endothelial cell monolayer system in vitro, we found that flux of adiponectin was significantly greater in monolayers cultured in high glucose media versus normal glucose. Collectively, the data suggest that in the STZD model, hyperglycemia is likely to be one of the principal determinants of altered vascular permeability of adiponectin.

In this study, we also focused on alterations in tight junction proteins as a potential mechanism underlying the effects observed here. We focused on claudin-7 based on the rationale from previous studies, which showed that shRNA-mediated reduction in endothelial cell claudin-7 levels increased flux of adiponectin across endothelial monolayers (9). Indeed, our data indicated that a decrease in claudin-7 may be one important alteration leading to increased vascular permeability in STZD mice. Furthermore, we found ZO-1 was not significantly changed in STZD hearts, although previously, hyperglycemia was shown to increase permeability of the blood-brain barrier (17), and retinal pigment epithelial cells (17, 41) through downregulation of occludin and ZO-1. Because AdipoR-mediated endocytosis has been shown to have important cellular signaling consequences, we also believed that this may contribute to a transcellular route of transport (10, 46). However, the data in Supplemental Fig. S4, showing no significant change in the level of cardiac AdipoR1 or AdipoR2 after hyperglycemia in mice or high glucose level in HDMEC, suggest that this is likely not a major player.

We used advanced in vitro platform of 3D microvascular networks on a chip to confirm the observation from 2D Transwell endothelial monolayer responses in a high-glucose environment. Generating endothelial monolayer of 3D vessels with multiple branches using programmed cellular dynamics in hydrogel allows one to better mimic in vivo vascular morphology (23). Another strength of the showing 3D microvasculature in microfluidic devices is perfusibility, which allows one to test the functionality of the vessels on a chip, as well as to better mimic the physiological environment with application of fluidic shear stress (21, 24, 44). Using paracellular tracers, many researchers have shown that the basal permeability of comparably large molecules (40–70 kDa dextran) was lower

than the permeability of smaller molecules (4–10 kDa dextran) (13, 18, 20). In this study, using the platform, we confirmed size-selective transport behavior and showed for the first time that movement of rhodamine-labeled full-length adiponectin was significantly impacted by hyperglycemia-mediated alteration of endothelial permeability.

In summary, we have shown that biodistribution of adiponectin can be altered in a diabetic environment. Data from a combination of temporal noninvasive imaging in mice, isolated vessels ex vivo and in vitro endothelial cell monolayers suggest that hyperglycemia increased vascular flux of adiponectin. We believe this may be an important determinant of adiponectin's physiological actions and could provide rationale for further investigation and be exploited from a therapeutic perspective.

GRANTS

This work was supported by a grant to G. Sweeney from Natural Sciences and Engineering Research Council (NSERC) and Canadian Institutes of Health Research (CIHR). G. Sweeney also acknowledges support from the Heart & Stroke Foundation via a Career Investigator Award. The research of B. Hinz was supported by the Canadian Institutes of Health Research (Grant 375597), the Canadian Foundation for Innovation, and the Ontario Research Foundation (Grant 36050). J. S. Jeon acknowledges support from Basic Science Research Program through the National Research Foundation of Korea funded by the Ministry of Education (2017R1D1A1B03030428).

DISCLOSURES

No conflicts of interest, financial or otherwise, are declared by the authors.

AUTHOR CONTRIBUTIONS

K.D., E.T., J.S.J., J.J., T.D.M., J.G., J.D.P., and G.S. conceived and designed research; N.Y., K.D., T.D., T.C., N.N., A.R., and S.K. performed experiments; N.Y., K.D., N.N., B.H., and S.K. analyzed data; N.Y., K.D., E.T., J.S.J., S.P.K., and G.S. interpreted results of experiments; N.Y., K.D., N.N., and S.K. prepared figures; N.Y. drafted manuscript; N.Y., K.D., T.D., T.C., N.N., A.R., E.T., S.K., J.S.J., J.J., T.D.M., J.G., J.D.P., S.P.K., and G.S. approved final version of manuscript; K.D., B.H., E.T., J.S.J., J.J., T.M., J.G., J.D.P., S.P.K., and G.S. edited and revised manuscript.

REFERENCES

1. **Alipoor E, Mohammad Hosseinzadeh F, Hosseinzadeh-Attar MJ.** Adipokines in critical illness: A review of the evidence and knowledge gaps. *Biomed Pharmacother* 108: 1739–1750, 2018. doi:10.1016/j.biopha.2018.09.165.
2. **Bhaumik S, DePuy J, Klimash J.** Strategies to minimize background autofluorescence in live mice during noninvasive fluorescence optical imaging. *Lab Anim (NY)* 36: 40–43, 2007. doi:10.1038/laban0907-40.
3. **Capucci MS, Hoffmann ME, De Groot A, Natarajan AT.** Streptozotocin-induced toxicity in CHO-9 and V79 cells. *Environ Mol Mutagen* 26: 72–78, 1995. doi:10.1002/em.2850260111.
4. **Chang KS, Stevens WC.** Endothelium-dependent increase in vascular sensitivity to phenylephrine in long-term streptozotocin diabetic rat aorta. *Br J Pharmacol* 107: 983–990, 1992. doi:10.1111/j.1476-5381.1992.tb13395.x.
5. **Combs TP, Marliss EB.** Adiponectin signaling in the liver. *Rev Endocr Metab Disord* 15: 137–147, 2014. doi:10.1007/s11154-013-9280-6.
6. **Dadson K, Liu Y, Sweeney G.** Adiponectin action: a combination of endocrine and autocrine/paracrine effects. *Front Endocrinol (Lausanne)* 2: 62, 2011. doi:10.3389/fendo.2011.00062.
7. **Dadson K, Turdi S, Boo S, Hinz B, Sweeney G.** Temporal and molecular analyses of cardiac extracellular matrix remodeling following pressure overload in adiponectin-deficient mice. *PLoS One* 10: e0121049, 2015. doi:10.1371/journal.pone.0121049.
8. **Dadson K, Turdi S, Hashemi S, Zhao J, Polidovitch N, Beca S, Backx PH, McDermott JC, Sweeney G.** Adiponectin is required for cardiac MEF2 activation during pressure overload induced hypertrophy. *J Mol Cell Cardiol* 86: 102–109, 2015. doi:10.1016/j.yjmcc.2015.06.020.
9. **Dang TQ, Yoon N, Chasiotis H, Dunford EC, Feng Q, He P, Riddell MC, Kelly SP, Sweeney G.** Transendothelial movement of adiponectin is restricted by glucocorticoids. *J Endocrinol* 234: 101–114, 2017. doi:10.1530/JOE-16-0363.
10. **Ding Q, Wang Z, Chen Y.** Endocytosis of adiponectin receptor 1 through a clathrin- and Rab5-dependent pathway. *Cell Res* 19: 317–327, 2009. doi:10.1038/cr.2008.299.
11. **Engin A.** Adiponectin-resistance in obesity. *Adv Exp Med Biol* 960: 415–441, 2017. doi:10.1007/978-3-319-48382-5_18.
12. **Esmaili S, Hemmati M, Karamian M.** Physiological role of adiponectin in different tissues: a review. *Arch Physiol Biochem* Nov. 18: 1–7, 2018. doi:10.1080/13813455.2018.1493606.
13. **Funamoto K, Yoshino D, Matsubara K, Zervantonakis IK, Funamoto K, Nakayama M, Masamune J, Kimura Y, Kamm RD.** Endothelial monolayer permeability under controlled oxygen tension. *Integr Biol* 9: 529–538, 2017. doi:10.1039/C7IB00068E.
14. **Goldstein BJ, Scalia RG, Ma XL.** Protective vascular and myocardial effects of adiponectin. *Nat Clin Pract Cardiovasc Med* 6: 27–35, 2009. doi:10.1038/ncpcardio1398.
15. **Günzel D, Fromm M.** Claudins and other tight junction proteins. *Compr Physiol* 2: 1819–1852, 2012. doi:10.1002/cphy.c110045.
16. **Günzel D, Yu AS.** Claudins and the modulation of tight junction permeability. *Physiol Rev* 93: 525–569, 2013. doi:10.1152/physrev.00019.2012.
17. **Hawkins BT, Lundeen TF, Norwood KM, Brooks HL, Egleton RD.** Increased blood-brain barrier permeability and altered tight junctions in experimental diabetes in the rat: contribution of hyperglycaemia and matrix metalloproteinases. *Diabetologia* 50: 202–211, 2007. doi:10.1007/s00125-006-0485-z.
18. **Ho YT, Adriani G, Beyer S, Nhan PT, Kamm RD, Kah JCY.** A facile method to probe the vascular permeability of nanoparticles in nanomedicine applications. *Sci Rep* 7: 707, 2017. doi:10.1038/s41598-017-00750-3.
19. **Iwabu M, Okada-Iwabu M, Yamauchi T, Kadowaki T.** Adiponectin/adiponectin receptor in disease and aging. *NPJ Aging Mech Dis* 1: 15013, 2015. doi:10.1038/npjamd.2015.13.
20. **Jeon JS, Bersini S, Gilardi M, Dubini G, Charest JL, Moretti M, Kamm RD.** Human 3D vascularized organotypic microfluidic assays to study breast cancer cell extravasation. *Proc Natl Acad Sci USA* 112: 214–219, 2015. [Erratum in *Proc Natl Acad Sci USA*. 112: E818, 2015.] doi:10.1073/pnas.1417115112.
21. **Jeon JS, Bersini S, Whisler JA, Chen MB, Dubini G, Charest JL, Moretti M, Kamm RD.** Generation of 3D functional microvascular networks with human mesenchymal stem cells in microfluidic systems. *Integr Biol* 6: 555–563, 2014. doi:10.1039/C3IB40267C.
22. **Johnson AM, Costanzo A, Gareau MG, Armando AM, Quehenberger O, Jameson JM, Olefsky JM.** High-fat diet causes depletion of intestinal eosinophils associated with intestinal permeability. *PLoS One* 10: e0122195, 2015. doi:10.1371/journal.pone.0122195.
23. **Kim S, Kim W, Lim S, Jeon JS.** Vasculature-on-a-chip for in vitro disease models. *Bioengineering (Basel)* 4: E8, 2017. doi:10.3390/bioengineering4010008.
24. **Kim S, Lee H, Chung M, Jeon NL.** Engineering of functional, perfusable 3D microvascular networks on a chip. *Lab Chip* 13: 1489–1500, 2013. doi:10.1039/c3lc41320a.
25. **Kolka CM, Bergman RN.** The barrier within: endothelial transport of hormones. *Physiology (Bethesda)* 27: 237–247, 2012. doi:10.1152/physiol.00012.2012.
26. **Kolka CM, Bergman RN.** The endothelium in diabetes: its role in insulin access and diabetic complications. *Rev Endocr Metab Disord* 14: 13–19, 2013. doi:10.1007/s11154-012-9233-5.
27. **Kusminski CM, McTernan PG, Schraw T, Kos K, O'Hare JP, Ahima R, Kumar S, Scherer PE.** Adiponectin complexes in human cerebrospinal fluid: distinct complex distribution from serum. *Diabetologia* 50: 634–642, 2007. doi:10.1007/s00125-006-0577-9.
28. **Liu Y, Palanivel R, Rai E, Park M, Gabor TV, Scheid MP, Xu A, Sweeney G.** Adiponectin stimulates autophagy and reduces oxidative stress to enhance insulin sensitivity during high-fat diet feeding in mice. *Diabetes* 64: 36–48, 2015. doi:10.2337/db14-0267.
29. **Liu Y, Sweeney G.** Adiponectin action in skeletal muscle. *Best Pract Res Clin Endocrinol Metab* 28: 33–41, 2014. doi:10.1016/j.beem.2013.08.003.
30. **Palanivel R, Ganguly R, Turdi S, Xu A, Sweeney G.** Adiponectin stimulates Rho-mediated actin cytoskeleton remodeling and glucose uptake via APPL1 in primary cardiomyocytes. *Metabolism* 63: 1363–1373, 2014. doi:10.1016/j.metabol.2014.07.005.

31. **Park M, Sweeney G.** Direct effects of adipokines on the heart: focus on adiponectin. *Heart Fail Rev* 18: 631–644, 2013. doi:10.1007/s10741-012-9337-8.
32. **Park M, Youn B, Zheng XL, Wu D, Xu A, Sweeney G.** Globular adiponectin, acting via AdipoR1/APPL1, protects H9c2 cells from hypoxia/reoxygenation-induced apoptosis. *PLoS One* 6: e19143, 2011. doi:10.1371/journal.pone.0019143.
33. **Raignault A, Bolduc V, Lesage F, Thorin E.** Pulse pressure-dependent cerebrovascular eNOS regulation in mice. *J Cereb Blood Flow Metab* 37: 413–424, 2017. doi:10.1177/0271678X16629155.
34. **Raza H, John A.** Streptozotocin-induced cytotoxicity, oxidative stress and mitochondrial dysfunction in human hepatoma HepG2 cells. *Int J Mol Sci* 13: 5751–5767, 2012. doi:10.3390/ijms13055751.
35. **Rutkowski JM, Halberg N, Wang QA, Holland WL, Xia JY, Scherer PE.** Differential transendothelial transport of adiponectin complexes. *Cardiovasc Diabetol* 13: 47, 2014. doi:10.1186/1475-2840-13-47.
36. **Sente T, Van Berendoncks AM, Hoymans VY, Vrints CJ.** Adiponectin resistance in skeletal muscle: pathophysiological implications in chronic heart failure. *J Cachexia Sarcopenia Muscle* 7: 261–274, 2016. doi:10.1002/jcsm.12086.
37. **Shin Y, Han S, Jeon JS, Yamamoto K, Zervantonakis IK, Sudo R, Kamm RD, Chung S.** Microfluidic assay for simultaneous culture of multiple cell types on surfaces or within hydrogels. *Nat Protoc* 7: 1247–1259, 2012. doi:10.1038/nprot.2012.051.
38. **Tao C, Sifuentes A, Holland WL.** Regulation of glucose and lipid homeostasis by adiponectin: effects on hepatocytes, pancreatic β cells and adipocytes. *Best Pract Res Clin Endocrinol Metab* 28: 43–58, 2014. doi:10.1016/j.beem.2013.11.003.
39. **Turer AT, Scherer PE.** Adiponectin: mechanistic insights and clinical implications. *Diabetologia* 55: 2319–2326, 2012. doi:10.1007/s00125-012-2598-x.
40. **Vasquez KO, Casavant C, Peterson JD.** Quantitative whole body biodistribution of fluorescent-labeled agents by non-invasive tomographic imaging. *PLoS One* 6: e20594, 2011. doi:10.1371/journal.pone.0020594.
41. **Villarroel M, García-Ramírez M, Corraliza L, Hernández C, Simó R.** Effects of high glucose concentration on the barrier function and the expression of tight junction proteins in human retinal pigment epithelial cells. *Exp Eye Res* 89: 913–920, 2009. doi:10.1016/j.exer.2009.07.017.
42. **Wang Y, Ma XL, Lau WB.** Cardiovascular adiponectin resistance: the critical role of adiponectin receptor modification. *Trends Endocrinol Metab* 28: 519–530, 2017. doi:10.1016/j.tem.2017.03.004.
43. **Wang ZV, Scherer PE.** Adiponectin, the past two decades. *J Mol Cell Biol* 8: 93–100, 2016. doi:10.1093/jmcb/mjw011.
44. **Whisler JA, Chen MB, Kamm RD.** Control of perfusable microvascular network morphology using a multiculture microfluidic system. *Tissue Eng Part C Methods* 20: 543–552, 2014. doi:10.1089/ten.tec.2013.0370.
45. **Yamauchi T, Iwabu M, Okada-Iwabu M, Kadowaki T.** Adiponectin receptors: a review of their structure, function and how they work. *Best Pract Res Clin Endocrinol Metab* 28: 15–23, 2014. doi:10.1016/j.beem.2013.09.003.
46. **Yoon N, Dang TQ, Chasiotis H, Kelly SP, Sweeney G.** Altered transendothelial transport of hormones as a contributor to diabetes. *Diabetes Metab J* 38: 92–99, 2014. doi:10.4093/dmj.2014.38.2.92.

Appendix C

Transendothelial movement of adiponectin is restricted by glucocorticoids.

Dang TQ, Yoon N, Chasiotis H, Dunford EC, Feng Q, He P, Riddell MC, Kelly SP, Sweeney G.

J Endocrinol. 2017 Aug;234(2):101-114.

HHS Public Access

Author manuscript

J Endocrinol. Author manuscript; available in PMC 2018 November 12.

Published in final edited form as:

J Endocrinol. 2017 August ; 234(2): 101–114. doi:10.1530/JOE-16-0363.

Transendothelial movement of adiponectin is restricted by glucocorticoids

Thanh Q. Dang[#1,#], **Nanyoung Yoon**[#1,#], **Helen Chasiotis**[1], **Emily C. Dunford**[2], **Qilong Feng**[3], **Pingnian He**[3], **Michael C. Riddell**[2], **Scott P. Kelly**[1], and **Gary Sweeney**[1,*]

[1]Department of Biology, Faculty of Science York University, Toronto, Canada

[2]School of Kinesiology and Health Science, Faculty of Health and Muscle Health Research Center, York University, Toronto, Canada

[3]College of Medicine, Department of Cellular and Molecular Physiology, Penn State University, USA.

[#] These authors contributed equally to this work.

Abstract

Altered permeability of the endothelial barrier in a variety of tissues has implications both in disease pathogenesis and treatment. Glucocorticoids are potent mediators of endothelial permeability and this forms the basis for their heavily-prescribed use as medications to treat ocular disease. However, the effect of glucocorticoids on endothelial barriers elsewhere in the body is less well-studied. Here we investigated glucocorticoid-mediated changes in endothelial flux of Adiponectin (Ad), a hormone with a critical role in diabetes. First, we used monolayers of endothelial cells *in vitro* and found that the glucocorticoid dexamethasone increased transendothelial electrical resistance and reduced permeability of polyethylene glycol (PEG, molecular weight 4000kDa). Dexamethasone reduced flux of Ad from the apical to basolateral side, measured both by ELISA and Western blotting. We then examined a diabetic rat model induced by treatment with exogenous corticosterone, which was characterized by glucose intolerance and hyperinsulinemia. There was no change in circulating Ad but less Ad protein in skeletal muscle homogenates, despite slightly higher mRNA levels, in diabetic versus control muscles. Dexamethasone-induced changes in Ad flux across endothelial monolayers were associated with alterations in the abundance of select claudin (CLDN) tight junction (TJ) proteins. shRNA-mediated knockdown of one such gene, *claudin-7*, in HUVEC resulted in decreased TEER and increased adiponectin flux, confirming the functional significance of Dex-induced changes in its expression. In conclusion, our study identifies glucocorticoid-mediated reductions in flux of Ad across endothelial monolayers *in vivo* and *in vitro*. This suggests that impaired Ad action in target tissues, as a consequence of reduced transendothelial flux, may contribute to the glucocorticoid-induced diabetic phenotype.

[*]Address for correspondence: Department of Biology, York University, 4700 Keele St, Toronto, M3J 1P3, Ontario, Canada. Tel: (1) 416-736-2100 (ext. 66635), gsweeney@yorku.ca.

[#]Equal contribution as co-first authors

Declaration of Interest

No conflicts of interest to disclose

Keywords

Adiponectin; Endothelial transport; Paracellular; Tight junctions; Glucocorticoids; Corticosterone; Hydraulic conductivity; Diabetes

Introduction

As the primary barrier to the movement of circulating endocrine factors from the bloodstream to the interstitial space, the endothelium plays a critical role in hormone action (Kolka and Bergman 2012; Yoon, et al. 2014). Endothelial permeability can significantly impact hormone action by preventing or delaying access of the hormone to target tissues (Kolka and Bergman 2012; Won, et al. 2011). Transendothelial solute movement can occur via the transcellular pathway where solutes are transported across the endothelium cell membrane or via the paracellular pathway where solutes passively move through the intercellular space between adjacent endothelial cells (Yoon et al. 2014) .Previous work has shown that hormone and nutrient concentrations in blood differ from surrounding cells on the tissue side of the blood vessel endothelium (Barrett, et al. 2011; Herkner, et al. 2003; Yang, et al. 1994).Of note, this has been best documented in the case of insulin where concentrations of the hormone are significantly lower in the target tissue than in the circulation (Kolka and Bergman 2012).

Glucocorticoids are among the most commonly prescribed anti-inflammatory and immunosuppressive medications worldwide (Clark and Belvisi 2012). They are also commonly used in oncology treatment (Lin and Wang 2016) and for the treatment of macular edema and, more recently, retinopathy (Agarwal, et al. 2015; Zhang, et al. 2014). However, glucocorticoids have been shown to have potent effects on restricting endothelial transport (Felinski and Antonetti 2005; Witt and Sandoval 2014) and they contribute to the development of diabetes at least in part by increasing hepatic glucose production and reducing GLUT4 translocation in muscle (Beaudry, et al. 2015) . Yet despite these observations, the potential importance of glucocorticoid-induced alterations in the transendothelial flux of circulating glucoregulatory hormones such as Ad is unclear.

Ad is one of the most abundant plasma proteins and exists in three different isoforms: low molecular weight (LMW; trimer), medium molecular weight (MMW; hexamer) and high molecular weight (HMW; oligomer) (Dadson, et al. 2011). Ad has important and beneficial anti-diabetic, anti-inflammatory and cardioprotective actions (Arita, et al. 2002; Dadson et al. 2011). Ad levels, in particular HMW, are decreased in obese individuals and this correlates with development of associated complications, including diabetes and cardiovascular disease (Kadowaki, et al. 2006; Peters, et al. 2013). Transendothelial movement of Ad across the blood-brain barrier (BBB) into cerebrospinal fluid (CSF) was studied and only LMW and MMW were found in the CSF, suggesting that passage of HMW complexes were restricted (Kubota, et al. 2007; Kusminski, et al. 2007; Neumeier, et al. 2007). This may be functionally significant since HMW Ad is often considered to be the most biologically active and physiologically relevant form (Dadson et al. 2011; Nanayakkara, et al. 2012). A recent study calculated the Stokes radii for the Ad oligomers

and found that endothelial barriers controlled Ad transport in a cell- and tissue-specific manner (Rutkowski, et al. 2014). Thus, emerging evidence suggests that Ad action may be at least in part mediated by endothelial transport, although whether this is influenced by glucocorticoid-induced changes in transendothelial permeability remains unknown.

Given the large size of Ad multimers it seem likely that transendothelial Ad movement is an important variable in determining it presence within, and action on, target tissues. Therefore we hypothesized that glucocorticoid-induced alterations in transendothelial permeability will modulate the transendothelial movement of Ad. In this regard, the objective of this study was to examine how glucocorticoid treatment of a cultured endothelium influences Ad flux in association with changes in permeability and apical junction protein abundance as well as investigate Ad content within the skeletal muscle in a diabetic rat model induced by exogenous glucocorticoid treatment. The overall goal of this work was to significantly advance our understanding of the glucocorticoid-induced diabetic phenotype by determining whether Ad movement out of the circulatory system might play a role in its pathogenesis.

Materials and methods

HUVEC cell culture and treatments

Normal primary human umbilical vein endothelial cells (HUVECs; Pooled, PCS-100–013) were obtained from ATCC (Manassas, VA, USA) and grown at 37°C and 5% CO_2 on uncoated T75 flasks in vascular cell basal medium (ATCC, PCS-100–030) containing 10% fetal bovine serum (FBS), VEGF endothelial cell growth kit (ATCC, PCS-100–041) and treated with DEX using 2% FBS (both medium were prepared without hydrocortisone hemisuccinate), 100 units/mL penicillin and 100 μg/mL streptomycin. Cells were kept frozen in medium containing 10% DMSO (Bio-Rad Laboratories Canada Ltd., Mississauga, ON, Canada). For experiments, passage 3 was used. Cells were counted using a haemocytometer and seeded onto permeable polyethylene terephthalate (PET) filters at the base of BD Falcon cell culture inserts (BD Biosciences, Mississauga, ON, Canada) at a density of 0.5×10^6 cells/insert.

Dexamethasone (DEX) was obtained from Sigma-Aldrich (Oakville, ON, Canada), and full-length Ad was produced in-house using a mammalian expression system (i.e. HEK 293 cells) according to methods described by (Wang, et al. 2002; Xu, et al. 2004). HUVECs were treated for 5 days with DEX (1 μM) starting 24 h after seeding cells into inserts, HUVECs were treated with DEX added to both apical and basolateral sides of inserts at concentrations indicated above

shRNA-mediated knockdown of claudin-7 in HUVEC

We used pGPU6/Neo-claudin-7 shRNA vector with target sequence (5'-GGCCATCAGATTGTCACAGAC-3') (GenePharma Co., Ltd., Shanghai, China). These were transfected into HUVEC using Lipofectamine™ 3000 Reagent (Invitrogen, Carlsbad, CA, USA) exactly according to manufacturer's protocol. Non-specific scrambed target sequence shRNA vector was used as control. Following selection with 50 ug/ml Neomycin (Sigma-Aldrich, Oakville, ON, CA) for 24 hours, cells were seeded onto inserts for analysis

of TEER, examining adiponectin flux or preparation of cell lysates to confirm claudin-7 knock-down.

Transendothelial electrical resistance (TEER),and [^{3}H]PEG4000 and Adflux

TEER was measured daily using chopstick electrodes (STX-2) connected to an EVOM voltohmmeter (World Precision Instruments, Sarasota, FL, USA). As a measure of paracellular permeability, apical to basolateral flux rates of [^{3}H] polyethylene glycol at 1 μCi; 1 h flux(molecular mass 4000 Da; PEG-4000; PerkinElmer, Woodbridge, ON, Canada)or Ad (10 μg/mL; 24 h flux) to apical culture medium were determined across HUVEC endothelia. [^{3}H]PEG-4000 in basolateral culture medium was detected using a liquid scintillation counter, Ad was detected using a mouse Ad ELISA kit (Antibody Immunoassay Services, Hong Kong) or Western blot. Permeability measurements were expressed according to calculations previously outlined by (Wood, et al. 1998).

L6 and H9C2 cell culture and treatment with HUVEC-conditioned medium

Rat myoblasts and cardiomyocytes at passage 22–30 were grown in α_AMEM(Life Technologies Inc., Manassas, MA, USA) and DMEM containing 10% FBS and 1% antibiotic-antimycotic (Wisent Inc., St- Bruno QC, Canada). Culture media from the basolateral compartment of HUVEC inserts were collected and applied.L6/ H9C2 cells were starved with medium containing 0.5% FBS and 1% antibiotic-antimycotic for 3 h prior to treatment with HUVEC-conditioned medium.

Quantitative real-time PCR analysis

Total RNA was isolated from control and DEX-treated HUVECs and from soleus skeletal muscle using TRIzol Reagent . Extracted RNA was then treated with DNase I and first-strand cDNA was synthesized using SuperScript III reverse transcriptase and oligo(dT)$_{12–18}$ primers (Life Technologies Inc.,Manassas MA, USA). Quantitative real-time PCR (qRT-PCR) analyses were conducted using gene specific primers. SYBR Green I Supermix (Bio-Rad Laboratories Canada Ltd.Mississauga, ON, Canada) and a Chromo4 Detection System (CFB-3240; Bio-Rad Laboratories Canada Ltd.) Samples were run in duplicate. For all qRT-PCR analyses, TJ protein mRNA expression was normalized to GAPDH transcript abundance. For the expression profile, TJ protein transcripts were expressed relative to occludin mRNA. For TJ protein transcripts that were not detected in HUVECs, normal human adult kidney cDNA was obtained (BioChain Institute, Inc., Newark, CA, USA) and used as a positive control in qRT-PCR reactions. Agarose gel electrophoresis verified single qRT-PCR products at predicted amplicon sizes from positive control reactions.

Animal model of diabetes induced by exogenous corticosterone treatment

We used a well-established hyperinsulinemic/hyperglycemic rodent model of chronic glucocorticoid treatment (Beaudry, et al. 2013; Beaudry et al. 2015; D'Souza A, et al. 2012; Shikatani, et al. 2012; Shpilberg, et al. 2012). Upon experiment cessation, the tibialis anterior (TA) and soleus skeletal muscles were excised and immediately frozen in liquid N_2 and kept at −80°C until future analysis.

Oral glucose tolerance test

Animals were fasted overnight (16 hours), 11 days after pellet implantation, and were administered an oral glucose tolerance test (OGTT, 1.5 g/kg body mass) on day 12 using glucometer (Bayer One Touch), additional fasted plasma was collected for later analysis of insulin concentrations via an ELISA 96-well kit (Crystal Chem, USA). Plasma for measurement of Ad concentration was obtained 7 days after pellet implantation at 0800 h and assessed using a mouse Ad ELISA kit (AIS, Hong Kong).

Measurement of hydraulic conductivity (Lp) in individually perfused rat mesenteric microvessel

Female Sprague-Dawley rats of 220 to 250 g (2 to 3 mo old, Sage Laboratory Animal, PA) were used for the experiments. All procedures and animal use were approved by the Animal Care and Use Committee at Pennsylvania State University. Inactin hydrate (Sigma) was used for anesthesia and given subcutaneously at 170 mg/kg body weight. Microvessel permeability was assessed by measuring Lp in individually perfused microvessels, which measures the volume of water flux across the microvessel wall. Details have been described previously (Yuan and He 2012; Yuan, et al. 2014).

Staining for metachromatic myosin ATPase

To identify skeletal muscle fiber type, a metachromatic myosin ATPase stain was performed using a modified protocol (Ogilvie and Feeback 1990). Sections were pre-incubated in an acidic buffer (pH=4.25) to differentially inhibit myosin ATPase within the different fiber types. In this protocol, type I fibers appear dark blue, type IIa appear light blue and type IIb and IIx are not apparent from each other and are classfied as IIb/x. These fibers appear almost white and are the largest. Images were acquired with a Nikon Eclipse 90i microscope and Q-imaging MicroPublisher with Q-Capture software at 10x magnification.

Immunohistochemistry of Ad and dystrophin in skeletal muscle

Tibialis anterior (TA) from Control and CORT treated rats were cryostat sectioned (10 μm thick) for analysis of muscle Ad content. Sections were stained as previously described (Krause, et al. 2008). Quantification was performed using Zen 2.0 software. The total Ad and dystrophin signal was determined bythe sum of red/green signal intensity obtained arbitrary values in the field of view. Diagram view intensity was recorded by the software in form of histograms. Intracellular quantification was done on Ad images (without dystrophin), images were changed to 8-bits on Image and the arbitrary intensity was calculated as mean intensity per area.

Western blot analysis

Control and DEX-treated HUVECs, and L6 or H9C2 cells treated with HUVEC-conditioned medium and soleus skeletal muscle were lysed in sample buffer (80 mMTris-HCl (pH 6.8), 2% (w/v) SDS, 20% glycerol, 3.3% (v/v) β-mercaptoethanol 0.01% w/v bromophenol blue) containing protease and phosphatase inhibitors (3 mM EDTA, 10 uM E64, 1 mM Na_3VO_4, 1 μMleupeptin, 1 μMpepstatin A, 1 μMokadaic acid and 200 μM PMSF). Apical and basolateral HUVEC-conditioned media collected from Ad flux experiments were

concentrated with Amicon Ultra-4 Centrifugal Filter Units with Ultracel-30 membranes (EMD Millipore, Billerica, MA, USA) and subjected to nondenaturing, nonreducing conditions to allow the analysis of the different forms of Ad (HMW >250 kDa, MMW ~180 kDa, and LMW ~90 kDa). Primary antibodies specific for the following proteins: T-cadherin (1:1000, R&D Systems), occludin (OCLN, 1:3000), tricellulin (TRIC, 1:3000), claudin-7 (CLDN-7, 1:500), CLDN-10 (1:800), CLDN-11 (1:1000), phospho-AMPKα (Thr172) (1:1000), phospho-p38 MAPK [pT180/pY182] (1:1000), Ad (1:1000),β-actin (1:1000). OCLN, TRIC, CLDN-7, CLDN-10 and phospho-p38 MAPK [pT180/pY182] antibodies were obtained from Life Technologies, CLDN-11 and Ad antibodies were purchased from EMD Millipore and Signalway Antibody (College Park, MD, USA) respectively, and phospho-AMPKα (Thr172) and β-actin antibodies were obtained from Cell Signaling Technology (New England Biolabs Ltd., Whitby, ON, CA). Protein detection using enhanced chemiluminescence (Bio-Rad) and quantification by densitometry using ImageJ analysis software. TJ protein expression was normalized to β-actin, Tubulin protein abundance.

Statistical analysis

All data are expressed as mean values ± SEM. A one-way analysis of variance (ANOVA) followed by a Student-Newman-Keuls test was used to determine significant differences ($P \leq 0.05$) between groups. When appropriate, a Student's t-test was also used. All statistical analyses were conducted using Prism 5, Excel SigmaStat 3.5 softwares.

Results

Dexamethasone induces endothelial tightening and inhibits Ad movement across endothelial cell monolayers

We first investigated the effect of dexamethasone (DEX), a synthetic glucocorticoid, on tightness of an endothelial monolayer of HUVECs. Addition of DEX to culture media significantly elevated TEER (Fig. 1A) and correspondingly reduced the endothelial permeability of the paracellular transport marker [^{3}H]PEG-4000 (Fig. 1B). Similar trends regarding permeability were observed in microvessels of DEX-treated rats. DEX treatment (n = 4) did not cause a significant reduction in baseline Lp compared to normal control group (n = 6), but lowered the mean value from 1.5 ± 0.1 to 1.1 ± 0.2 ($\times 10^{-7}$ cm/s/cm H_2O). When each vessel was exposed to platelet activating factor (PAF, 10 nM) that is known to cause transient increases in Lp(Zhou and He 2011), microvessels in DEX-treated rats showed significantly attenuated Lp response. The mean peak Lp value was reduced from 11.1 ± 1.8 (normal control) to 6.0 ± 0.4($\times 10^{-7}$ cm/s/cm H_2O, Figure 1C). We then assessed flux of Ad from the apical to basolateral side of HUVEC monolayer and found a reduced total amount of Ad in basolateral media after DEX treatment (Fig. 1D–F). When monitoring absolute flux rates in control cells, Ad flux rate was 4.4 ± 0.12 cm $s^{-1} \times 10^{-9}$ which significantly decreased after DEX treatment to 3.2 ± 0.30cm $s^{-1} \times 10^{-9}$ (Fig. 1D). Following a 24 h flux period, Ad levels detected in basolateral media were 64.8 ± 5.7 ng/mL. Using Western blotting to examine various oligomeric forms of Ad LMW (~90 kDa), MMW (~180 kDa) and HMW (>250 kDa), we found that flux of all forms was reduced by DEX (Fig. 1E&F). Additionally, the functional activity of Ad appearing in basolateral media was

confirmed by using this media to treat L6 skeletal muscle cells and H9C2 cells derived from rat heart ventricle. In both cell types the media increased AMPK phosphorylation (supplementary Figure 1A–B).

Dexamethasone treatment alters transcript and protein abundance of select TJ proteins in HUVEC monolayers

A tissue expression profile of transcripts encoding 26 TJ proteins in HUVECs revealed the presence of 15 (Fig. 2A). The most abundant transcript was found to be *CLDN-11*, while *CLDN-7, CLDN-12* and *ZO-1* exhibited relatively high abundance and *OCLN, TRIC, CLDN-10* and *CLDN-15* exhibited moderate levels of abundance (Fig 2A). Transcripts not detected in HUVECs included *CLDN-3, −4, −5, −8, −9, −16, −17, −18, −19, −23* and *−25* (Fig. 2A & Supplementary figure 1C). Human kidney cDNA was used as a positive control for transcripts that were not detected in HUVECs (Supplementary figure 1C). To explore the response of TJ proteins to DEX- treatment, we first compared mRNA abundance of expressed target genes in HUVECs. DEX increased *CLDN-6* mRNA abundance while *CLDN-2, −20, −22, −24* and *ZO-1* mRNA showed significant decreases (Fig. 2B). DEX treatment had no significant effect on mRNA encoding *OCLN*, *TRIC, CLDN-1, −7, −10, −11 −12* and *−15*(Fig. 2B). Following DEX treatment, the protein abundance of CLDN-1, −7, −11 and ZO-1 was examined and found to be significantly upregulated following DEX treatment when compared to the control group (Fig. 2C, D). On the other hand, CLDN-10 protein levels were significantly decreased when compared with the expression in control conditions (Fig. 2C, D). In order to validate the functional significance of Dex-induced changes in expression of tight juntion proteins we used shRNA to target claudin-7 and this effectively reduced its expression by 71% on average (Fig. 3A). Furthermore, HUVEC with reduced levels of claudin-7 showed reduced TEER and a small but significant increase in flux of adiponectin from apical to basolateral side (Figs 3B–D).

Examination of changes in transcellular endothelial flux

The possible contribution of transcellular receptor-mediated Ad movement across HUVEC monolayers was then investigated by analysis of expression levels of three identified Ad receptors. Intracellular Ad content in these cells was detected, although at low level, and expression levels did not change significantly with DEX treatment (Fig. 4A). However, DEX significantly increased T-cadherin protein abundance (Fig. 4B), but had no effect on protein abundance of AdipoR1 and AdipoR2 (Fig. 4C).

Skeletal muscle Ad content in a rat model of exogenous glucocorticoid-induced diabetes

We then examined whether the increased endothelial cell barrier tightness observed after DEX treatment would be paralleled in a diabetic rodent model of chronic glucocorticoid exposure. As expected based on previously published work (D'Souza A et al. 2012; Shikatani et al. 2012; Shpilberg et al. 2012), two weeks of exogenous corticosterone (CORT) treatment resulted in severe fasting hyperinsulinemia and impaired glucose tolerance (Supp Fig 2A). In addition, CORT treatment caused mild/moderate elevations in fasted blood glucose concentrations (5.12± 0.2 mM to 8.3 ± 1.88 mM, Supp Fig 2B) despite the significantly increased fasted insulin concentrations (0.76±0.25 ng/ml to 4.68±0.72 ng/ml , Supp Fig 2C). CORT treatment also caused a change in skeletal muscle fibre type

composition; a switch from predominantly slow to fast-twitch skeletal muscle fibers, within the tibialis anterior muscle (Supp Fig 2D).

To explore whether CORT-treatment affects circulating Ad levels, we measured plasma Ad levels in these animals before CORT pellet implantation and at 7 days post pellet implantation, at 0800h. Circulating Ad levels were unaffected by CORT treatment (Fig 5. A). Interestingly, there was an apparent elevation in skeletal muscle Ad mRNA levels (Fig 5. B), yet Ad protein content was significantly reduced (Fig 5. C&D). Upon immunohistochemical analyses, we also observed that the total amount of Ad was decreased in skeletal muscle from the COR-treated rats versus control rats (Fig 5. E–H). Dystrophin, was used to assess the structural integrity of the skeletal muscle and was unaffected by CORT treatment. Representative images are shown (Fig 5. E) with quantification of the total and intracellular Ad signal (Fig 5. G–H). Since CORT-treatment is known to preferentially target fast-twitch skeletal muscle (Beaudry et al. 2015), representative images accordingly depict smaller IIb/x fiber area (Fig. 4D) within the CORT-treated rats. CORT-treatment was also found to cause a significant reduction in individual myocyte size (Fig. 5F).

AdipoR abundance in a rat model of exogenous glucocorticoid-induced diabetes

Both Ad receptor isoforms (*AdipoR1* and *AdipoR2*) genes were expressed in rat soleus skeletal muscle and although an apparent increase in *AdipoR1* mRNA abundance was seen in the diabetic rat model, neither was significantly altered (Fig. 6 A,B). However, a significantly increased level of ADIPO-R1 protein (approximately 3.4 fold compared to the control) was seen (Fig. 6F). There were no changes in ADIPO- R2 nor in T- Cadherin protein levels (Fig. 6E, G).

CORT treatment altered Tight Junction genes in rat soleus skeletal muscle after 2 weeks

We then measured changes in mRNA abundance of tight junction, *Cldn-1, −2, −3, −4,−5, −6, −7, −9, −10, −11, −12, −24,−14, −15, −19, −20, −22, −23* and *Ocln, T*ricand *Z0–1* were found to be no significant changes with in diabetic rat skeletal muscle (Fig. 6C), with only *Cldn −5, −10, −11, −22* significantly decreased (Fig. 6D).

Discussion

Glucocorticoids are potential mediators of endothelium permeability. Our study was designed investigate the its influence on endothelium permeability and consequently the changes in Ad movement across the endothelium barrier and the underlying mechanism. More recently, a similar proposed mechanism for regulation of Ad action was suggested both by us and others (Rutkowski et al. 2014; Yoon et al. 2014). To the best of our knowledge, the regulation of this process by glucocorticoids had not been studied before. Our vitro model using DEX treated HUVEC and CORT treated rats to integrate the established observations that glucocorticoids can restrict paracellular transport across various endothelia (Keaney and Campbell 2015; Rao, et al. 2015; Rochfort and Cummins 2015) with the fact that glucocorticoids, commonly prescribed medications, have numerous side effects, including insulin resistance and diabetes (Beaudry et al. 2015). Furthermore, we examined whether the emerging phenomenon that transendothelial movement of Ad may

regulate the anti-diabetic effects of this hormone and whether this was regulated by glucocorticoids (Rutkowski et al. 2014; Yoon et al. 2014). Specifically, our approach involved the use of endothelial cell monolayers and individually perfused intact microvessels to examine whether glucocorticoid altered Ad flux was through reduced microvessel permeability. We also used a rat model of diabetes induced by exogenous glucocorticoid treatment to determine changes in Ad content in muscle as well as peripheral insulin sensitivity.

As indicated in the introduction, strong rationale for this work comes from previous studies with other circulating hormones, most notably insulin. Concentrations of insulin at the cell surface have been shown to be very different from those observed in plasma in microdialysis experiments (Herkner et al. 2003; Sjostrand, et al. 1999), direct interstitial sampling (Bodenlenz, et al. 2005) and lymph measurements (Chiu, et al. 2008; Yang et al. 1994). It was noted that insulin-mediated glucose uptake lagged behind the increase in plasma insulin (Freidenberg, et al. 1994), whereas in cultured skeletal muscle cells, insulin-mediated glucose uptake occurs within 10 min (Somwar, et al. 2001). The time delay seen in vivo (Freidenberg et al. 1994) reflects a delay in insulin access to the myocyte which is mediated in part via altered paracellular or transcellular endothelial transport. Thus, modification of access to skeletal muscle can have major effects on insulin action and metabolism, suggesting that reaching the interstitial space is the limiting factor for insulin-mediated glucose uptake (Kolka and Bergman 2012). Indeed, delivery of insulin to the interstitial space has been shown to be altered by diet (Kubota, et al. 2011).

We confirmed the ability of the synthetic glucocorticoid DEX to alter endothelial transport properties, in this case of HUVEC monolayers, as indicated by changes in TEER and PEG-4000. Similar effects were observed in DEX-treated rats, where we saw a significant reduction of permeability in rat mesenteric venules. We then showed that DEX reduced Ad flux across cultured endothelial monolayers by ELISA detection of total Ad content. Western blotting of Ad isoforms indicated that all three oligomeric forms of Ad (trimer, hexamer and oligomer) were reduced in basolateral media from DEX-treated cells, and although the magnitude of change was more evident in the case of LMW adiponectin, all isoforms were significantly altered and we do not believe this data infers a preferential restriction of LMW flux. This demonstration of restricted flux is important to establish from several perspectives. First, many studies have suggested that oligomeric high molecular weight complexes of Ad are most tightly correlated with insulin resistance (Liu, et al. 2007; Pajvani, et al. 2004). Second, the concept that endothelial transport regulated Ad action was also proposed by a recent study which estimated the size of different Ad forms by calculating a Stokes radius (Rutkowski et al. 2014). The Stokes radii were 3.96 nm for trimeric Ad, 6.01 nm for hexameric Ad and 10.1 nm for various HMW oligomeric forms (Rutkowski et al. 2014) and these sizes are likely to be in the range that can be physically obstructed or facilitated by changes in endothelial cell tight junction size. Indeed, it was concluded that Ad bioavailability and action in target cells was attenuated under stressed conditions due to reduced trans-endothelial transport (Rutkowski et al. 2014). We concur that regulation of Ad flux across endothelium is particularly relevant since the target tissues where Ad mediates its physiological effects have a wide-range of endothelial permeability. Liver, for example has highly fenestrated endothelium that may permit the passage of HMW

Ad, which has potent effects on hepatic metabolism. In contrast, the central effects of HMW Ad may be limited by its transport across the comparatively tighter blood brain barrier (Yoon et al. 2014).

The well-established effect of glucocorticoids to restrict endothelial transport has been proposed to be mediated via regulation of TJ and adherens junction (AJ) proteins (Blecharz, et al. 2008; Felinski and Antonetti 2005). Strands of transmembrane and cytosolic proteins form TJ and AJ complexes that regulate permeability between endothelial cells (Gunzel and Fromm 2012). Functional characteristics of the vertebrate TJ complex are dependent on the variable assemblage of TJ proteins such as occludin (OCLN), tricellulin (TRIC) and in particular, claudins (CLDNs) which directly establish the TJ barrier and form the backbone of TJ strands, while cytosolic ZO-1 and other cortical TJ proteins provide structural support to the TJ complex (Gunzel and Fromm 2012). The CLDN superfamily consists of at least 27 isoforms in mammals and the incorporation of specific CLDN isoforms in TJs can modulate TJ barrier function by making the paracellular pathway tighter or leakier (Gunzel and Yu 2013). The main observations in our study were increased CLDN-7 and decreased CLDN-10 protein abundance in HUVEC in response to DEX and these changes may underlie the functional properties of paracellular transport limiting Ad flux. Little is known about CLDN-7, although CLDN-7 knockout is lethal in murine models and it seems that CLDN-7 most likely facilitates anion movement across vertebrate epithelia. CLDN-7 was previously found to form a complex with the epithelial cell adhesion molecule (EpCAM) which enhanced cell-cell interaction (Krug, et al. 2012; Verma and Molitoris 2015) . We suggested that the functional role of CLDN-7 in our model is tightening of the endothelium in association with an increase in abundance, and that this may help to explain, in part, the restricted movement of Ad in DEX-treated HUVEC as well CORT-treated rats. Further supporting this idea, a reprevious studies which have found that CLDN-7 (−/−) can cause colonic inflammation and enhance the paracellular flux of small organic solutes (Tanaka, et al. 2015), as well as observations that CLDN-7 (−/−) results in the presence of intercellular gaps below TJs and cell matrix loosening (Ding, et al. 2012). Thus, we used shRNA to target claudin-7 in HUVEC and observed that this caused a decrease in TEER and increase in adiponectin flux across monolayers, further indicating an important mechanistic role for Dex-mediated changes in claudin-7 expression. Interestingly, another group found that NLRP3 inflammasome promoted endothelial disruption via production of HMGB1 to disrupt the junctions and increased paracellular permeability (Chen, et al. 2015). Finally, (Tatum, et al. 2010) reported that urine Na(+), Cl(−), and K(+) were significantly increased in CLDN-7(−/−) mice compared with that of CLDN-7(+/+) mice. Taken together, the studies outlined above and our data indicate an important functional consequence for CLDN-7 reduction and compromised epithelial permeability as the result of tight junction disruption, and this supports the view that increased CDLN-7 abundance, as seen in these experiments, may contribute to endothelial tightening and reduced Ad flux.

In contrast, CLDN-10 isoforms in vertebrate epithelia have been described to impart both charge and size selective properties to the paracellular pathway. Previous studies investigated the role of CLDN-10 deficient mice using Cre-Lox found that serum phosphate concentration was 28% higher and serum Mg^{2+} concentration was almost two-fold higher in cKO mice compared with controls. However, the same study also found that CLDN-10

transports molecules in a charged selective manner (Breiderhoff, et al. 2012). To the best of our knowledge, Ad is uncharged. Therefore, the transport of Ad is less likely to be affected by CLDN-10. Nevertheless, it would be very interesting to explore whether the consistent decrease in CLDN-10 observed in this study has a functional role in the modulation of Ad transport across the endothelium barrier.

In the glucocorticoid-induced diabetic rodent model used here, a decrease in CLDN-10 mRNA expression in skeletal muscle was also observed. Although changes in expression profiles of other tight junction proteins do not entirely match the changes in HUVEC treated directly with DEX, this is not entirely surprising since there are multiple factors impinging upon tight junction protein expression in skeletal muscle tissue *in vivo*.

We believe that reduced paracellular transport is the main mechanism of reduced Ad flux observed, yet we also tested possible indicators of altered transendothelial flux (Yoon et al. 2014). In DEX-treated endothelial cells, there was no major change in ADIPO-R1 or ADIPO-R2 mRNA and protein expression, although in skeletal muscle homogenates, ADIPO-R1 protein expression levels increased significantly in CORT-treated animals. This may reflect a compensatory mechanism to reduced Ad availability in order to increase sensitivity to available Ad. We also observed that DEX increased expression of T-cadherin in HUVEC. T-cadherin has been identified as a non-functional receptor for Ad (Hug, et al. 2004). This is in agreement with a previous study showing that DEX enhanced T-cadherin expression in human osteosarcoma cells (Bromhead, et al. 2006). One possible interpretation of our finding is that binding to endothelial T-cadherin may trap Ad in the vasculature, as has recently been proposed (Matsuda, et al. 2015).

We also investigated potential alterations in endothelial transport of Ad in a rodent model of glucocorticoid-induced diabetes (Shpilberg et al. 2012). In these rats, we found normal circulating Ad levels but significantly reduced total Ad protein content within skeletal muscle without an accompanying decrease in muscle Ad gene expression. This suggests less flux of Ad from circulation could be a contributory mechanism. Indeed, upon immunohistochemical analysis we found reduced Ad content in the interstitial space. Although not a direct comparison to the *in vitro* studies we used here, it suggests that skeletal muscle Ad availability, and thus action, may be limited in this animal model possibly contributing to its diabetic phenotype (Beaudry et al. 2013; Beaudry et al. 2015; Beaudry, et al. 2014; Shpilberg et al. 2012; Yoon et al. 2014).

In conclusion, our study indicates that glucocorticoid-mediated tightening can reduce flux of Ad across endothelial monolayers, and that this may be due to alterations in the expression profile of tight junction proteins. Furthermore, in a rat model of diabetes induced by exogenous glucocorticoids, we observed reduced interstitial and intracellular levels of Ad in skeletal muscle. Thus, we propose that reduced Ad action in target tissues, as a consequence of reduced endothelial flux from circulation to interstitial space, may contribute to the diabetic phenotype occurring after glucocorticoid treatment. Since glucocorticoids are one of the most commonly prescribed medications, our discovery of reduced Ad transport in response to glucocorticoids is a particularly important and novel finding with potentially far-reaching consequences.

Supplementary Material

Refer to Web version on PubMed Central for supplementary material.

Acknowledgements

We also greatly appreciate the contribution of Dr. Tara Haas via advice on quantifications of skeletal muscle tissue immunostaining.

Funding

This work was initially funded by an operating grant to GS from Canadian Institutes of Health Research and then by Natural Science and Engineering Research Council of Canada Discovery Grants to GS, SPK and MCR. PH was funded by the National Institutes of Health (US) HL56237 and DK097391. GS also acknowledges Career Investigator support from Heart & Stroke Foundation of Ontario.

References

1. Agarwal A, Sarwar S, Sepah YJ & Nguyen QD 2015 What have we learnt about the management of diabetic macular edema in the antivascular endothelial growth factor and corticosteroid era? Curr Opin Ophthalmol 26 177–183. [PubMed: 25784111]
2. Arita Y, Kihara S, Ouchi N, Maeda K, Kuriyama H, Okamoto Y, Kumada M, Hotta K, Nishida M, Takahashi M, et al. 2002 Adipocyte-derived plasma protein adiponectin acts as a platelet-derived growth factor-BB-binding protein and regulates growth factor-induced common postreceptor signal in vascular smooth muscle cell. Circulation 105 2893–2898. [PubMed: 12070119]
3. Barrett EJ, Wang H, Upchurch CT & Liu Z 2011 Insulin regulates its own delivery to skeletal muscle by feed-forward actions on the vasculature. Am J Physiol Endocrinol Metab 301 E252–263. [PubMed: 21610226]
4. Beaudry JL, D'Souza A M, Teich T, Tsushima R & Riddell MC 2013 Exogenous glucocorticoids and a high-fat diet cause severe hyperglycemia and hyperinsulinemia and limit islet glucose responsiveness in young male Sprague-Dawley rats. Endocrinology 154 3197–3208. [PubMed: 23766132]
5. Beaudry JL, Dunford EC, Leclair E, Mandel ER, Peckett AJ, Haas TL & Riddell MC 2015 Voluntary exercise improves metabolic profile in high-fat fed glucocorticoid-treated rats. J Appl Physiol (1985) 118 1331–1343. [PubMed: 25792713]
6. Beaudry JL, Dunford EC, Teich T, Zaharieva D, Hunt H, Belanoff JK & Riddell MC 2014 Effects of selective and non-selective glucocorticoid receptor II antagonists on rapid-onset diabetes in young rats. PLoS One 9 e91248. [PubMed: 24642683]
7. Blecharz KG, Drenckhahn D & Forster CY 2008 Glucocorticoids increase VE-cadherin expression and cause cytoskeletal rearrangements in murine brain endothelial cEND cells. J Cereb Blood Flow Metab 28 1139–1149. [PubMed: 18231113]
8. Bodenlenz M, Schaupp LA, Druml T, Sommer R, Wutte A, Schaller HC, Sinner F, Wach P & Pieber TR 2005 Measurement of interstitial insulin in human adipose and muscle tissue under moderate hyperinsulinemia by means of direct interstitial access. Am J Physiol Endocrinol Metab 289 E296–300. [PubMed: 15769794]
9. Breiderhoff T, Himmerkus N, Stuiver M, Mutig K, Will C, Meij IC, Bachmann S, Bleich M, Willnow TE & Muller D 2012 Deletion of claudin-10 (Cldn10) in the thick ascending limb impairs paracellular sodium permeability and leads to hypermagnesemia and nephrocalcinosis. Proc Natl Acad Sci U S A 109 14241–14246. [PubMed: 22891322]
10. Bromhead C, Miller JH & McDonald FJ 2006 Regulation of T-cadherin by hormones, glucocorticoid and EGF. Gene 374 58–67. [PubMed: 16516410]
11. Chen Y, Pitzer AL, Li X, Li PL, Wang L & Zhang Y 2015 Instigation of endothelial Nlrp3 inflammasome by adipokine visfatin promotes inter-endothelial junction disruption: role of HMGB1. J Cell Mol Med 19 2715–2727. [PubMed: 26293846]

12. Chiu JD, Richey JM, Harrison LN, Zuniga E, Kolka CM, Kirkman E, Ellmerer M & Bergman RN 2008 Direct administration of insulin into skeletal muscle reveals that the transport of insulin across the capillary endothelium limits the time course of insulin to activate glucose disposal. Diabetes 57 828–835. [PubMed: 18223011]
13. Clark AR & Belvisi MG 2012 Maps and legends: the quest for dissociated ligands of the glucocorticoid receptor. Pharmacol Ther 134 54–67. [PubMed: 22212616]
14. D'Souza A M, Beaudry JL, Szigiato AA, Trumble SJ, Snook LA, Bonen A, Giacca A & Riddell MC 2012 Consumption of a high-fat diet rapidly exacerbates the development of fatty liver disease that occurs with chronically elevated glucocorticoids. Am J Physiol Gastrointest Liver Physiol 302 G850–863. [PubMed: 22268100]
15. Dadson K, Liu Y & Sweeney G 2011 Adiponectin action: a combination of endocrine and autocrine/paracrine effects. Front Endocrinol (Lausanne) 2 62. [PubMed: 22649379]
16. Ding L, Lu Z, Foreman O, Tatum R, Lu Q, Renegar R, Cao J & Chen YH 2012 Inflammation and disruption of the mucosal architecture in claudin-7-deficient mice. Gastroenterology 142 305–315. [PubMed: 22044670]
17. Felinski EA & Antonetti DA 2005 Glucocorticoid regulation of endothelial cell tight junction gene expression: novel treatments for diabetic retinopathy. Curr Eye Res 30 949–957. [PubMed: 16282129]
18. Freidenberg GR, Suter S, Henry RR, Nolan J, Reichart D & Olefsky JM 1994 Delayed onset of insulin activation of the insulin receptor kinase in vivo in human skeletal muscle. Diabetes 43 118–126. [PubMed: 8262308]
19. Gunzel D & Fromm M 2012 Claudins and other tight junction proteins. Compr Physiol 2 1819–1852. [PubMed: 23723025]
20. Gunzel D & Yu AS 2013 Claudins and the modulation of tight junction permeability. Physiol Rev 93 525–569. [PubMed: 23589827]
21. Herkner H, Klein N, Joukhadar C, Lackner E, Langenberger H, Frossard M, Bieglmayer C, Wagner O, Roden M & Muller M 2003 Transcapillary insulin transfer in human skeletal muscle. Eur J Clin Invest 33 141–146. [PubMed: 12588288]
22. Hug C, Wang J, Ahmad NS, Bogan JS, Tsao TS & Lodish HF 2004 T-cadherin is a receptor for hexameric and high-molecular-weight forms of Acrp30/adiponectin. Proc Natl Acad Sci U S A 101 10308–10313. [PubMed: 15210937]
23. Kadowaki T, Yamauchi T, Kubota N, Hara K, Ueki K & Tobe K 2006 Adiponectin and adiponectin receptors in insulin resistance, diabetes, and the metabolic syndrome. J Clin Invest 116 1784–1792. [PubMed: 16823476]
24. Keaney J & Campbell M 2015 The dynamic blood-brain barrier. FEBS J 282 4067–4079. [PubMed: 26277326]
25. Kolka CM & Bergman RN 2012 The barrier within: endothelial transport of hormones. Physiology (Bethesda) 27 237–247. [PubMed: 22875454]
26. Krause MP, Liu Y, Vu V, Chan L, Xu A, Riddell MC, Sweeney G & Hawke TJ 2008 Adiponectin is expressed by skeletal muscle fibers and influences muscle phenotype and function. Am J Physiol Cell Physiol 295 C203–212. [PubMed: 18463233]
27. Krug SM, Gunzel D, Conrad MP, Lee IF, Amasheh S, Fromm M & Yu AS 2012 Charge-selective claudin channels. Ann N Y Acad Sci 1257 20–28. [PubMed: 22671585]
28. Kubota N, Yano W, Kubota T, Yamauchi T, Itoh S, Kumagai H, Kozono H, Takamoto I, Okamoto S, Shiuchi T, et al. 2007 Adiponectin stimulates AMP-activated protein kinase in the hypothalamus and increases food intake. Cell Metab 6 55–68. [PubMed: 17618856]
29. Kubota T, Kubota N, Kumagai H, Yamaguchi S, Kozono H, Takahashi T, Inoue M, Itoh S, Takamoto I, Sasako T, et al. 2011 Impaired insulin signaling in endothelial cells reduces insulin-induced glucose uptake by skeletal muscle. Cell Metab 13 294–307. [PubMed: 21356519]
30. Kusminski CM, McTernan PG, Schraw T, Kos K, O'Hare JP, Ahima R, Kumar S & Scherer PE 2007 Adiponectin complexes in human cerebrospinal fluid: distinct complex distribution from serum. Diabetologia 50 634–642. [PubMed: 17242917]
31. Lin KT & Wang LH 2016 New dimension of glucocorticoids in cancer treatment. Steroids 111 84–88. [PubMed: 26930575]

32. Liu Y, Retnakaran R, Hanley A, Tungtrongchitr R, Shaw C & Sweeney G 2007 Total and high molecular weight but not trimeric or hexameric forms of adiponectin correlate with markers of the metabolic syndrome and liver injury in Thai subjects. J Clin Endocrinol Metab 92 4313–4318. [PubMed: 17698903]
33. Matsuda K, Fujishima Y, Maeda N, Mori T, Hirata A, Sekimoto R, Tsushima Y, Masuda S, Yamaoka M, Inoue K, et al. 2015 Positive feedback regulation between adiponectin and T-cadherin impacts adiponectin levels in tissue and plasma of male mice. Endocrinology 156 934–946. [PubMed: 25514086]
34. Nanayakkara G, Kariharan T, Wang L, Zhong J & Amin R 2012 The cardio-protective signaling and mechanisms of adiponectin. Am J Cardiovasc Dis 2 253–266. [PubMed: 23173099]
35. Neumeier M, Weigert J, Buettner R, Wanninger J, Schaffler A, Muller AM, Killian S, Sauerbruch S, Schlachetzki F, Steinbrecher A, et al. 2007 Detection of adiponectin in cerebrospinal fluid in humans. Am J Physiol Endocrinol Metab 293 E965–969. [PubMed: 17623750]
36. Ogilvie RW & Feeback DL 1990 A metachromatic dye-ATPase method for the simultaneous identification of skeletal muscle fiber types I, IIA, IIB and IIC. Stain Technol 65 231–241. [PubMed: 1703671]
37. Pajvani UB, Hawkins M, Combs TP, Rajala MW, Doebber T, Berger JP, Wagner JA, Wu M, Knopps A, Xiang AH, et al. 2004 Complex distribution, not absolute amount of adiponectin, correlates with thiazolidinedione-mediated improvement in insulin sensitivity. J Biol Chem 279 12152–12162. [PubMed: 14699128]
38. Peters KE, Beilby J, Cadby G, Warrington NM, Bruce DG, Davis WA, Davis TM, Wiltshire S, Knuiman M, McQuillan BM, et al. 2013 A comprehensive investigation of variants in genes encoding adiponectin (ADIPOQ) and its receptors (ADIPOR1/R2), and their association with serum adiponectin, type 2 diabetes, insulin resistance and the metabolic syndrome. BMC Med Genet 14 15. [PubMed: 23351195]
39. Rao A, Pandya V & Whaley-Connell A 2015 Obesity and insulin resistance in resistant hypertension: implications for the kidney. Adv Chronic Kidney Dis 22 211–217. [PubMed: 25908470]
40. Rochfort KD & Cummins PM 2015 The blood-brain barrier endothelium: a target for pro-inflammatory cytokines. Biochem Soc Trans 43 702–706. [PubMed: 26551716]
41. Rutkowski JM, Halberg N, Wang QA, Holland WL, Xia JY & Scherer PE 2014 Differential transendothelial transport of adiponectin complexes. Cardiovasc Diabetol 13 47. [PubMed: 24552349]
42. Shikatani EA, Trifonova A, Mandel ER, Liu ST, Roudier E, Krylova A, Szigiato A, Beaudry J, Riddell MC & Haas TL 2012 Inhibition of proliferation, migration and proteolysis contribute to corticosterone-mediated inhibition of angiogenesis. PLoS One 7 e46625. [PubMed: 23056375]
43. Shpilberg Y, Beaudry JL, D'Souza A, Campbell JE, Peckett A & Riddell MC 2012 A rodent model of rapid-onset diabetes induced by glucocorticoids and high-fat feeding. Dis Model Mech 5 671–680. [PubMed: 22184636]
44. Sjostrand M, Holmang A & Lonnroth P 1999 Measurement of interstitial insulin in human muscle. Am J Physiol 276 E151–154. [PubMed: 9886961]
45. Somwar R, Kim DY, Sweeney G, Huang C, Niu W, Lador C, Ramlal T & Klip A 2001 GLUT4 translocation precedes the stimulation of glucose uptake by insulin in muscle cells: potential activation of GLUT4 via p38 mitogen-activated protein kinase. Biochem J 359 639–649. [PubMed: 11672439]
46. Tanaka H, Takechi M, Kiyonari H, Shioi G, Tamura A & Tsukita S 2015 Intestinal deletion of Claudin-7 enhances paracellular organic solute flux and initiates colonic inflammation in mice. Gut 64 1529–1538. [PubMed: 25691495]
47. Tatum R, Zhang Y, Salleng K, Lu Z, Lin JJ, Lu Q, Jeansonne BG, Ding L & Chen YH 2010 Renal salt wasting and chronic dehydration in claudin-7-deficient mice. Am J Physiol Renal Physiol 298 F24–34. [PubMed: 19759267]
48. Verma SK & Molitoris BA 2015 Renal endothelial injury and microvascular dysfunction in acute kidney injury. Semin Nephrol 35 96–107. [PubMed: 25795503]

49. Wang Y, Xu A, Knight C, Xu LY & Cooper GJ 2002 Hydroxylation and glycosylation of the four conserved lysine residues in the collagenous domain of adiponectin. Potential role in the modulation of its insulin-sensitizing activity. J Biol Chem 277 19521–19529. [PubMed: 11912203]
50. Witt KA & Sandoval KE 2014 Steroids and the blood-brain barrier: therapeutic implications. Adv Pharmacol 71 361–390. [PubMed: 25307223]
51. Won SM, Lee JH, Park UJ, Gwag J, Gwag BJ & Lee YB 2011 Iron mediates endothelial cell damage and blood-brain barrier opening in the hippocampus after transient forebrain ischemia in rats. Exp Mol Med 43 121–128. [PubMed: 21278483]
52. Wood CM, Gilmour KM, Perry SF, Part P & Walsh PJ 1998 Pulsatile urea excretion in gulf toadfish (Opsanus beta): evidence for activation of a specific facilitated diffusion transport system. J Exp Biol 201 805–817. [PubMed: 9464961]
53. Xu A, Yin S, Wong L, Chan KW & Lam KS 2004 Adiponectin ameliorates dyslipidemia induced by the human immunodeficiency virus protease inhibitor ritonavir in mice. Endocrinology 145 487–494. [PubMed: 14592951]
54. Yang YJ, Hope ID, Ader M & Bergman RN 1994 Importance of transcapillary insulin transport to dynamics of insulin action after intravenous glucose. Am J Physiol 266 E17–25. [PubMed: 8304440]
55. Yoon N, Dang TQ, Chasiotis H, Kelly SP & Sweeney G 2014 Altered transendothelial transport of hormones as a contributor to diabetes. Diabetes Metab J 38 92–99. [PubMed: 24851202]
56. Yuan D & He P 2012 Vascular remodeling alters adhesion protein and cytoskeleton reactions to inflammatory stimuli resulting in enhanced permeability increases in rat venules. J Appl Physiol (1985) 113 1110–1120. [PubMed: 22837164]
57. Yuan D, Xu S & He P 2014 Enhanced permeability responses to inflammation in streptozotocin-induced diabetic rat venules: Rho-mediated alterations of actin cytoskeleton and VE-cadherin. Am J Physiol Heart Circ Physiol 307 H44–53. [PubMed: 24778164]
58. Zhang X, Wang N, Schachat AP, Bao S & Gillies MC 2014 Glucocorticoids: structure, signaling and molecular mechanisms in the treatment of diabetic retinopathy and diabetic macular edema. Curr Mol Med 14 376–384. [PubMed: 24467200]
59. Zhou X & He P 2011 Temporal and spatial correlation of platelet-activating factor-induced increases in endothelial [Ca(2)(+)]i, nitric oxide, and gap formation in intact venules. Am J Physiol Heart Circ Physiol 301 H1788–1797. [PubMed: 21873500]

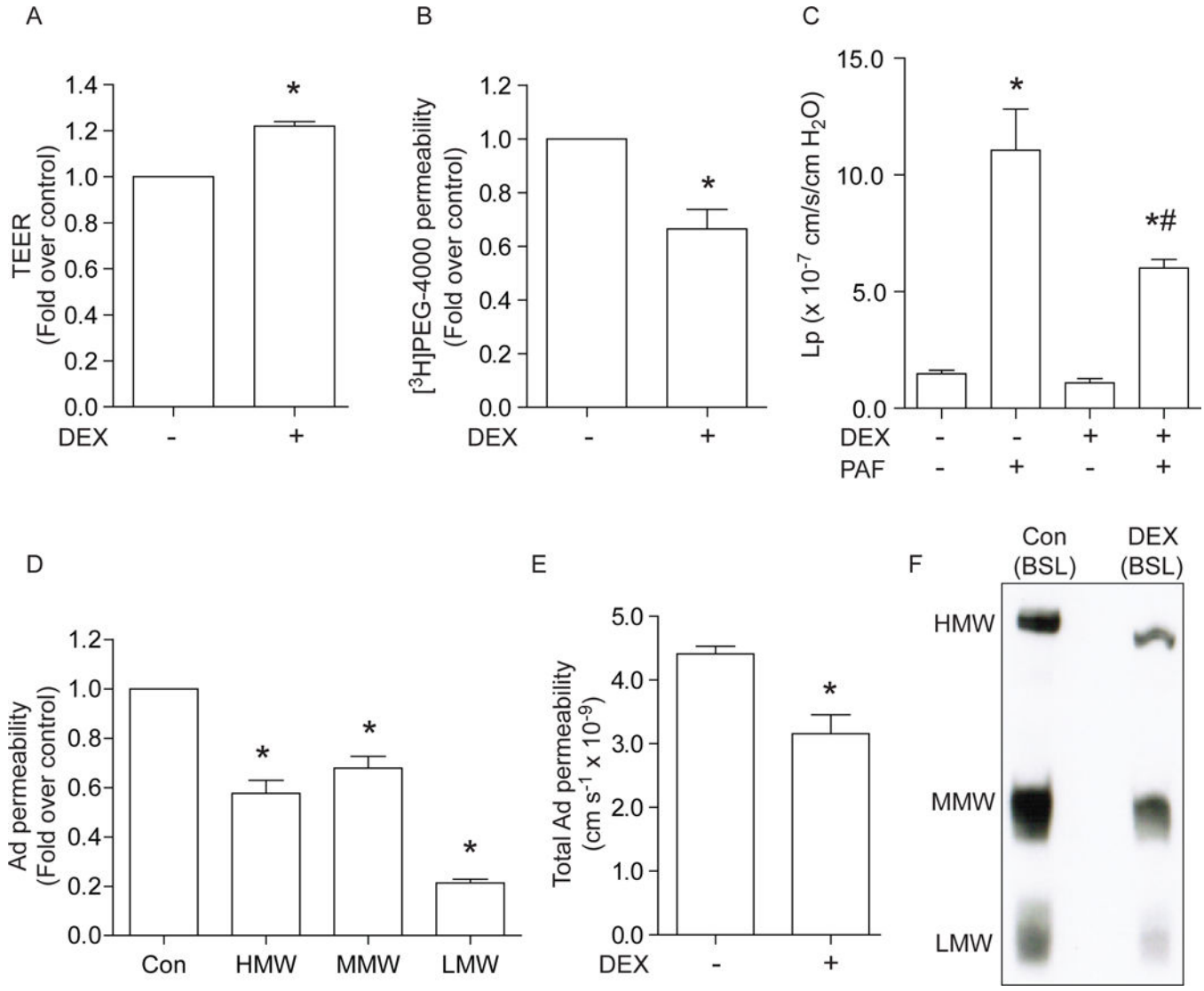

Figure 1:

Effects of DEX on permeability. HUVECs (Human Umbilical Vein Endothelial Cell) were seeded onto permeable polyethylene terephthalate (PET) filters and treated with or without 1μM of DEX every other day in both top and bottom of compartments. Tightness of the monolayer was measured on the 5th day of DEX treatment. A) Transendothelial Electrical Resistance (TEER). B) [^{3}H]PEG-4000 permeability across HUVEC monolayer. C) Measurements of hydraulic conductivity (Lp) in individually perfused mesenteric venulesfrom normal (n = 6) and Dex-treated(n = 4) rats. DEX treatment significantly attenuated the Lp responses to PAF that was known to cause transient increases inLp. D–F) 10 μg of full-length Ad was added onto the apical side. After 24 hrs, the medium on basolateral was collected. D) Total Ad amount was quantified using ELISA. E) The collected basolateral medium was concentrated and separated by PAGE. 3 forms of Ad are labeled as LMW (~90 kDa), MMW (~180 kDa), HMW (>250 kDa). F) Representative Western blot for full-length Ad flux across control and Dex-treated monolayers. Data are

expressed as mean values ± SEM (n = 4–8). *Significant difference ($P \leq 0.05$) from control (Con) group.

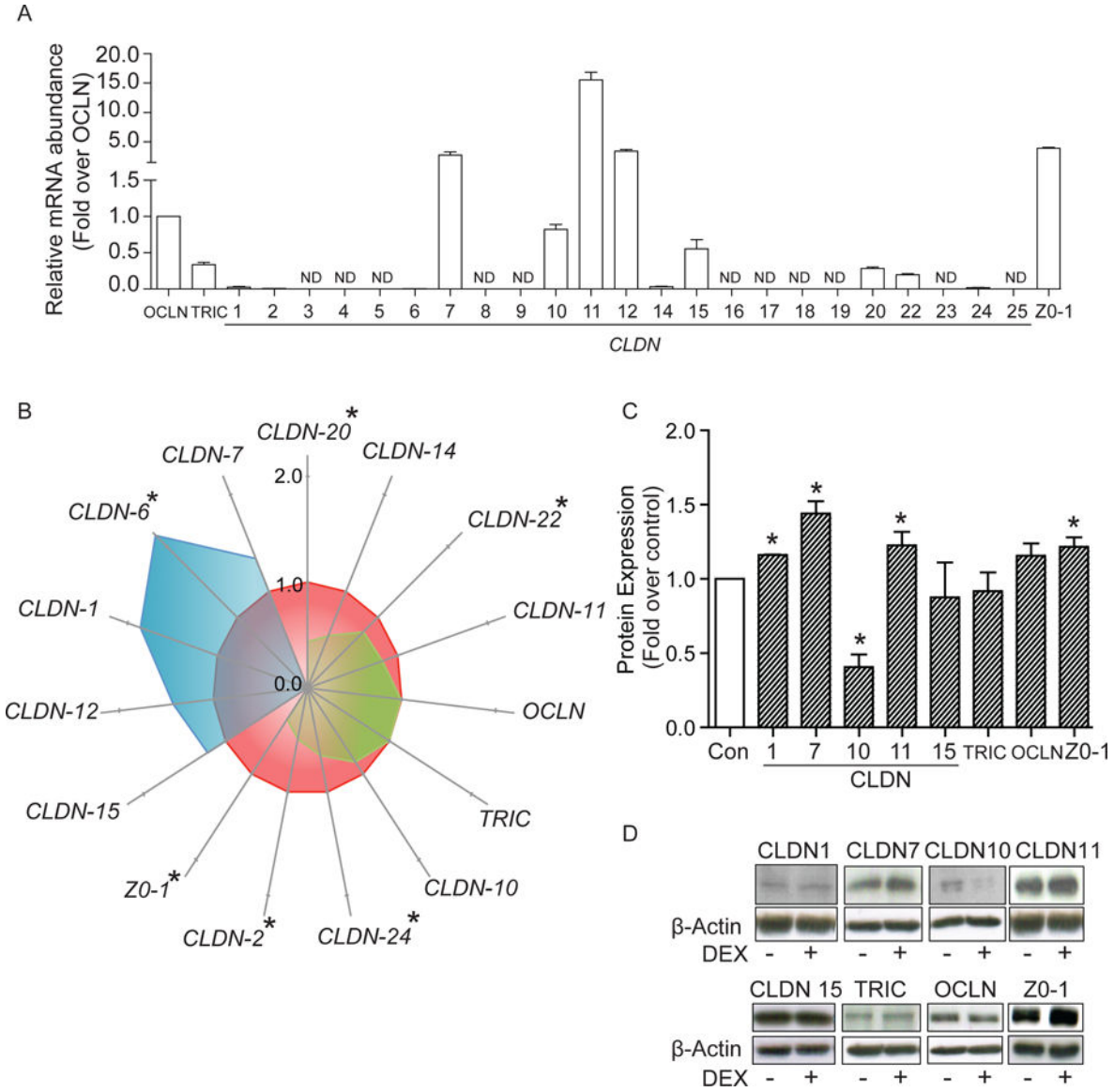

Figure 2:

Effect of DEX on Tight Junction Components. A) mRNA abundance by qRT-PCR analysis. HUVECs grown to confluence on permeable PET inserts. Total RNA was isolated from control cells on the 5th day. Transcript abundance was normalized to *GAPDH* and each gene examined was expressed relative to *OCLN* transcript abundance. B) TJ transcript levels in DEX-treated cells were normalized to *GAPDH*, and expressed relative to the control group (Blue - increasing compared to control; Green- decreasing compared to control). Data are expressed as mean values ± SEM (n = 3–5). C) Protein abundance in HUVECs grown on cell culture inserts. Protein abundance were normalized toβ-ACTIN, and expressed relative to the control group. D) Representative Western blots of CLDN- 1, −7, −10, −11, −15, TRI, OCC, Z0–1. Data are expressed as mean values ± SEM (n = 3–8). * indicates significant difference ($P \leq 0.05$) from control (Con) group.

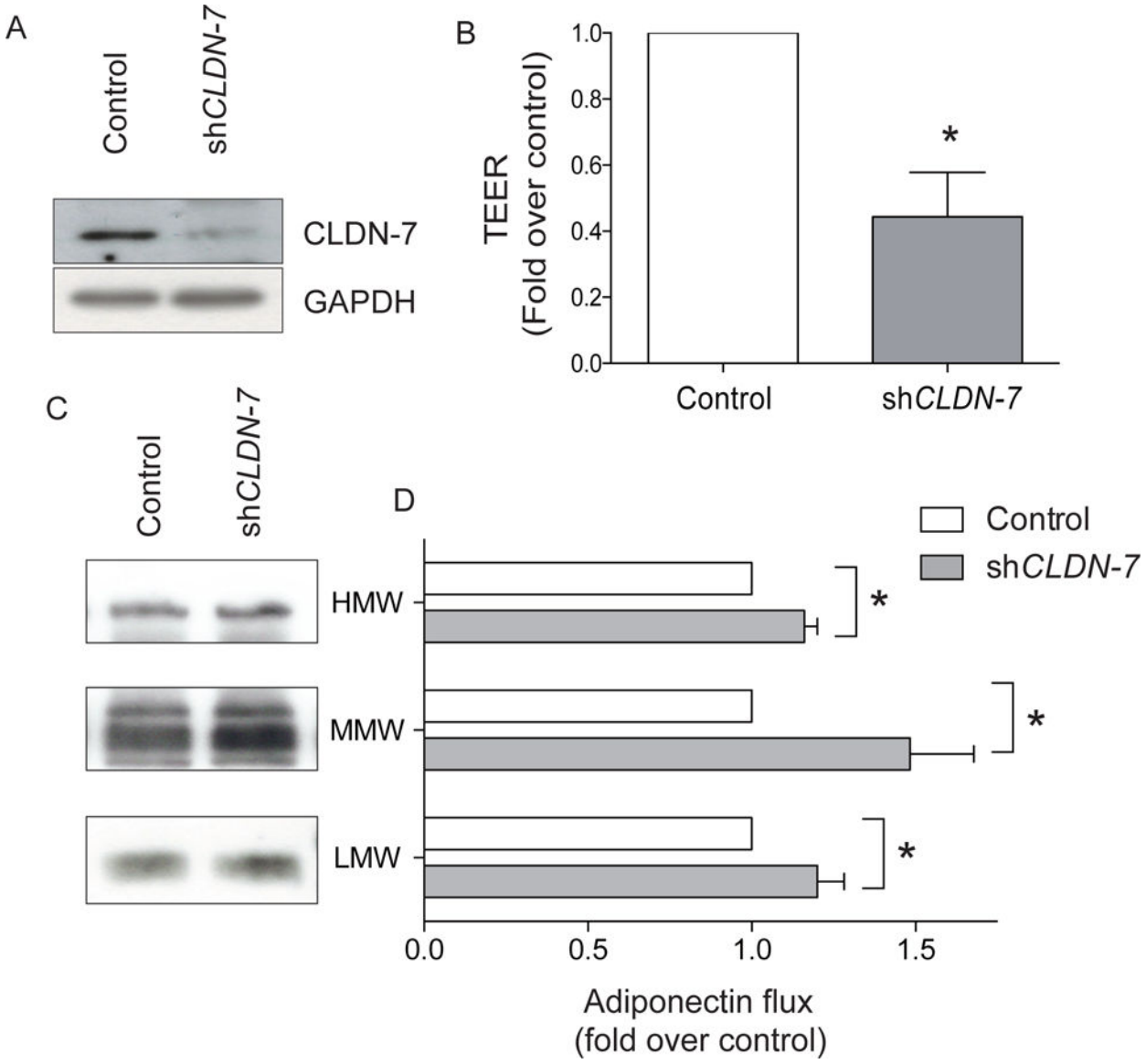

Figure 3:

Knockdown of claudin-7 alters transendothelial electrical resistance and adiponectin flux. We used shRNA to reduce levels of claudin-7 in HUVEC and average efficiency of knockdown was 71% with a representative Western blot shown in A. In cells transfected with scrambled (Control) or claudin-7 shRNA we then tested TEER (B) and flux of adiponectin with representative Western blot shown in C and quantitation in D. In B and D values are mean ± SEM (n = 3) and *indicates significant difference ($P \leq 0.05$) from control group.

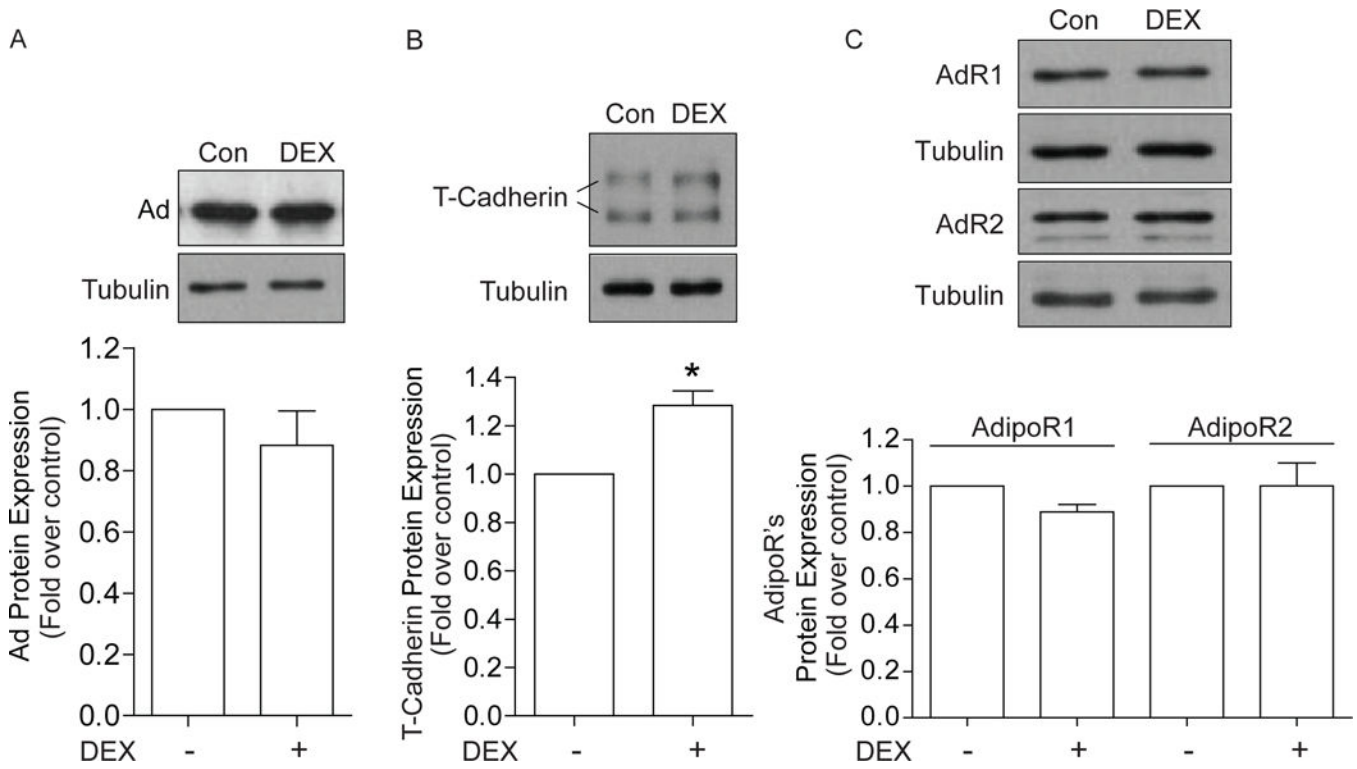

Figure 4:

Expression of Ad and its receptors in HUVEC. A) Ad expression in HUVECs treated with DEX after 5 days. B) T- CADHERIN expression in HUVECs with DEX treatment. C) ADIPO -R1/ -R2 expression in HUVECs. Data are expressed as mean values ± SEM (n = 3–6). *indicates significant difference ($P \leq 0.05$) from control (Con) group.

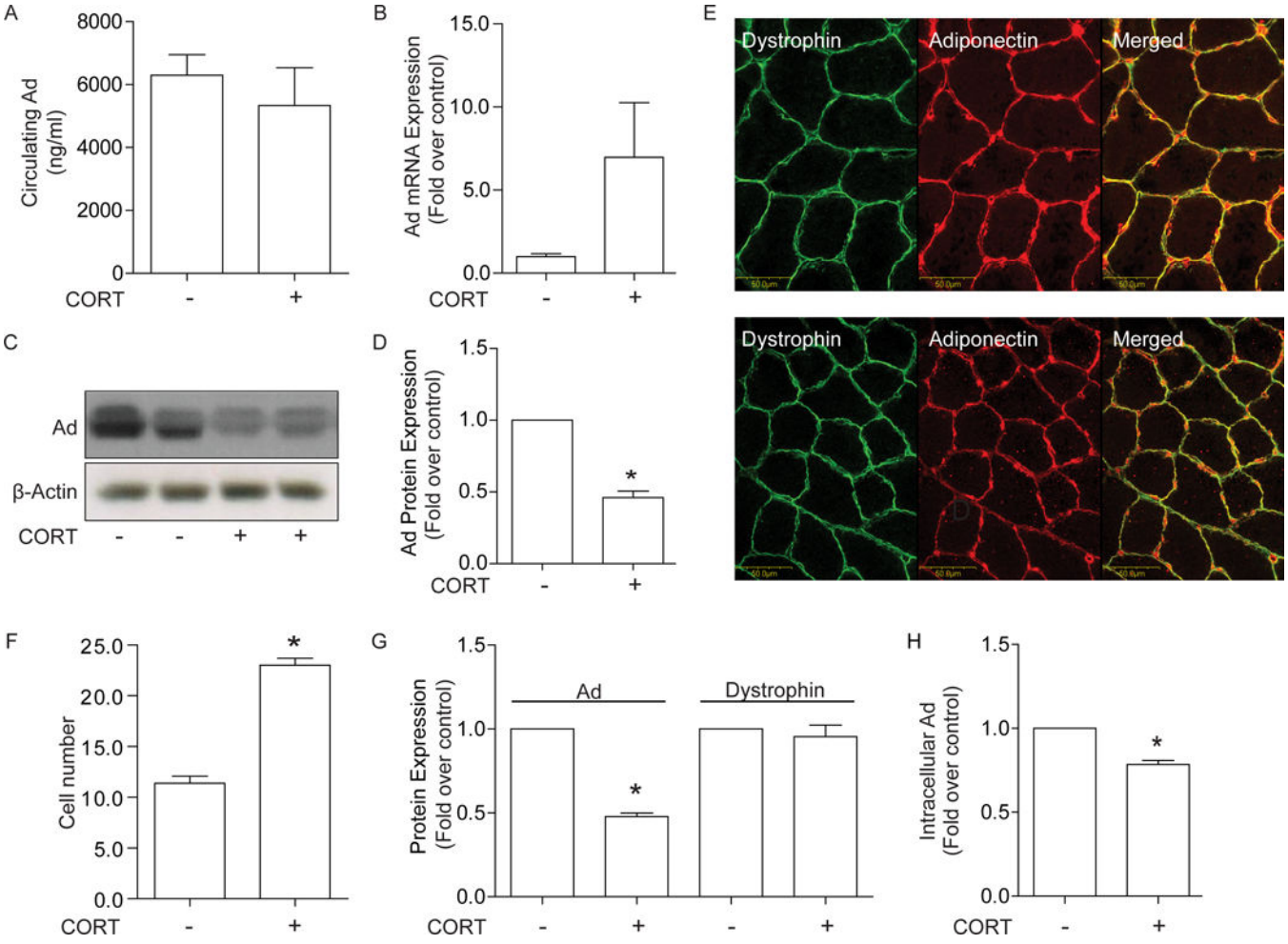

Figure 5:

Ad level in CORT treated animals. A) Using ELISA, circulating Ad was calculated in 1 week treated rat serum. B) Ad mRNA expression after 14 days of CORT. C&D) Representative Western blotting and quantitation of reduced Ad (~30 kDa) in soleus skeletal muscle. E) Immunohistochemical detection of dystrophin (green), Ad (red) in skeletal muscle isolated from rats after 2 weeks of CORT treatment, together with quantitation in F. G) Quantification of changes in intracellular Ad levels and H) cell number. Quantification of Ad shown as the intensity expressed per cell in arbitrary units and are expressed as mean values ± SEM (n = 3–5).* indicates significant difference ($P \leq 0.05$) from control (Con) group.

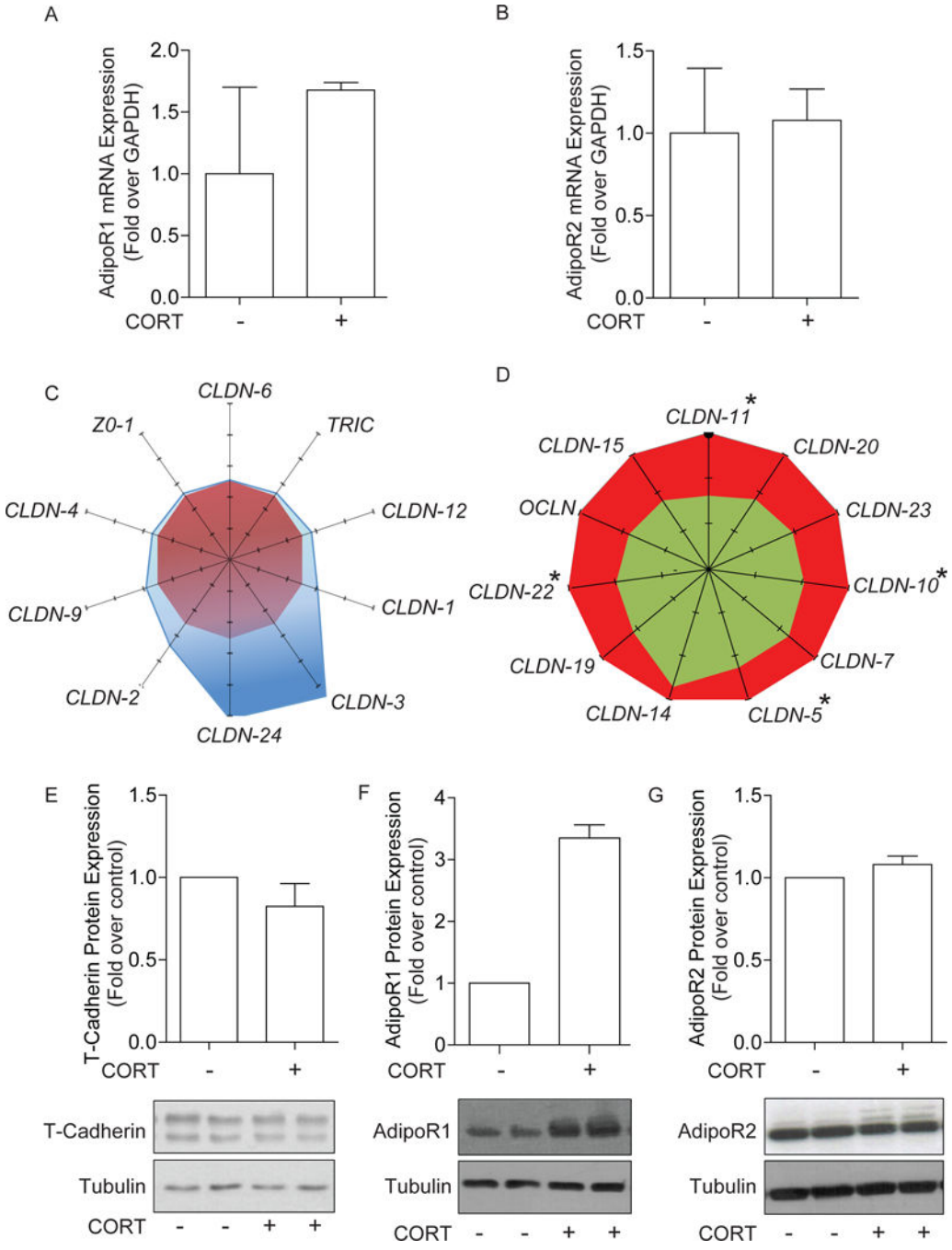

Figure 6:

Ad receptor expression in skeletal muscle. Rats were treated with CORT for 2 weeks. A,B) mRNA expression of Ad and its receptors after 14 days of CORT. Data are expressed as mean values ± SEM (n = 4–5). C–D) mRNA profile of tight junction in soleus skeletal muscle isolated from 2 weeks CORT- treated rats. mRNA abundance by qRT-PCR analysis. Transcript abundance was normalized to GAPDH mRNA abundance, and mRNA abundance for each gene examined was expressed relative to control group transcript abundance. Control group gene transcript were normalized to 1. C) mRNA profile of TJ that are

increased after 2 weeks CORT treatment compared to control. Blue- CORT- treated, Red- Control. D) TJ genes that are decreased after 2 weeks of CORT treatment. . E–G) Protein expression in soleus. E) T- CADHERIN. F) Ad receptor 1. G) Ad receptor 2. Data are expressed as mean values ± SEM (n = 3). * indicates significant difference ($P \leq 0.05$) from control group.

Appendix D

Altered transendothelial transport of hormones as a contributor to diabetes.

Yoon N, Dang TQ, Chasiotis H, Kelly SP, Sweeney G.

Diabetes Metab J. 2014 Apr;38(2):92-9.

Review
Pathophysiology

Diabetes Metab J 2014;38:92-99
http://dx.doi.org/10.4093/dmj.2014.38.2.92
pISSN 2233-6079 · eISSN 2233-6087

dmj
DIABETES & METABOLISM JOURNAL

Altered Transendothelial Transport of Hormones as a Contributor to Diabetes

Nanyoung Yoon, Thanh Q. Dang, Helen Chasiotis, Scott P. Kelly, Gary Sweeney

Department of Biology, York University, Toronto, ON, Canada

The vascular endothelium is a dynamic structure responsible for the separation and regulated movement of biological material between circulation and interstitial fluid. Hormones and nutrients can move across the endothelium either via a transcellular or paracellular route. Transcellular endothelial transport is well understood and broadly acknowledged to play an important role in the normal and abnormal physiology of endothelial function. However, less is known about the role of the paracellular route. Although the concept of endothelial dysfunction in diabetes is now widely accepted, we suggest that alterations in paracellular transport should be studied in greater detail and incorporated into this model. In this review we provide an overview of endothelial paracellular permeability and discuss its potential importance in contributing to the development of diabetes and associated complications. Accordingly, we also contend that if better understood, altered endothelial paracellular permeability could be considered as a potential therapeutic target for diabetes.

Keywords: Adherens junctions; Adiponectin; Endocrine; Endothelial transport; Hormones; Insulin; Paracellular; Tight junctions; Transcellular

INTRODUCTION

Structure and function of endothelium

A monolayer of endothelial cells lines the entire circulatory system of the body. This endothelium acts as a barrier which regulates the exchange of hormones, proteins and small molecules between the vascular compartment and the interstitial space [1,2]. The actions of a hormone or nutrient on a target tissue is implicitly dependent upon the ability of these factors to gain access to the target and numerous studies have indicated that hormone and nutrient concentrations in blood differ from those surrounding cells on the tissue side of the blood vessel endothelium [3-11]. In this regard, it is our contention that the significance of the endothelium as a regulator of hormone and substrate access to target tissues is often underappreciated. Endothelial permeability can be regulated by two distinct pathways: 1) the transcellular pathway where solutes are actively transported across the endothelium, primarily via caveolae-mediated transcytosis; or 2) the paracellular pathway where solutes passively move through the intercellular space between adjacent endothelial cells (Fig. 1).

TRANSCELLULAR TRANSPORT

The transcellular movement of solutes involves energy-dependent trafficking of vesicles across the endothelium [2]. This often requires their recognition by receptors in caveolae on the luminal surface of the endothelium, may involve vesiculo-vacuolar organelles or occur via transcellular channels [2]. Caveolae, cholesterol- and sphingolipid-rich non-clathrin-coated pits, are abundant in endothelial cells. After ligand binding to receptors in caveolae, dynamin-mediated endocytosis occurs followed by vectorial transport and fusion of the vesicle with basolateral membrane, resulting in the release of contents by

Corresponding author: Gary Sweeney
Department of Biology, York University, 4700 Keele Street, Toronto, ON, M3J 1P3, Canada
E-mail: gsweeney@yorku.ca

exocytosis [2]. As a general concept, transcellular vesicle trafficking is important in the transport of larger macromolecules across the endothelium since the paracellular route is typically capable of restricting passage of solutes larger than 3 nm in radius [12,13].

PARACELLULAR TRANSPORT

The paracellular mode of transport across endothelia depends upon concentration gradients between blood and interstitial fluid. One regulatory mechanism of paracellular movement involves tight junctions (TJs) which are composed of strands of transmembrane and cytosolic proteins that closely control paracellular flux and have been established to be important in regulating hormone transport [4,12,14]. As a component of the cell-cell junction of endothelia, the TJ provides a selective barrier to solute movement between cells [13]. The permselectivity of the TJ barrier is dependent on the variable assemblage of TJ proteins that comprise the complex. Proteins such as occludin, tricellulin, and claudins directly establish the TJ barrier and form the backbone of TJ strands while the cytosolic proteins, such as ZO-1, provide structural support to the TJ complex. The incorporation of specific TJ protein isoforms can enhance TJ barrier function (i.e., make TJs tighter) or form channels to increase TJ permeability (i.e., make TJs leakier) [13]. Importantly, skeletal muscle and heart vasculature have continuous endothelium with TJs between cells (Fig. 2) [15,16]. However, the liver and spleen have a discontinuous endothelium with large holes, which allow rapid equilibration of plasma with the underlying tissue [15,16]. It was suggested that this expedited exposure of the liver to plasma solute changes may partly explain its earlier susceptibility to insulin resistance [17]. Indeed, the precise architecture of TJs varies between different vascular beds, with TJs being either dominant at the apical point

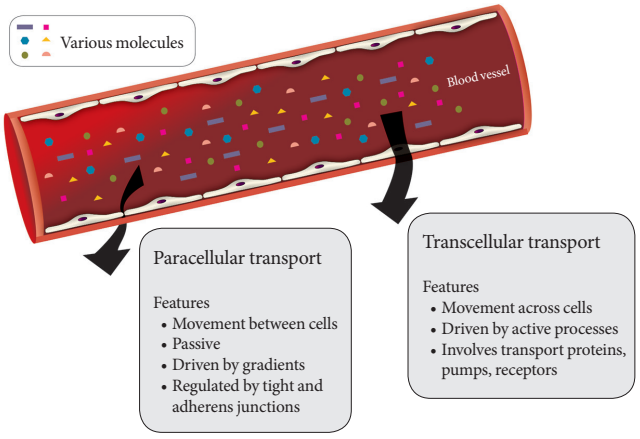

Fig. 1. Routes of transendothelial transport. A schematic representation of paracellular and transcellular routes for transport of blood-borne hormones and solutes to interstitial space of underlying tissue.

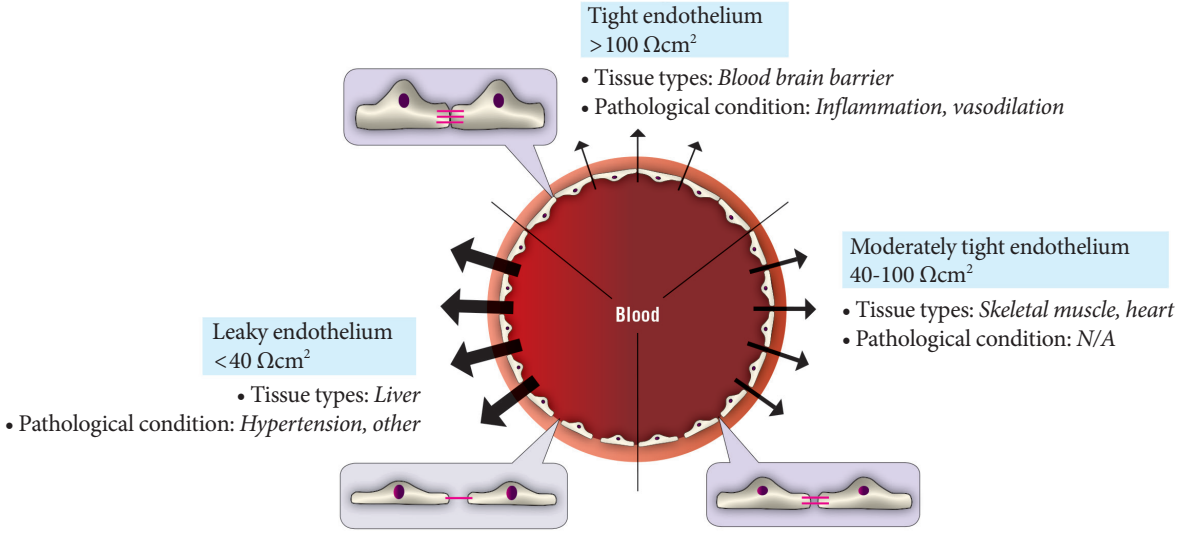

Fig. 2. Diversity of paracellular transport characteristics in different vascular beds. The size and structure of tight junctions varies significantly between different tissues and in this figure we summarize this by defining three arbitrary categories of leaky, moderately tight and tight endothelia. The typical resistance values associated with these definitions and examples of tissues where each category of endothelium is characteristic is shown. N/A, not applicable.

of intercellular space or intermingled with adherens junctions (AJs). Therefore, there is no doubt that transendothelial paracellular flux in certain vascular beds is more susceptible to changes in TJ composition and structure. Furthermore, changes in paracellular transport leading to endothelial hyperpermeability is a significant problem in vascular inflammation associated with diabetes, cancer, ischaemia-reperfusion injury, thrombisis, trauma, sepsis, and adult respiratory distress syndrome [18]. Importantly, despite the tremendous interest in adipokines over recent years very few studies have examined the critical step whereby and factors secreted by adipose tissue, or other tissues, must enter the circulation via capillaries or lymph. Paracellular movement is very likely to be a major regulatory step in this process. Indeed, it has been demonstrated that lymph/capillary partitioning of adipokines is dependent upon their molecular size and proposed that this will have important ramifications for their regional and systemic distribution and subsequent physiological effects [19].

It is also important to realize that crosstalk exists between 1) transcellular and paracellular routes of transport across endothelia and 2) TJs and AJs of endothelia. An example of the former is that in caveolin-1 knockout mice, or upon siRNA-mediated reduction of caveolin-1, altered TJ assembly in small capillaries and veins increased paracellular transport of albumin [20-22]. In the latter case, it has been shown that vascular endothelial (VE)-cadherin mediated signaling can regulate the expression of TJ proteins and consequently alter barrier function [2].

Indeed, evidence suggests that AJs also play a crucial role in regulating vascular permeability. They are comprised of calcium-dependent VE-cadherin in complex with a range of interacting partners, such as β-catenin and p120-catenin [2] and the expression of VE-cadherin is a specific early developmental marker for endothelial lineage. Deletion of the VE-cadherin gene induces embryonic lethality due to early collapse of the vasculature [23]. Increased vascular permeability occurs when VE-cadherin homophilic binding is inhibited. AJ stability is also critically regulated by phosphorylation [2]. More specifically, phosphorylation of VE-cadherin at catenin binding sites induced internalisation and thus alterations in vascular permeability. Interestingly, recent work demonstrated that phosphorylation of these residues (tyrosine 658 and 685 of VE-cadherin) occurs constitutively in veins but not arteries, correlating with enhanced leakiness in venous vessels [24]. Furthermore, single point mutations in VE-cadherin (Y658F and Y685F) reduce paracellular permeability by blocking internalisation of VE-cadherin [24].

ENDOTHELIAL DYSFUNCTION IN DIABETES

The concept of endothelial dysfunction in diabetes is well established [25]. However, this typically refers to vascular functions independent of transendothelial solute flux. The endothelium is also a dynamic interface that responds to various stimuli and synthesizes and liberates vasoactive molecules such as nitric oxide, prostaglandins and endothelin. Accordingly, vascular complications in diabetes include outcomes occurring in large (atherosclerosis, cardiomyopathy) and small (retinopathy, nephropathy, neuropathy) vessels [26]. We believe that diabetes-induced deleterious alterations in paracellular solute movement also represents a form of endothelial dysfunction which should be fully characterized to establish its physiological significance.

STUDIES ON TRANSENDOTHELIAL TRANSPORT OF HORMONES

Transport of insulin has been perhaps the best studied example. Insulin concentration at the target cell surface has been shown to be very different from that in plasma by approaches including microdialysis [7,8], direct interstitial sampling [9], and lymph measurements [5,6]. Furthermore, early temporal studies have demonstrated that insulin-mediated glucose uptake in muscle lags behind increases in plasma insulin [27], In contrast, when using cultured skeletal muscle cells, the addition of recombinant insulin has been shown to stimulate glucose uptake almost immediately (maximal at~10 minutes) [28]. The time delay seen *in vivo* has led to the suggestion that reaching the interstitial space is the limiting factor for insulin-mediated glucose uptake [14]. Thus, modification of access to skeletal muscle can have major effects on insulin action and subsequent metabolism [14,29]. Indeed, the efficiency and extent of insulin delivery to the interstitial space can be inhibited physiologically by diet [30]. The mechanism via which insulin crosses the endothelium is at least in part via the paracellular pathway and for more information on this topic readers are referred to recent excellent review articles by Kolka and Bergman [14,31].

Recent years have seen great interest in the role of adipo-

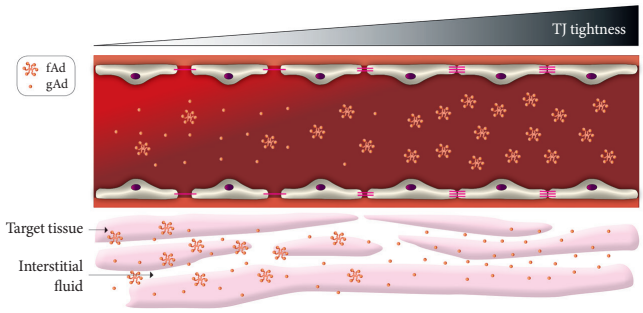

Fig. 3. Paracellular movement of adiponectin. A conceptual model showing the potential significance of paracellular transendothelial movement of adiponectin. When vascular endothelium is leaky (left side) there is significant flux of all forms of adiponectin from bloodstream to interstitial space. However, as endothelium becomes tighter there is likely to be a gradient of decrease in high molecular weight or other multimeric forms of adiponectin whereas the smaller globular fragment of adiponectin may still be able to access underlying target tissue such as skeletal muscle. TJ, tight junctions; fAd, full length adiponectin; gAd, globular adiponectin.

nectin in the pathophysiology of diabetic complications [32-34]. Numerous studies have now established that adiponectin can act on various targets to mediate antidiabetic, anti-inflammatory, antiatherosclerotic, and cardioprotective effects [32,34,35]. Thus, enhancing adiponectin action is considered as a therapeutically beneficial strategy. Adiponectin circulates in the blood as three multimeric complexes; low molecular weight (LMW; trimer), medium molecular weight (MMW; hexamer) and high molecular weight (HMW; oligomer), and in obese and diabetic patients reduced circulating levels of adiponectin have been observed. In addition, cleavage of adiponectin by leukocyte derived elastase generates a C-terminal globular fragment of adiponectin which mediates important functional effects. It is likely that delivery of adiponectin to the interstitial space is a major, yet underestimated, determinant of its function. Given the size range of the biologically active forms of adiponectin (16 kDa for globular form and >500 kDa for HMW) there is considerable potential for selective paracellular transport of adiponectin, particularly in different vascular beds. HMW adiponectin is often considered to be the most biologically active and most relevant form with respect to the metabolic syndrome, and we speculate that given the large size of the HMW form, transendothelial movement may prove to be a significant rate-limiting step in its physiological actions (Fig. 3). Indeed, it has been proposed that HMW adiponectin mediates beneficial metabolic effects primarily by acting on liver [34], whereas the globular form is thought to have more potent metabolic effects in skeletal muscle [33]. These observations could be explained by the leaky and moderately tight paracellular barriers present in vascular beds of these respective tissues, although this is likely an oversimplification (Fig. 3). As far as we are aware, no studies have directly examined the paracellular movement of adiponectin in skeletal muscle and liver.

Studies of adiponectin movement across the blood-brain barrier (BBB) have indicated that only LMW and MMW, but not HMW forms were found in cerebralspinal fluid [36-38]. Surprisingly, there are only a few studies examining interstitial adiponectin levels. One found that interstitial concentrations of adiponectin in human adipose tissue were ~25-fold lower than plasma [39] while the other found that exercise increased interstitial adiponectin levels, which were around 20% of plasma concentration [40]. We hypothesize that the magnitude of gradient between plasma and interstitial levels of adiponectin in skeletal muscle may be higher due to existence of a tighter endothelial barrier within the muscle vasculature. Indeed, this may be highly significant as it has been shown that hyperinsulinemia differentially affects the compartmental (interstitial and circulating) distribution of the adiponectin complexes in lean and insulin-resistant, obese individuals [41]. We have recently shown that adiponectin moves across cultured endothelial monolayers via a paracellular route and that this movement was reduced by hormonal or physical manipulation of TJs.

TJ COMPOSITION AND PROTEIN EXPRESSION IN DIABETES

Studies examining changes in TJ composition and protein expression in diabetes have not been extensive but have so far yielded numerous consistent observations in the study of diabetic complications. For example, reductions in ZO-1 have been observed in kidney glomeruli, the retina, BBB and intestine of various diabetic models [42-46]. Localization of ZO-1 in glomeruli was also investigated by electron microscopy and found to redistribute from the podocyte membrane to the cytoplasm in the diabetic kidney [47]. Several reports have indicated that both occludin and claudin-5 were reduced in diabetic retina or BBB [44-46,48,49]. Hence, expression or localization of TJ proteins appear to be susceptible to a diabetic environment and contribute to complications such as retinopathy and nephropathy. More widespread analysis is now needed, particularly in metabolically active tissues. Knockout mouse models have

been generated for various TJ proteins, including occludin and claudin-1, 2, 4, 5, 7, 9, 11, 14, 15, 16, 18, and 19 [50-63]. Little to no information was given regarding their metabolic phenotype, however in one study using $Cldn2^{-/-}Cldn15^{-/-}$ double-knockout mice the animals died from malnutrition related to defective absorption of glucose, amino acids and fats [63]. These models may prove valuable in elucidating the significance of alterations in transendothelial hormone flux in determining metabolic dysfunction in diabetes.

THERAPEUTIC POTENTIAL OF TARGETING ENDOTHELIAL TRANSPORT

Based on the above description of the importance of endothelial transport in diabetes, it is evident that developing therapeutic strategies which manipulate paracellular flux may prove useful. Indeed, a literature review indicates that various agents are already available; such as peptides which bind to integral TJ proteins, siRNA and antisense oligonucleotides targeting TJ proteins, various toxins, lipids, and activators or inhibitors of kinases and phosphatases that regulate junction assembly and function have all been shown to regulate paracellular permeability [64]. Nevertheless, there is an innate risk in therapeutics which globally alter transendothelial permeability and so it will be desirable to elicit changes in a localized or tissue-specific manner, or to targeting specific components of TJs which allow more controlled and selective changes in permeability [65]. One example of a current therapeutic approach targeting TJs is the use of glucocorticoids as a locally applied treatment for diabetic retinopathy. The mechanism of action is thought to involve, at least in part, restoration of barrier function in the retinal vasculature by modifying TJ composition and structure [66]. Therefore, it is attractive to speculate that controlled manipulation of paracellular transport may be applicable to improving metabolic dysfunction in diabetes.

CONCLUSIONS

The endothelial monolayer is an important rate-limiting determinant of hormone and substrate access to target tissues. Previous studies focusing on insulin suggest that impaired delivery of insulin from plasma to interstitial space in obesity may contribute to metabolic insulin resistance and diabetes. Since adiponectin is known to mediate beneficial antidiabetic effects, and the molecular weight of biologically active forms of adiponectin ranges widely, we propose that paracellular transport may be a major determinant of transendothelial adiponectin flux. In particular, the research community has often accepted that fact that the HMW oligomeric form of adiponectin targets liver and not muscle whereas the small globular portion has 'more potency' in skeletal muscle. This was initially attributed to the higher binding affinity of globular fragment of adiponectin to skeletal muscle cell membranes which were thought to express more adiponectin receptor AdipoR1 isoform. However, such data are not consistent and easier access of the smaller globular adiponectin across the relatively tight endothelial monolayer found in skeletal muscle vasculature, in comparison with liver, may be significant. Thus, TJ-mediated, or AJ-mediated, alterations in adiponectin access to tissues from the vasculature are likely to be of important functional significance. Numerous studies in kidney and retina have indicated that expression of various TJ proteins is altered in diabetes; however, the changes in metabolic target tissues of adiponectin and their physiological significance still need to be established. The principal mechanisms responsible for altered TJ composition and structure in diabetes must also be elucidated, with likely mediators including hyperglycemia, hyperinsulinemia, free fatty acids or tumor necrosis factor-α.

Overall, the paracellular permeability of the endothelial barrier is a tightly regulated process which can be dynamically adjusted in response to various mediators. The potential contribution to metabolic dysfunction in diabetes is apparent yet the precise significance has likely been somewhat underestimated. We believe that further investigation of TJ-mediated changes in hormone or substrate flux in diabetes and characterization of their functional significance will shed additional light on the pathophysiology of disease and identify potential therapeutic opportunities.

CONFLICTS OF INTEREST

No potential conflict of interest relevant to this article was reported.

ACKNOWLEDGMENTS

Related work in the authors laboratories is funded by Canadian Diabetes Association (G.S.), Heart & Stroke Foundation of Canada (G.S.), Canadian Institutes of Health Research (G.S.), and Natural Sciences and Engineering Research Council (S.

P.K.). We also wish to express sincere thanks to Haemin Kwak, School of the Art Institute of Chicago (haeminkwak88@gmail.com) for graphic design expertise in producing all figures in this manuscript.

REFERENCES

1. Pries AR, Kuebler WM. Normal endothelium. Handb Exp Pharmacol 2006;176 Pt 1:1-40.
2. Goddard LM, Iruela-Arispe ML. Cellular and molecular regulation of vascular permeability. Thromb Haemost 2013;109:407-15.
3. Chiu JD, Kolka CM, Richey JM, Harrison LN, Zuniga E, Kirkman EL, Bergman RN. Experimental hyperlipidemia dramatically reduces access of insulin to canine skeletal muscle. Obesity (Silver Spring) 2009;17:1486-92.
4. Kolka CM, Harrison LN, Lottati M, Chiu JD, Kirkman EL, Bergman RN. Diet-induced obesity prevents interstitial dispersion of insulin in skeletal muscle. Diabetes 2010;59:619-26.
5. Chiu JD, Richey JM, Harrison LN, Zuniga E, Kolka CM, Kirkman E, Ellmerer M, Bergman RN. Direct administration of insulin into skeletal muscle reveals that the transport of insulin across the capillary endothelium limits the time course of insulin to activate glucose disposal. Diabetes 2008;57:828-35.
6. Yang YJ, Hope ID, Ader M, Bergman RN. Importance of transcapillary insulin transport to dynamics of insulin action after intravenous glucose. Am J Physiol 1994;266:E17-25.
7. Sjostrand M, Holmang A, Lonnroth P. Measurement of interstitial insulin in human muscle. Am J Physiol 1999;276:E151-4.
8. Herkner H, Klein N, Joukhadar C, Lackner E, Langenberger H, Frossard M, Bieglmayer C, Wagner O, Roden M, Muller M. Transcapillary insulin transfer in human skeletal muscle. Eur J Clin Invest 2003;33:141-6.
9. Bodenlenz M, Schaupp LA, Druml T, Sommer R, Wutte A, Schaller HC, Sinner F, Wach P, Pieber TR. Measurement of interstitial insulin in human adipose and muscle tissue under moderate hyperinsulinemia by means of direct interstitial access. Am J Physiol Endocrinol Metab 2005;289:E296-300.
10. Maggs DG, Jacob R, Rife F, Lange R, Leone P, During MJ, Tamborlane WV, Sherwin RS. Interstitial fluid concentrations of glycerol, glucose, and amino acids in human quadricep muscle and adipose tissue: evidence for significant lipolysis in skeletal muscle. J Clin Invest 1995;96:370-7.
11. Barrett EJ, Wang H, Upchurch CT, Liu Z. Insulin regulates its own delivery to skeletal muscle by feed-forward actions on the vasculature. Am J Physiol Endocrinol Metab 2011;301:E252-63.
12. Gunzel D, Yu AS. Claudins and the modulation of tight junction permeability. Physiol Rev 2013;93:525-69.
13. Gunzel D, Fromm M. Claudins and other tight junction proteins. Compr Physiol 2012;2:1819-52.
14. Kolka CM, Bergman RN. The barrier within: endothelial transport of hormones. Physiology (Bethesda) 2012;27:237-47.
15. Aird WC. Phenotypic heterogeneity of the endothelium: I. Structure, function, and mechanisms. Circ Res 2007;100:158-73.
16. Aird WC. Phenotypic heterogeneity of the endothelium: II. Representative vascular beds. Circ Res 2007;100:174-90.
17. Kim SP, Ellmerer M, Van Citters GW, Bergman RN. Primacy of hepatic insulin resistance in the development of the metabolic syndrome induced by an isocaloric moderate-fat diet in the dog. Diabetes 2003;52:2453-60.
18. Kumar P, Shen Q, Pivetti CD, Lee ES, Wu MH, Yuan SY. Molecular mechanisms of endothelial hyperpermeability: implications in inflammation. Expert Rev Mol Med 2009;11:e19.
19. Miller NE, Michel CC, Nanjee MN, Olszewski WL, Miller IP, Hazell M, Olivecrona G, Sutton P, Humphreys SM, Frayn KN. Secretion of adipokines by human adipose tissue in vivo: partitioning between capillary and lymphatic transport. Am J Physiol Endocrinol Metab 2011;301:E659-67.
20. Schubert W, Frank PG, Woodman SE, Hyogo H, Cohen DE, Chow CW, Lisanti MP. Microvascular hyperpermeability in caveolin-1 (-/-) knock-out mice: treatment with a specific nitric-oxide synthase inhibitor, L-NAME, restores normal microvascular permeability in Cav-1 null mice. J Biol Chem 2002;277:40091-8.
21. Miyawaki-Shimizu K, Predescu D, Shimizu J, Broman M, Predescu S, Malik AB. siRNA-induced caveolin-1 knockdown in mice increases lung vascular permeability via the junctional pathway. Am J Physiol Lung Cell Mol Physiol 2006;290:L405-13.
22. Razani B, Engelman JA, Wang XB, Schubert W, Zhang XL, Marks CB, Macaluso F, Russell RG, Li M, Pestell RG, Di Vizio D, Hou H Jr, Kneitz B, Lagaud G, Christ GJ, Edelmann W, Lisanti MP. Caveolin-1 null mice are viable but show evidence of hyperproliferative and vascular abnormalities. J Biol Chem 2001;276:38121-38.
23. Gory-Faure S, Prandini MH, Pointu H, Roullot V, Pignot-Paintrand I, Vernet M, Huber P. Role of vascular endothelial-cadherin in vascular morphogenesis. Development 1999;126:2093-102.
24. Orsenigo F, Giampietro C, Ferrari A, Corada M, Galaup A, Sigismund S, Ristagno G, Maddaluno L, Koh GY, Franco D,

Kurtcuoglu V, Poulikakos D, Baluk P, McDonald D, Grazia Lampugnani M, Dejana E. Phosphorylation of VE-cadherin is modulated by haemodynamic forces and contributes to the regulation of vascular permeability *in vivo*. Nat Commun 2012; 3:1208.
25. Ding H, Triggle CR. Endothelial dysfunction in diabetes: multiple targets for treatment. Pflugers Arch 2010;459:977-94.
26. Symons JD, Abel ED. Lipotoxicity contributes to endothelial dysfunction: a focus on the contribution from ceramide. Rev Endocr Metab Disord 2013;14:59-68.
27. Freidenberg GR, Suter S, Henry RR, Nolan J, Reichart D, Olefsky JM. Delayed onset of insulin activation of the insulin receptor kinase in vivo in human skeletal muscle. Diabetes 1994; 43:118-26.
28. Somwar R, Kim DY, Sweeney G, Huang C, Niu W, Lador C, Ramlal T, Klip A. GLUT4 translocation precedes the stimulation of glucose uptake by insulin in muscle cells: potential activation of GLUT4 via p38 mitogen-activated protein kinase. Biochem J 2001;359:639-49.
29. Barrett EJ, Rattigan S. Muscle perfusion: its measurement and role in metabolic regulation. Diabetes 2012;61:2661-8.
30. Kubota T, Kubota N, Kumagai H, Yamaguchi S, Kozono H, Takahashi T, Inoue M, Itoh S, Takamoto I, Sasako T, Kumagai K, Kawai T, Hashimoto S, Kobayashi T, Sato M, Tokuyama K, Nishimura S, Tsunoda M, Ide T, Murakami K, Yamazaki T, Ezaki O, Kawamura K, Masuda H, Moroi M, Sugi K, Oike Y, Shimokawa H, Yanagihara N, Tsutsui M, Terauchi Y, Tobe K, Nagai R, Kamata K, Inoue K, Kodama T, Ueki K, Kadowaki T. Impaired insulin signaling in endothelial cells reduces insulin-induced glucose uptake by skeletal muscle. Cell Metab 2011; 13:294-307.
31. Kolka CM, Bergman RN. The endothelium in diabetes: its role in insulin access and diabetic complications. Rev Endocr Metab Disord 2013;14:13-9.
32. Scheid MP, Sweeney G. The role of adiponectin signaling in metabolic syndrome and cancer. Rev Endocr Metab Disord. Epub 2013 Sep 10. http://dx.doi.org/10.1007/s11154-013-9265-5.
33. Liu Y, Sweeney G. Adiponectin action in skeletal muscle. Best Pract Res Clin Endocrinol Metab 2014;28:33-41.
34. Ye R, Scherer PE. Adiponectin, driver or passenger on the road to insulin sensitivity? Mol Metab 2013;2:133-41.
35. Park M, Sweeney G. Direct effects of adipokines on the heart: focus on adiponectin. Heart Fail Rev 2013;18:631-44.
36. Kubota N, Yano W, Kubota T, Yamauchi T, Itoh S, Kumagai H, Kozono H, Takamoto I, Okamoto S, Shiuchi T, Suzuki R, Satoh H, Tsuchida A, Moroi M, Sugi K, Noda T, Ebinuma H, Ueta Y, Kondo T, Araki E, Ezaki O, Nagai R, Tobe K, Terauchi Y, Ueki K, Minokoshi Y, Kadowaki T. Adiponectin stimulates AMP-activated protein kinase in the hypothalamus and increases food intake. Cell Metab 2007;6:55-68.
37. Neumeier M, Weigert J, Buettner R, Wanninger J, Schaffler A, Muller AM, Killian S, Sauerbruch S, Schlachetzki F, Steinbrecher A, Aslanidis C, Scholmerich J, Buechler C. Detection of adiponectin in cerebrospinal fluid in humans. Am J Physiol Endocrinol Metab 2007;293:E965-9.
38. Kusminski CM, McTernan PG, Schraw T, Kos K, O'Hare JP, Ahima R, Kumar S, Scherer PE. Adiponectin complexes in human cerebrospinal fluid: distinct complex distribution from serum. Diabetologia 2007;50:634-42.
39. Nielsen NB, Hojbjerre L, Sonne MP, Alibegovic AC, Vaag A, Dela F, Stallknecht B. Interstitial concentrations of adipokines in subcutaneous abdominal and femoral adipose tissue. Regul Pept 2009;155:39-45.
40. Hojbjerre L, Rosenzweig M, Dela F, Bruun JM, Stallknecht B. Acute exercise increases adipose tissue interstitial adiponectin concentration in healthy overweight and lean subjects. Eur J Endocrinol 2007;157:613-23.
41. Murdolo G, Hammarstedt A, Schmelz M, Jansson PA, Smith U. Acute hyperinsulinemia differentially regulates interstitial and circulating adiponectin oligomeric pattern in lean and insulin-resistant, obese individuals. J Clin Endocrinol Metab 2009; 94:4508-16.
42. Omran OM. Effects of thymoquinone on STZ-induced diabetic nephropathy: an immunohistochemical study. Ultrastruct Pathol 2014;38:26-33.
43. Shan CY, Yang JH, Kong Y, Wang XY, Zheng MY, Xu YG, Wang Y, Ren HZ, Chang BC, Chen LM. Alteration of the intestinal barrier and GLP2 secretion in Berberine-treated type 2 diabetic rats. J Endocrinol 2013;218:255-62.
44. Shin JY, Sohn J, Park KH. Chlorogenic acid decreases retinal vascular hyperpermeability in diabetic rat model. J Korean Med Sci 2013;28:608-13.
45. Bhattacharjee PS, Huq TS, Potter V, Young A, Davenport IR, Graves R, Mandal TK, Clement C, McFerrin HE, Muniruzzaman S, Ireland SK, Hill JM. High-glucose-induced endothelial cell injury is inhibited by a Peptide derived from human apolipoprotein E. PLoS One 2012;7:e52152.
46. Liu C, Wu J, Zou MH. Activation of AMP-activated protein kinase alleviates high-glucose-induced dysfunction of brain microvascular endothelial cell tight-junction dynamics. Free

Radic Biol Med 2012;53:1213-21.
47. Rincon-Choles H, Vasylyeva TL, Pergola PE, Bhandari B, Bhandari K, Zhang JH, Wang W, Gorin Y, Barnes JL, Abboud HE. ZO-1 expression and phosphorylation in diabetic nephropathy. Diabetes 2006;55:894-900.
48. Antonetti DA, Barber AJ, Khin S, Lieth E, Tarbell JM, Gardner TW. Vascular permeability in experimental diabetes is associated with reduced endothelial occludin content: vascular endothelial growth factor decreases occludin in retinal endothelial cells: Penn State Retina Research Group. Diabetes 1998;47:1953-9.
49. Barber AJ, Antonetti DA, Gardner TW. Altered expression of retinal occludin and glial fibrillary acidic protein in experimental diabetes: the Penn State Retina Research Group. Invest Ophthalmol Vis Sci 2000;41:3561-8.
50. Gow A, Southwood CM, Li JS, Pariali M, Riordan GP, Brodie SE, Danias J, Bronstein JM, Kachar B, Lazzarini RA. CNS myelin and sertoli cell tight junction strands are absent in Osp/claudin-11 null mice. Cell 1999;99:649-59.
51. Saitou M, Furuse M, Sasaki H, Schulzke JD, Fromm M, Takano H, Noda T, Tsukita S. Complex phenotype of mice lacking occludin, a component of tight junction strands. Mol Biol Cell 2000;11:4131-42.
52. Furuse M, Hata M, Furuse K, Yoshida Y, Haratake A, Sugitani Y, Noda T, Kubo A, Tsukita S. Claudin-based tight junctions are crucial for the mammalian epidermal barrier: a lesson from claudin-1-deficient mice. J Cell Biol 2002;156:1099-111.
53. Ben-Yosef T, Belyantseva IA, Saunders TL, Hughes ED, Kawamoto K, Van Itallie CM, Beyer LA, Halsey K, Gardner DJ, Wilcox ER, Rasmussen J, Anderson JM, Dolan DF, Forge A, Raphael Y, Camper SA, Friedman TB. Claudin 14 knockout mice, a model for autosomal recessive deafness DFNB29, are deaf due to cochlear hair cell degeneration. Hum Mol Genet 2003;12:2049-61.
54. Nitta T, Hata M, Gotoh S, Seo Y, Sasaki H, Hashimoto N, Furuse M, Tsukita S. Size-selective loosening of the blood-brain barrier in claudin-5-deficient mice. J Cell Biol 2003;161:653-60.
55. Miyamoto T, Morita K, Takemoto D, Takeuchi K, Kitano Y, Miyakawa T, Nakayama K, Okamura Y, Sasaki H, Miyachi Y, Furuse M, Tsukita S. Tight junctions in Schwann cells of peripheral myelinated axons: a lesson from claudin-19-deficient mice. J Cell Biol 2005;169:527-38.
56. Tamura A, Kitano Y, Hata M, Katsuno T, Moriwaki K, Sasaki H, Hayashi H, Suzuki Y, Noda T, Furuse M, Tsukita S, Tsukita S. Megaintestine in claudin-15-deficient mice. Gastroenterology 2008;134:523-34.
57. Nakano Y, Kim SH, Kim HM, Sanneman JD, Zhang Y, Smith RJ, Marcus DC, Wangemann P, Nessler RA, Banfi B. A claudin-9-based ion permeability barrier is essential for hearing. PLoS Genet 2009;5:e1000610.
58. Muto S, Hata M, Taniguchi J, Tsuruoka S, Moriwaki K, Saitou M, Furuse K, Sasaki H, Fujimura A, Imai M, Kusano E, Tsukita S, Furuse M. Claudin-2-deficient mice are defective in the leaky and cation-selective paracellular permeability properties of renal proximal tubules. Proc Natl Acad Sci U S A 2010;107:8011-6.
59. Tatum R, Zhang Y, Salleng K, Lu Z, Lin JJ, Lu Q, Jeansonne BG, Ding L, Chen YH. Renal salt wasting and chronic dehydration in claudin-7-deficient mice. Am J Physiol Renal Physiol 2010;298:F24-34.
60. Will C, Breiderhoff T, Thumfart J, Stuiver M, Kopplin K, Sommer K, Gunzel D, Querfeld U, Meij IC, Shan Q, Bleich M, Willnow TE, Muller D. Targeted deletion of murine Cldn16 identifies extra- and intrarenal compensatory mechanisms of Ca2+ and Mg2+ wasting. Am J Physiol Renal Physiol 2010;298:F1152-61.
61. Hayashi D, Tamura A, Tanaka H, Yamazaki Y, Watanabe S, Suzuki K, Suzuki K, Sentani K, Yasui W, Rakugi H, Isaka Y, Tsukita S. Deficiency of claudin-18 causes paracellular H+ leakage, up-regulation of interleukin-1β, and atrophic gastritis in mice. Gastroenterology 2012;142:292-304.
62. Fujita H, Hamazaki Y, Noda Y, Oshima M, Minato N. Claudin-4 deficiency results in urothelial hyperplasia and lethal hydronephrosis. PLoS One 2012;7:e52272.
63. Wada M, Tamura A, Takahashi N, Tsukita S. Loss of claudins 2 and 15 from mice causes defects in paracellular Na+ flow and nutrient transport in gut and leads to death from malnutrition. Gastroenterology 2013;144:369-80.
64. Gonzalez-Mariscal L, Hernandez S, Vega J. Inventions designed to enhance drug delivery across epithelial and endothelial cells through the paracellular pathway. Recent Pat Drug Deliv Formul 2008;2:145-76.
65. Deli MA. Potential use of tight junction modulators to reversibly open membranous barriers and improve drug delivery. Biochim Biophys Acta 2009;1788:892-910.
66. Felinski EA, Antonetti DA. Glucocorticoid regulation of endothelial cell tight junction gene expression: novel treatments for diabetic retinopathy. Curr Eye Res 2005;30:949-57.